UNIVERSITAT DE BARCELONA

Insights into the role of GPRC5B in the pathophysiology of MLC disease

Adrià Pla Casillanis

UNIVERSITAT DE BARCELONA

Insights into the role of GPRC5B in the pathophysiology of MLC disease

Programa de Doctorat en Biomedicina

Tesi doctoral: **Adrià Pla Casillanis**

Tesi realitzada sota la direcció de: **Dr. Raúl Estévez Povedano**

Departament de Ciències Fisiològiques

Facultat de Medicina. Campus Bellvitge

Universitat de Barcelona, Desembre 2022

PROGRAMA DE DOCTORAT EN BIOMEDICINA

UNIVERSITAT DE BARCELONA

Memòria presentada per optar al grau de doctor per la Universitat de Barcelona, 2022

ADRIÀ PLA CASILLANIS

L'interessat,

Adrià Pla Casillanis

El director de la tesi,

Raúl Estévez Povedano

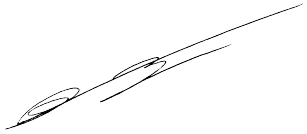

Departament de Ciències Fisiològiques, UB

ABSTRACT

Megalencephalic Leukoencephalopathy with Subcortical Cysts (MLC) is a rare genetic disorder characterized by macrocephaly and white matter vacuole formation. The pathogenesis of this disease is suggested to be due to an impaired water and ionic homeostasis by glial cells. MLC disease is caused by mutations in either *MLC1* or *GLIALCAM* genes. They encode for membrane proteins that form a complex in astrocytes, although its exact function is still unclear. GlialCAM has also been reported to act as the auxiliary subunit of the chloride channel ClC-2. In addition, recent studies also identified the G-protein-coupled receptor GPRC5B as an important member of the GlialCAM/MLC1 interactome and relevant to the regulation of related physiological processes. The main objective of this thesis is to determine the role of GPRC5B and signaling events in MLC pathophysiology. We characterized that GPRC5B regulates the expression of a novel GlialCAM/MLC1 interacting protein, Vascular Cell Adhesion Molecule 1 (VCAM-1). Also, we proved that this regulation is dependent on Fyn kinase activity via GPRC5B, and that MLC1 has a negative modulatory effect on this regulation. We also showed that GlialCAM forms oligomeric structures at the plasma membrane of astrocytes via lateral interactions between IgC2 domains from adjacent GlialCAM proteins. Moreover, we propose that mutations in *GLIALCAM* that encode for residues that are located in GlialCAM IgC2 domain are pathogenic because they increase the stability of GlialCAM oligomeric structures. We give evidence that this endocytosis is physiologically mediated by GPRC5B. Furthermore, we show that phosphorylation events are important in the regulation of the activity of chloride channels within GlialCAM/MLC1 interactome. We observed that GPRC5B has a negative modulatory effect on volume-regulated anion channel (VRAC) activity via Fyn. Last, we identified dephosphorylation events in specific Serine residues in ClC-2 as triggers of the described changes in the subcellular localization of the channel, together with altered gating properties, that occur in astrocytes in depolarizing conditions.

TABLE OF FIGURES

ABBREVIATIONS

- AJ: Adherent junctions
- APS: Ammonium Persulfate
- AraC: Cytosine β-D-arabinofuranoside
- BBB: Blood-brain barrier
- BCA: Bicinchoninic acid assay
- Bp: Base pair
- BSA: Bovine serum albumin
- CAM: Cell adhesion molecule
- cDNA: Complementary deoxyribonucleic acid
- CNS: Central nervous system
- CSF: Cerebrospinal fluid
- DAPI: 4',6-diamidino-2-phenylindole
- DCPIB: 4-(2-butyl-6,7-dichloro-2-cyclopentylindan-1-on-5-yl)oxybutyric acid
- DMSO: Dimethyl sulfoxide
- DNA: Deoxyribonucleic acid
- DGC: Dystrophin glycoprotein complex
- ECL: Enhanced chemiluminescence substrate
- E. coli: Escherichia coli
- EDTA: Ethylenediaminetetraacetic acid
- ER: Endoplasmic reticulum
- FBS: Fetal bovine serum
- GFP: Green fluorescent protein
- GABA: γ-Aminobutyric acid
- GPCR: G-protein-coupled receptor
- HRP: Horseradish peroxidase
- i.e.: Id est
- Ig: Immunoglobulin
- ITRs: Inverted terminal repeats
- kDa: kilodalton
- KI: Knock-in
- KO: Knock-out
- LRRC8: Leucine-rich-repeat-containing protein

- MBP: Myelin basic protein
- MOI: Multiplicity of infection
- MRI: Magnetic resonance imaging
- NTPs: Nucleoside triphosphate
- PBS: Phosphate-buffered saline
- PDZ: PSD-95/Zona occludens domain
- PCR: Polymerase chain reaction
- PFA: Paraformaldehyde
- PMSF: Phenylmethylsulfonyl fluoride
- RNase: Ribonuclease
- RNA: Ribonucleic acid
- RT-PCR: Reverse transcription polymerase chain reaction
- RVD: Regulatory volume decrease
- RVI: Regulatory volume increase
- SDS: Sodium dodecyl sulfate
- shRNA: short hairpin RNA
- TAE: Tris-acetate-EDTA buffer
- TEMED: Tetramethylethylenediamine
- TBS: Tris saline buffer
- TJ: Tight junctions
- TTBS: TBS-Tween 20
- VRAC: Volume-regulated anion channel
- VSOAC: Volume-sensitive organic osmolyte anion channel
- WB: Western Blot
- WT: Wild type

INTRODUCTION

The main purpose of this thesis was to gain a better insight into the pathophysiology of Megalencephalic Leukoencephalopathy with Subcortical Cysts by better understanding the physiological role and the regulation of the proteins known to be involved in it. Several former – and future – theses in this lab share this aim. However, this project has focused particularly on the role of GPRC5B on MLC pathogenesis.

We studied the interplay between GPRC5B and VCAM-1 as a recently identified member of the GlialCAM/MLC1 interactome. We continued to tackle the mechanisms underlying pathogenicity of GlialCAM mutations focusing on those located at the GlialCAM IgC2 domain. Finally, we improved our understanding of the role of GPRC5B and signaling pathways on the regulation of chloride channels VRAC and ClC-2.

In this introduction, we first sum up MLC and its main features, both at a clinical and at a genetic-biological level. We present MLC1 and GlialCAM, as well as the known information regarding their role in MLC pathogenesis based on their mutations. We describe the role of astrocytes and chloride channels within them, especially regarding cell volume regulation and potassium buffering since these processes are functionally linked to MLC.

The second part of the introduction is an overview of G-Protein-coupled receptors (GPCRs) and their classification, focusing on orphan receptors GPR37, GPR37L1 and GPRC5 family for their relevance in the CNS.

Last, given the relevance of GlialCAM and VCAM-1 to this work, we also review Cell Adhesion Molecules (CAMs), focusing on their main properties and classification. VCAM-1 will be thoroughly covered in this section.

1. MLC, A LEUKODYSTROPHY

1.1 CNS OVERVIEW

The Central Nervous System (CNS) consists of two basic cell types: neurons and glial cells. Neurons transmit rapid electric signals in form of action potentials (APs). All cells within the CNS that do not possess this ability are considered glia. Neurons form networks of cells and are connected to each other through specialized intercellular adhesion sites known as synapses. In the neuronal signaling process, the AP propagates through the axon of the neuron to the pre-synaptic region of the cell. There, the release of neurotransmitters takes place, and they bind to the receptors displayed at the post-synaptic membrane of a second neuron. This neuron will continue transmitting the electric signal. As for glial cells, they locate around neuronal somas, axons, and synapses across the whole nervous system (NS) (Allen and Barres, 2005).

Glial cells are the most abundant cells in the brain. They are classified according to morphology, functions, and the NS structure around which the glial cell is located. In mammals, glial cells are divided in four types: microglia, astrocytes, ependymal cells and oligodendrocytes (Kettenmann and Verkhratsky, 2011). Microglia are the CNS resident immune cells, and they derive from hematopoietic lineage. Astrocytes are the most abundant cell type; they are big and star-shaped. The classical view on astrocytes considers these cells to be providing trophic and structural support to CNS neurons. Ependymal cells are connected through adherent, gap, and tight junctions. They form the cerebral epithelium, and they are an important part of the blood-brain barrier (BBB). Last, oligodendrocytes show a small soma with long, branched prolongations. Their main role is to produce myelin sheaths to wrap neuronal axons.

Myelin is the specialized plasma membrane of oligodendrocytes. Its configuration consists of concentric layers around the axon. These layers alternate electrodense layers with clear layers. The electrodense layers are consequence of fusion between membranes, and clear areas are due to extracellular matrix fusion. Mature myelin is the laminar structure resulting from all these layers compacted. Every myelin sheath is found around axons divided in segments called internodes. The internodes provide the axons with electrical insulation. Nonetheless, there are areas between internodes that are not wrapped – therefore not insulated. These zones are called Ranvier nodes. Internodal areas are dense ion channels and transporters, which are responsible for regenerating APs at the end of

each internode. This phenomenon by which AP is regenerated 'jumping' from one node to the next one is what we know as saltatory conduction (Huxley and Stämpfli, 1949). It allows for rapid nervous impulse transmission and minimizes its energy expense.

Myelinated axons form the white matter, which takes approximately half the volume of the human brain. Myelination occurs during the first stages in postnatal brain development (Kamholz, 1996). The cells responsible for this process are oligodendrocyte precursor cells (OPCs). During development, OPCs migrate from germinal zones to ensheathe unmyelinated axons. Nonetheless, their maintenance is tightly regulated by astrocytes. Both formation and maintenance of white matter is essential to neuronal network connectivity, which is the basis of brain function (Domingues et al., 2016, Liedtke et al., 1996).

Mutations in myelin-related genes and changes in white matter structure are linked to a wide array of neurologic and psychiatric disorders. Autoimmune diseases can result in myelin damage (i.e. multiple sclerosis). Genetic diseases and environmental-derived disorders can also impair myelin function. Within the genetic diseases that affect myelin we find leukodystrophies.

1.2 Demyelinating Leukodystrophies

Leukodystrophy is the name given to a group of genetic disorders characterized by alterations in the formation, development, or maintenance of white matter in the CNS. The term *leukodystrophy* comes from Greek: *leuko* translates to white, *dys* translates to abnormal, *troph* translates to growth.

Within leukodystrophies we find diverse diseases from a pathological standpoint. Common clinical features are the genetic determination of the illness and white matter affection. Nonetheless, all white matter affections with an inflammatory, autoimmune, or environmental origin are not considered leukodystrophies. In terms of clinical evolution, leukodystrophies are also variable. They can be progressive, lethal, static, or even ameliorate with time.

Leukodystrophy-linked genes are heterogenous. Unsurprisingly, they encode for key components in white matter function and maintenance. The increasing number of identified genes and this heterogeneity lead to changes in the classification of these diseases over time for a better fit with available data. Initially, classification derived from

the pathological feature of white matter defect. Classical classification divided leukodystrophies in four groups: hypomyelinating (deficient myelin production), demyelinating (myelin degradation), dysmyelinating (biochemically and structurally abnormal myelin production), and myelinolytic (vacuolated myelin) (Naidu, 1999).

Recently, Dr Marjo van der Knaap proposed a new classification (Figure 1) that includes defects in astrocytes, neurons, microglia and blood vessels to the existing criteria, based on oligodendrocytes and white matter themselves (van der Knaap and Bugiani, 2017).

- Myelin disorders
  - Hypomyelination
    - a. Pelizaeus-Merzbacher disease [224]
    - b. Peripheral neuropathy, central hypomyelination, Waardenburg-Hirschsprung [36]
    - c. Cx47-related Pelizaeus-Merzbacher-like disease [36]
    - d. Hypomyelination of early myelinated structures [104]
  - Demyelination
    - a. Metachromatic leukodystrophy [214]
    - b. Multiple sulfatase deficiency [214]
    - c. Globoid cell leukodystrophy (Krabbe disease) [214]
    - d. X-linked adrenoleukodystrophy, cerebral from [173]
  - Myelin vacuolization
    - a. Mitochondrial diseases with leukoencephalopathy [159]
    - b. Phenylketonuria [94]
    - c. Canavan disease [91]
    - d. Other selected disorders of amino acid metabolism [2]
    - e. Cx32-related (X-linked) Charcot-Marie-Tooth disease [45]
- Astrocytopathies
  - a. Alexander disease [25]
  - b. Megalencephalic leukoencephalopathy with subcortical cysts [23]
  - c. ClC-2-related disease [45]
  - d. Vanishing white matter [48]
  - e. Aicardi-Goutières syndrome and variants [255]
  - f. Oculodentodigital dysplasia (Cx43) [1]
  - g. Giant axonal neuropathy [135]
- Leuko-axonopathies
  - a. Hypomyelination with atrophy of the basal ganglia and cerebellum [80]
  - b. Hypomyelination with congenital cataract [66]
  - c. Early-onset neuronal degenerative disorders
    - 1. Gangliosidosis GM1 and GM2 [75, 250]
    - 2. Infantile neuronal ceroid lipofuscinosis [79]
    - 3. *AGC1*-related disease [265, 268]
    - 4. *AIMP1*-related diseases [58]
    - 5. *HSPD1*-related disease [134]
  - d. Pol III-related leukodystrophies [269]
  - e. Leukoencephalopathy with brainstem and spinal cord involvement and high lactate [231]
  - f. Hypomyelination with brainstem and spinal cord involvement and leg spasticity [216]
  - g. Giant axonal neuropathy [135]
- Microgliopathies
  - a. *CSF1R*-related disorders [153, 179]
    - 1. Hereditary diffuse leukoencephalopathy with spheroids
    - 2. Pigmentary ortochromatic leukodystrophy
  - b. Nasu-Hakola disease [193]
- Leuko-vasculopathies
  - a. Cerebral AD arteriopathy with subcortical infarcts and leukoencephalopathy [162]
  - b. Cerebral AR arteriopathy with subcortical infarcts and leukoencephalopathy [162]
  - c. Cathepsin A-related arteriopathy with strokes and leukoencephalopathy [31]
  - d. Cerebral amyloid angiopathy [162]
  - e. Leukoencephalopathy with calcifications and cysts [98]

The table is meant to give examples and not to be exhaustive

AD autosomal dominant, *AR* autosomal recessive

Figure 1. A new classification of leukodystrophies. Extracted from van der Knaap and Bugiani, 2017.

1.3 Megalencephalic Leukoencephalopathy with Subcortical Cysts (MLC)

Megalencephalic Leukoencephalopathy with Subcortical Cysts (MLC) is a genetic disorder within the group of vacuolating leukodystrophies. It is a childhood-onset, rare disease. However, its prevalence increases in populations where consanguinity is

common (Topcu et al., 1998). Moreover, such observations were consistent in Agrawal community in East India (Gorospe et al., 2004), Jewish families in Lebanon and Turkey (Ben-Zeev et al., 2002), and many others. Endogamy and consanguinity are important factors in the appearance of rare diseases, both present in a lot of MLC patients.

Clinical criteria are the bases of the diagnosis of the disease, especially by means of Magnetic Resonance Imaging (MRI) (Figure 2):

- Macrocephaly during the first year of life. The extent of macrocephaly is variable, ranging up to 4 to 6 SD above population mean for some patients. From this point, head growth is reduced to normal. The growth curve for head size in MLC individuals continues a parallel evolution
- Motor function slow decline, mild cerebellar ataxia and spasticity. These symptoms typically appear in late-childhood and adolescence. Patients show difficulty walking and postural instability
- Dysarthria
- Epileptic seizures in early stages
- Cognitive impairment. It is mild and late-onset
- Behavioral problems
- Altered MRI scans:
    - Bilateral atrophy and swelling in brain hemispheres. Abnormally diffuse white matter
    - White matter in the corpus callosum, internal capsule and brain stem are better preserved. Subcortical regions and periventricular areas in the occipital brain are also less affected
    - White matter in the cerebellum is not swollen, although signal is lightly abnormal
    - Subcortical cysts in the anterior-temporal brain. Cysts can grow in number and size with time. In some cases, they can expand to the great majority of white matter
    - With the evolution of the disease, cerebral atrophy replaces inflammation in white matter. MRI signal can go back to normality in some individuals
    - Gray matter is unaffected

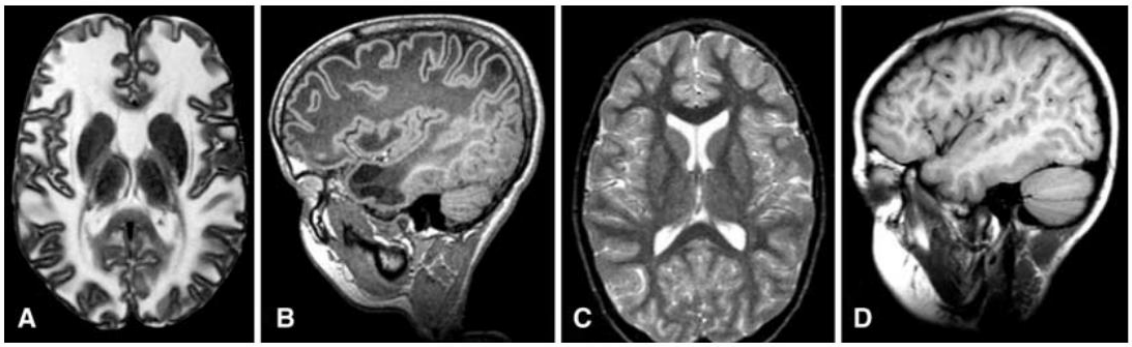

Figure 2. MRI of the brain of an MLC patient. Comparison between an MRI from an MLC patient (**A, B**) and one from a healthy individual (**C, D**). The images observed correspond transverse sections from T2-weighted MRI scans in **A** and **C**, while sagittal views featured in **B** and **D** correspond to T1-weighted MRI scans. Comparing the two transverse sections we observe that white matter in the patient is swollen and shows abnormal diffusion. In sagittal views, we observe subcortical cysts in the anterior-temporal region as well as the parietal subcortical area. Extracted from (Leegwater et al., 2002).

Information about life span for MLC patients is still lacking because the disease is of recent discovery. According to some studies, patients can live up to their forties or fifties (Saijo et al., 2003, Singhal, 2005). However, other individuals die in their teens or twenties. The most dramatic case reported was an MLC patient passing away due to status epilepticus at the age of three (van der Knaap et al., 2003)

Clinical phenotype is also variable severity-wise, even for different patients bearing the same mutation or among relatives (Blattner et al., 2003). This fact implies an influence of environmental factors on the disease clinic.

A study conducted on a group of patients that were displaying differences in MRI brought novel conclusions to MLC field (van der Knaap et al., 2010). During the first years of life, the patients showed MLC symptoms. However, they ameliorated in time. Patients displayed a mild phenotype: macrocephaly during the first years, small cognitive impairment, and difficulty in motor function without ataxia nor spasticity. Epileptic seizures were also present in this subset of patients, although the condition improved with age (López-Hernández et al., 2011a). MRI scans from these patients displaying the benign phenotype are depicted in **Figure 3**.

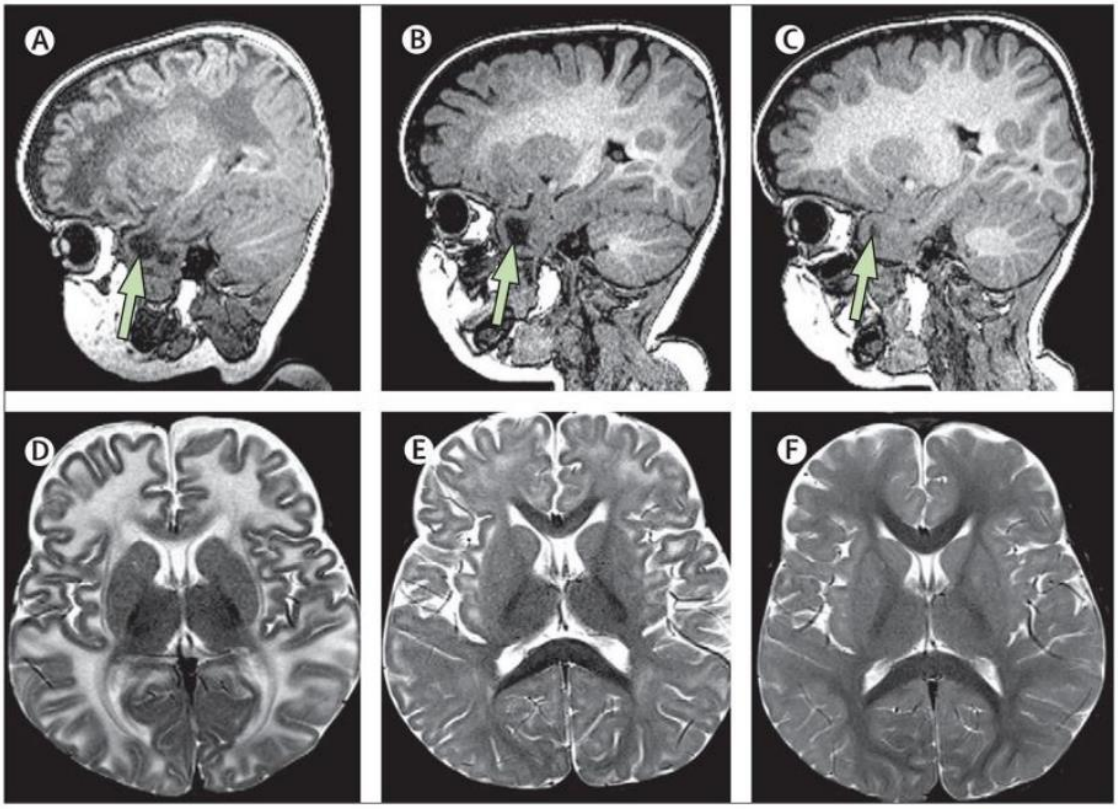

Figure 3. MRI from MLC patients with benign phenotype (MLC2B). Images **A,D** belong to a patient of 9 months of age. **B, E** belong to a patient of 18 months of age. **C, F** belong to a patient of 42 months of age. At the first time point, MRI scans perfectly match the profile of 'classic MLC. The other two patients show improvement in white matter appearance, as well as a decrease in cyst size (arrows). Extracted from (van der Knaap et al., 2012).

Therefore, according to the clinic there are two types of patients within MLC: those who show the 'classical' phenotype, and those who show a remitting phenotype (benign). In more recent cases, some patients suffering 'classical' MLC improved at an MRI level. However, symptom remission did not accompany these improvements (Arnedo et al., 2014a). As will be explained later in this introduction, genetic differences are responsible for these different variants of the disease.

Another key finding in the process of understanding MLC pathology was to determine that the concentration of various osmolytes was smaller in the brain of MLC individuals. This observation, made by proton-magnetic resonance spectroscopy, suggested that water would be accumulating in cerebral tissue (Brockmann et al., 2003, Sener, 2003).

Consistently, histological studies revealed spongiform degeneration of white matter and vacuole formation in outer myelin layers. On the other hand, innermost layers were

unaltered (Figure 4) (van der Knaap et al., 1996). In most cases, a single myelin layer surrounds the vacuole. In spite of that, myelin multilayers can surround these water accumulations. The fact that these vacuoles are observed in outer parts of the myelin could translate into low effects on nervous impulse transmission.

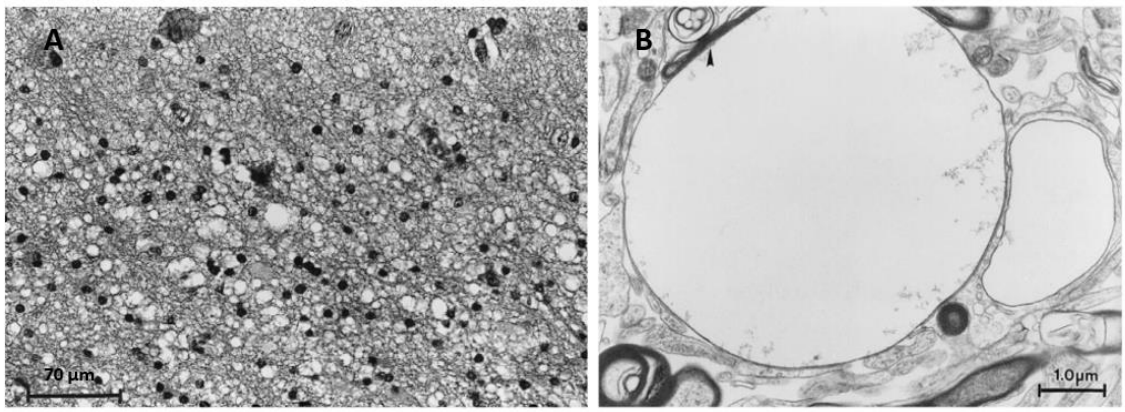

Figure 4. Vacuoles in the white matter of an MLC patient. **A** Hematoxylin-eosin (HE) staining from the neighboring area between neocortex and subcortical white matter. The uppermost quarter of the image shows the neocortex, with a normal histological appearance. Below that border, white matter is dense in vacuoles. **B** Electron microscopy (EM) image of a vacuole from the outer layer of a myelin sheath. This figure is adapted from (van der Knaap et al., 1996).

1.3.1 MLC Genetics. From MLC1 Identification to GlialCAM Discovery

The first gene linked to MLC pathology received the name *MLC1* [MIM604004] (Leegwater et al., 2002). The locus for *MLC1* is 22q13.33. The gene comprises 26 kb and 12 exons, the first of them being non-coding. There are two splice variants currently described (NM_015166.3 and NM_139292.2). They differ in 5' region from the first exon, although they result in the same mRNA that encodes the same MLC1 protein. The literature contains over 100 MLC1 mutant variants linked to the disease. Around 50% of these mutations are missense, 28% are either deletions or insertions, while 22% are splicing mutations. Finally, 1 every 50 mutations is a nonsense variant (Ilja Boor et al., 2006, Cao et al., 2016, Kariminejad et al., 2015, van der Knaap et al., 2012).

Around 76% of MLC patients bear mutations in *MLC1* (Leegwater et al., 2002, Topcu et al., 1998). Their inheritance pattern is autosomal recessive. In addition, only a tiny proportion of cases are due to a *de novo* mutation combined with an inherited mutation. MLC patients bearing mutations in *MLC1* present the classic phenotype. Hence, this variant is known as MLC1. For this variant, there is no genotype-phenotype correlation.

In fact, patients displaying the same mutation can manifest variable disease severity (Leegwater et al., 2002).

Around 22% of MLC patients harbor mutations in a different gene called *GLIALCAM (or HEPACAM)* [MIM611642]. This was the second gene described to be MLC-causing. Its locus is 11q24.2 and it comprises 17 kb, with 7 exons and a non-coding sequence in 3' end. Mutations in *GLIALCAM* originate two distinct phenotypes. The first phenotype is MLC classic phenotype, inherited in an autosomal recessive manner. This disease variant is MLC2A. Most of the mutations responsible for this variant are missense. On the other hand, the second phenotype is the benign phenotype, and it is known as MLC2B (van der Knaap et al., 2010, López-Hernández et al., 2011a). Its inheritance pattern is autosomal dominant and only due to missense mutations (Arnedo et al., 2014a, van der Knaap et al., 2012).

There is a small percentage of MLC patients (2%) that do not display mutations in neither *MLC1* nor *GLIALCAM*. This evidence suggests that a yet to be described third disease-causing gene might exist (Bosch and Estévez, 2020).

1.3.2 MLC1 Protein

1.3.2.1 Generalities, Expression, and Localization Studies of MLC1

MLC1 encodes for an integral transmembrane protein that receives the same name. It has a length of 377 amino acids and its molecular weight is 41 kDa. MLC1 function remains unknown up to date. However, MLC1 orthologs prove that the protein is highly conserved in myelin-producing vertebrate species, including zebrafish (Sirisi et al., 2014).

As was previously hypothesized by previous predictive models, AlphaFold MLC1 structural models (Jumper et al., 2021, Varadi et al., 2022) suggested that MLC1 consists of 8 transmembrane domains (TMD) with both N-terminal and C-terminal regions inside the cell (Boor et al., 2005). Regarding the fold, the model predicted a 4+4 structural repeat, involving transmembrane regions 1-4 and 5-8 (Figure 5**A, B**). This brings up the possibility of *MLC1* gene being a result of a gene duplication. (Estévez et al., 2018). Moreover, a significant number of missense mutations in *MLC1* locate at interfaces between MLC1 repeats (Figure 5**C**). Combined with the observation that these mutations usually lead to protein instability and further degradation (Duarri et al., 2008, Petrini et al., 2013), we hypothesize that proper interaction between MLC1 internal repeats is crucial for the correct folding and ER sorting of the protein (Pla-Casillanis et al., 2022).

Recently, some authors reported homo-trimeric complex in detergent micelles and proteoliposomes (Hwang et al., 2021). This would also suggest that interaction interphases between monomeric subunits would be required for protein stability.

Protein folding is predictive of protein function. In this regard, Figure 5**D** shows that the algorithm PDBeFold reveals similar fold for TMD1-4 to a prokaryotic copper storage protein (PDB ID 6Q6B). This is compatible with the belief of an ion-sensing role for MLC1 (Estévez et al., 2018).

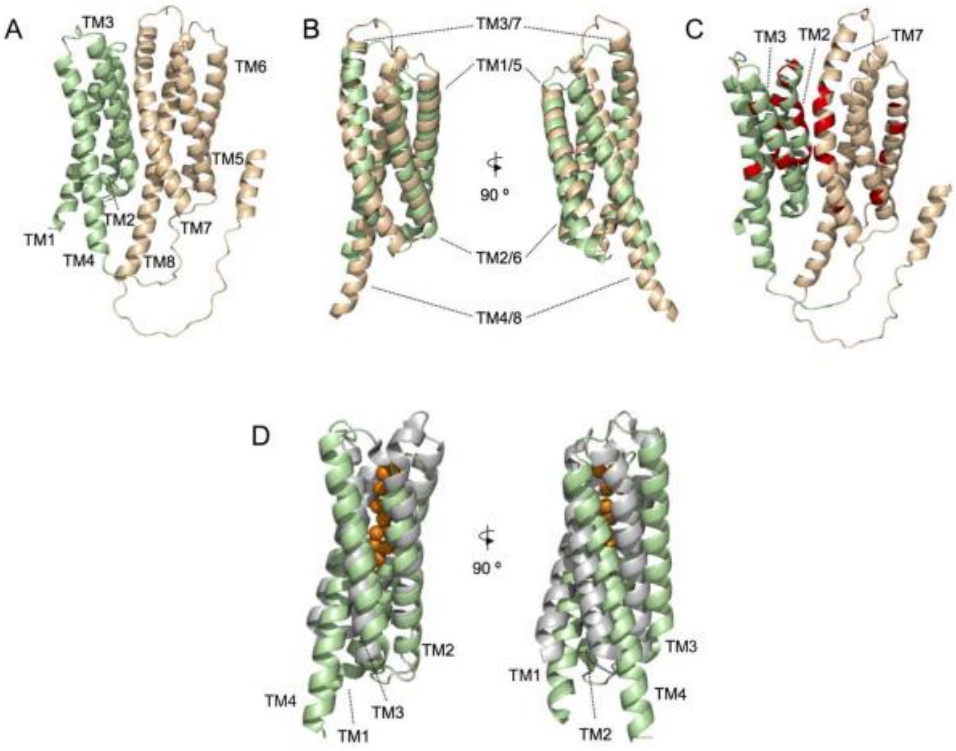

Figure 5. Structural models of MLC1. A Alphafold structural model of monomeric MLC1. TMD1-4 and 5-8 are displayed in pale green and wheat, respectively. **B** Structural superimposition of the two MLC1 subdomains, comprised of TMs 1 to 4 (pale green) and 5 to 8 (wheat), respectively. The image shows two different views, rotated by 90º. **C** Summary of MLC-causing mutations (red) depicted in the MLC1 structural model. Preferential localization of mutated residues is the interaction surface defined by the two MLC1 subdomains (TMD1-4 (pale green) and TMD5-8 (wheat)). **D** Structural superimposition of MLC1 structural model TMD1-4 (pale green) and a prokaryotic soluble copper storage protein from *Streptomyces lividans* (light grey) (PDB ID 6Q6B). Two different views, rotated by 90º, are shown. Adapted from (Pla-Casillanis et al., 2022).

MLC1 protein is mainly expressed in the brain, although it is also present in leukocytes (Boor et al., 2005). Within the brain, we find MLC1 in Bergmann glia and in astrocytes in perivascular, subependymal, and subpial areas. As opposed to what was initially reported, neither oligodendrocytes, microglia nor neurons express MLC1 (Boor et al.,

2005, Schmitt et al., 2003, Teijido et al., 2004). High-resolution EM (immunogold) carried out in both rodent and human samples reveal that MLC1 is located in astrocyte-astrocyte junctions in the perivascular area (**Figure 6B**) (Duarri et al., 2011, Teijido et al., 2007).

To study MLC1 at a biochemical level, primary cultures of astrocytes are the main experimental model. Initial studies in cultured astrocytes indicated that MLC1 was intracellular and co-localized with endoplasmic reticulum (ER) and endosomal markers (Ambrosini et al., 2008). Latter studies showed that treating astrocytes with cell cycle inhibitors such as Cytosine β-D-arabinofuranoside (AraC) lead to MLC1 localizing in the plasma membrane and astrocytic junctions (**Figure 6A**) (Duarri et al., 2011). With this treatment, the model replicated *in vitro* what was observed *in vivo* for MLC1 biochemical behavior. Thus, cell cycle-arrested cultured astrocytes were validated as model to study MLC.

The use of this model allowed to determine that MLC1 protein co-localizes with tight junction components, like ZO-1 and occludin. Such co-localization also exists with adherens junction proteins, like β-catenin and N-cadherin (Duarri et al., 2011). The same pattern was observed between MLC1 and proteins from the dystrophin-associated glycoprotein complex (DGC), also by means of immunoprecipitation. Among other functions, DGC is involved in aquaporin and potassium channels anchoring in astrocytic endfeet at the BBB. In MLC brain tissue, absence of MLC is correlated with altered expression of proteins within DGC. This data indicates that DGC and MLC1 are functionally linked, although this mechanism is not thoroughly unraveled (Ambrosini et al., 2008, Boor et al., 2007). Also, MLC1 expression is not altered in the dystrophin KO mouse model (Duarri et al., 2011).

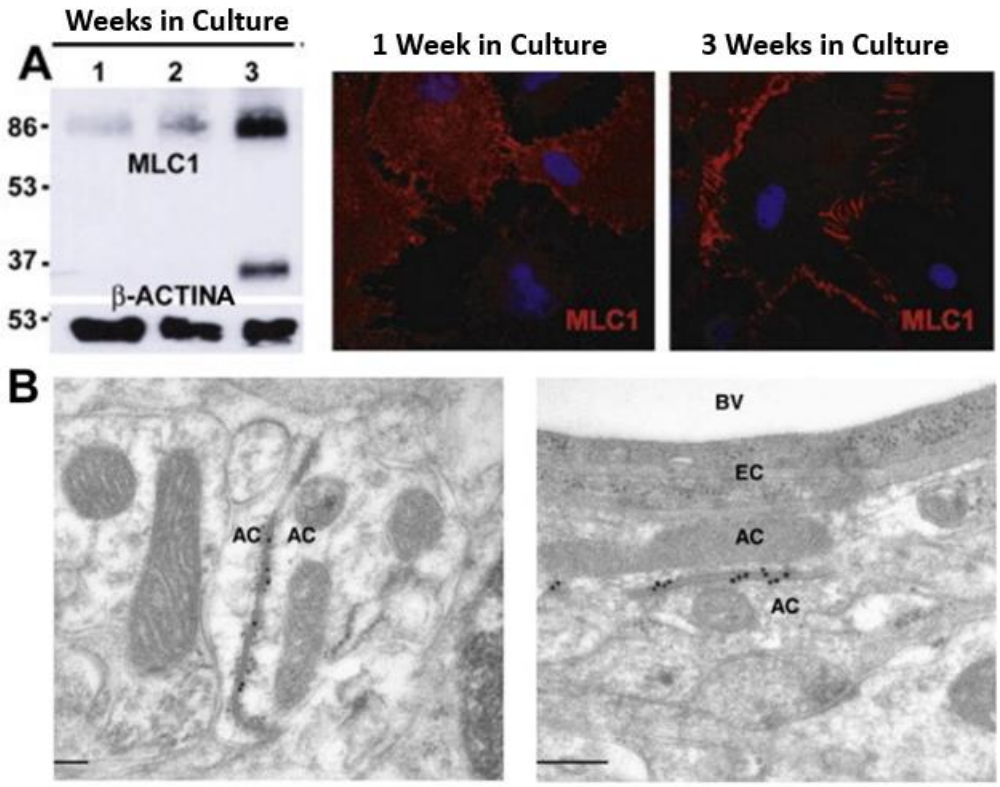

Figure 6. MLC1 localization in primary cultured astrocytes and at a tissular level. A Correlation between MLC1 levels by western blot (*left*) and localization at astrocyte-astrocyte junctions by immunofluorescence assays (*middle, right*). After 3 weeks of treatment with AraC, MLC1 levels gradually increase to reach peak expression. At this moment, the observed phenotype replicates in vivo observations for MLC1 localization. **B** EM images of MLC1 localization at astrocyte-astrocyte junctions, both in astroglial processes (*left*) and perivascular zones (*right*). AC: astrocyte, EC: endothelial cell, BV: blood vessel. Scale bar: 0,25 µm. Image modified from (Teijido et al., 2007).

1.3.2.2 Structure and Function of MLC1 Protein, and Impact of MLC1 Mutations

The structure of MLC1 protein is yet to be resolved up to date. As mentioned in this introduction, from an evolution standpoint it would be reasonable that MLC1 originated from the duplication of a smaller gene encoding a protein with 4 TMDs. A reason to believe that is that fourth and eighth TMD feature a segment rich in polyleucine, while the loop between TMD4 and TMD5 is not conserved in MLC orthologs (unlike the first and second 'half' of the protein). Further experiments supported this hypothesis (Estévez et al., 2018). When MLC1 is split in two halves by this intracellular loop between TMD4 and TMD5, the two splits reach the plasma membrane only when co-expressed in *X. laevis* oocytes. Therefore, the two halves interact and restore function (**Figure 7B**).

More experimental evidence is consistent with the idea of homo-oligomerization for MLC1. When analyzing MLC1 expression by WB, protein bands are detected at

molecular weights around 37 and 72 kDa bands from the protein ladder. These should belong to monomeric and dimeric MLC1 structures. In addition, protein-protein interaction (PPI) Split-TEV assays confirmed MLC1 ability to homo-oligomerize (**Figure 7C**) (Capdevila-Nortes et al., 2012).

Since the identification of MLC1, various studies analyzed the protein at a biochemical level (**Figure 7A**). First, MLC1 displays a putative glycosylation site between TMD3 and TMD4. However, it is not glycosylated in heterologous expression cell systems (Teijido et al., 2004). Second, both N-terminal domain and C-terminal domain are phosphorylated by Protein Kinases A and C (PKA and PKC) at Serin 27. Serin 339 is phosphorylated as well, only by PKC (Lanciotti et al., 2010). Third, the analysis of MLC1 sequence of amino acids reveals an N-terminal putative ER retention motif based on arginine (*RXR*, where *X* is any amino acid). Such analysis also brings up potential unconfirmed phosphorylation sites (Brignone et al., 2015) and a caveolin-binding motif (**Figure 7A**). MLC1 is present in caveolin lipid rafts from rodent-derived astrocytes (Lanciotti et al., 2010).

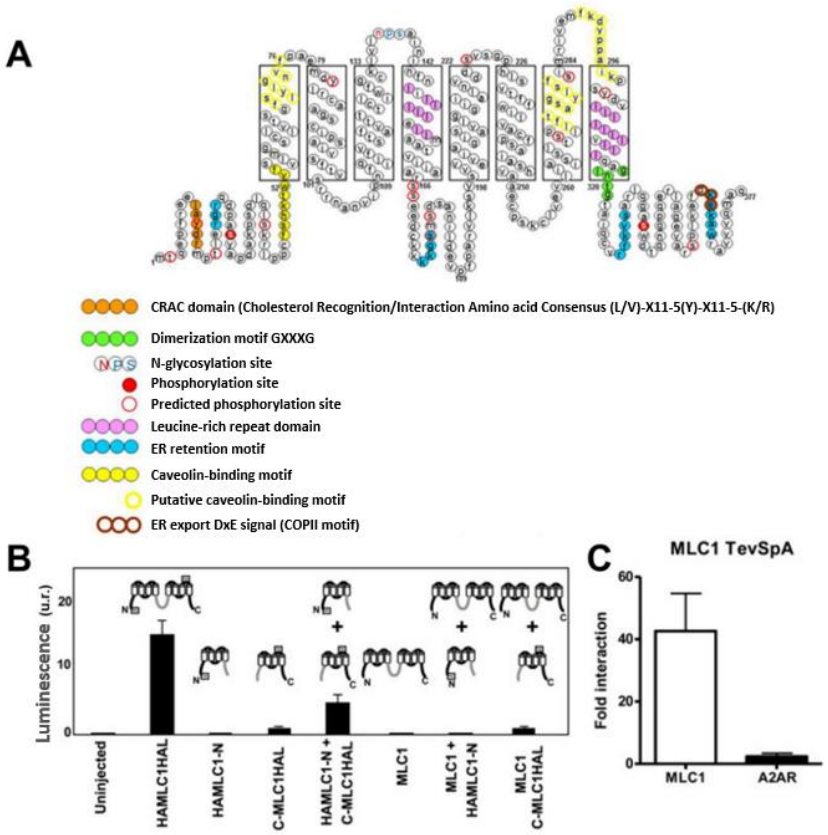

Figure 7. Biochemical properties of MLC1. A Summarized consensus information regarding the main post-translational modifications, domains and motifs described for MLC1. Putative and predictive information is represented with hollow circles, confirmed information is plotted in regular circles. Modified

from (Brignone et al., 2015). **B** Surface expression of MLC1 in X. laevis oocytes. MLC1 was expressed either whole or divided in two equal splits by intracellular loop between TMD4 and TMD5. The two splits are HAMLC1-N and C-MLC1HAL in the graph. We observe that both splits do not reach the plasma membrane by themselves. However, they do so when co-expressed, albeit partially. **C** Split-TEV analysis of MLC1 homo-oligomerization. As we can see, the experiment confirmed this ability using A2AR as a negative control. Modified from (Estévez et al., 2018).

MLC1 mutations are found along the gene (Leegwater et al., 2002). Most missense mutations are responsible for a reduction in protein expression levels that is accompanied by a reduction in membrane surface protein presence (Lanciotti et al., 2010, Montagna et al., 2006, Teijido et al., 2004). The proposed mechanism behind this observation is that the mutation should lead to protein misfolding, resulting in an unstable protein to be degraded either right in the ER or in lysosomes. While some mutated forms of MLC1 can reach plasma membrane, they are targeted for lysosomal degradation either way (Duarri et al., 2008).

Physiological MLC1 localization combined with the classic phenotype of MLC suggest that MLC1 could have a role in ionic and fluid homeostasis (Simard and Nedergaard, 2004). Bioinformatic predictions showed homology between MLC1 and shaker-like voltage-gated potassium channel (Kv1.1), although low in identity (less than 20% of the amino acids) (Teijido et al., 2004). Again, the combination between this finding and the fact that MLC patients develop vacuoles supported the idea of MLC1 being an ion channel, or to work like a transporter linked to water homeostasis. Unfortunately, results from experiments carried out in heterologous expression systems rejected this idea (Teijido et al., 2004).

The study of the physiological role of MLC1 has also used mouse KO model for *Mlc1*. The animals are a good early-stage disease model (**Figure 8**), since they display increased water content in the brain, progressive vacuole formation in the white matter, and morphological changes in perivascular astrocytes right before myelin vacuolation (Dubey et al., 2015, Hoegg-Beiler et al., 2014). In primary cultured astrocytes, lack of MLC1 is also responsible for intracellular vacuoles (Duarri et al., 2011, Sirisi et al., 2014). Such results prompted a reanalysis of patient-derived brain biopsies, which confirmed vacuole formation in perivascular astrocytes (Duarri et al., 2011). Up until that moment, vacuole formation was thought to be limited at outer myelin layers (van der Knaap et al., 1996).

In summary, astrocytic integrity is compromised in MLC patients and such process can be checked histologically.

A recent study reported that *Mlc1*$^{-/-}$ animals manifest spontaneous epileptic activity, with a diminished seizure threshold and altered extracellular potassium dynamics (Dubey et al., 2018). Again, the combination of these results with the vacuolizing phenotype in the white matter of these animals is consistent with the hypothesis of MLC1 being functionally linked to water and ion homeostasis.

In the same regard, primary cultured astrocytes derived from *Mlc1*$^{-/-}$ animals have impairments in volume-regulated anion channel (VRAC) activity and the associated physiological cell volume regulation compensatory mechanism (Regulatory Volume Decrease or RVD). Lack of MLC1 leads to a reduction in VRAC activity, but not total abolishment (Capdevila-Nortes et al., 2013, Dubey et al., 2015). Lymphoblasts from MLC patients with undetectable MLC1 protein levels also show impaired VRAC activity (Petrini et al., 2013, Ridder et al., 2011).

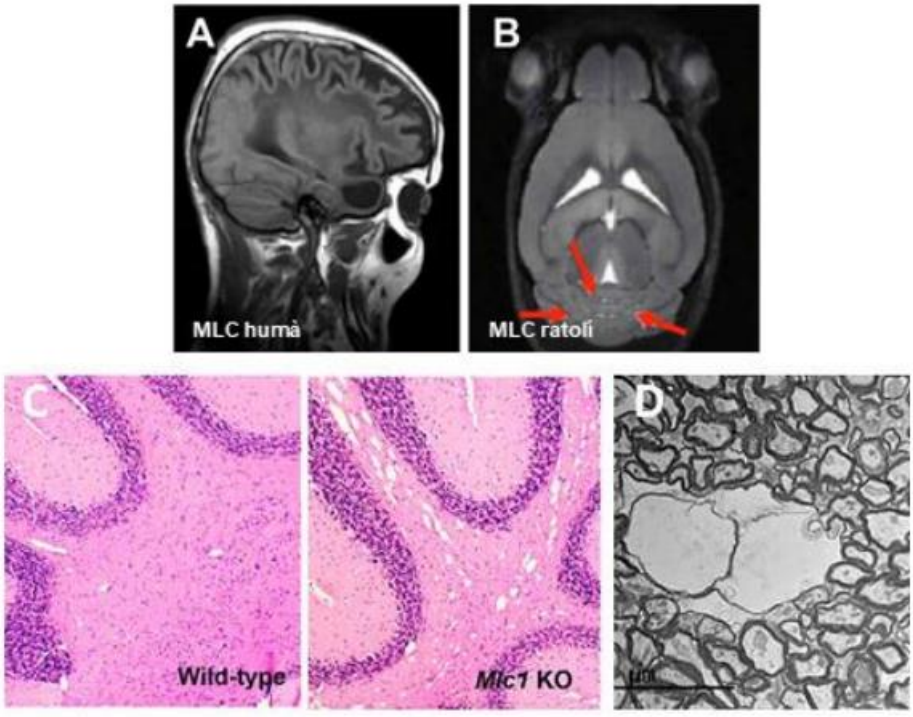

Figure 8. Vacuolizing phenotype in mouse *Mlc1*$^{-/-}$ model replicates human disease. MRIs from an MLC patient (**A**) and a mouse *Mlc1*$^{-/-}$ (**B**), respectively. Red arrows in **B** point at areas with water accumulation. **C** HE stainings on cerebellar white matter from wild-type (WT) (*left*) and *Mlc1*$^{-/-}$ (*right*) samples. Tissue from KO animals shows vacuole formation. **D** EM image from vacuoles in *Mlc1*$^{-/-}$ mice. Modified from (Bosch and Estévez, 2020).

Alternatively, MLC1 overexpression leads to increased VRAC activity in primary cultured astrocytes. VRAC controls chloride efflux and other osmolytes during RVD (Ernest et al., 2005, Pasantes-Morales et al., 2006). This was the first functional alteration described in MLC. However, the interplay between VRAC and MLC1 is yet to be fully understood. Some biochemical studies revealed that MLC1 and LRRC8A (VRAC's main subunit) do not co-localize nor directly interact, suggesting an indirect regulation of channel's activity (Elorza-Vidal et al., 2018).

Other approached used by researchers in this field when tackling potential MLC1 partners or interactors was Membrane Yeast Two-Hybrid (MYTH) and affinity immunoprecipitation. Such studies allowed the identification of Na^+/K^+ ATP-ase (Brignone et al., 2011), Kir4.1, calcium-permeable TRPV4, and V-ATPase (Brignone et al., 2014). This ATP-ase regulates endosomal acidity and it is a vacuolar proton pump. Nonetheless, up to date no experimental evidence proves the direct interaction between these described proteins and MLC1 or GlialCAM.

Last, MLC1 overexpression triggers Epidermal Growth Factor Receptor (EGFR) degradation while inhibits EGF-modulated calcium influx, ERK1/2 activation, phospholipase Cγ1 (PLC γ1) activation, and calcium-activated potassium channel KCa3.1. All these pathways regulate astrocyte proliferation (**Figure 9**) (Lanciotti et al., 2016). Consistently, MLC1 absence in astrocytes leads to increased ERK1/2 phosphorylation (Elorza-Vidal et al., 2018). Taken together, these findings suggest that MLC1 can effectively participate in intracellular signaling pathways.

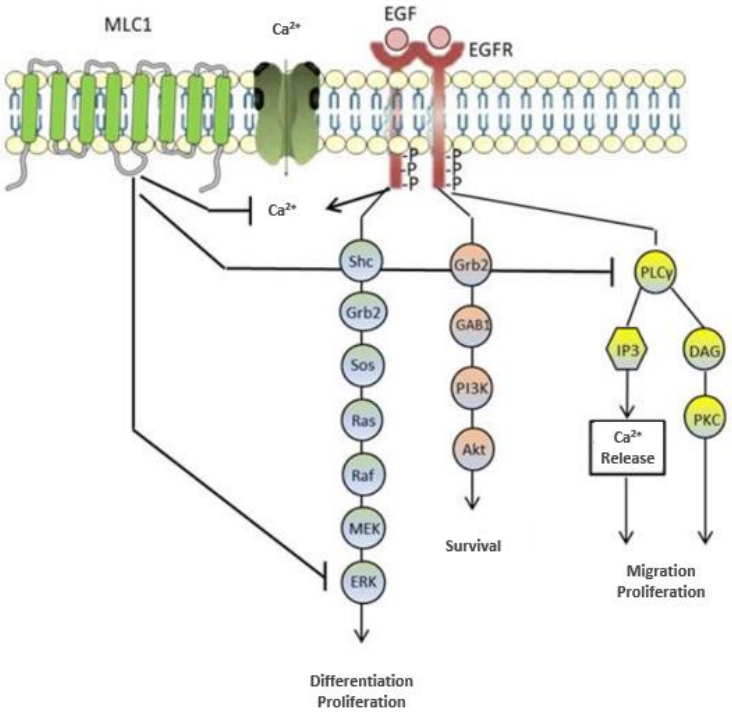

Figure 9. Schematic representation of EGFR-activated signaling pathways on which MLC1 exerts a inhibitory effect in human astrocytoma cells U251. Modified from (Lanciotti et al., 2016).

1.3.3 GlialCAM Protein

1.3.3.1 Generalities, Expression and Localization Of GlialCAM

Human *HEPACAM* gene encodes for a glial and hepatic cell adhesion molecule known as HepaCAM or GlialCAM (as will be referred to in this thesis) (Favre-Kontula et al., 2008, Chung Moh et al., 2005). The protein has a length of 417 amino acids and its molecular weight is around 72 kDa. It was identified as an adhesion cell molecule belonging to Ig Superfamily (Moh et al., 2005).

Biochemical studies predict GlialCAM to be a protein with a single transmembrane segment, two extracellular Immunoglobulin-like loops (IgV in N-terminal end and IgC2 following TMD), and an intracellular C-terminal domain or cytoplasmic tail. In the extracellular domain, GlialCAM features 6 putative N- and O-glycosylation as well as a signal peptide (**Figure 10**) (Gaudry et al., 2008, Chung Moh et al., 2005). In the intracellular region there is a SRC Homology 3 domain (SH3) and various potential phosphorylation sites by serin/threonine kinases and tyrosine kinases (Moh et al., 2005). At the cell surface, it forms cis- homodimers.

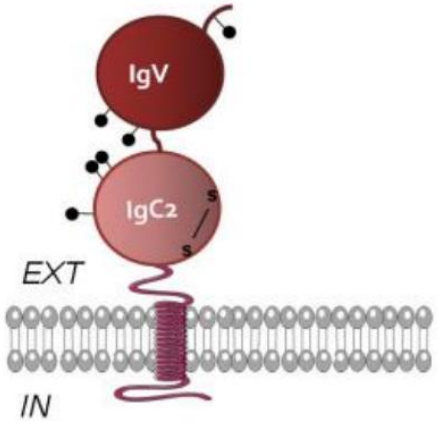

Figure 10. Schematic representation of GlialCAM secondary structure. GlialCAM predicted topology follows the typical Immunoglobulin Superfamily CAM (IgSF CAM) structure. There are two Ig-like domains in the extracellular region (IgV, IgC2), a single transmembrane segment and a cytoplasmic C-terminal tail. Black circles represent putative glycosylation sites. In IgC2 domain, we find a structural disulfide bond. EXT: extracellular region, IN: intracellular region.

The first work to identify GlialCAM believed it to be a tumor suppressor protein. Researchers found that GlialCAM expression levels were lower in hepatocellular carcinoma, while it acted as an antiproliferative agent *in vitro* (Chung Moh et al., 2005). A posterior publication identified GlialCAM cDNA in a library for the human brain. Also, the expression levels were high in the nervous system (Spiegel et al., 2006) in comparison to hepatic levels. In addition, *Glialcam*$^{-/-}$ mice do not show an increase in tumor frequency (Hoegg-Beiler et al., 2014). In the CNS, GlialCAM expression pattern is mostly glia-enriched white matter, ependymal cells in ventricular zones, astrocytic junctions and the astrocyte-blood vessel contact areas (Favre-Kontula et al., 2008). As per cell types, astrocytes and oligodendrocytes are the ones displaying higher expression of GlialCAM. As seen in mice, GlialCAM expression correlates with Myelin Basic Protein (MBP) expression in the developing brain. This clearly suggests that GlialCAM could be involved in the myelination process. Consistent with this idea, GlialCAM is present along different stages of oligodendrocyte differentiation *in vitro*. Similarly, GlialCAM expression levels are higher during the first 3 years of human life. These levels stabilize and begin to slowly decline from around the age of 5 years (Bugiani et al., 2017).

There is co-localization between GlialCAM and MLC1 in astrocytic junctions, as seen by EM on brain slices (Figure 11) (López-Hernández et al., 2011a). The stability of such co-localization depends on the interaction with actin cytoskeleton (Duarri et al., 2011, Chung Moh et al., 2005). Noteworthy, both MLC1 and GlialCAM are functionally linked to

caveolae. Caveolae are special types of lipid rafts involved in the compartmentalization of intracellular signal transduction components, in transport processes, in endocytosis, and in transcytosis (Ambrosini et al., 2008, Lanciotti et al., 2010, Chung Moh et al., 2005, Sowa, 2012).

As for the biochemical behavior of GlialCAM, Split-TEV assays revealed that it homo oligomerizes in *cis*- through the extracellular domain of the protein (López-Hernández et al., 2011b). At the same time, this oligomerization is important for the interaction between the actin cytoskeleton and the cytoplasmic tail of GlialCAM, necessary for the localization of GlialCAM at astrocyte-astrocyte junctions (Capdevila-Nortes et al., 2015). In addition, GlialCAM also shows *trans*- interaction with neighboring GlialCAM molecules from surrounding cells (Capdevila-Nortes et al., 2015, Hoegg-Beiler et al., 2014). However, *in vitro* studies characterizing patient-derived mutations in GlialCAM proved that *cis*- interactions need to be previously established for *trans*- interactions to take place (López-Hernández et al., 2011b).

1.3.3.2 Structure and Function of GlialCAM Protein

GlialCAM as MLC1 β-subunit

Proteomic assays identified MLC1-interacting subunits. These studies used 3 different antibodies against N-terminal end of MLC1 on solubilized membranes obtained from brain tissue. GlialCAM resulted to be the second most abundant protein detected in quantitative Mass Spectrometry (MS) assay, while MLC1 was the first, as expected (López-Hernández et al., 2011a).

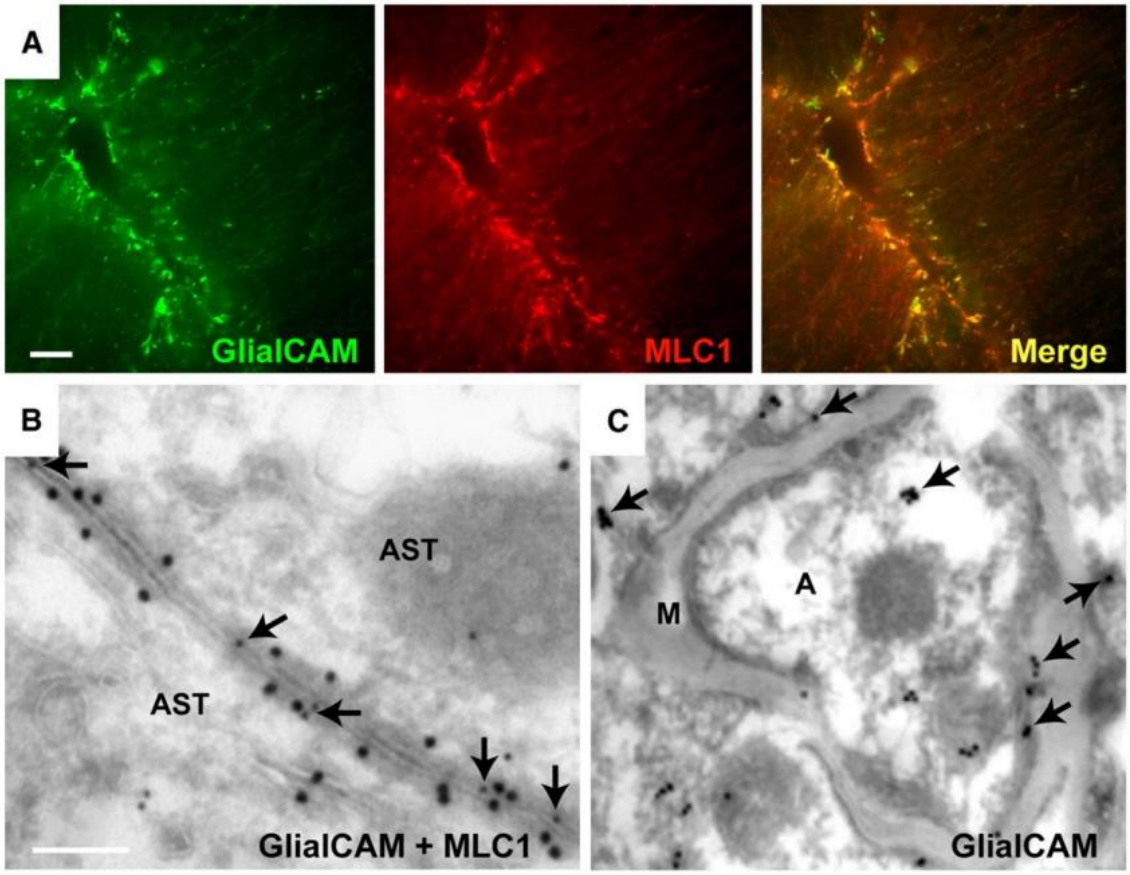

Figure 11. GlialCAM and MLC1 localization studies in brain tissue. A Immunofluorescence assays performed in cerebellum tissue reveal co-localization (yellow, *right*) between GlialCAM (green, *left*) and MLC1 (red, *middle*) at the endfeet of perivascular astrocytes. **B** Double Immunogold EM stainings in human brain tissue confirms co-localization between GlialCAM and MLC1 at astrocyte-astrocyte junctions. **C** Post-embedding Immunogold EM stainings show GlialCAM localization inside the axons, in contact regions between myelin and axons, and in cells surrounding myelin (López-Hernández et al., 2011a).

These findings lead to a thorough characterization of the interaction between MLC1 and GlialCAM. The project started with approaches such as co-immunoprecipitation, Fluorescence Resonance Energy Transfer (FRET), Bioluminescence Resonance Energy Transfer (BRET), and Split-TEV. All of them confirmed direct interaction between the two partners. Further *in vitro* experiments on protein localization in HeLa cells proved that MLC1 shifted its subcellular localization upon co-transfection with GlialCAM, compared to the localization observed when heterologously expressed alone. Specifically, MLC1 moved from ER or being scattered in the plasma membrane to be enriched at cell-cell junctions (**Figure 12**) (López-Hernández et al., 2011a, López-Hernández et al., 2011b).

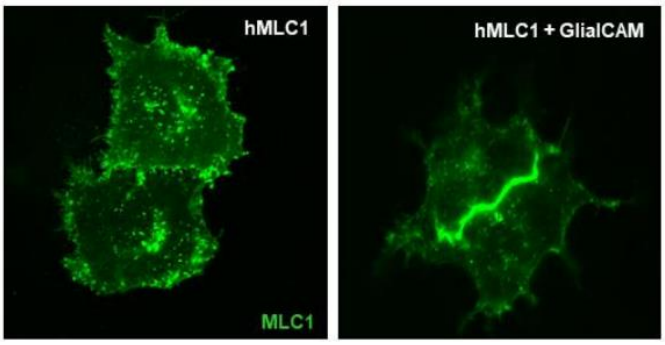

Figure 12. MLC1 subcellular localization in HeLa cells changes upon co-expression with GlialCAM. Immunofluorescence assays reveal that the presence of GlialCAM targets MLC1 to cell-cell junctions (López-Hernández et al., 2011b).

Exact GlialCAM function in glial cells remains obscure. In astrocytes, MLC1 acts as β-subunit of MLC1. This means that MLC1 requires GlialCAM for its proper traffic to cell-cell junctions from the ER (López-Hernández et al., 2011b). That is, GlialCAM acts as a chaperone for MLC1 (Capdevila-Nortes et al., 2013).

Glialcam$^{-/-}$ mice suffer from macrocephaly, elevated water content in the brain, astrocyte cell swelling, and progressive vacuole formation in myelin. Also, in these animals MLC1 expression levels are lower, and MLC1 is mislocalized in Bergmann glia and perivascular astrocytes. This phenotype is further evidence of GlialCAM's role as chaperone for MLC1. Also, it is very similar as the phenotype observed in *Mlc1*$^{-/-}$ animals (Bugiani et al., 2017, Hoegg-Beiler et al., 2014).

MLC1 also exerts an effect on GlialCAM. While proper expression and apparent subcellular location of GlialCAM are independent of MLC1 when the protein is expressed *in vitro*, MLC1 increases the frequency of GlialCAM enrichment at cell-cell junctions. This suggests MLC1 could be involved in the correct enriched localization of GlialCAM at cell-cell junctions (López-Hernández et al., 2011b). In primary cultured astrocytes derived from *Mlc1*$^{-/-}$ animals there is no defect in GlialCAM localization when the cells are cultured in physiological conditions. However, GlialCAM is internalized upon culture in depolarizing conditions (potassium-enriched medium). Moreover, the absence of MLC1 leads to GlialCAM mislocalization *in vivo*, especially in Bergmann glia and perivascular astrocytes (Dubey et al., 2015, Hoegg-Beiler et al., 2014). Thus, both *in vitro* and *in vivo* behaviors for GlialCAM in the absence of MLC1 are consistent. Last, studies in zebrafish model for absence of mlc1 also show mislocalization for GlialCAM (Sirisi

et al., 2014). Thus, MLC1 and GlialCAM cooperate for a mutual correct protein expression and localization.

GlialCAM as ClC-2 auxiliary subunit

The fact that GlialCAM is expressed in cell types where MLC1 is absent (i.e. astrocytes) suggests GlialCAM might have additional properties and functions independent of MLC1. Further proteomic and immunoprecipitation assays on solubilized mouse brain membranes identified allowed the identification of a third highly abundant protein: chloride channel ClC-2 (Barrallo-Gimeno et al., 2015, Jeworutzki et al., 2012).

This channel is ubiquitous across cell types. In the human brain, it is detectable in neurons, astrocytes, and oligodendrocytes (Jeworutzki et al., 2012). ClC-2 and GlialCAM are expressed at the same time in both astrocytes and oligodendrocytes, while MLC1 is only expressed in astrocytes.

PPI experiments like Split-TEV and co-immunoprecipitation validated the direct interaction between GlialCAM and MLC1. Immunofluorescence assays in HeLa cells determined that ClC-2 is only present at cell-cell junctions upon co-expression with GlialCAM, as was the case for MLC1 (**Figure 13A**). Interestingly, GlialCAM induces modifications in the biophysical properties of ClC-2. GlialCAM increases current amplitude, and it alters ClC-2 rectification properties. Thus, ClC-2 is open also at positive membrane potentials when GlialCAM is present (**Figure 13B**) (Jeworutzki et al., 2012). In this regard, the first three amino acids in the transmembrane segment of GlialCAM (Serin, Leucin and Tyrosine residues) are essential for ClC-2 electrophysiological activity but they do not participate in ClC-2 trafficking to cell-cell junctions (Capdevila-Nortes et al., 2015).

Since ClC-2 expression pattern is wider than GlialCAM expression pattern, GlialCAM would be an auxiliary subunit for ClC-2 instead of being an obligatory subunit. The latter would be the case for MLC1.

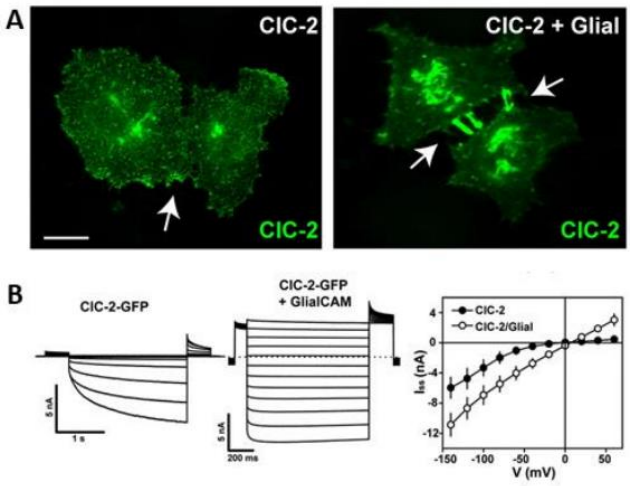

Figure 13. GlialCAM-mediated changes in ClC-2 localization and function. A Immunofluorescence assays in HeLa cells that exemplify the differences in enrichment at cell-cell junctions that ClC-2 (*green*) undergoes upon co-expression with GlialCAM. In the image from the left, ClC-2 signal is diffuse and scattered across the plasma membrane. In the image from the right, ClC-2 is enriched at cell-cell junctions (López-Hernández et al., 2011b). **B** Electrophysiological recordings of ClC-2 activity with or without GlialCAM in the system. Biophysical properties of the channel change with GlialCAM presence: rectification disappears with GlialCAM, and the channel is open at positive voltages (Ohmic channel). *Right* I-V curve. Modified from (Jeworutzki et al., 2012).

On the other hand, ClC-2 and MLC1 co-expression does not affect ClC-2 functional properties (López-Hernández et al., 2011a). Nonetheless, co-immunoprecipitation experiments and Proximity Ligation Assays (PLA) suggest that MLC1 is necessary for the interaction between GlialCAM and ClC-2 to happen. In fact, a recent work by our research group demonstrates that MLC1, GlialCAM and ClC-2 form a ternary complex under depolarizing conditions (**Figure 14**) (Sirisi et al., 2017). This observation was made in primary cultured astrocytes incubated with potassium-enriched culture medium. At a physiological level, the formation of MLC1/GlialCAM complex induces ClC-2 trafficking to cell-cell junctions and the forementioned changes in its electrical properties, thus allowing a chloride influx that balances potassium accumulation. The mechanism by which ClC-2 associates with MLC1/GlialCAM is not clear up to date, although it is dependent on L-type calcium channels and calcium-dependent calpains (Sirisi et al., 2017).

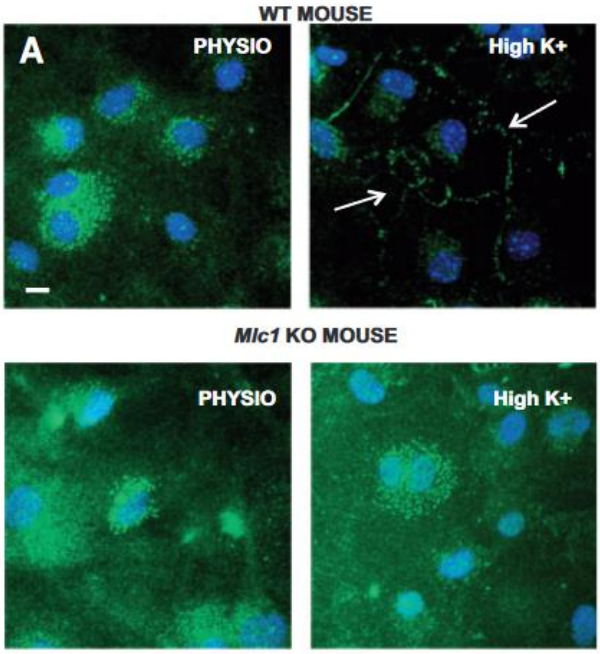

Figure 14. Depolarization induces ClC-2 trafficking to cell-cell junctions in WT mouse primary cultured astrocytes, but not in Mlc1$^{-/-}$ -derived astrocytes. The figure shows immunofluorescence assays in wild-type primary cultured astrocytes and in *Mlc1*$^{-/-}$-derived astrocytes, incubated with both physiological and potassium-enriched solutions (Depolarizing, high K^+, 60 mM) for 6 hours. Arrows point at ClC-2 (green) at cell-cell junctions, which only happens upon potassium-enriched incubation in WT cells. Scale bar: 20 µM. Extracted from (Sirisi et al., 2017).

In both *Mlc1*$^{-/-}$ and *Glialcam*$^{-/-}$ animals, ClC-2 is mislocalized in Bergmann glia, perivascular astrocytes, and oligodendrocytes (Bugiani et al., 2017, Hoegg-Beiler et al., 2014). The fact that ClC-2 is not properly localized in oligodendrocytes in *Mlc1*$^{-/-}$ suggests that MLC1/GlialCAM could be regulating ClC-2 activity in these cells through interaction with astrocytes (Hoegg-Beiler et al., 2014).

1.3.3.3 Mutations in *GLIALCAM* Gene

MLC patients bearing recessive mutations in *GLIALCAM* lose MLC1 function and develop the same phenotype as patients bearing recessive mutations in MLC1. Similarities are both at the MRI level and at the clinical level. On the contrary, heterozygous dominant mutations in *GLIALCAM* lead to benign phenotype. These patients develop symptoms of the disease but they ameliorate, potentially resulting in remission of white matter alterations (van der Knaap et al., 2010, López-Hernández et al., 2011b).

All missense mutations in *GLIALCAM* from MLC patients affect GlialCAM extracellular region. The only exception is mutation W263X, which introduces a stop codon at the transmembrane segment. Within the extracellular region, dominant mutations are present in IgV domain only, while recessive mutations can be found anywhere from the extracellular region (**Figure 15A**).

Unlike mutations in *MLC1*, most *GLIALCAM* missense mutations do not compromise protein expression. Their effect is in homo-oligomerization in *cis*-, and in localization at cell-cell junctions (**Figure 15B**) (López-Hernández et al., 2011b).

Such is the case for *GLIALCAM* dominant mutations. However, in this group there are some exceptions. Mutation D128N leads to proper homo oligomerization but the protein does not enrich at cell-cell junctions. Mutation K135Del does not lead to apparent effects. Another property of these mutations is that they are not able to target either MLC1 or ClC-2 to cell-cell junctions, although interaction by these proteins with GlialCAM is not affected (Arnedo et al., 2014b, López-Hernández et al., 2011b).

Some of the recessive mutations also lead to the same biochemical behavior. Other mutations (R73W, P148S, S196Y, D211N) do not display any of the defects (Arnedo et al., 2014a, Arnedo et al., 2014b, López-Hernández et al., 2011b). Moreover, any of these mutations alters GlialCAM effect on ClC-2 biophysical properties.

Later, studies performed by researchers in our group identified that some of these mutant GlialCAM proteins (K135Del, S196Y, D211N) are resistant to depolarization-induced internalization in primary cultured astrocytes derived from *Mlc1*$^{-/-}$ animals. While incubation with potassium-enriched medium leads to GlialCAM WT internalization in these astrocytes, the mutant proteins stay enriched at cell-cell junctions (Sirisi et al., 2014).

Also, while GlialCAM is necessary for correct MLC1 expression and protein levels (Jeworutzki et al., 2012, López-Hernández et al., 2011b, López-Hernández et al., 2011a), overexpression of either dominant or recessive MLC-causing GlialCAM mutations is sufficient for proper MLC1 expression levels. However, MLC1 is not targeted to cell-cell junctions and VRAC activity is altered (Capdevila-Nortes et al., 2013). Therefore, the problem with these mutations is at a functional level.

Finally, biochemical studies indicate that localization defects in recessive GlialCAM mutant variants are rescued by WT protein. This defect is not solved in dominant mutations (Elorza-Vidal et al., 2020, López-Hernández et al., 2011a). The generation of a *knock-in* (KI) mouse model for *Glialcam* bearing an MLC-causing dominant mutation allowed to confirm these findings in an *in vivo* model, since heterozygous mice also developed a phenotype (Hoegg-Beiler et al., 2014). A recent work published by our research group showed that the reason why some disease-causing GlialCAM mutations are dominant is that they are located at GlialCAM IgV domain interacting surfaces and disrupt either *cis*- or *trans*- interactions necessary for proper protein function (Elorza-Vidal et al., 2020).

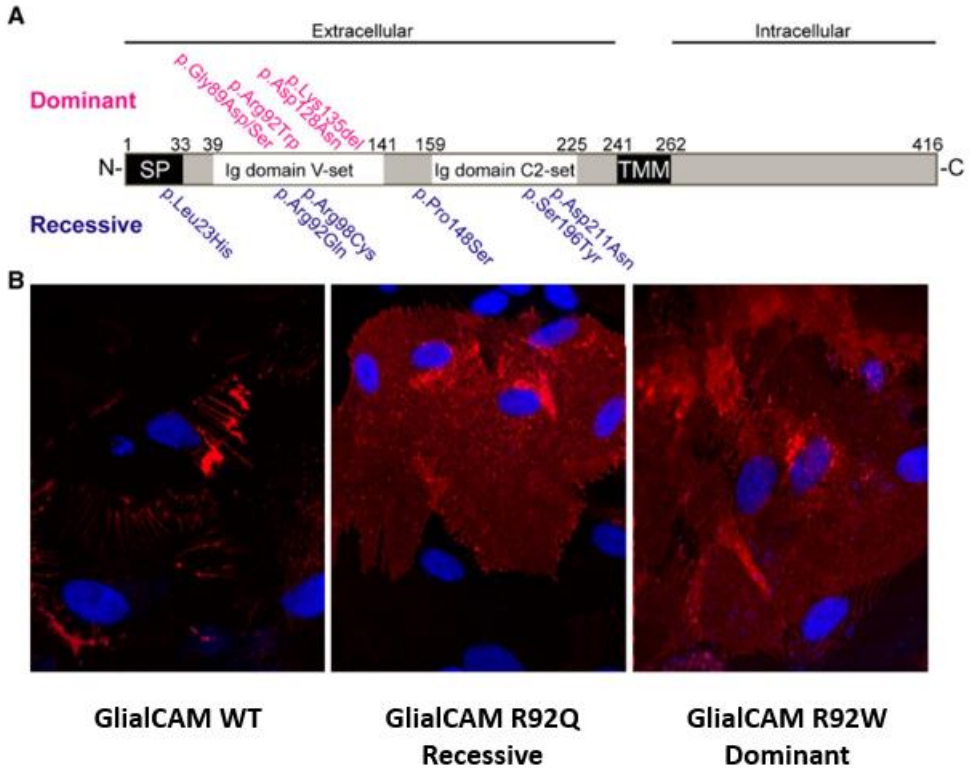

Figure 15. GlialCAM mutations affect protein localization. A Schematic representation of missense mutations identified for *GLIALCAM*, sorted by the domain in which the encoded residue is found upon protein folding. Dominant mutations are written in pink, recessive mutations are written in blue. SP: signal peptide, TMM: transmembrane segment. **B** IF assays in cultured astrocytes heterologously expressing the WT (*left*), a recessive mutant (R92Q, *middle*), or a dominant mutant (R92W, *right*). GlialCAM (red) is mislocalized in both cases when compared to the WT protein. Figure modified from (López-Hernández et al., 2011a).

1.3.4 Chloride Channels in MLC Pathogenesis

1.3.4.1 Astrocyte Generalities: Morphology and Function

As already mentioned in the first chapter of this introduction, astrocytes are the most abundant cell type in the brain, while they are essential for the proper function of the nervous system. The first description of glial cells by Camillo Golgi and Michael von Lenhossek already estimated that astrocytes account for almost 50% of brain volume.

Astrocytes are distributed across gray and white matter. Their morphology is highly complex, since they display a star-shaped morphology and present multiple ramifications **Figure 16**. Also, these cells show polarization in two domains, both highly ramified. One reaches neighbouring neurons and the other one extends to contact blood vessels (Benarroch, 2005, Lundgaard et al., 2014, Nedergaard et al., 2003). One the one hand, astrocytes can contact several neuronal soma and hundreds of dendrites from different neurons (Benarroch, 2005, Theodosis et al., 2008). On the other hand, astrocytes also contact with 90% of the cerebral vasculature through astrocytic endfeet. The characteristic cytoskeletal component of astrocytes is the glial fibrillary acidic protein (GFAP), which is a filament protein (Bignami et al., 1972, Bovolenta et al., 1984, Kimelberg, 2004).

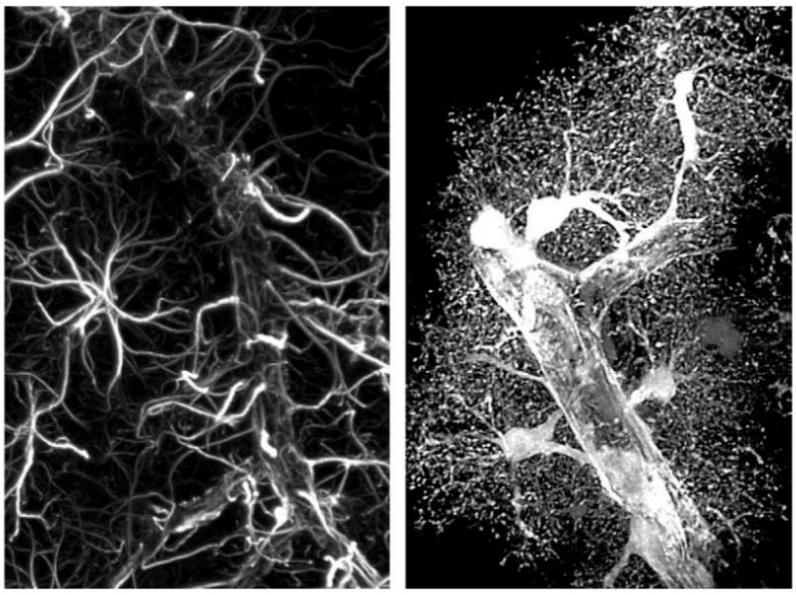

Figure 16. Astrocyte morphology. Stainings of rat cortex using GFAP as astrocytic markers (right) or with over-expression of eGFP in a group of astrocytes. Extracted from (Simard and Nedergaard, 2004).

According to morphology, there are two populations of astrocytes. The first population is protoplasmatic astrocytes, mostly present in grey matter. These cells exhibit branches and prolongations around the cell body. From a developmental standpoint, they belong to radial glia lineage. The second population is fibrous astrocytes, which are mainly localized along myelinated fibre tracts in the white matter forming long fibre-like processes. These astrocytes, in turn, arise from progenitor cells of the subventricular zone (Molofsky et al., 2012, Nash et al., 2011, Wang and Bordey, 2008).

However, there is high heterogeneity within each population of astrocyte. The anatomical environment of each cell and the specific developmental origin seem to be responsible for that (Hewett, 2009, Wang and Bordey, 2008). Moreover, it is important to note that the great majority of data and observations published on astrocyte physiology and morphology come from studies on rodents. Structural and phylogenetic analyses on human astrocytes indicate that some properties could be different. Morphologically, human astrocytes would be bigger and more complex. Also, the cells would have unique gene profiling (Dossi et al., 2018, Lundgaard et al., 2014, Vasile et al., 2017).

Although they are a heterogenous cell type, astrocytes share numerous cellular characteristics. All of them are scarce in organelles in the cytoplasm, they display specific astrocytic filaments, their nuclei are irregular, and contain elevated expression of K^+ channels at the cell membrane. This last feature leads to slight leakage of K^+, which is responsible for the distinctive low membrane resistance of astrocytes (Mori and Leblond, 1969, Peters, 2007, Zhou et al., 2009).

Astrocyte heterogeneity directly translates into a wide array of roles linked to these cells. A lot of physiological processes and functions involved in brain homeostasis are due to the action of astrocytes. First, they modulate neurotransmitter-based excitatory signals. Second, they protect neurons from oxidative stress. Third, they participate in the regulation of stem cell proliferation as well as axonal migration. Fourth, they contribute to maintain BBB. In addition, they control energetic metabolism through the coupling of blood flow to neuronal needs by increasing availability of oxygen and glucose (Abbott et al., 2006, Howarth, 2014, Iadecola and Nedergaard, 2007). Also, they are responsible for glymphatic flow. This process consists in the exchange of soluble substrates between cerebrospinal fluid (CSF) and interstitial fluid in the brain. It is aimed at the clearance of solutes through veins, mainly taking place during sleep. (Iliff and Nedergaard, 2013, Iliff et al., 2012, Xie et al., 2013). Furthermore, astrocytes control synaptic activity by

uptaking released K^+ and neurotransmitters (i.e. glutamate) during neuronal activity. This property is needed for the facilitation of fast repetitive neurotransmission, especially in Bergmann Glia. Last, astrocytes are involved in regulating cell volume, pH, and the buffering of extracellular K^+ (Benarroch, 2005, Blackburn et al., 2009, Oberheim et al., 2006).

Another suggested role for astrocytes is their involvement in myelin formation and maintenance. Through astrocyte-oligodendrocyte coupling, astrocytes would be providing metabolic support and homeostatic control necessary to create a proper environment for myelination to occur (Barnett and Linington, 2013, Lundgaard et al., 2014).

Next in this introduction, we will review astrocytic mechanisms of volume regulation and K^+ buffering, which are essential for proper glial homeostasis. Specifically, we will focus on the role of ClC-2 and VRAC chloride channels.

1.3.4.2 Regulation of Astrocytic Cell Volume

The human cranium is a vessel with limited space available. For this reason, regulation of cell volume changes is crucial: an expanded brain results in compression of the blood vessels. This can induce hypoxia or ischemia, which compromise neuronal survival. A physiological adaptation that astrocytes feature is their high permeability to water, which is provided by the presence of aquaporin channels (AQPs) in the membrane, specifically AQP4. AQPs are water channels mainly found in astrocytic endfeet. Since they are passive transporters, they allow bi-directional water exchange between blood vessels and brain cells (Amiry-Moghaddam et al., 2003a). Events such as nutrient transport, neurotransmitter release, protein degradation, or vesicular secretion, lead to changes in osmolyte concentration. These changes elicit water movements to maintain osmotic equilibrium. In consequence, there are changes in cellular volume. Hence, reduction of osmolytes in the extracellular medium induces hypoosmotic swelling. At the same time, increases in extracellular osmolyte concentration induce cell shrinkage.

All cell types activate physiological mechanisms to regulate cellular volume in response to osmotic changes. These processes are named RVD or RVI. As opposed to RVD, Regulatory Volume Increase (RVI) is the mechanism in charge of increasing cell volume after hyperosmotic cell shrinkage. Several ionic co-transporters such as the $Na^+/K^+/Cl^-$ NKCC1, Na^+/H^+ and Cl^-/HCO_3-exchangers, as well as amino acid transporters mediate

this process (Jayakumar and Norenberg, 2010, Jayakumar et al., 2011, Larsen et al., 2014). On the other hand, Regulatory Volume Decrease (RVD) restores cell volume after hypoosmotic swelling by mobilizing osmolyte ($Na^+/K^+/Cl^-$ ions amino acids and amines mainly) and water release from the cell (Benfenati and Ferroni, 2010, Kimelberg, 2004, Kimelberg et al., 2006, Pasantes-Morales et al., 2006, Pasantes-Morales and Vázquez-Juárez, 2012).

Focusing on RVD, we know that this process is triggered by cellular swelling after a hypoosmotic shock. This induces water entry at the astrocyte through AQP4 aimed at balancing intracellular and extracellular osmotic concentrations (Mola et al., 2016). The cell usually detects this increased volume because it causes a raise of intracellular Ca^{2+} levels, as well as changes in the cytoskeleton. These signals would be initiated by proteins like Transient Receptor Protein Channels (TRPC), tyrosine-kinase receptors (TKRs) or GPCRs (Benfenati and Ferroni, 2010, Malarkey et al., 2008, Pasantes-Morales et al., 2006).

The non-selective calcium channel Transient Receptor Potential cation channel subfamily V member 4 (TRPV4), also known as Transient Receptor Potential Vanilloid 4, is another protein thought to be key in the detection of changes in astrocytic volume (Benfenati et al., 2007, Benfenati et al., 2011, Liu et al., 2006). Elevations of cytosolic Ca^{2+} concentration mediates RVD in astrocytes (McCarty and O'Neil, 1992). Such elevations lead to IKca channel activation, which induces K+ and Cl+ efflux. In turn, this KCl efflux is one of the main events in RVD (Mola et al., 2016). In addition, a functional link between TRPV4 and AQP4 is suggested. TRPV4 can mediate AQP4 expression in astrocytes (Lafrenaye and Simard, 2019), while TRPV4 inhibition reduces brain oedema (Jie et al., 2015, Ryskamp et al., 2015). Calcium entry through TRPV4 would be behind this gene expression regulation (Jo et al., 2015). Unfortunately, the mechanism underlying this interaction is controversial. It is not clear whether TRPV4 or AQP4 would be the main RVD trigger. However, it has been proved that TRPV4 and AQP4 co-express in astrocytic plasma membrane, while deficits of both proteins decelerate cell shrinkage (Chmelova et al., 2019). A proposed mechanism would be that TRPV4 and AQP4 form a complex in astrocytic endfeet surrounding blood vessels, coupling water entry and osmotic stress to signalling cascades that mediate RVD responses (Benfenati and Ferroni, 2010, Benfenati et al., 2011). A recent study found that TRPV4 activation is independent

of osmolality-associated AQP4 permeability, which would oppose to the discussed mechanisms (Wang and Parpura, 2018).

In this regard, increases in intracellular Ca^{2+} induce the activation of Bestrophin 1, a Ca^{2+}-activated chloride channel. It is not hypoosmotic swelling but rather increases in intracellular Ca^{2+} that directly regulate it. Nonetheless, while this channel modulates cell volume in the fly (Stotz and Clapham, 2012), in mammals its physiological role is more related to glial tonic release of GABA (Lee et al., 2010, Oh and Lee, 2017).

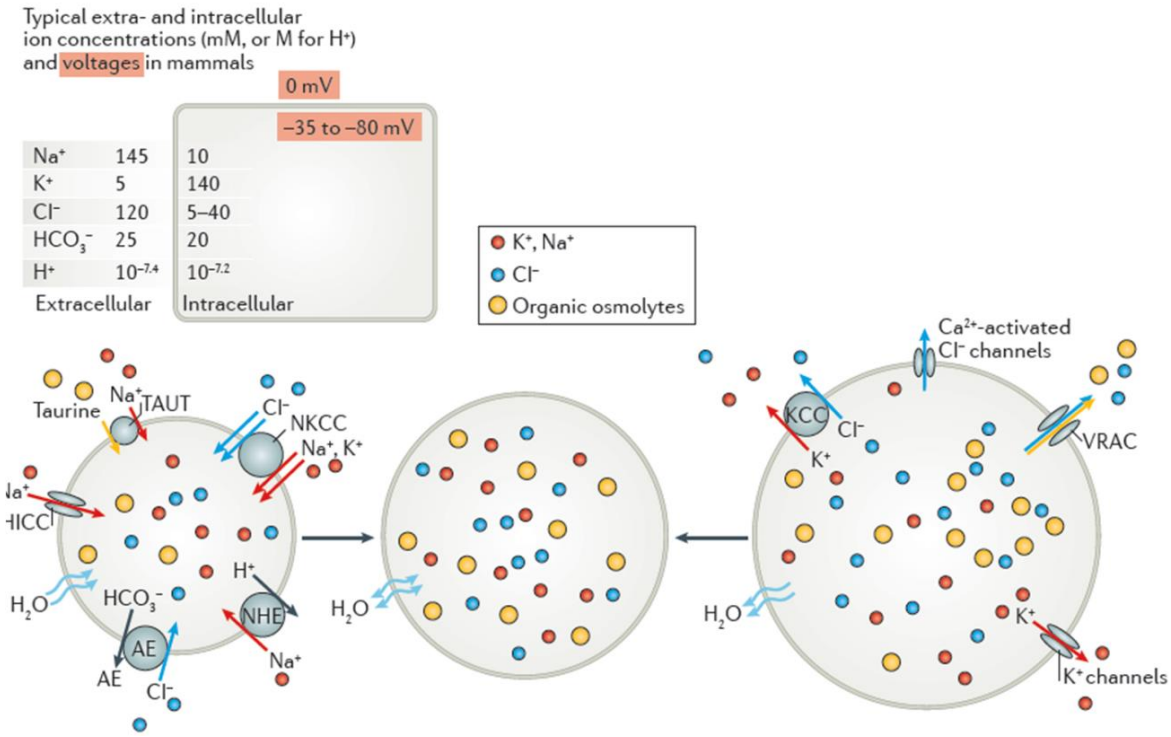

Figure 17. Summary of cell volume regulation processes. The figure features a schematic representation of RVI (*left* and RVD (*right*). In RVI we find activation of Na^+/H^+ exchangers, anion exchangers, and Na-K-Cl (NKCC) cotransporters. This leads to increased intracellular levels of Na^+ and Cl^-, that are followed by swelling of shrunken cells until volume restoration by water flow through AQP4 to recover osmotic balance. The opposite effect takes place in RVD. By a similar mechanism, swollen cells recover their volume after the release of K^+, Cl^- and organic osmolytes like taurine. K^+/Cl^- (KCC) cotransporters but especially VRAC/LRRC8 channels are key players in the transport of ion and organic osmolytes outside the cell. In addition, cell swelling can induce a rise in intracellular Ca^{2+} concentration, in which case Cl^- may also exit through various Ca^{2+}-activated Cl^- channels. Cl^- exit must be electrically balanced by K^+ efflux, which can occur through a range of constitutively open or swelling-activated K^+ channels. Inset: typical extra- and intracellular concentrations of ions involved in mammalian volume regulation. From (Jentsch, 2016).

In summary (**Figure 17**), cells regulate their volume by adjusting the levels of intracellular osmolytes (mainly Cl^-, K^+, Na^+ ions and small organic molecules). Different ion channels and transporters activate upon cell swelling to release those osmolytes at the

extracellular medium. This osmolyte efflux is coupled to water exit through AQP4, which restores cell volume. Among the channels involved in this activity, we find ClC chloride channels, VRAC or VSOAC channels, and K^+ channels like Kir4.1 (Benfenati and Ferroni, 2010; Kimelberg et al., 1990, 2006; Pasantes-Morales et al., 2006).

1.3.4.2.1 The VRAC channel: LRRC8 heteromers

As just reviewed, the volume regulated anion channel (VRAC) is a ubiquitously expressed ion channel activated in response to cell swelling. Thus, it is crucial for cell volume regulation. VRAC activity is one of the main players in RVD because it drives the efflux of Cl^-, along with several other anions. In astrocytes, as well as in other CNS cells, VRAC activity is essential for KCl release. In turn, this release is the basis of the process of RVD. The ion accumulated in astrocytes usually is K^+ that results from neuronal activity and nervous impulse transmission. However, astrocytic negative membrane potential restricts direct K^+ efflux unless a previous anion release occurs. This is accomplished by Cl^- efflux, mostly mediated by VRAC.

The first swelling-activated chloride currents identified belonged to the activity of VRAC or VSOAC (Volume sensitive organic osmolyte anion channel). From an electrophysiological standpoint, the currents displayed similarities in their properties regardless of the cell type of identification (Hoffmann et al., 2009, Jentsch, 2016, Nilius et al., 1997, Strange et al., 1996). These common properties are activation by cell swelling, moderate outward rectification, intermediate conductance, and time-dependent inactivation at high positive potentials. Moreover, a property of VRAC is its permeability to small molecules such as amino acids, glutamate, or taurine. Nonetheless, it is mostly defined by its selectivity to anionic molecules in the following order: $SCN^- > I^- > NO_3^- > Br^- > Cl^- > F^- > HCO_3^-$ > gluconate (Akita and Okada, 2014, Jentsch, 2016, Nilius and Droogmans, 2003).

Among other physiological functions, published data links VRAC to transepithelial ion transport, cell proliferation, cell migration, apoptosis, and release of bioactive molecules. Specifically speaking of astrocytes, impairments of the role of VRAC in the control of astrocyte volume are behind several pathologies. Some examples are traumatic brain injury, stroke, hyponatremia, hyperammonaemia, or epilepsy (Akita and Okada, 2014, Kimelberg et al., 1990, Kimelberg et al., 2006, Mongin, 2016). Interestingly, the astrocytic cell compartments that undergo the most dramatic swelling are processes in contact with blood vessels (Kimelberg, 2005). An interesting finding was that even if

VRAC activation is a protective mechanism from cellular oedema, excessive VRAC activation may also be detrimental for brain integrity through the release of excitotoxic glutamate and aspartate. *In vivo*, blocking VRAC in animal models of stroke protected against brain injury (Akita and Okada, 2014, Kimelberg, 2005, Liu et al., 2006).

Less is known about the role of VRAC when brain homeostasis is stable. Some studies claim VRAC involvement in astrocytic control of hypothalamic neuroendocrine structures. Also, some believe that the release of glutamate and taurine by VRAC contributes to astrocyte-neuron communication. Another possibility is that VRAC is susceptible of being activated upon intracellular signals even in the absence of astrocytic swelling. For instance, a mechanism could involve GPCR signaling through Ca^{2+} or cAMP as secondary messengers. Such process takes place in other cell types, ending in the release of glutamate or other gliotransmitters (Bourque and Oliet, 1997, Crépel et al., 1998, Mongin, 2016).

For years, VRAC activity was known but its molecular identity remained unresolved. The first postulated candidates featured P-glycoprotein, ClC-2, ClC-3, Bestrophin 1, pI_{cl}, among others. Eventually, all of them proved wrong (Strange et al., 1996, Pedersen et al., 2015). It was not until recently that the work of two independent groups determined that the essential component of VRAC is the protein called Leucine-Rich Repeat-Containing 8 A (LRRC8A) (Qiu et al., 2014, Voss et al., 2014). These works described that VRAC consisted of a heteromeric complex of LRRC8 proteins, where LRRC8A isoform is the essential subunit for channel formation. Up to date, there are reports of five members of LRRC8 proteins in chordate organisms, named from A to E (Abascal and Zardoya, 2012, Sawada et al., 2003). These proteins present four TMDs and a cytoplasmic leucine-rich repeats domain (LRRD) featuring 17 Leucine-Rich Repeats (LRRs) at the C-terminus. As seen in **Figure 18**, this LRR domains forms a bended structure that exposes a large surface area, which would be mediating protein-protein interactions (Kajander et al., 2006). Last, sequence alignment studies for LRRC8 suggest a common origin and structure similarities with pannexin proteins, which participate in the formation of gap-junctions (Abascal and Zardoya, 2012).

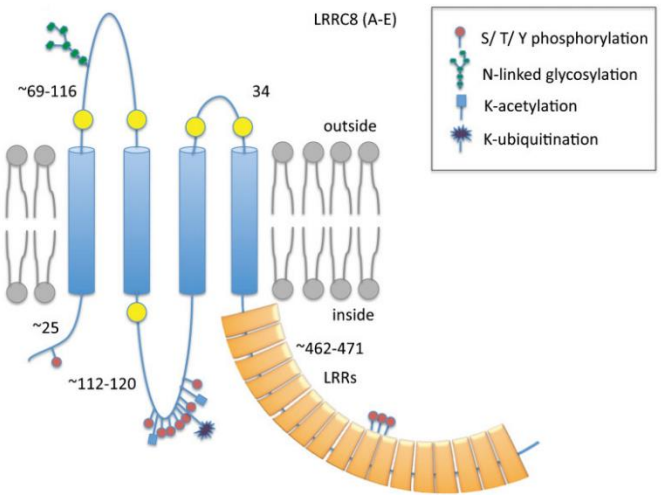

Figure 18. Schematic representation of LRRC8 topology and general features. In the figure, yellow spheres indicate conserved cysteines. Other post-translational modifications are K-ubiquitination, K-acetylation, N-linked glycosylation, and phosphorylation (*legend*). In the cytoplasmic domain, each of the 17 leucine-rich repeats correspond to an orange box. Extracted from (Abascal and Zardoya, 2012).

Mutations in *LRRC8A* gene cause congenital agammaglobulinemia and lack of B cells (Sawada et al., 2003). Alternatively, the *Lrrc8a*$^{-/-}$ mouse model displays a similar defect but in T cell development and function. These animals displayed pre- and postnatal mortality along with several tissue abnormalities (Kumar et al., 2014) (**Figure 19A**). The fact that VRAC is ubiquitous and its relevance in homeostasis maintenance might explain the observed phenotype. LRRC8A and D proteins are indeed ubiquitous, whereas the rest of LRRC8 proteins show a more restrictive expression pattern. LRRC8B is enriched in CNS cells, in lymphocytes, and in monocytes during peripheral stimulation. On the other hand, LRRC8C expression is restricted to immune cells (Abascal and Zardoya, 2012).

The stoichiometry of heteromeric LRRC8 complexes forming VRAC is likely to consist of six subunits (hexameric complexes). The authors that identified VRAC molecular identity found that although LRRC8A is the essential subunit, at least one accessory B or E subunit is needed for to elicit VRAC currents (Voss et al., 2014). Various recent studies point out that different LRRC8 complexes composition-wise may mediate distinct and specific VRAC activities while showing substrate specificities. For instance, LRRC8D subunit seems necessary for channel resistance to Pt-based antitumor drugs (Planells-Cases et al., 2015). LRRC8E would be primarily involved in the transport of negatively charged molecules like aspartate, while LRRC8D appears to allow the transport of molecules in a charge-independent manner. Thus, it would allow the transport of electrically neutral molecules (taurine, GABA, or myo-inositol), negatively charged

aspartate, partially positive compounds like cisplatin, and even positive compounds like lysine (Lutter et al., 2017).

Heteromeric complexes of three or more VRAC subunits is also suggested by some authors (Jentsch, 2016, Lutter et al., 2017).

In astrocytes, LRRC8 A-D genes express at different levels. LRRC8A expression is necessary for glutamate and taurine release in primary cultured astrocytes (Hyzinski-García et al., 2014) (**Figure 19B**). Also, LRRC8A or LRRC8D deletion leads to the suppression of uncharged osmolytes efflux. At the same time, release of charged osmolytes is dependent of either LRRC8A or LRRC8C+LRRC8E, while it would be independent of LRRC8D (Schober et al., 2017).

Last, it is important to highlight the technical difficulties of studying LRRC8/VRAC. First, heterologous overexpression of LRRC8A *in vitro* reduces endogenous VRAC currents rather than increasing them. Moreover, overexpression of LRRC8 paralogs does not achieve increases in VRAC current densities. Therefore, such studies require a heterologous system with total LRRC8A ablation where only heterologously expressed LRRC8A protein is in the system. In fact, an ideal experimental model would be a system with all LRRC8 subunits eliminated. Such would be the perfect background for overexpression studies of different channel combinations, aimed at further understanding VRAC stoichiometry and its impact in VRAC function (Jentsch, 2016, Mongin, 2016, Voss et al., 2014). In our group, we study VRAC using *X. laevis* oocytes as the experimental system. They are interesting because they do not show endogenous VRAC activity except for a low background LRRC8A current that can be neglected. This characteristic makes these cells suitable for heterologous expression of LRRC8 proteins. Moreover, we discovered that fluorescent tags fused at the C-terminal domain of LRRC8 proteins increased the total current amplitude measured for the channel without altering its intrinsic properties. In summary, these features make for a robust experimental model to study VRAC *in vitro* (Gaitán-Peñas et al., 2016).

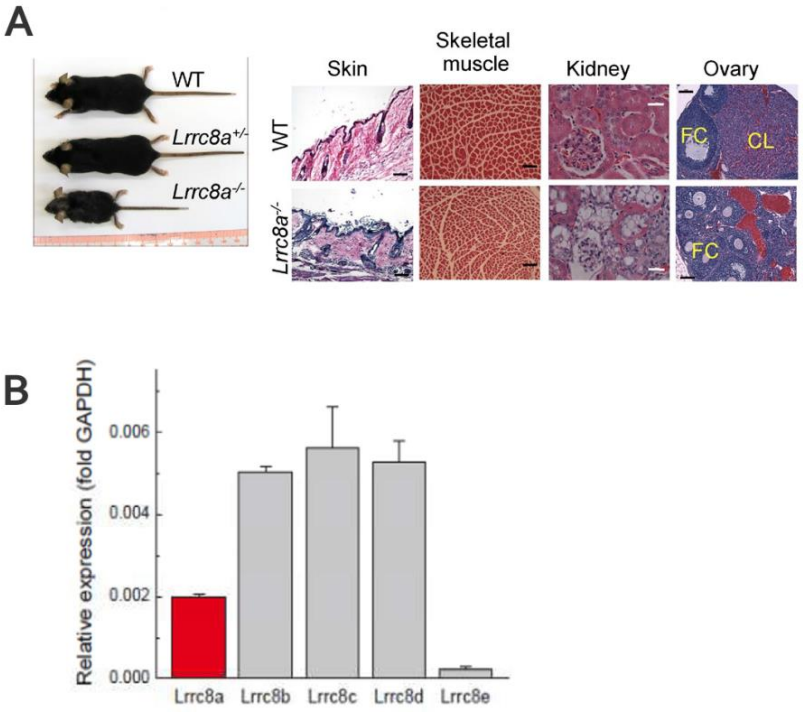

Figure 19. LRRC8 proteins in mammalian tissue. A Macroscopic phenotype of *Lrrc8a*$^{-/-}$ mice. KO animals are smaller in terms of body size than WT animals (*left*). HE stainings (*right*) show tissue abnormalities in the same KO animals. Skin, skeletal muscle, ovary and kidney are affected. Extracted from (Kumar et al., 2014). **B** mRNA expression levels for the different LRRC8 subunits in primary rat astrocytes. Lrrc8b-d are more than twice the expression of Lrrc8a. Lrrc8e show the lesser mRNA expression among all subunits. Extracted from (Hyzinski-García et al., 2014).

1.3.4.3 Potassium Spatial Buffering and Formation of Glial Networks

Physiological neuronal activity results in big, rapid changes in extracellular K^+ concentration. This increase is due to the low volume of extracellular space in the human CNS (Kume-Kick et al., 2002, Nicholson and Syková, 1998). Basal extracellular K^+ concentration is stable around 3 mM. Upon neuronal activity, this value spikes at 10-12 mM due to K^+ release by neurons (Connors et al., 1982, Gutnick et al., 1979, Heinemann and Lux, 1977). Importantly, K^+ changes can impact a wide variety of physiological processes within neurons, like membrane potential, synaptic transmission, or activation of voltage gated channels. Therefore, buffering these changes in extracellular K^+ concentration is key to maintain cerebral homeostasis. When these mechanisms do not work properly, extracellular K^+ concentration can reach values as high as 60 mM. These levels are pathological (i.e. spreading depression or anoxia), since they compromise CNS function (Somjen, 2002, Vyskocil et al., 1972).

Hence, these K+ fluctuations need to be rapidly counteracted by various physiological mechanisms. That includes passive diffusion and active transport of K^+. At a cellular level, K^+ buffering occurs via glial or neuronal uptake of K^+ ions through these specific channels or transporters. In general, however, mechanisms of K^+ buffering are classified into either mechanisms involved in K^+ direct uptake or mechanisms responsible for K^+ spatial buffering.

The latter of the two is the best characterized mechanism for K^+ clearance in the brain, also known as potassium siphoning in classical studies in Müller glia (Kofuji et al., 2000, Newman, 1985, Newman and Reichenbach, 1996). It consists in the dispersion of local high extracellular K^+ concentrations to areas with low concentration, thanks to the formation of a glial syncytium (Kofuji and Newman, 2004, Rash, 2010). Specifically, astrocytes are the glial cell most directly involved in this syncytium formation. They are connected through gap junctions, thus leading to the formation of a K^+-permeable network across which ions circulate in order to be redistributed. This allows the restoration of physiological concentrations in the extracellular compartment, maintaining them compatible with neuronal activity (Benfenati and Ferroni, 2010, Clausen, 1992, Cotrina et al., 1998).

The inwardly rectifying K^+ channel Kir4.1 is the main modulator of K^+ redistribution from perineural areas to perivascular zones. Since its astrocytic expression is high, it is responsible for most of K^+ conductance in this cell type (Butt and Kalsi, 2006, Olsen et al., 2006). Other cell types that express this channel are oligodendrocytes, Bergmann glia, and Müller glia. Kir4.1 allows bidirectional movement of K^+ depending on transmembrane gradient (Higashi et al., 2001, Kalsi et al., 2004). Aside of Kir4.1, other channels involved in K^+ uptake are rSlo and Kv1.5 (Price et al., 2002, Roy et al., 1996). All of them participate in this buffering of K^+ to the areas with low concentration. Noteworthy, it is astrocytic endfeet that present specific high conductance for potassium. Consistently, high K^+ fluxes have been recorded at the endfeet following neuronal activity (Newman, 1984, Orkand et al., 1966). Such elicited currents correspond to K^+ finally being released into blood stream.

The other group of K^+ clearance mechanisms is direct astrocytic uptake. Mainly, NKCC1 cotransporter or the Na^+/K^+ ATPase pump can mediate this process (D'Ambrosio et al., 2002, Larsen et al., 2014, Wang et al., 2012). Net entry of cations requires either anion influx (i.e. Cl^-) or efflux of other cations (i.e. Na^+) to preserve electroneutrality. This

cotransport is active in astrocytes in response to high extracellular K^+ concentrations (Hertz et al., 2000, Tas et al., 1989). This Cl^- entry may be via NKCC1 or through specific Cl^- channels. It has been suggested that spatial buffering combines with an approximately equimolar KCl transport (Dietzel et al., 1989).

Since glial uptake of K^+ reduces extracellular osmolarity and increases intracellular osmolarity, there must be an accompanying water influx to glial cells. As previously reviewed, there appears to be co-expression of the water channel AQP4 with Kir4.1 at the astrocyte endfeet. The hypothesis is that both proteins would cooperate to facilitate these water movements. AQP4 may also be modulating extracellular space volume homeostasis after neuronal activity (Haj-Yasein et al., 2012, Nagelhus et al., 2004). If that were true, glial cells would be able to activate osmoregulatory processes to compensate osmotic resulting of water movements. In this regard, one study linked water permeability and AQP4 function regulation to intracellular cAMP-dependent signaling in a context of high extracellular K^+ concentration (Song and Gunnarson, 2012).

In addition, both Kir4.1 and AQP4 colocalize with syntrophin, a protein within the dystrophin glycoprotein complex (DGC) (Amiry-Moghaddam et al., 2003b, Benfenati and Ferroni, 2010). DGC would be anchoring AQP4, since *Syntrophin*$^{-/-}$ mice lose AQP4 localization at perivascular astrocytic endfeet. Also, the animals have problems in K^+ clearance (Amiry-Moghaddam et al., 2003b). Nonetheless, Kir4.1 is unaffected in these knockout animals. This could imply that Kir4.1 does not interact functionally with AQP4 in the process of potassium clearance and the associated water movement (Zhang and Verkman, 2008). This does not exclude that Kir4.1 is essential for efficient uptake of K^+ by glial cells, regardless of the lack of functional involvement with AQP4 in this process (Chever et al., 2010).

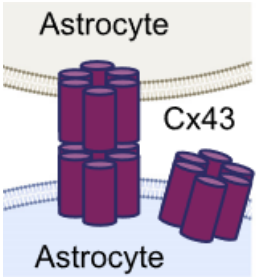

Figure 20. Connexin 43 forms Gap junctions in astrocytes. Connexin 43 forms hemichannels, which interact to establish Gap junctions. Extracted from (Baldwin et al., 2021).

Last, other essential elements in the process of K^+ siphoning are connexins. These proteins constitute the gap junctions that connect the astro-glial network for ionic transport. Connexins (Cx) are membrane proteins that form complexes of 6 connexin subunits, which are the hemichannels. These complexes can be either homomeric or heteromeric. Two hemichannels (one of each adjacent cell) align and establish a gap junction (Figure 20**).** These gap junctions are permeable to ions and facilitate substrate fluxes (Abrams and Scherer, 2012, Nualart-Marti et al., 2013). Astrocytes express mainly Cx43, also Cx30 and Cx26 (Nagy et al., 2004). The Cx43/Cx30 double knockout mouse model was where the role of gap junctions in K^+ buffering was discovered. These animals present vacuole formation in myelin structures, similar to the phenotype that *Kir4.1*$^{-/-}$ mice develop (Menichella et al., 2006, Wallraff et al., 2006). Interestingly, AQP4 suppression in astrocytes decreases Cx43 expression and impairs cell-cell functional coupling (Nicchia et al., 2005).

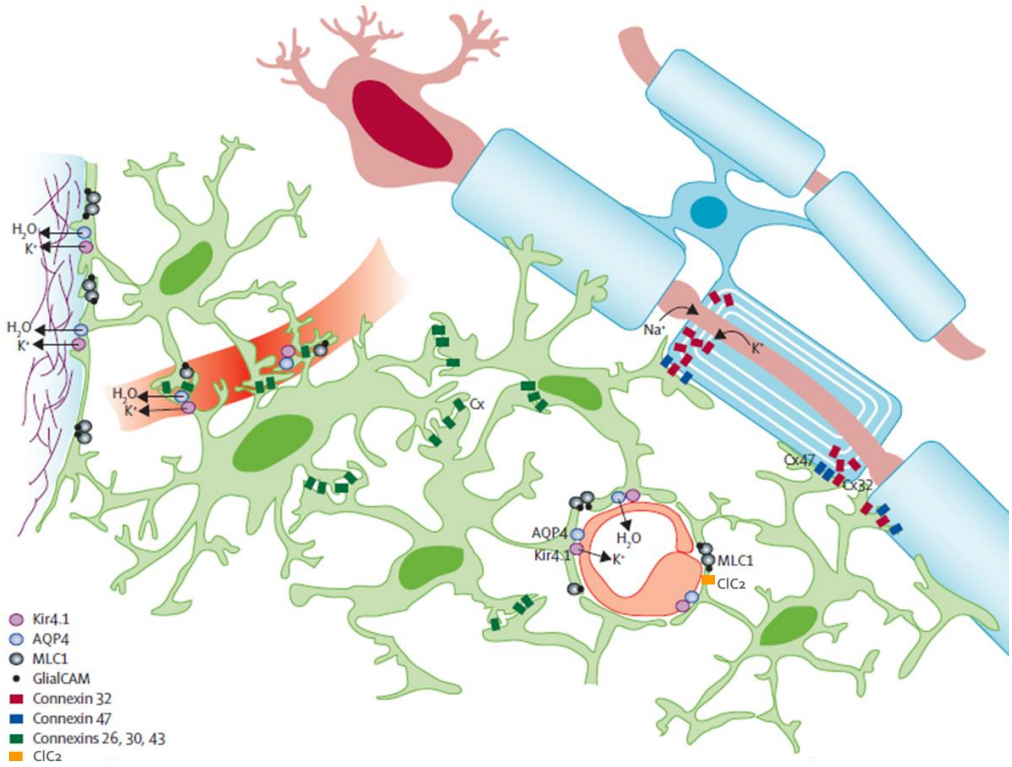

Figure 21. Schematic representation of the panglial **syncytium.** As seen in the figure, Na^+ enters the axon at Ranvier nodes, while K^+ exits at the paranodal axonal plasma membrane. In the myelin sheath, Cx32 forms gap junctions that drive K^+ out through the different layers and towards astrocytes surrounding myelin. Cx32 and Cx47 form the gap junctions that communicate outer myelin with astrocytes. There, K^+ circulates across the astrocytic network through gap junctions consisting of Cx43 pores. Ions reach the astrocytic endfeet and they transfer to pericapillary and subpial spaces through Kir4.1, accompanied by water efflux through AQP4. MLC1/GlialCAM complexes and ClC-2 are also featured in the scheme. Adapted from (van der Knaap et al., 2012).

Classically, the term used to refer to the functional network of astrocytes for potassium buffering is panglial syncytium (Figure 21). This network consists of the astrocytes and oligodendrocytes connected via gap junctions, which extend from spinal cord and ventricles to the vascular epithelia (Nedergaard et al., 2003, Rash, 2010, Simard and Nedergaard, 2004). Connexins (Cx43/47 or Cx30/32) are present in oligodendrocytes, both in the external myelin sheaths and within the myelinated fibres contacting Ranvier nodes. Connexins are essential for the maintenance of myelin homeostasis, to the point that their suppression leads to myelin vacuolation (Altevogt and Paul, 2004, Menichella et al., 2003, Rash, 2010). Apart from regulating K^+, this glial network would be playing an essential role regulating pH, glutamate homeostasis, glucose traffic, and even in controlling vascular tone (Bekar and Nedergaard, 2013).

1.3.4.3.1 The ClC-2 chloride channel

ClC-2 is one out of the nine members belonging to the family of Voltage-dependent chloride channels (ClCs). ClCs participate in a wide range of physiological processes, in which they contribute with voltage-dependent transport of Cl^- ions across cell membranes. Some members of this family are located in the plasma membrane, while others act in intracellular organelle membranes. Moreover, various of these ClCs interact with auxiliary subunits that are important for their proper function and subcellular trafficking (Figure 22). The affection of ClCs or their auxiliary subunits are disease-causing. These diseases are known as chloride channelopathies, and they are genetic disorders (Jentsch et al., 2005; Poroca et al., 2017; Thiemann et al., 1992).

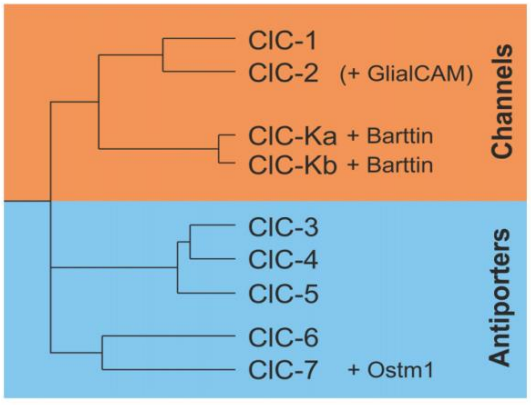

Figure 22. Classification of ClC chloride channels. The ClC family comprises 9 members, divided into four plasma membrane chloride channels (ClC-1, ClC-2 and ClCKa/b) and five intracellular antiporters (ClC-3, ClC-4, ClC-5, ClC-6 and ClC-7). ClC-2, ClCKs and ClC-7 interact with auxiliary subunits, which also appear on the Figure. Exacted from (Stölting et al., 2014).

CLCN2 gene encodes for ClC-2 channel in humans. ClC-2 is expressed in a wide array of tissues. We find ClC-2 in the brain, kidney, pancreas, skeletal muscle, gastrointestinal tract, among others (Gründer et al., 1992, Thiemann et al., 1992). Within the brain, ClC-2 is present in pyramidal hippocampal neurons and interneurons (Smith et al., 1995). It is also found in astrocytic endfeet surrounding blood vessels (Jeworutzki et al., 2012, Sík et al., 2000), as well as in oligodendrocytes (Blanz et al., 2007).

ClC-2 is classically described as being localized at basolateral membranes of polarized cells. However, its rapid recycling ends with large part of the channels detected intracellularly, where is suggested to be associated to membrane compartments (Cornejo et al., 2009).

1.3.4.3.1.1 Structure and Biophysical Properties of ClC-2

ClC-2 protein consists of 907 amino acids and weighs around 100 kDa. ClC-2 structure is common to ClC channels and transporters (Dutzler, 2007, Weinreich and Jentsch, 2001). The channel forms a homo-dimeric double-barrel structure, as could be confirmed thanks to the crystallization of ClC bacterial channels. This breakthrough also revealed independent pores or protopores for each monomer, with filter selectivity for chloride ions. Specifically, one ClC-2 subunit consists of 18 transmembrane helices (named from A to R) followed by a cytosolic C-terminus tail containing two conserved cystathionine-ß-synthase (CBS) motifs (Dutzler et al., 2002). **Figure 23** includes a visual representation of ClC-2 structure and topology. These CBS domains are essential for correct intracellular trafficking and may be involved in protein oligomerization (Estévez et al., 2004, Ponting, 1997).

Furthermore, crystallization of bacterial ClCs also served to establish the permeability sequence of ClC-2: $Cl^- > Br^- > I^- > F^-$. This sequence is very similar to its family members ClC-1 and ClC-0 (Jentsch et al., 2002, Stölting et al., 2014, Thiemann et al., 1992).

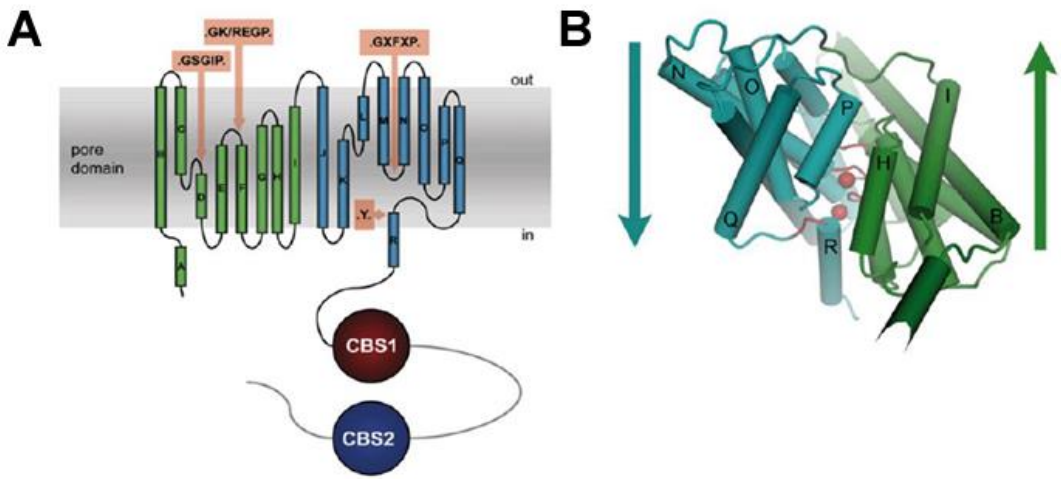

Figure 23. Topology and features of ClC-2 channel. A Schematic representation of transmembrane topology for ClC-2 subunits. The image shows helices A to R, the sequences that contribute to the chloride selectivity filter (arrows) and the two intracellular CBS motifs. Noteworthy, helices A-R can be divided in two equal 8-segment halves, with antiparallel orientations (B-I vs J-Q, green helices vs blue helices). **B** Putative tridimensional structure of ClC-2 in terms of folding and orientation. Extracted from (Dutzler, 2007).

Hyperpolarization is the main activation stimulus for ClC-2. Upon hyperpolarization, ClC-2 open in a very short time course, and its voltage-dependent gating can be modulated by Cl^- and H^+ (pH-dependent). Thus, increases in the intracellular chloride concentration shift the voltage dependence of the channel to a more positive voltage, activating the channel (Poroca et al., 2017). Also, mild acidification of extracellular pH activates ClC-2. However, further pH reduction leads to a decrease in currents (Niemeyer et al., 2004). Hypotonic-induced cell swelling is another factor that leads to channel activation, a mechanism that is involved in RVD response (Jentsch et al., 1999, Jordt and Jentsch, 1997, Niemeyer et al., 2004, Niemeyer et al., 2009, Thiemann et al., 1992)

ClC-2 currents present a slow time-course, and inward rectification (**Figure 24).** After activation at negative potentials, voltage steps back to positive potentials result in a very slow current deactivation. Mutagenesis studies determined that the intracellular N-terminus of the channel was essential for voltage-dependent and pH-dependent activation (Jordt and Jentsch, 1997). Complementarily, the activation and deactivation of ClC-2 gating is faster upon some deletions or modifications of the C-terminal domain. These findings suggest a modulatory function of this domain on ClC-2 gating properties (Gründer et al., 1992, Garcia-Olivares et al., 2008, de Santiago et al., 2005).

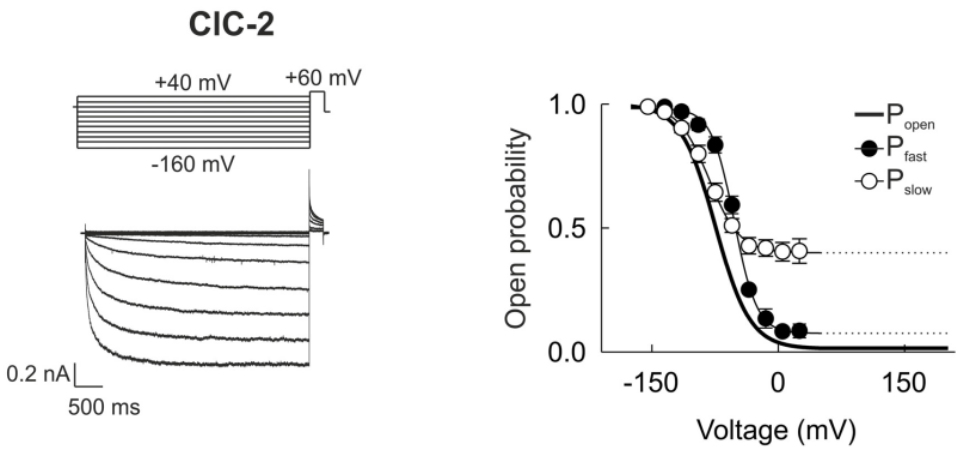

Figure 24. Representative whole-cell patch clamp responses from ClC-2. *Left* Currents elicited applying the specified protocol. *Right* voltage dependence of the probabilities of either the fast gate (full circle) or the common gate (blank circle) to be open (Stölting et al., 2014).

Regarding the gating of the channel, there are two different mechanisms that have been classically proposed: a fast gate and a slow gate. A fast gating process occurs when a single protopore turns active independently, mostly due to a conformational change. It is the component dependent on voltage, chloride concentration and pH. On the other hand, a slow gating (or common gating) mechanism consists in the simultaneous opening of both protopores through the cooperative movement of both CBS domains (Accardi and Pusch, 2000, Estévez and Jentsch, 2002, Saviane et al., 1999, Stölting et al., 2014)

Before GlialCAM discovery as a ClC-2 β auxiliary subunit, the only described proteins that modulate ClC-2 were Hsp90 and Hsp70. Both are cellular stress associated proteins and activate the channel by facilitating channel opening and increasing sensibility to intracellular Cl^- (Hinzpeter et al., 2006). JAK2 kinase could also be modulating ClC-2, according to some authors (Hosseinzadeh et al., 2012), while ATP depletion-related metabolic stress could also be involved in the regulation of ClC-2 activity (Dhani et al., 2008) through a lack of internalization of ClC-2.

1.3.4.3.1.2 Role of ClC-2 in Glial Physiology

The exact function of ClC-2 in the brain is not yet elucidated. The ubiquitous expression of ClC-2 is compatible with the thought of differential functions of the channel depending on the cell type. Arguably, chloride channels in the brain could be involved in the regulation of a wide array of physiological processes, such as cell volume regulation, control of intracellular Cl^- concentrations in inhibitory GABAergic neurons, and the regulation of ionic homeostasis of Cl^- and K^+ at the astrocyte-oligodendrocyte junction

(Blanz et al., 2007, Jentsch et al., 1999, Jentsch et al., 2002, Smith et al., 1995, Zúñiga et al., 2004). In this regard, some authors suggested a direct role of ClC-2 in the control of neuronal excitability by preventing Cl^- accumulation at GABAergic synapses (Ratté and Prescott, 2011, Rinke et al., 2010). Some studies linked ClC-2 to idiopathic generalized epilepsy (D'Agostino et al., 2004, Kleefuss-Lie et al., 2009), but they are controversial (Niemeyer et al., 2010).

A relevant model to understand the function of ClC-2 is the KO model. *Clcn2* knockout mice showed degeneration of male germ cells and photoreceptors (Bösl et al., 2001, Edwards et al., 2010). There are reports of severe defects in absorptive ion transport in the colon as well (Catalán et al., 2012). Regarding the role of ClC-2 in glial cells, the most interesting findings were that lack of ClC-2 induces vacuolization in external myelin sheaths, showing a phenotype that reproduces with high fidelity that of MLC patients (Blanz et al., 2007). Also, it alters hippocampal neurotransmission in aging mice (Cortez et al., 2010). However, this model does not develop major neurological defects (Blanz et al., 2007). The study of a possible link of *CLCN2* mutations with MLC ruled out this hypothesis (Scheper et al., 2010). Nonetheless, mutations in the *CLCN2* gene are indeed associated with a mild leukoencephalopathy (Depienne et al., 2013, Giorgio et al., 2017, Zeydan et al., 2017), that also features infertility (Di Bella et al., 2014), and secondary paroxysmal kinesigenic dyskinesia (Hanagasi et al., 2015). This disease is known as LKPAT (acronym for Leukoencephalopathy with Ataxia), and it is a *CLCN2*-related leukoencephalopathy (CC2L). *CLCN2* mutations related to CC2L severely impair channel function and trafficking (Gaitán-Peñas et al., 2017). Conversely, other works linked gain-of-function mutations in *CLCN2* to familial hyperaldosteronism (Fernandes-Rosa et al., 2018, Scholl et al., 2018).

All these data from CC2L patients combined with the observations on the phenotype of *Clcn2*$^{-/-}$ mice reinforces the idea of a role of glial ClC-2 in controlling ionic homeostasis. Given the similarities between the vacuolizing phenotype caused by the lack of ClC-2 and the vacuolization caused by ablation of astro-glial Connexins 32 and 47, or due to the lack of Kir4.1, a clear hypothesis is that ClC-2 is involved in potassium siphoning (Blanz et al., 2007). Moreover, this observation is consistent with the fact that alterations in potassium clearance trough glial syncytium lead to demyelinating problems (Rash, 2010).

2. G-PROTEIN-COUPLED RECEPTORS IN THE CENTRAL NERVOUS SYSTEM

2.1 GENERALITIES OF G-PROTEIN-COUPLED RECEPTORS

G-Protein-coupled receptors (GPCR) are membrane proteins involved in cell signaling processes in animals. At a structural level, they feature 7 α-helix segments that cross the plasma membrane and that are connected by protein loops. Since N-terminal domain is extracellular and C-terminal domain is intracellular, the protein contains three intracellular loops and three extracellular loops (**Figure 25**) (Venkatakrishnan et al., 2013).

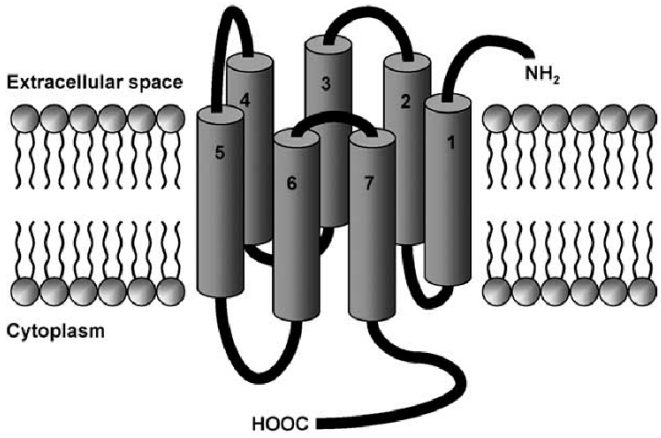

Figure 25. GPCR topology. The figure is a schematic representation of the structural topology of GPCRs. These receptors are also known as 7TMRs (7 Transmembrane-spanning receptors) due to their 7 TMDs. We see the intracellular and extracellular loops, with the extracellular N-terminal domain and the C-terminal cytoplasmic tail. Extracted from (Tikhonova and Costanzi, 2009).

GPCRs are a large superfamily of proteins expressed on the plasma membrane that receive extracellular stimuli and initiate signal transduction events in response to these stimuli (Tikhonova and Costanzi, 2009). A wide variety of ligands interact with GPCRs, either endogenous or exogenous. Some examples are neurotransmitters, metals, odorant molecules, peptides, proteins, fatty acids, amino acids, light photons, etc. These signaling molecules control a lot of distinct physiological processes, such as cell differentiation, cell death, changes in blood pressure, immune responses, tumor progression, among many others. The number of processes that GPCRs participate in, the vast array of pathologic conditions that involve GPCRS, combined with the common molecular architecture of all GPCRs, makes them a perfect target for drug development efforts. In

fact, up to a third of the drugs medically prescribed act on GPCRs (Lappano and Maggiolini, 2011, Rosenbaum et al., 2009, Tikhonova and Costanzi, 2009).

Around 800 genes in the human genome encode for GPCRs, which represent 2 % of the total genome (Fredriksson et al., 2003, Jacoby et al., 2006). Approximately 100 genes out of these 800 genes do not have an identified ligand that activates the GPCR that they encode for. These are known as orphan GPCRs (Lagerström and Schiöth, 2008). The normal binding of a ligand to its receptor can happen in three distinct mechanisms: through a pocket conformed by TMDs, through extracellular loops, or through N-terminal domain (Jacoby et al., 2006).

The canonical mechanism of signal transduction activation mediated by GPCR requires three main components: the GPCR itself, a heterotrimeric G protein, and an effector protein that produces second messengers. These, in turn, activate target proteins that trigger the cellular response. Regarding the G protein, it is heterotrimeric because it consists of three different subunits: α, β, and γ. The G protein shifts between two states: inactive and active. It is inactive when it is bound to GDP, and it is active when it is bound to GTP.

The mechanism starts with the interaction between the cytoplasmic tail of the GPCR and the G protein. Active G protein is unstable and the trimer splits into an α subunit and a βγ dimer. The dimer interacts with the effector protein that starts producing second messengers, which trigger the cellular response. However, effector proteins can sometimes directly elicit the cellular response. The signaling is terminated upon the hydrolysis of GTP bound to G_α subunit by its own intrinsic GTPase activity. G_α bound to GDP leads to the inactive state of the G protein, in which the three subunits reconstitute the heterotrimer (Milligan and Kostenis, 2006).

The effector system releases molecules that act as second messengers that initiate signaling cascades (**Figure 26**). One of the main GPCR effectors is Adenylyl Cyclase (AC), which produces cAMP at an intracellular level. Another important effector is Phospholipase C (PLC), that breaks by hydrolysis the compound phosphatidylinositol 4,5-biphosphate (PIP_2) into two phospholipids, inositol triphosphate (IP_3) and diacylglycerol (DAG). Generally, IP_3 binds to calcium channels located at intracellular compartments, such as the ER, and activates them. This results in the release of calcium

to the cytosol. On the other hand, DAG interacts with protein kinases that phosphorylate proteins (Eglen et al., 2007, Hendriks-Balk et al., 2008).

Heterotrimeric G proteins can be classified into 4 subfamilies depending on structural and functional homology of G_α subunit: G_s, $G_{i/0}$, $G_{q/11}$, and $G_{12/13}$ (Hollmann et al., 2005, Offermanns, 2003). Their main features are (Milligan and Kostenis, 2006, Yudin and Rohacs, 2018):

- G_s: the effector protein is AC. The resulting increase in cAMP levels leads to signaling cascades activation. For instance, it activates Protein Kinase A (PKA)
- $G_{q/11}$: it leads to intracellular calcium concentration increase
- G12/13: it activates small GTPases like RhoA, and Phospholipase D (PLD). They are involved in cytoskeleton changes that affect cell shape and motility
- Gi/0: the main effectors are potassium channels, typically. They inhibit AC.

A key finding in the study of GPCR signaling was the discovery of the role of β-arrestin in the process. Specifically, the binding of the ligand to the GPCR can induce the recruitment of β-arrestin in a G-protein-independent manner, which is key to desensitization of the receptor. Also, β-arrestin can activate signaling pathways like Mitogen-activated Protein Kinase (MAPK) pathway. This pathway leads to the activation by phosphorylation of proteins such as ERK1/2, RAF-1, or MEK1. MAPK pathway is pivotal to cell cycle control and to the regulation of transcription and apoptosis. Some studies even link β-arrestin 1 to oncogene activation (DeWire et al., 2007).

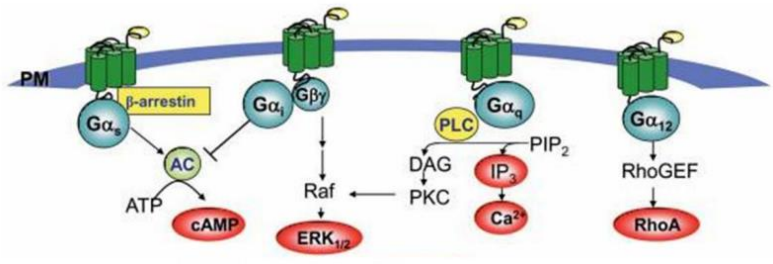

Figure 26. Schematic summary of the main signaling pathways activated by G-Protein-coupled receptors. Upon interaction with the stimulus, $G_{\alpha s}$ activates AC, while $G_{\alpha i}$ inhibits it. $G_{\beta\gamma}$ activate ERK pathways. $G_{\alpha q}$ activate PLC, producing second messengers that lead to increases in intracellular calcium concentrations and protein kinase C (PKC) activity. $G_{\alpha 12}$ activates small GTPases like RhoA. Modified from (Cheng et al., 2010).

As described, the cellular response varies according to the ligand or stimulus that interacts with the GPCR. Thus, the compounds that act on GPCRs can also be classified in different categories: agonists, partial agonists, inverse agonists, and antagonists. Agonists bind to the receptor and activate it. Partial agonists bind to the receptor and activate it, but the elicited response is not maximal. Inverse agonists bind to the receptor and reduce its constitutive activity. Last, antagonists bind to the receptor and do nothing but block the agonist binding (Park et al., 2008).

However, the binding of ligands to GPCRs not only lead to intracellular responses via G proteins. Simultaneously, a negative feedback process takes place. This is what we call desensitization (Drake et al., 2006). Desensitization aims at reducing excessive cell response to avoid potential negative effects. This process involves GPCR-specific intracellular kinases 1-7 (GRK1-7), as well as other kinases like PKA or PKC. GRK1-7 phosphorylate GPCRs upon agonist binding, which is the homologous desensitization. On the other hand, PKA and PKC do the same in a ligand-independent manner. Thus, it is the heterologous desensitization. The final step of this process is the recruitment of β-arrestin, which terminates the signal transduction by blocking the binding between G-protein and GPCR. However, β-arrestin activity also features the induction of GPCR internalization. Clathrin-coated vesicle formation units (clathrin complex, AP-2) recognize phosphorylated β-arrestin, thus leading to receptor endocytosis (Claing et al., 2002). Four types of β-arrestin are known up to date (β-arrestin 1-4). β-arrestin 1 and 4 are expressed in the retina, and they are mostly related to phototransduction. β-arrestin 2 and 3 are ubiquitous. Last, GPCRs are re-sensitized upon dephosphorylation by protein phosphatases and protein turnover to the plasma membrane. However, proteins can also be targeted for degradation at this point (Métayé et al., 2005).

2.2 GPCR CLASSIFICATION

The GCRDb (G-protein-coupled-receptor database) project by Kolakowsi proposed the first GPCR classification. It divided these proteins into seven groups, each one receiving a letter from A to F, and O (Davies et al., 2007, Kolakowski, 1994). The classification was updated to the final six classes, keeping what is known as the A-F system. It is based on amino acid sequence and functional similarities (Foord et al., 2005). Some authors proposed another classification based on the phylogenetic tree of approximately 800 human GPCR sequences (Hu et al., 2017) named GRAFS. It divided GPCRs into five

families (G for Glutamate, R for Rhodopsin, A for Adhesion, F for Frizzled, S for Secretin; GRAFS) (Schiöth and Fredriksson, 2005). However, the A-F system is more widely spread. In this system, A-C families make up for the great majority of GPCRs (**Figure 27**).

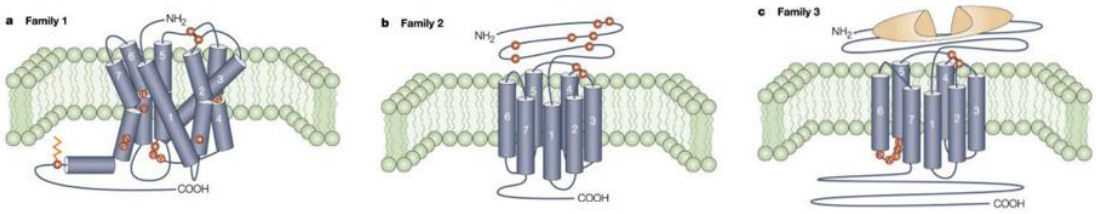

Figure 27. Schematic representation of the three main GPCR families. Family 1 corresponds to class A GPCRs, family 2 equals class B, family 3 is class C. In red, conserved amino acids across family members. For the class C receptors, Venus Flytrap module is pictured in ocre. Modified from (George et al., 2002).

Class A: Rhodopsin-like GPCRs

It is the largest GPCR family, with around 90 % of all GPCRs. It includes odorant receptors and small ligand receptors. The crystal structure of rhodopsin receptor (Palczewski et al., 2000) revealed alterations in helicoidal domain by the presence of amino acids like proline, that results in TMD tilting. These receptors feature a disulfide bond connecting extracellular loops 1 and 2, while a lot of the receptors belonging to this family contain a palmitoylated cysteine residue in the C-terminal end. This residue anchors the receptor to the plasma membrane.

Class B: secretin family receptors

This family includes 15 receptors for peptide hormones (Alexander et al., 2013). These receptors comprise a large N-terminal extracellular domain and a TMD that contains the 7 TM segments of every GPCR (Bortolato et al., 2014). The N-terminal domain includes various cysteine residues that form disulfide bonds (Ulrich et al., 1998). The peptide hormones that are ligands for these GPCRs are of small molecular weight. Some examples are glucagon, calcitonin, and secretin. The N-terminal ectodomain is the binding site for these ligands (Jacoby et al., 2006).

Class C: metabotropic glutamate receptor family

The main GPCRs within this family are metabotropic glutamate receptors (mGluRs), $GABA_B$ receptors, and Ca^{2+}-sensing receptors, sweet and amino acid taste receptors, pheromone receptors, and several orphan receptors, like GPRC5 family (Bräuner-Osborne et al., 2007).

mGluRs are subclassified into three groups based on sequence homology, G protein coupling, and ligand selectivity. Group I (mGlu 1 and 5) couple to G_q/G_{11} and active PLCβ. Group II (mGlu 2, 3) and group III (mGlu 4, 6, 7, and 8) couple to $G_{i/0}$, thus inhibiting AC and directly regulating ion channels (among other downstream partners) via $G_{\beta\gamma}$ release.

From a structural standpoint, this family is unique. N-terminal domain is exceptionally large, which contains a Venus Flytrap (VFT) module and a cysteine rich domain or CRD, except for the $GABA_B$ receptor. Ligand binding site is within the VFT module. Also, to be functional, class C GPCRs need to previously dimerize, either as homodimers or heterodimers. For instance, $GABA_B$ receptors are obligatory heterodimers of $GABA_{B1}$ and $GABA_{B2}$ while mGluRs are typically homodimers (**Figure 28**).

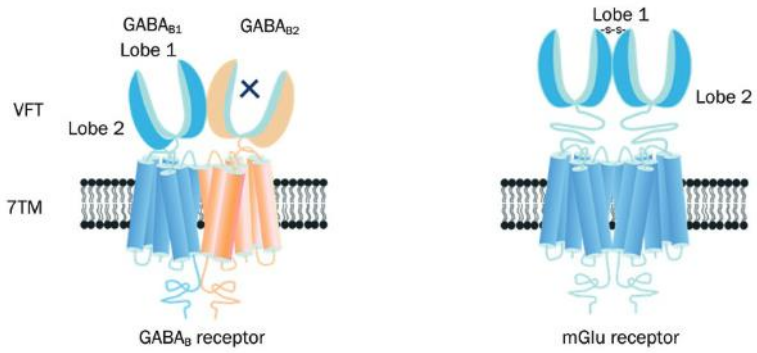

Figure 28. Schematic representation of two prototypical class C GPCRs as heterodimer (GABAB receptor) and homodimer (mGluR). $GABA_B$ is an obligatory heterodimer, in which $GABA_{B1}$ binds endogenous ligands and $GABA_{B2}$ activates G protein. While the VFT module is directly linked to the 7TM segments in $GABA_B$ receptors, in mGluRs this VFT connects to the 7TM via the CRD. mGluRs form homodimers with two binding sites per dimer (one per subunit). Extracted from (Chun et al., 2012).

Class F: frizzled

It is a minor class, formed by receptors necessary for Wnt binding and Hedgehog signaling. Therefore, they are involved in embryonic development, and cell division and polarity (Foord et al., 2002).

2.3 GPCRs IN CELL VOLUME REGULATION

The activation of a GPCR upon binding to its ligand triggers a cellular response that initiates several physiological processes at different levels, as just reviewed. In this regard, we discussed that proteins from the G_q family mediate PLC-dependent generation of IP_3 and DAG, which lead to mobilization of Ca^{2+} to the intracellular space and PKC activation (Vázquez-Juárez et al., 2008). The increased calcium concentration, in turn, is responsible for an osmolyte efflux within RVD (Pasantes-Morales and Morales Mulia, 2000). VRAC is one of the main channels involved in this osmolyte efflux. Various studies suggest that the osmolyte efflux consequence of high intracellular calcium concentrations via the binding of a GPCR with its ligand is similar in a wide variety of cell types. For instance, the glutamate efflux upon ATP or thrombin-mediated activation of purinergic receptors, or PAR-1 activation in cultured astrocytes, are some examples of this (Mongin and Kimelberg, 2002, Ramos-Mandujano et al., 2007). Consistent with the involvement of PKC within these Ca^{2+}-dependent mechanisms, inhibitors for PKC seem to reduce glutamate and taurine efflux in cultured astrocytes (Mongin and Kimelberg, 2005). Other downstream partner proteins are calmodulin (CaM) and calcium/calmodulin-dependent kinase II (CaMKII) (Franco et al., 2004).

However, there is indeed GPCR activity affecting osmolyte efflux that works in a calcium-independent manner. Noteworthy, cell swelling results in taurine release in calcium-dependent manner but also calcium-independent. In murine fibroblasts, G_i-mediated receptor activity that involves cAMP signaling also boosts taurine efflux (Heacock et al., 2006). Common to all these mechanisms, the described osmolyte efflux occurs via VRAC, essentially.

Changes in cell volume also translate into changes in the actin cytoskeleton as an adaptive mechanism. G proteins that recruit Rho-GTPase are responsible (Pedersen et al., 2001). Rho establishes dynamic interactions with proteins that regulate ion channels and transporters within RVD (Nilius et al., 1999). Rho signaling leads to the formation of an

actin-based platform that coordinates proteins that could activate current activation in response to cell swelling, resulting from Cl^-, K^+ and organic osmolytes efflux (Pedersen et al., 2002, Tilly et al., 1996). Noteworthy, Rho activation is not a direct consequence of the cell swelling stimulus, but rather mediated by other molecules that sense this swelling. It is the case of integrin receptors, growth factor receptors, among others (**Figure 29**) (Carton et al., 2002).

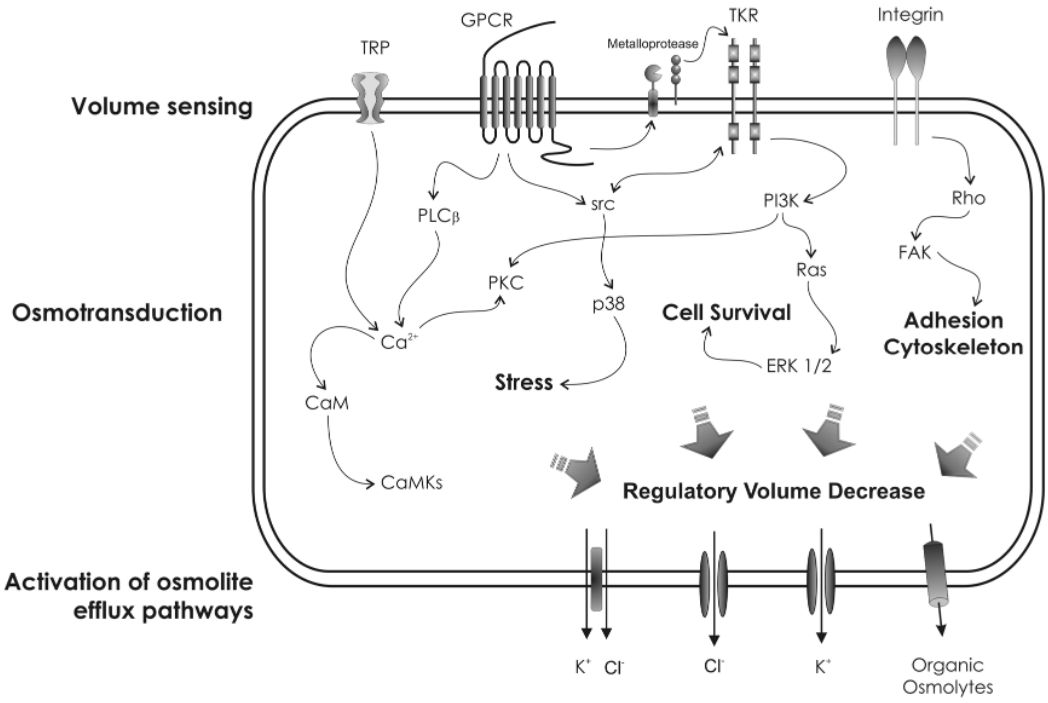

Figure 29. Model for molecular mechanisms involved in RVD for cell volume restoration. The figure represents the distinct elements that intervene in the different pathways involved in the three main steps that contribute to RVD cell recovery after hypoosmotic swelling: volume sensing, osmotransduction, and osmolyte efflux pathway activation. The scheme also features their suggested interplay. Also, the model includes other responses evoked as part of the adaptive responses of the cell to volume changes. These are: adhesion processes, cytoskeleton remodeling, stress-sensing, and cell survival pathways. TRP: transient receptor potential channels, GPCR: G-protein-coupled receptors, TKR: Tyrosine kinase activity receptors, PLCβ: phospholipase C β, src: proto-oncogene tyrosine-protein kinase Src, PI3K: phosphoinositide 3-kinases or phosphatidylinositol 3-kinases, PKC: Protein Kinase C, FAK: focal adhesion kinase, ERK1/2: extracellular signal-regulated kinase 1/2, CaM: calmodulin, CamKII: calcium/calmodulin-dependent kinase II. Extracted from (Vázquez-Juárez et al., 2008).

2.4 THE ORPHAN RECEPTORS GPR37 AND GPR37L1

GPR37 and GPR37L1 are orphan GPCRs within class A rhodopsin-like family. They relate with endothelin receptors and other GPCRs activated by peptides. Specifically, GPR37 (or hET(B)R-LP) shows a 40 % homology with endothelin receptors type B (ET_BR), and Bombesin (Bn) receptors BB1 and BB2 (Imai et al., 2001, Marazziti et al., 1997, Marazziti et al., 1998). Posterior studies identified GPR37L1 (ET(B)R-LP-2), which shared 68 % sequence similarity and 48 % identity with GPR37 (Valdenaire et al., 1998). The phylogenetic information and identity of these receptors are featured in **Figure 30**.

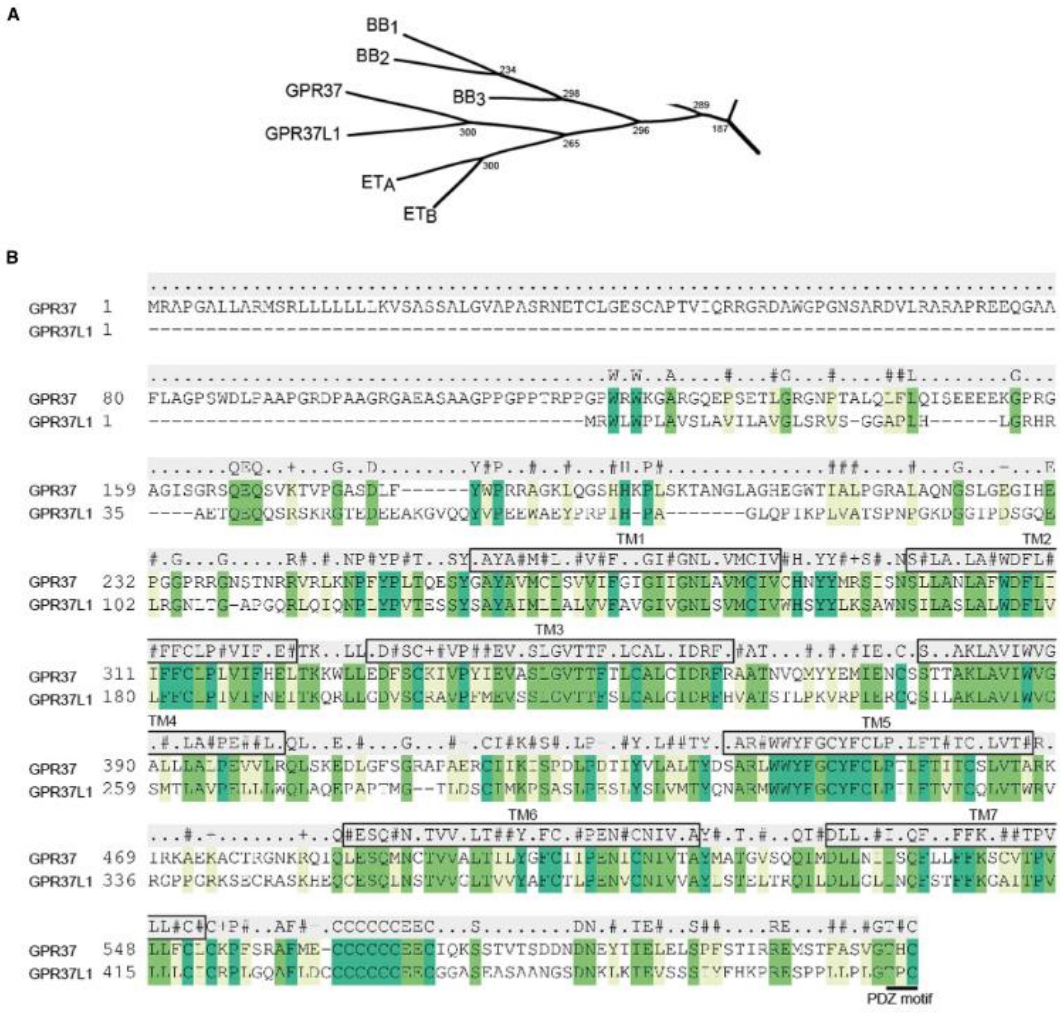

Figure 30. GPR37, GPR37L1, and their closest relatives. A Phylogenetic tree illustrating the relationship between endothelin receptors, bombesin receptors, and GPR37 and GPR37L1. **B** Alignment between human GPR37 and GPR37L1. The highlighted areas correspond to sequence conservation in TM segments. Regarding conservation, maintained residues are noted above the alignment. Regarding similarity: #: hydrophobic, +: positively charged, -: negatively charged. Boxes indicate predicted TM segments, underlining in C-terminal end marks PDZ motif. Extracted from (Smith, 2015).

Both GPR37 and GPR37L1 are highly expressed in the CNS. GPR37 is predominantly present in the cerebellum, corpus callosum, spinal cord, putamen, caudate nucleus, substantia nigra, and the hippocampus (Donohue et al., 1998, Marazziti et al., 1997, Takahashi and Imai, 2003, Zeng et al., 1997). Regarding cell types, oligodendrocytes are the main cell type expressing GPR37, while some subset of neurons in the substantia nigra also express GPR37 significantly (Imai et al., 2001). On the other hand, only glial cells express GPR37L1, mostly Bergmann glia astrocytes in the cerebellum (Marazziti et al., 2013).

The ligand for neither GPCR is known up to date. However, several studies aimed at identifying the endogenous agonist for GPR37 and GPR37L1. This topic is still controversial and continuously under debate. Given the similarity between these receptors and endothelin receptors and Bn receptors, the first approach was to assess whether endothelin or related peptides could activate signaling via GPR37 or GPR37L1. The studies ruled out this possibility (Leng et al., 1999, Valdenaire et al., 1998, Zeng et al., 1997).

One study claimed that head activator (HA) neuropeptide was the ligand for GPR37 (Rezgaoui et al., 2006). However, various groups tried to replicate the results of the study and none of them found evidence that HA could lead to GPR37 internalization. Also, HA comes from the invertebrate Hydra, and no vertebrate equivalent exists. Thus, HA was not the ligand for GPR37 (Davenport et al., 2013, Dunham et al., 2009). More recently, two novel candidates to be GPR37 and GPR37L1 ligands appeared. One was neuroprotective and glioprotective factor prosaposin, the second one was a peptide derivative, known as prosaptide (Meyer et al., 2013). Studies *in vitro* do not confirm the validity for neither (Liu et al., 2018, Smith, 2015). Therefore, GPR37 and GPR37L1 continue to be orphan GPCRs up to date.

Information on the structure of GPR37 and GPR37L1 is very lacking. GPR37 is tricky for heterologous expression due to intrinsic difficulties in protein folding in the *de novo* synthesis. Thus, in heterologous systems, GPR37 trafficking to the plasma membrane is troublesome. Also, the elimination of both extracellular and intracellular ends affected GPR37 expression and localization in the plasma membrane. Both GPCRs display a PDZ motif in the final region of their C-terminal domain, which acts as a facilitator of the

receptor trafficking to the plasma membrane through the interaction with third proteins, like Syntenin-1 (Dunham et al., 2009).

2.4.1 Knockout Models for GPR37 and GPR37L1

GPR37 is also known as Parkin-associated endothelin-like receptor or Pael-R. As indicated by this alternative name, a lot of published studies centered on the potential involvement of GPR37 in Parkinson's disease, also focusing on its potential regulatory role in the dopaminergic system.

Parkin is a E3 ubiquitin ligase protein that has GPR37 as a substrate and targets it for proteasomal degradation (Dev et al., 2003). Mutations in *PRKN*, the human gene encoding for Parkin, cause the early-onset and autosomal recessive form of Parkinson's disease. The lack of Parkin would lead to a toxic accumulation of GPR37 due to deficient degradation of the receptor. Hence, dopaminergic cells in the substantia nigra expressing GPR37 die, thus leading to the disease progression (Shimura et al., 2000, Sriram et al., 2005, Zhang et al., 2000). Consistently, Lewy bodies from patient-derived samples contained GPR37 accumulated in the nucleus (Murakami et al., 2004).

On the other hand, *Gpr37*$^{-/-}$ mice show that the protein is important in the regulation of oligodendrocyte differentiation and myelin formation. The knockout animals suffer from precocious oligodendrocyte differentiation, thus leading to hypermyelination of the CNS that originates at early in the development and continues until mice adulthood (Yang et al., 2016). Both in the brain and in primary cultured oligodendrocytes from *Gpr37*$^{-/-}$ feature elevated ERK1/2 phosphorylation levels. Interestingly, the pharmacological suppression of MEK 1/2 and ERK1/2 in this model achieved a reversion in the effect of the lack of Gpr37. Oligodendrocytes did not differentiate prematurely and cell proliferation was unaltered (Keshet and Seger, 2010). In addition, the resulting AC inhibition led to a further inhibition of the translocation of ERK1/2 to the nucleus. This suggests that this is the pathway that would normally activate GPR37. In the same regard, cAMP levels increased in *Gpr37*$^{-/-}$ mice (Afshari et al., 2001).

Published data on GPR37L1 physiological role is scarce in comparison to the work devoted to elucidating GPR37L1. The group led by Dr Daniela Marazziti studied the effect of GPR37L1 in the development and behavior of mice using the knockout model. Immunofluorescence assays show that Gpr37l1 expression levels gradually increase in Bergmann glia from the first neonatal stages up until adulthood. Knockout mice present

precocious cerebellar development due to the premature reduction of granule neuron progenitors cells proliferation, along with premature Bergmann glia and Purkinje cell maturation. These changes in phenotype occur during neonatal development in mice, while neither cytohistologic nor anatomical differences exist between WT and KO animals (**Figure 31**) (Marazziti et al., 2013). Such GPR37L1 effects link to Sonic Hedgehog (Shh) signaling pathway alterations, since this pathway is described to induce granule neuron progenitor proliferation and Bergmann glia maturation. During postnatal development of the cerebellum, both astrocytes and granule neuron progenitor cells express high levels of those proteins involved in Shh pathway, such as Patched-1 (Ptch1) and the GPCR Smoothened (Smo) (Ruat et al., 2012, Vaillant and Monard, 2009). There is basal interaction between Ptch1 and Smo that represses the signaling via this GPCR. When Shh interacts with this complex, Smo is released and intracellular mitogenic downstream signal transduction takes place (Ho and Scott, 2002). GPR37L1 interacts with Ptch1 in periciliary membranes from Bergmann glia astrocytes and modulates the formation of the primary neuronal cilium (Huangfu et al., 2003, Kim et al., 2010, Marazziti et al., 2013). In the absence of GPR37L1, expression levels and internalization of Ptch1 are higher. Therefore, these KO astrocytes proliferate with a higher ratio in comparison to WT astrocytes. These Ptch1 alterations lead to an elevation in synthesis and Shh endogenous secretion, that will lead to MAPK hyperphosphorylation (La Sala et al., 2020).

From a behavioral standpoint, the animals show enhanced motor skills (Marazziti et al., 2013) and a greater susceptibility to convulsions upon induction of different intensity currents (Giddens et al., 2017). In 2018, the firs evidence of the involvement of GPR37L1 and pathological conditions appeared. Exome sequencing allowed to link a human GPR37L1 variant (p.Lys349>Asn) with progressive myoclonus epilepsy (PME). This variant was present in five patients within a consanguineal family, and it displayed an autosomal recessive inheritance pattern (Giddens et al., 2017).

Studies in KO animals for each GPCR were useful to identify which signaling pathways they modulate. Both GPCRs seem to inhibit AC via $G_{i/o}$. Thus, the absence of these GPCRs leads to an increase in cAMP levels and an activation of MAPK signaling, which leads in turn to the phosphorylation of ERK1/2 for the activation of these enzymes (La Sala et al., 2020, Yang et al., 2016).

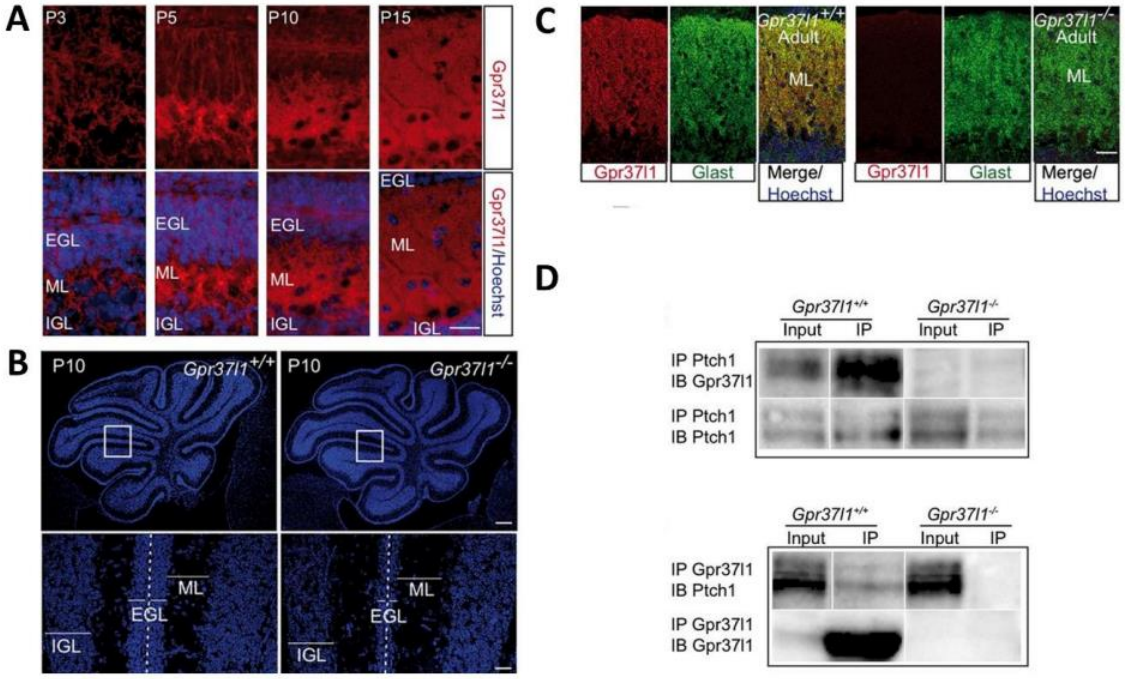

Figure 31. Gpr37l1 expression and comparative cerebellar morphology in different developmental stages of WT and Gpr37l1$^{-/-}$ mice. A Immunofluorescence images labeling Gpr37l1 (red) and cell nuclei (Hoechst, blue) in tissue samples obtained from pups at postnatal days (P) P3, P5, P10 and P15. Scale bar: 25 µm. **B** Nuclear Hoechst staining of cerebellum from WT mice and *Gpr37l1*$^{-/-}$ mice. The molecular layer is thicker in KO animals, whereas the external granular layer is thinner. Upper scale bar: 250 µm, lower scale bar: 25 µm. **C** Immunofluorescence images labeling Gpr37l1 (red) and Glast (green), with nuclear Hoechst stainings (blue). The panel includes experiments in WT animals vs KO animals, both groups in adult stages. In WT animals, Gpr37l1 colocalizes with Glast, the high-affinity glutamate transporter in Bergmann glia astrocytes. Scale bar: 25 µm. **D** Coimmunoprecipitation studies to analyse interaction between Ptch1 and Gpr37l1 in cerebellum extracts from WT and KO mice at P10. EGL: external granular layer, IGL: inner granular layer, ML: molecular layer. Modified from (Marazziti et al., 2013).

2.5 GPRC5 FAMILY

2.5.1 Generalities and Classification

GPRC5 receptors are heterotrimeric orphan receptor within class C (metabotropic glutamate receptor family) GPCRs, group IV. The identification of these receptors occurred in a context of cancer cells, where the gene encoding for these proteins appeared to be induced by retinoic acid. Hence, the first name that GPRC5 receptors received was RAIG (Retinoic Acid Inducible Gene) (Cheng and Lotan, 1998).

The 7 TM segments from GPRC5 receptors show conservation from invertebrates to mammals. The only identified ortholog for GPRC5 receptors in invertebrates is BOSS receptor, from *Drosophila melanogaster* (Kohyama-Koganeya et al., 2008). On the other

hand, there are four GPRC5 subtypes in mammals: GPRC5A (RAIG1), GPRC5B (RAIG2), GPRC5C (RAIG3), AND GPRC5D (RAIG4) (Robbins et al., 2000).

Class C GPCRs typically feature the binding site within N-terminal domain. However, GPRC5 receptors possess an exceptionally short N-terminal domain. For instance, BOSS N-terminal domain is even longer than the one in GPRC5 receptors. This indicates that the ability of binding a ligand of these receptors might have been lost throughout evolution (Kim et al., 2012).

GPRC5	Tissue distribution	Cellular localization	KO mice	Proposed function and signalling
GPRC5A	Lung, colon, urinary bladder	PM, ER, Golgi Extracellular vesicular exosomes	Lung tumours	Tumour suppressor gene, NF-κB and STAT3 signalling
GPRC5B	Brain, adipose tissue, kidney, mammary grand	PM, Golgi Extracellular vesicular exosomes	Defect in cerebellar motor learning resistant to obesity, low milk production	SFK-signalling domain formation Pro-inflammatory effects Cardiac fibrosis, breast cancer
GPRC5C	Brain, kidney, liver	PM Extracellular vesicular exosomes	Regulation of hematopoietic system Lower blood pH and higher urine pH	Thromboembolism. Kidney liver function
GPRC5D	Hair follicle, pancreas, B cell	PM Extracellular vesicular exosomes	?	Hard-keratinized structures Multiple myeloma antigen

Figure 32. Main properties of GPRC5 family members. PM: plasma membrane, ER: Endoplasmic reticulum. Extracted from (Hirabayashi and Kim, 2020).

Every member of the GPRC5 family shows a singular distribution pattern across different tissues, while they link to different pathological conditions (**Figure 32**). GPRC5A and GPRC5D are non-neuronal. GPRC5A can be found in the lungs and in the colon, while GPRC5D is present in the skin and in pancreatic tissue (Tao et al., 2007). Also, GPRC5A is a tumor suppressor protein in the lung. Mice with Gprc5a deficits improve at an inflammatory level due to NF-κB activation in lung epithelial cells (Deng et al., 2010). Also, hypoxia induces GPRC5A activity in cancer cells (Greenhough et al., 2018).

On the other hand, GPRC5B and GPRC5C express ubiquitously but are particularly abundant in the CNS. Mostly, they are enriched at the cerebellum, adipose tissue, and placenta (Tao et al., 2007). At an mRNA level, GPRC5B is strongly expressed in taste buds, the olfactory bulb and Purkinje cells. There is a strong regulation in GPRC5B expression during development, and it continues throughout life and aging (Sano et al., 2011). GPRC5C is very important for kidney homeostasis. The receptor localizes at the apical membrane of proximal tubules, while the absence of Gprc5c in KO mice leads to disruptions in acid-base equilibrium. Blood pH is lower in these animals and urine pH is

higher compared to WT animals (Rajkumar et al., 2018). Regarding GPRC5D, its *in vivo* functions remain unraveled up to date (Inoue et al., 2004). Nonetheless, all GPRC5 receptors share the property of being glycosylated as well as secreted in extracellular exosomes (Kwon et al., 2014).

Given its relevance for this thesis, a specific chapter of this introduction will be dedicated to GPRC5B. This receptor is the only GPRC5 that plays a role in psychiatric conditions like Attention Deficit Hyperactivity Disorder (ADHD) (Albayrak et al., 2013), bipolar disorder, and severe depression (Tomita et al., 2013). It plays an important role in the adipose tissue, as well.

2.5.2 GPRC5B Receptor

As reviewed, GPRC5B receptor is ubiquitous but cerebellum-enriched. It participates in motor learning and spontaneous activity evoked by novel environmental stimuli (Sano et al., 2011, Sano et al., 2018). Moreover, it is fairly abundant in the adipose tissue, allegedly playing an important role in obesity (Tekola-Ayele et al., 2019). At a subcellular level, it localizes at the plasma membrane, Golgi apparatus and exosomes. Also, it mediates extracellular vesicle transport and tubule formation. This last property was observed *in vitro* for Madin-Darby canine kidney cells (Kwon et al., 2014).

In the cerebellum, GPRC5B levels increase in the axons of Purkinje cells, as reported in mice. These neurons are the only output neurons from the cerebellar cortex. They make synaptic contacts with cells from the deep cerebellar nuclei early after birth (Garin and Escher, 2001). These observations raised the hypothesis for the role of GPRC5B in neural circuitry development and in cerebellum-mediated motor control. The absence of GPRC5B, either in all CNS or limited to Purkinje cells, leads to abnormal inflammation in the distal region of Purkinje cells axons. However, dendrite morphology does not show alterations. Indeed, the axons of Purkinje cells from *Gprc5b*$^{-/-}$ mice do not develop synapse-associated structures, their mitochondria are dysfunctional, and they accumulate within inflamed areas. In these affected axons, there is an increase in local Reactive Oxygen Species (ROS) activity, which have oxidative stress-inducing ability. ROS generation is due to mitochondrial dysfunction. ROS increase simultaneous to ATP production, they provoke oxidative stress-induced cellular dysfunction, impairing synapse formation between Purkinje cells and deep cerebellar nuclei. In turn, this compromises long-term motor learning skills (Sano et al., 2018).

GPRC5B levels in the adipose tissue are also remarkably high (Sano et al., 2011). Even if the exact role of GPRC5B remains to be fully understood, a genome-wide association study uncovered the correlation between *GPRC5B* gene expression and Body Mass Index (BMI) (Speliotes et al., 2010). A published work observed that *Gprc5b*$^{-/-}$ mice weighted less than WT animals upon being fed a high-fat diet (HFD) at 16 weeks of age. Also in this study, WT animals showed greater hepatic steatosis due to lipid accumulation in the liver, while their adipose tissue was heavier. Moreover, KO animals displayed reduced insulin resistance, as well as less adipose tissue chronic inflammation combined with smaller adipocyte size. Indeed, the production of inflammatory cytokines like TNF-α, and macrophage infiltration in the adipose tissue were also lower in the Gprc5b-deficient animals. These and other metabolic parameters like circulating glucose and insulin, or leptin concentrations, ameliorated in *Gpcr5b*$^{-/-}$ animals. Such parameters are tightly linked to obesity progression. The phenotype could be due to increased metabolic rate and enhanced thermogenesis processes (Kim et al., 2012).

At a molecular level, GPRC5B is a phosphoprotein that contains several phosphorylation sites. Mass spectrometry analyses reveal eight phosphorylated serin residues and two phosphorylated threonine residues at the C-terminal region, along with three phosphorylated tyrosine residues with high conservation across evolution (**Figure 33A**). Specifically, these tyrosine residues are Tyr^{307}, Tyr^{330}, and Tyr^{383}. Some *in vitro* studies show that the kinase that phosphorylates these residues is Fyn, a kinase that belongs to the Src family. GPRC5B recruits Fyn through its SH2 domain when it is active. Fyn is the effector that modulates inflammatory responses that GPRC5B is involved in (**Figure 33B,C**). Fyn activity within this context goes via NF-κB pathway (see chapter 3.2.3.1 from this introduction) (Kim et al., 2012).

Other tissues or cell types also feature GPRC5B activity via NF-κB. This is the case for cardiomyocytes or cardiac fibroblasts, where it would be playing a role in some pathologic conditions (von Samson-Himmelstjerna et al., 2019). On the other hand, a recent work related GPRC5B activity with TGF-β/Smad3 pathway and JAK-STAT/IFN-γ in pancreatic β-cells. Interestingly, these pathways participate in fibrotic and inflammatory processes, respectively (Atanes et al., 2018).

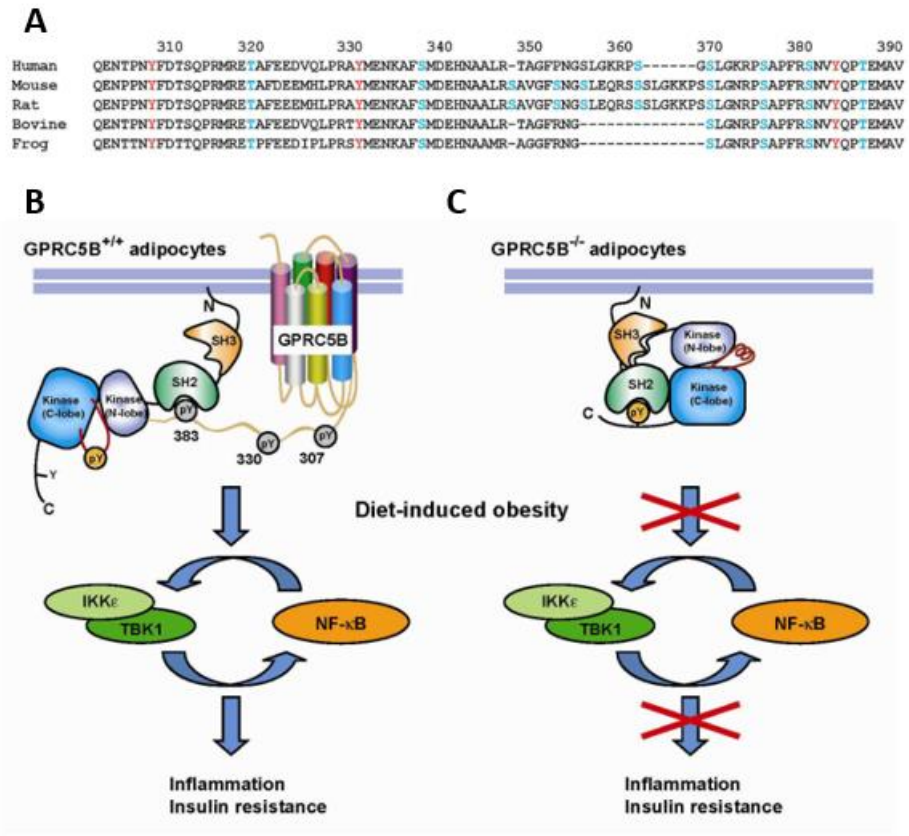

Figure 33. GPRC5B properties and modulation of the inflammatory response in the adipose tissue. **A** Alignment for GPRC5B in different species. Conserved phosphorylation sites belong to C-terminal domain. Phosphotyrosine (red), phosphoserine and phosphothreonine (blue) residues are highlighted. **B** Upon high-fat diet (HFD), GPRC5B and Fyn-SH2 domain interact. Then, Fyn activity increases locally, stimulating the positive feedback stablished for NF-kB pathway and leading to adipose tissue inflammation and insulin resistance, obesity hallmarks. **C** In the absence of GPRC5B, Fyn activity does not increase, and NF-kB loop is maintained at low, basal levels. Extracted from (Kim et al., 2012).

3. CELL ADHESION MOLECULES IN THE CNS. STRUCTURAL FEATURES OF IGCAM MOLECULES WITH SIMILARITY TO GLIALCAM

GlialCAM is a cell adhesion molecule discovered in human hepatocellular carcinoma (Moh et al., 2005) and later found to be present in glial cells (Favre-Kontula et al., 2008). Its exact function remains obscure, but mutations in the gene encoding for GlialCAM are cause of MLC disease. This suggests a strong physiological role for GlialCAM in glial cells, potentially in ionic homeostasis (López-Hernández et al., 2011a).

Like GlialCAM, many other cell adhesion molecules play a wide variety of physiological roles in different cell types within the CNS.

In this last introduction chapter, we provide a brief summary on cell adhesion molecules identified in the CNS. First, we will introduce the immunoglobulin-like cell adhesion molecule (IgCAM) superfamily. After, we will focus on its structural highlights, given that GlialCAM belongs to this superfamily of cell adhesion molecules.

3.1 GENERALITIES AND PHYSIOLOGICAL ROLES OF CAMS IN THE CNS

Cell adhesion molecules are important in a lot of key physiological processes such as cell differentiation, contact inhibition of cell growth, and apoptosis. They are important both during development and during adulthood, since these processes allow correct tissue organization at developmental stages but also tissue regeneration in the adult. In addition, correct brain morphology and development of highly specialized functions require proper cell adhesion (Cavallaro and Dejana, 2011, Ogita et al., 2010).

Cell adhesion is a concept that includes contacts. In general, this means cell-cell contacts and cell-matrix junctions. The first of the two is crucial for both tissue and organ formation and maintenance. Cell-cell junctions can be classified into symmetric (contact is due to the interaction between identical cells and identic proteins), asymmetric (different proteins establish the contact between same cell types), or heterotypic intercellular junctions (neither cells nor proteins in contact match). Moreover, cell-cell junctions can be further classified according to the type of interaction that is being established, since cell-cell junctions comprise various junctional complexes of high specialization. This gives rise to three different types of junctions: tight junctions, adhesive junctions, and gap junctions.

Tight junctions (TJs) connect cells while they serve as a physical barrier. Thus, they prevent the passage of soluble molecules through the gaps between cells, acting like a seal. Within adhesive junctions mediating side-to-side cell interactions, we find Adherens junctions (AJs) and desmosomes. Both are adhesive intercellular contacts that connect neighbouring cells and collaborate in tissue stability. However, AJs interact with actin cytoskeleton, while desmosomes interact with intermediate filament cytoskeleton. Both structures contribute to epithelial integrity and provide the machinery for homeostatic intercellular rearrangements (Garrod and Chidgey, 2008, Rübsam et al., 2018). Last, gap junctions consist of the union between channels directly connecting two cells, which enable intercellular transmission of molecules through them (Cavallaro and Dejana, 2011, Ogita et al., 2010).

Cell adhesion molecules (CAMs) are cell surface proteins that mediate the interaction between adjacent cells, or even between cells and the extracellular matrix (ECM). There are four main families of adhesion molecules: integrins, cadherins, selectins, and members of the immunoglobulin-like superfamily (IgSF). Specifically, CAMs are glycoproteins with large extracellular domains that mediate these interactions (Kozlova et al., 2020, Ren et al., 2011). Moreover, these interactions can be divided into homophilic (between identical CAMs) or heterophilic (between different adhesion molecules). In addition, CAMs propagate intracellular signals, thanks to their connections with signalling networks that control several cellular responses. Therefore, these adhesive proteins not only maintain tissue integrity but also modulate cell behaviour in response to the surrounding microenvironment (Cavallaro and Dejana, 2011, Togashi et al., 2009).

Neurons and glial cells express multiple families of CAMs (**Figure 34**). Neuronal and axonal growth, and synapse formation and maintenance depend on CAMs (Shapiro et al., 2007). Synapses are highly specialized intercellular communication units, highly asymmetrical, while containing several adhesion structures. Astrocyte-synapse interactions also play important roles during neuronal network development. Communication between astrocytes and neurons are important in synaptic transmission, axonal conduction, and modulation of neuronal networks (Brümmendorf and Rathjen, 1996, Togashi et al., 2009, Washbourne et al., 2004).

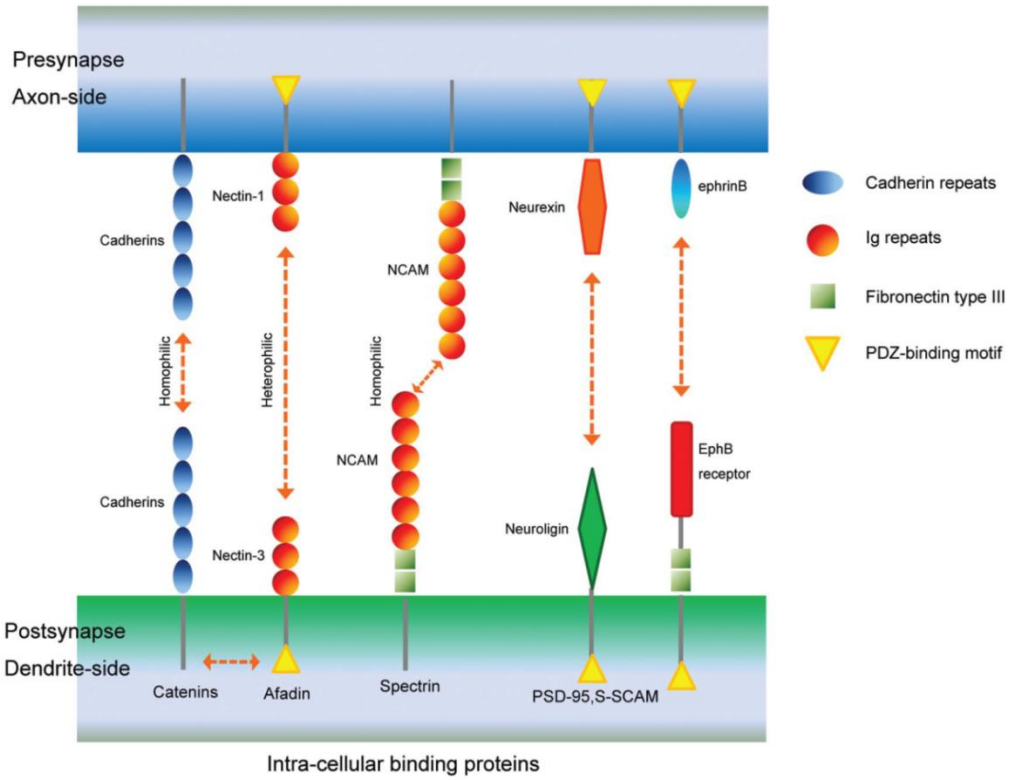

Figure 34. Schematic representation of CAMs participating in the synapse formation. The diagram shows adhesion molecules with their extracellular domains depicted. Most molecules associate contain PDZ-binding motifs (yellow triangles) to form multimolecular scaffolds beneath pre- and post-synaptic membranes. Extracted from (Togashi et al., 2009).

Last, adhesion molecules are key in the configuration and integrity of the BBB (**Figure 35**). The BBB is a selective barrier formed by the endothelial cells surrounding cerebral capillaries, together with perivascular elements (astrocytic end-feet, perivascular neurons, pericytes). These cells involved conform the neurovascular unit (Cecchelli et al., 2007). At the level of the microvascular endothelium, the barrier that separates circulating blood from the brain extracellular fluid consists in tight junctions composed of claudins, occludins, and junctional addhesion molecules (JAMs). Adherens junctions are also key to maintain the seal for the paracellular route, but they are less apical than TJs. In addition, all these junctional proteins are directly or indirectly associated with scaffold protein ZO-1, which links them to the actin cystoskeleton (Hashimoto and Campbell, 2020).

Outer to the BBB and right after the perivascular space, the astrocytic endfeet engulf the microvascular wall in what is known as glia limitans. The combined action of these two barriers controls the access of molecules or immune cells to the CNS. Indeed, in response to inflammation there is tight junction formation in the glia limitans to act as a secondary

barrier to restrict activated T cell infiltration. This is likely to compensate for the tight junction downregulation in the BBB in response to CNS inflammation (Chow and Gu, 2015, Horng et al., 2017, Quintana, 2017).

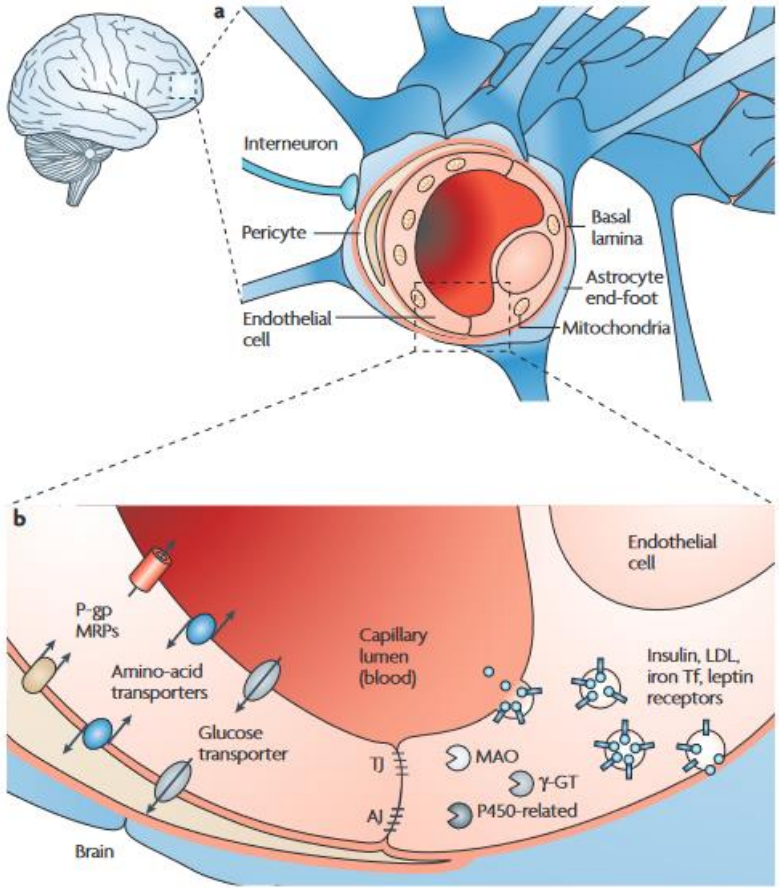

Figure 35. The blood-brain barrier (BBB). A Schematic representation of the BBB, established by the interaction between endothelial cells and perivascular elements. **B** Zoomed picture of the molecular composition of the BBB, formed by TJs and AJs. Also, the presence of enzymes and transporters around the BBB is an indicator of its dynamic metabolic activity. Extracted from (Cecchelli et al., 2007).

3.1.1 Classification and Examples of Cell Adhesion Molecules of the CNS

As just reviewed, there are basically four families of CAMs. Several adhesion molecules have been identified as taking part in neuron-neuron and neuron-astrocyte interactions.

Cadherins

Cadherins constitute a large superfamily comprising more than 100 proteins. There are several subfamilies according to the tissue in which they are found: epithelial cadherin (e-cadherin) in epithelial cells; neural cadherin (n-cadherin) in the nervous system; or vascular endothelial cadherin (ve-cadherin) in endothelia. Another classification for this

family is the division between classic cadherins and protocadherins (Brümmendorf and Rathjen, 1996, Ogita et al., 2010, Takeichi, 2007).

On the one hand, classic cadherins are single-pass transmembrane proteins with five cadherin repeats in their extracellular domains. These proteins are Ca^{2+}-dependent and establish homophilic interactions, except for limited subtypes. Through their conserved cytoplasmic domain, they bind to catenins, which connect them to the actin cytoskeleton. The cadherin-catenin complex is the molecular identity of adherens junctions, located in the apical portion of the junctions. There, they establish a signaling centre that comprises various cystoskeletal and signaling proteins. Cadherin-catenin connection allows cadherins to regulate actin polymerization, which is important to regulate cell-cell adhesion. In this regard, the main function of cadherins at the adherens junctions is to promote homotypic cellular adhesion, creating and maintaining tissue integrity. Classic cadherins are mostly expressed in the nervous system, correlating with neuronal connectivity and synaptic contacts, including axodendritic contacts (Takeichi, 2007).

On the other hand, protocadherins have a variable number of cadherin repeats in the extracellular domain. Also, their cytoplasmic domain does not signal through catenins. They are also synapse-bound, mostly expressed both in neurons and astrocytes. Some published data highlights the relevance of protocadherins in neuron-astrocyte communication, together with delay in synapse formation that impairments in this process induce (Dewa and Arimura, 2022, Garrett and Weiner, 2009). However, the function of these cadherins remains poorly understood. Since synapses eventually form, an additional role for protocadherins in bidirectional neuron-glia communication seems reasonable (Li et al., 2010).

Nectins

Nectins and nectin-like molecules belong to the superfamily of immunoglobulin-like (Ig-like) proteins. They can form *trans* homo- or heterodimers in a Ca^{2+}-independent manner. Heterotypic complexes (typically between nectin-1 and nectin-3, with nectin-1 being expressed in presynaptic terminals and nectin-3 in postsynaptic terminals) establish stronger trans-interacting adhesion than homotypic complexes (Sakisaka and Takai, 2004).

Nectins bind to Afadin protein, which connects nectins to the actin cytoskeleton. Nectin induces intracellular signalling and reorganization of the actin cytoskeleton, which are

necessary for the formation of both adherens and tight junctions (Ogita et al., 2010). Several mental disorders feature defects in Nectins. One hypothesis is that these mutations would be that altered AJs lead to defective synaptic function, specifically due to defective junctions between axons and dendritic spines (Beaudoin, 2006, Ogita et al., 2010). Interestingly, some authors described the expression of one type of Nectin (Nectin-2δ) in astrocytes using a co-culture of neurons and astrocytes. The protein was present on the plasma membranes of astrocytic perivascular endfeet processes facing the basal membrane of blood vessels. Ablation of this Nectin caused degeneration of astrocytic perivascular processes and neurons in the brain (Miyata et al., 2016). Topology for the described proteins is depicted in **Figure 36**.

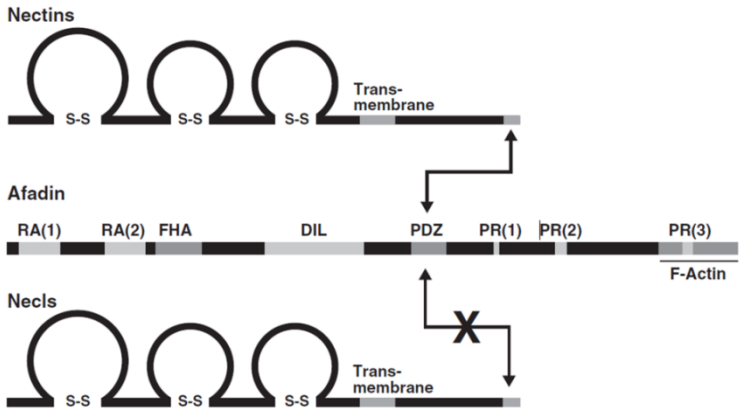

Figure 36. Topology of Nectin, Nectin-like molecules (Necls), and Afadin. Nectin and Necls possess three Ig-like domains in the extracellular region, a single transmembrane segment, and a cytoplasmic tail. Also, Nectins contain a consensus motif for interaction with PDZ domain of Afadin. Afadin further interacts with F-actin, thus binding the Nectin-Afadin complex to the cytoskeleton. Necls do not feature this PDZ-interacting domain, so they do not directly bind to Afadin. Extracted from (Ogita et al., 2010).

NCAMs

Neural cell adhesion molecules (NCAMs) also belong to the Ig-like superfamily. NCAMs display 5 Ig-like domains and 2 fibronectin-III repeats. NCAM can display either homophilic or heterophilic interactions with different ligands such as FGFR, L1-CAM adhesion molecule or TAG-1 (Togashi et al., 2009, Walsh and Doherty, 1997). NCAMs are widely expressed in development as well as in adult brain, and it is essential for axon migration and synaptic plasticity. It displays a large amount of the negatively charged sugar, polysialic acid (PSA), that seems to be mediating axonal fasciculation (Monnier et al., 2001).

SynCAM1

SynCAM1 is yet another protein belonging to the Ig-like superfamily with homophilic binding properties. SynCAM1 is present in developing neurons, where it is necessary to shape the migrating growth cones. Moreover, it contributes to the adhesive differentiation of their axo-dendritic contacts. The cytosolic tails of SynCAM 1 and β-neurexins are highly conserved throughout evolution, a fact that highlights their physiological relevance (Robbins et al., 2010, Stagi et al., 2010).

Neuroligin and β-neurexins

Neuroligin and β-neurexins form heterotypic adhesions important in synaptogenesis (**Figure 37**). The two are different families of single-pass transmembrane domain proteins. On the one hand, neuroligins are a postsynaptic acetylcholinesterase-like (ACE-like) domain-containing protein. On the other hand, β-neurexins are presynaptic laminin-globular-domain-containing protein (Baig et al., 2017, Cao and Tabuchi, 2017, Togashi et al., 2009). When these proteins interact trans-synaptically, they induce synapse formation while promoting its maturation. Several mutations or variants of both genes are linked to neurodevelopmental disorders, such as autism spectrum disorders (Cao and Tabuchi, 2017).

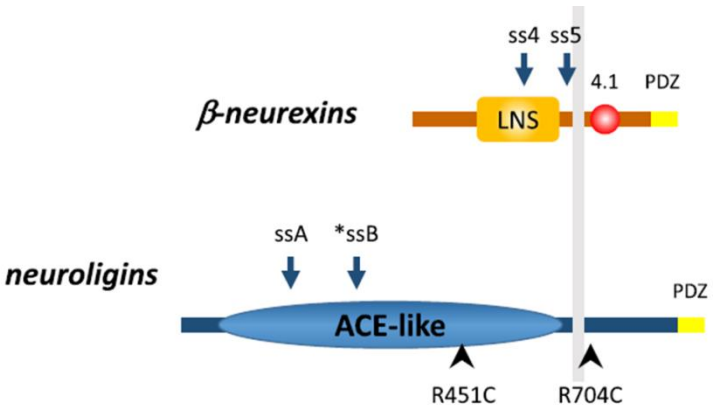

Figure 37. Domain structure of β-neurexins and neuroligins. The schematic representation of β-neurexins and neuroligins includes specific laminin-globular domains (LNS) and ACE-like domain. Arrows indicate alternative splicing sites that are linked to disease. Adapted from (Cao and Tabuchi, 2017).

3.2 IgCAMs: Structural Features and Focus on JAM and CAR Proteins.

Immunoglobulin-like cell adhesion molecules or IgCAMs are among the largest groups of adhesion molecules. IgCAMs are particularly abundant in the NS. Some remarkable examples of neural IgCAMs are NCAM, VCAM-1, and L1 family members.

IgCAMs are cell surface glycoproteins. Topologically, they feature a variable number of immunoglobulin domains on their extracellular region, together with a single transmembrane pass, and a cytoplasmic tail. Regarding their function, IgCAMs mediate calcium-independent cell–cell adhesion through homophilic *trans*- interactions. Therefore, an IgCAM binds to the same IgCAM protein belonging to the adjacent cell. Furthermore, IgCAMs typically form zipper-like structures that are similar to those described for cadherins. This structure comes from *trans*-interactions at cell-cell contacts in combination with *cis*- homophilic binding on the same cell surface. Then, the anchoring of the cytoplasmic tail of the IgCAMs to cytoskeletal components further stabilizes these zipper-like structures. Such cytoskeletal proteins range from actin, to ankyrins, and spectrins. This anchorage is essential for IgCAM-mediated triggering of different signaling cascades (**Figure 38**).

However, IgCAMs also establish heterophilic *cis*- and *trans*-interactions. The other molecules can be members of the IgCAM superfamily, integrins, cadherins, growth factor receptors, or even components of the extracellular matrix (Brümmendorf and Rathjen, 1996, Cavallaro and Dejana, 2011, Volkmer et al., 2013).

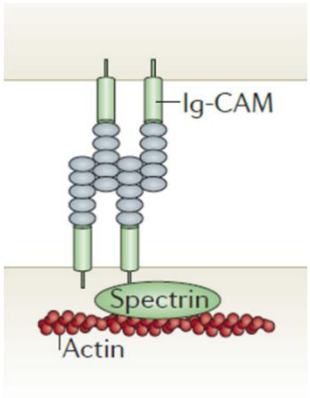

Figure 38. Schematic representation of IgCAM homophilic interactions, both trans- (between molecules from neighboring cells), and cis- (between molecules from the same membrane). The complexes anchor to actin cytoskeleton by actin-binding proteins like Spectrin. Extracted from (Cavallaro and Dejana, 2011).

IgCAM adhesion is required for the execution of diverse biological functions by these proteins. Thus, tight regulation of this process should be key. Some candidate regulatory mechanisms are local clustering through binding to scaffolding proteins, proteolytical shedding of IgCAM ectodomains, or rapid plasma membrane turnover. Flexibility of IgCAMs ectodomains could also be important to this end. Such domains could adopt distinct conformations, leading to changes in their adhesion activity. This translates into a shift in the monomer-oligomer balance (Brümmendorf and Rathjen, 1996, Cavallaro and Dejana, 2011, Volkmer et al., 2013).

GlialCAM structure is yet to be resolved. However, some work towards determining GlialCAM structural features is developed in this thesis. Hence, in this chapter we focus on structural features of adhesion molecules of the Immunoglobulin-like Superfamily (Ig-SF) since it is the family where GlialCAM belongs. Based on their similarity with GlialCAM, we approach this review of structural features of IgCAMs by the review of JAM1 and CAR structural features, the structure of which is available (**Figure 39**).

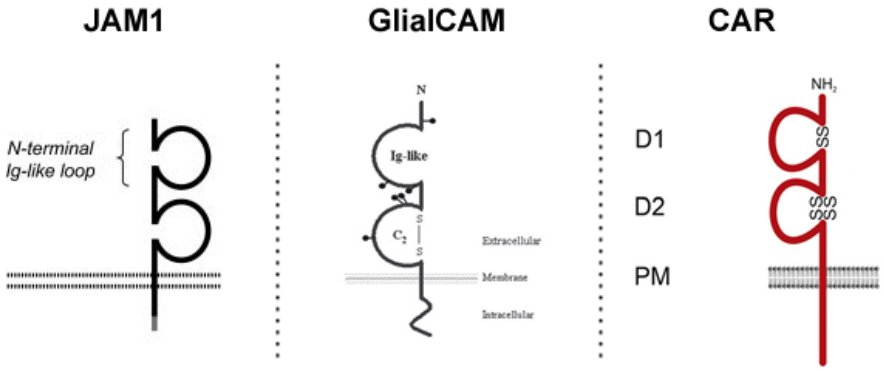

Figure 39. Summary of structural topological highlights of JAM1, GlialCAM and CAR molecules. All of them are single-pass membrane proteins (with a single transmembrane domain), in addition to a cytoplasmic tail. At the extracellular region, they display two N-terminal Ig-like domains. These domains establish homophilic interactions with other adhesion molecules (Mandell et al., 2005, Matthäus et al., 2017, Moh et al., 2005).

3.2.1 JAM molecules. JAM1 structural features

Junctional adhesion molecules (JAMs) are adhesion molecules found in epithelial tight junctions, where they regulate epithelial barrier function. JAM1 is the main member of this family, and the more extensively studied. Up to date, three homologues to JAM-1 have been reported, namely JAM-2, JAM-3, AND JAM-4. JAM-2 is expressed primarily on endothelial cells, JAM-3 is expressed on leukocytes, and JAM-4 is reported to be expressed in kidney and intestinal epithelia (Aurrand-Lions et al., 2001, Hirabayashi et al., 2003, Mandell et al., 2004, Mandell et al., 2005).

F11R gene encodes for JAM-1, which consists of 36-40 kDa. Its extracellular domain includes two Ig-like domains: a membrane-distal V-type Ig-like domain (IgV), and a membrane-proximal C2-type Ig-like domain (IgC2). IgV includes two *N*-glycosylation sites. A single-pass TMD connects the extracellular part to the plasma membrane, while its short cytoplasmic C-terminal tail ends in a type II PDZ-binding motif (Aurrand-Lions et al., 2001). Published data suggests that the N-terminal Ig-like loop is responsible for relevant JAM1 functions such as tight junction assembly, platelet aggregation, and reovirus binding. In addition, these Ig-like domains can form JAM-1 homodimers, which also appear to be of high relevance for its function (Liang et al., 2000, Mandell et al., 2004, Mandell et al., 2005). On the other hand, the cytoplasmic domain mediates interactions important for downstream intracellular activities. For instance, the C-terminal PDZ-binding motif has been reported to bind various junction-associated scaffolding proteins such as ZO-1, AF-6, ASIP, and CASK (Ebnet et al., 2003, Fanning and Anderson, 2009).

The crystal structure of human JAM-1 (Prota et al., 2003) confirmed two concatenated Ig-type domains at the N-terminal extracellular region of the protein. The domains, called D1 and D2, display a pronounced bend at the domain interface (**Figure 40**). D1 domain includes two antiparallel β-sheets, meaning it belongs to the variable type (V-set) of Ig-like domains (Bork et al., 1994). Regarding D2 domain, although its fold resembles that of D1, it is classified as intermediate type (I-set) Ig-like domain.

Furthermore, hJAM-1 molecules form homophilic dimers (**Figure 40**). Extensive ionic and hydrophobic contacts between N-terminal domains help stabilize the structure. The dimer dependence on ionic interactions is partially responsible for a dynamic hJAM-1 dimer interface. Such interface differs from conventional interfaces in its highly polar character, which enables it to undergo reconfigurations. This can be easily observed upon

comparison of the different dimeric structures for hJAM1 and murine mJAM1, especially considering the great degree of residue conservation at the interface. One hypothesis is that this polar interface may facilitate transitions between monomeric and dimeric forms of JAM1 (Kostrewa et al., 2001, Prota et al., 2003).

From an expression pattern standpoint, JAM-1 is present in endothelial and epithelial cells. JAM-1 homodimer formation is crucial for epithelial barrier function, as highlighted by the alteration in cell morphology and permeability in epithelia upon deletion of putative homodimer interface. Also, JAM-1 suppression reduces epithelial interactions with ECM through B1 integrins (Mandell et al., 2005).

In epithelial cells, Nectins within adherent junctions first recruit JAMs. Afterwards, Nectins interact at the apical zones of adhesive junctions with other CAMs, like Claudin and Occludin. Thus, tight junctions form, leading to polarization of epithelial cells (Ogita et al., 2010). During the process of cell contact formation, JAM-1 colocalizes with E-cadherin and ZO-1 in primordial spot-like AJs (Ebnet et al., 2003).

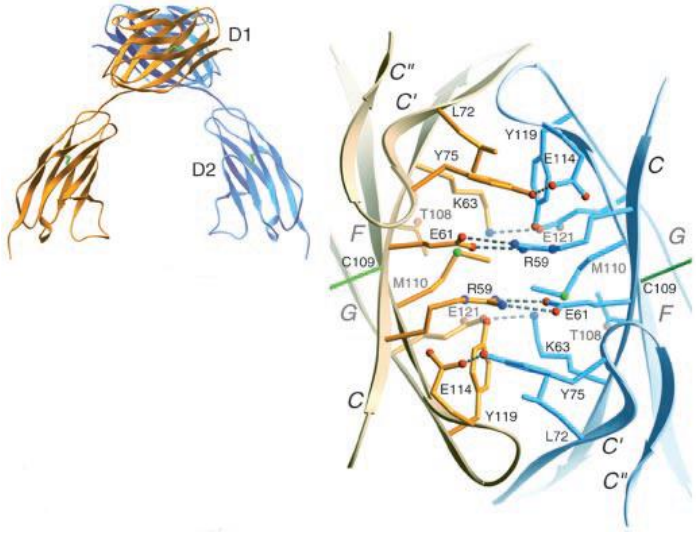

Figure 40. Schematic representation of the Structure of hJAM1 D1D2 extracellular domain. The figure features a hJAM-1 dimer displayed in ribbons (*left*), and a zoomed interface between two interacting hJAM-1 monomers (*right*). In this second drawing, broken cylinders represent hydrogen bonds and salt bridges. Amino acids are also specified in one-letter code. Adapted from (Prota et al., 2003).

The region that is involved in the establishment of homodimers was revealed thanks to the use of specific antibodies, peptides and recombinant proteins targeted at the extracellular domain of JAM-1. These biochemical studies confirmed the residues 111-123 within the N-terminal Ig-like loop as the interacting interface. Disruption of this

sequence led to dysfunction of JAM-1 in the epithelial barrier, combined with elimination of its enrichment at cell-cell contacts (Mandell et al., 2004).

3.2.2 CAR receptor. CAR structural features.

The coxsackievirus–adenovirus receptor (CAR) was originally identified due to its involvement in the attachment of group B coxsackieviruses and adenoviruses to the surface of cells (Bergelson et al., 1997). CAR and CAR-related proteins are Ig-like cell adhesion molecules that, in combination with JAMs, belong to a structural subgroup within the larger subgroup of CTX (the cortical thymocyte marker in *Xenopus*) (Matthäus et al., 2017, Weber et al., 2007).

At a topological level, CARs feature two extracellular Ig-like domains in the extracellular N-terminal region, a single transmembrane segment, and a C-terminus intracellular domain. Like was the case for JAMs, the most apical N-terminal domain of CAR is an IgV domain (D1), whereas the membrane proximal domain is an IgC2 domain (D2) (**Figure 41**). Regarding the C-terminus, it also binds to PDZ-containing scaffolding proteins (Bergelson et al., 1997, Cohen et al., 2001, Honda et al., 2000).

CARs are abundant in the nervous system during development, in addition to being uniformly distributed. They enrich at membranes facing the basal lamina or the ventricular side. However, CAR expression is downregulated and restricted to specific regions at early postnatal stages. They are also present in epithelial cells, specifically located at the basolateral membrane of intercellular junctions. There, CARs associate with ZO-1 to become part of the tight junction complex. Last, they are part of the intercalated discs in the heart (Dorner et al., 2005, Freimuth et al., 2008).

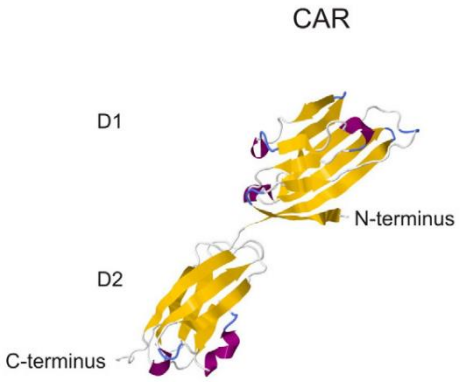

Figure 41. Crystal structure of the complete extracellular portion of CAR molecule, showing both D1 and D2 Ig-like domains. D1 is an IgV domain, whereas D2 is an IgC2 domain. From (Matthäus et al., 2017).

Crystal structures of the full extracellular region of CAR protein reveal that CAR forms U-shaped homodimers through N-terminal D1 Ig domains in a similar fashion to JAM-1 homodimers (**Figure 42**) (Patzke et al., 2010, van Raaij et al., 2000, Verdino et al., 2010). CAR dimer was hypothesized to exist only within the same cell, following *cis*-homophilic interactions. Several analyses indicate that homophilic binding would be achieved by D1-D2 and D2-D2 interactions. These would mean involvement of *trans*-interactions between opposing CAR molecules, essential for cell attachment. Furthermore, D2 Ig-like domain of CAR has also been described to interact with ECM glycoproteins like fibronectin. These interactions appear to be important for proper CAR function, especially regarding neurite extension, and adhesion to extracellular matrices (Patzke et al., 2010, Volkmer et al., 2013). On the other hand, the D1 domain seems to participate in heterophilic interactions, for instance with JAM-like proteins or with Coxsackievirus (van Raaij et al., 2000, Verdino et al., 2010).

A summarized model for CAR a flexible ectodomain is proposed, which enables a conformational shift resulting in *cis*- or *trans*-homophilic CAR interactions (Volkmer et al., 2013).

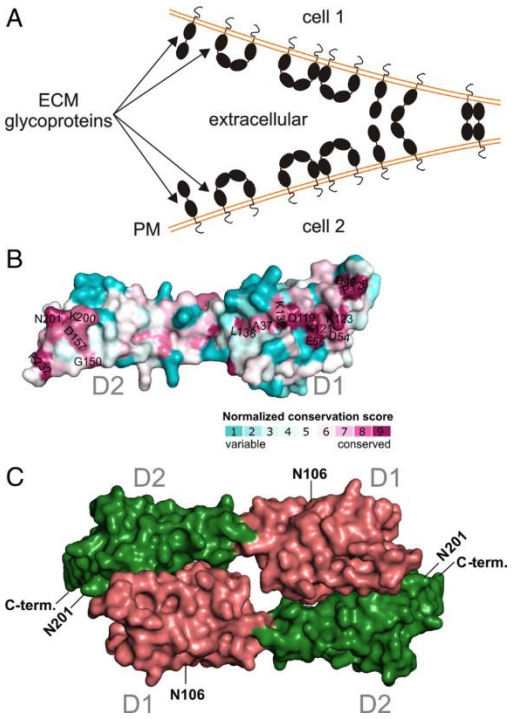

Figure 42. Summary of molecular CAR interactions. A Summary of putative molecular homophilic interactions between CAR molecules in *cis*- (*left*, forming a U-shaped structure by D1-D1 interface binding) or in *trans*- (*right*), with D1-D2 antiparallel interaction. **B, C** Proposed model for two D1-D2 CAR dimeric interaction, based on molecular docking simulations. Molecular contact surfaces corresponding to D1 and D2 are colored pink and green, respectively. Glycosylation sites (N106 and N201) and C-terminal ends are labeled. Normalized conservation score is indicated by a color code. Extracted from (Patzke et al., 2010).

3.2.3 Vascular Cell Adhesion Molecule 1 (VCAM-1)

Vascular cell adhesion molecule 1 or VCAM-1 also belongs to the Ig-SF of cell adhesion molecules. As such, it is a type-I membrane protein and cell surface glycoprotein typically expressed in endothelial cells. In humans, *VCAM1* gene encodes for the protein, which weights around 90 kDa.

At a topological level, VCAM-1 features an extracellular region containing 6 to 7 Ig-like domains, 1 TMD, and 1 C-terminal cytoplasmic tail. Regarding the extracellular region of VCAM-1, Ig domains 1 and even 4 are responsible for ligand-binding functions. Among ligands for VCAM-1, we highlight α4β1 and α4β7 integrins. In addition, Ig-like domains contain *N*-glycosylation sites that bind to galectin-3 on eosinophiles (Kong et al., 2018, Schlesinger and Bendas, 2015). VCAM-1 is an important element in the inflammatory response. For instance, the binding of α4β1 integrin (also known as VLA-4) to VCAM-1 is essential for its regulation of rolling and firm adhesion of leukocytes to the endothelium, as well as leukocyte transmigration. The molecular and signaling pathway responsible for these properties are further detailed in **Figure 43** (Alon et al., 1995, Cerutti and Ridley, 2017, Deem et al., 2007, Wittchen, 2009).

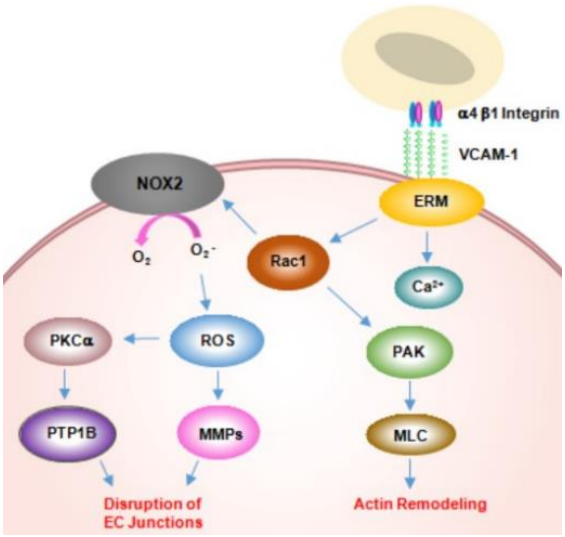

Figure 43. α4β1 integrin binding to VCAM-1 in activated endothelial cells is necessary for leukocyte rolling. The figure shows the downstream signaling pathway resulting from α4β1 integrin and VCAM-1 interaction. Binding initiates a calcium flux and Rac1 activation, leading to NADPH oxidase 2 (NOX2) activity, that generates ROS. Such molecules activate PKCα, which is responsible for phosphorylation of protein tyrosine phosphatase 1B (PTP1B) to activate it. This kinase is essential for VCAM-1-mediated leukocyte transendothelial migration. The same molecules trigger Matrix Metalloproteases (MMP) activity, that disrupt endothelial cell-cell junctions with the same aim. Rac1 also acts via Rac1-p21-activated protein kinase-myosin light chain signaling pathway, that leads actin stress fiber formation and actin cytoskeleton remodeling. Adapted from (Kong et al., 2018).

Several factors activate the expression of VCAM-1, including pro-inflammatory cytokines like TNF-α, ROS, oxidized low density lipoprotein, high glucose concentration, and toll-like receptor (TLR) agonists (Cook-Mills et al., 2011).

3.2.3.1 Inflammation, NF-κB Signaling Pathway and VCAM-1

TNF-α is a pro-inflammatory cytokine produced by immune cells, namely macrophages, T-cells, and Natural Killer Cells (Chatzantoni and Mouzaki, 2006). The TNFα-converting enzyme cleaves the molecule to give a soluble 17 kDa portion. This fragment binds to TNF receptor 1 (TNFR1), which oligomerizes to form a homotrimer and becomes active.

Upon binding of the ligand, TNFR recruits adaptor proteins to the intracellular domain and induces several signaling pathways. Specifically, intracellular domain of TNFR features a death domain (DD). This domain recruits TNFR1-associated death domain protein (TRADD) and interacts with TNF receptor-associated factor 2 (TRAF2), receptor-interacting protein 1 (RIP1), and cellular inhibitor of apoptosis proteins (cIAP1/2). These complexes activate transforming growth factor-β-activated kinase 1 (TAK1) signaling complex, and the inhibitor of κB (IκB) kinase (IKK) complex. The first one includes TAK1, TAK1 binding proteins 2 and 3 (TAB2 and TAB3). The second one features NF-κB essential modulator (NEMO) and IKKα and IKKβ.

TAK1 complex triggers MAPK signaling cascades. C-jun N-terminal kinase (JNK), P38, and AP1 get activated. IKK complex, on the other hand, activates NF-κB pathway thanks to the phosphorylation of IκB. In summary, TNFR1 signaling leads to AP1 and NF-κB enhancement, which result in the expression of target genes such as E-selectin, intracellular adhesion molecule-1 (ICAM-1), and VCAM-1 (Brenner et al., 2015, Kalliolias and Ivashkiv, 2016). A summary of these pathways is displayed in **Figure 44.**

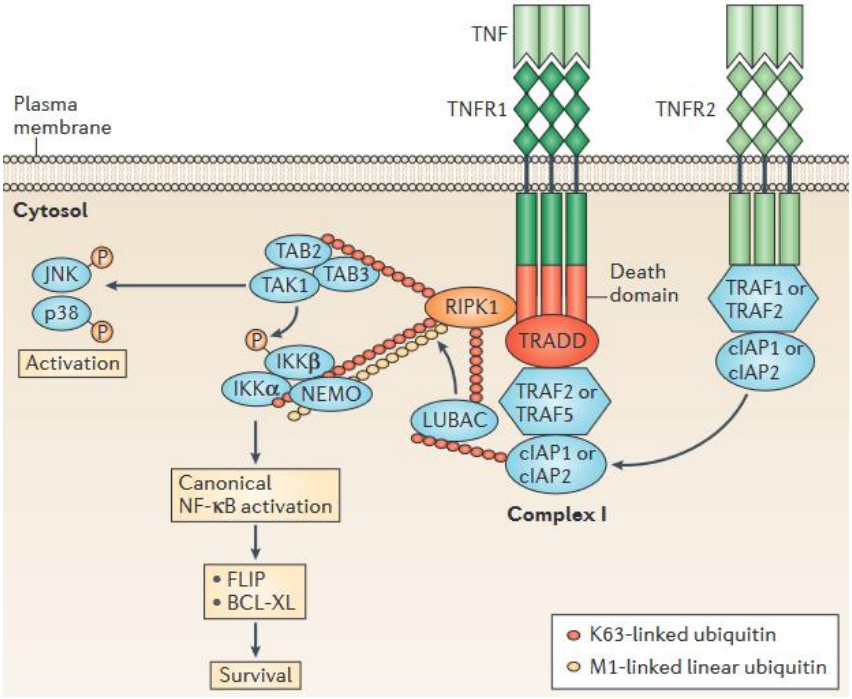

Figure 44. TNFR1 downstream signaling leads to NF-κB activation, resulting in VCAM-1 upregulation. The figure summarizes the main signaling pathway linking TNF-α and NF-κB signaling, which results in VCAM-1 upregulation in inflammatory contexts. Extracted from (Brenner et al., 2015).

OBJECTIVES

Megalencephalic Leukoencephalopathy with subcortical Cysts (MLC) is a rare genetic disease. Mutations in *MLC1* and *GLIALCAM* are identified as responsible for the development of MLC. The function of neither protein is clear up to date, and the pathophysiological mechanisms underlying the disease are not yet fully understood. For this reason, no effective therapy is available for MLC patients nowadays.

Previous works in our group have shown the wide array of proteins that are functionally related with GlialCAM and MLC1, together with the number of physiological processes in which they participate. Recently, GPRC5B was discovered to be part of this network. While some preliminary data on the functional relationship between GPRC5B and MLC-related proteins was described, various questions are unsolved. Indeed, this thesis is aimed at gaining knowledge on the molecular mechanisms underlying GPRC5B regulation of the pathophysiological processes related to MLC disease. The specific objectives are:

1. Study the role of GPRC5B on the regulation of VCAM-1 expression levels using rat primary astrocytes as a model. Analyze potential modulatory effects on this regulation by the GlialCAM/MLC1 complex.

2. Study the pathogenicity of patient-derived mutations in *GLIALCAM* encoding for amino acid residues located at IgC2 domain of the GlialCAM protein. Determine a potential link of GPRC5B activity on the function of GlialCAM related to its IgC2 domain.

3. Study the role of signaling and GPRC5B on the regulation of chloride channels ClC-2 and VRAC activity. Characterize the specific effects of phosphorylation events within these regulatory mechanisms.

METHODS

1. MOLECULAR BIOLOGY TECHNIQUES

In this thesis we cloned genes of our interest to express them in cellular models. Several molecular biology techniques were used to successfully clone these genes in different bacterial or eukaryotic expression vectors. The generation of the clones was carried out by Polymerase Chain Reaction (PCR) technique to replicate DNA, together with the application of Gateway technology (developed by Invitrogen) as the vector expression system.

1.1 DNA CLONING: PCR

The PCR technique allowed us to synthesize and/or replicate DNA fragments for our research from templates.

MATERIALS

- KOD hot start DNA Polymerase (Novagen) kit
    - Polymerase buffer 10X
    - dNTPs 2 mM
    - MgSO4 25 mM
    - KOD polymerase 1 U/µL
- Primer oligonucleotides, forward and reverse (10 µM)
- Template DNA (100 ng/µL)
- Milli-Q H_2O
- Thermocycler
- Individual PCR tubes

PROTOCOL

1. Prepare the PCR mix for each reaction in an individual tube. The final volume of each reaction is 50 µL
    - Polymerase buffer 10X: 5 µL
    - dNTPs 2 mM: 5 µL
    - $MgSO_4$ 25 mM: 3 µL
    - KOD polymerase 1 U/µl: 1 µL
    - Forward and reverse oligonucleotides 10 µM: 1,5 µL each
    - Template DNA (100 ng/µl): Adjust volume according to template concentration

- Milli-Q H_2O: up to 50 µL

2. Centrifuge the mix using a short run
3. Place the reaction tubes in the Thermocycler
4. Set the PCR protocol as follows

Start	2 minutes at 95°C	
Denaturalization	30 seconds at 95°C	X 25 cycles
Annealing	30 seconds at 55°C	
Elongation	1 minute 30 seconds at 70°C	
Final Elongation	10 seconds at 95°C	

1.1.1 Splicing by overlap extension PCR

One application of the PCR technique highly used in this project is the generation of point mutations, small insertions, or deletions on the template DNA. This technique requires the cloning of two separate fragments containing the mutation by standard PCR reaction, followed by a second PCR reaction aimed at overlapping the two fragments. This application of the PCR is known as Splicing by Overlap Extension (SOE).

PROTOCOL

1. Prepare the PCR mix for each reaction in an individual tube. The final volume of each reaction is 100 µL
   - Polymerase buffer 10X: 10 µL
   - dNTPs 2mM: 10 µL
   - $MgSO_4$ 25mM: 6 µL
   - KOD polymerase 1 U/µl: 2 µL
   - Forward and reverse oligonucleotides 10 µM: 3 µL each
   - DNA Fragment 1 (100 ng/µl): 7 µL
   - DNA Fragment 2 (100 ng/µl): 7 µL
   - Milli-Q H_2O: up to 100 µL

2. Centrifuge the mix using a short run
3. Place the reaction tubes in the Thermocycler
4. Set the PCR protocol as follows

Start	2 minutes at 95°C	
Denaturalization	30 seconds at 95°C	X 25 cycles
Annealing	30 seconds at 55°C	
Elongation	1 minute* 30 seconds at 70°C	
Final Elongation	10 seconds at 95°C	

*1 minute / kilobase of replicated DNA fragment length

1.2 DNA ELECTROPHORESIS AND PURIFICATION

PCR products obtained from a PCR reaction need to be checked and sometimes purified. With this purpose, in our group we run these samples in a non-denaturalizing agarose gel electrophoresis. DNA migration depends on its molecular weight, and it can be monitored using a molecular weight marker.

MATERIALS

For agarose gel electrophoresis:

- Mould tray
- Well comb
- Electrophoresis tank
- Power supply
- TAE 50X (Tris-Base 2 M, Acetic acid 1 M, EDTA 50 mM)
    - TAE 1X (TAE 50X diluted in distilled H_2O)
- Loading buffer 6X (EDTA 40 mM, SDS 0,1%, Ficol 400 30%, Bromophenol blue 0,2%)
- Agarose gel 1-2% (in TAE 1X) with 0,5-1% Ethidium bromide
- GeneRuler (ThermoFisher Scientific) DNA molecular weight ladder
- Eppendorf tubes

For DNA purification:

- High Pure PCR product purification kit (Roche) containing:
    - Centrifuge tubes (2 mL) with coupled columns
    - Binding buffer (Guanidine-thiocyanate 3 M, Tris-HCl 10 mM, Ethanol 5% (v/v), pH 6,6)
    - Washing buffer (NaCl 20 mM, Tris-HCl 2 mM, pH 7,5 and Ethanol)
- Milli-Q water
- Eppendorf tubes
- Blades
- Dry bath

PROTOCOL

For agarose gel electrophoresis:

1. Prepare DNA samples, bringing loading buffer to a final concentration of 1X
2. Prepare 1-2% agarose gel with Ethidium bromide 0,5-1% in TAE 1X
    a. For standard gels, a total volume of 100 mL is our choice. For purification gels, a total volume of 150 mL is recommended
3. Heat agarose solution in TAE 1X to dissolve it
4. Wait for ten minutes before adding Ethidium bromide to the agarose solution
5. Pour the agarose solution onto the mould tray with the well comb already placed. Let it cool and polymerize
6. Remove the well comb
7. Place the gel in the electrophoresis tank and cover with TAE 1X
8. Load the DNA samples mixed with loading buffer into the wells of the gel alongside the DNA gene ladder
9. Run the electrophoresis at 80-100 mV until the desired level of DNA migration
10. Visualize the gel in a UV transilluminator
    a. Cut the bands of interest and remove from the gel using a blade, if needed for DNA purification
    b. Collect the bands in a fresh Eppendorf tube
11. Acquire a photo of the gel

For DNA purification:

In this thesis, DNA purification was used in two distinct applications. The first one was to retrieve DNA inside an agarose band from running a PCR. The second one was within adenovirus production. Specifically, this process was aimed at getting rid of salts and undesired molecules in the DNA to be transfected (see chapter 3.1)

1. Add 500 µL of the binding buffer to the Eppendorf tube containing the agarose band
    a. Use 250 µL of binding buffer if we are working with DNA in solution for adenovirus production. The rest of the protocol is the same for both cases
2. Heat at 60°C in a dry thermal bath until the agarose is melted (around 5 minutes)
3. Transfer the sample to a column coupled to the 2 mL Eppendorf tube from the Purification Kit
4. Centrifuge at 13 000 rpm for 1 minute and discard SN
5. Add 500 µL of the washing buffer to the column
6. Centrifuge at 13 000 rpm for 1 minute and discard SN
7. Add 200 µL of the washing buffer to the column
8. Centrifuge at 13 000 rpm for 1 minute and discard SN
9. Transfer the column to a 1,5 mL Eppendorf tube
10. Elute DNA
    a. Add 50 µL of Milli-Q water and incubate at RT for 1 min
    b. Centrifuge at 13 000 rpm for 1 minute
11. Quantify DNA in a Nanodrop, if desired

1.3 DNA CLONING EXPRESSION SYSTEM: GATEWAY SYSTEM

A key step in DNA cloning is the insertion of our DNA of interest into a plasmid or vector. The resulting circular DNA is called a construct, which is ultimately used for the expression of the cloned genes or DNA fragments in living systems. This is key to perform functional assays or to assess the effect of protein overexpression.

For this purpose, in this thesis we used the Gateway system (Invitrogen) plasmid cloning methodology. Gateway technology is based on site-specific recombination between lambda phage sequences involved in both integration (reaction: attB x attP → attL + attR) and excision (reaction: attL x attR → attB + attP) into the *E. coli* genome. This system

allows the forementioned insertion of desired DNA to a wide array of different vectors containing lambda phage-recognized sequences. Furthermore, this reaction is reversible.

The first step in standard Gateway cloning is the addition of attB1 and attB2 sequences flanking the DNA of interest. This is obtained through a PCR reaction using specific primers designed to incorporate these ends. The primers should contain the att regions followed by the next 18 to 25 nucleotides of the sequence from our template DNA of interest. It is important that these oligonucleotides feature either the Kozak sequence (ACC) necessary to signal for the beginning of gene translation, or the termination codon in the case of the oligonucleotide corresponding to the end of the DNA sequence.

The following is an example of the sequence of the primers used to introduce the attBs in the target DNAs:

*att*B1 (*forward*): 5'-GGGGACAAGTTTGTACAAAAAAGCAGGCTTAACC-(GEN)-3'
*att*B1 *Kozak*

*att*B2 (*reverse*): 5'-GGGGACCACTTTGTACAAGAAAGCTGGGT TAG-(GEN)-3'
*att*B2 *stop*

Figure 45. Examples of AttB1 and AttB2 sequences necessary to clone DNA inserts.

The flanked insert generated by PCR needs to be run in an agarose gel, checked, and purified (see chapter 1.2). Once this DNA is ready, BP reaction can be set to proceed with the cloning of our gene of interest into the donor vector

Figure 46. Summary of BP Clonase II reaction. DNA already flanked by att sequences recombines with a donor vector by B and P sequences to give the final entry clone.

In addition, commercially available donor vectors (pDONR221) contain a lethal gene for negative selection (ccdB) as well as a kanamycin resistance (KanR) gene. When proper recombination takes place, the insert is swapped with ccdB gene. Thus, we generate a by-product DNA featuring the lethal gene which will not be present in our desired clone. In the Gateway system, this plasmid containing the insert flanked by attL sequences is called Entry Clone.

Antibiotic resistance and the lethal gene are useful in latter stages of DNA cloning process. Specifically, upon expression in E. coli for DNA amplification and purification. Bacteria expressing the correct entry clones will survive and proliferate when cultured in LB medium supplemented with Kanamycin.

However, Gateway technology offers us the possibility to clone several DNAs altogether into a single final vector. One useful application of this feature is to fuse molecular tags, epitopes, or even fluorescent proteins to our protein of interest. Noteworthy, this addition can be directed to either the N-terminal end or the C-terminal end. This Gateway variant is named Multisite Gateway two-fragment cloning. Specific recombination to clone different DNA fragments simultaneously and in a certain order is possible depending on the att sequences that flank each of them.

The sequence of the primers used to introduce the attBs in the target DNAs are the following:

*att*B1 (*forward*): 5'-GGGGACAAGTTTGTACAAAAAAGCAGGCTTAACC-(GEN)-3'
*att*B1 *Kozak*

*att*B5R (*reverse*): 5'-GGGGACAACTTTTGTATACAAAGTTGT-(GEN)-3'
*att*B5R

*att*B5 (*forward*): 5'-GGGGACAACTTTGTATACAAAAGTTGNN-(GEN)-3'
*att*B5

*att*B2 (*reverse*): 5'-GGGGACCACTTTGTACAAGAAAGCTGGGT TAG-(GEN)-3'
*att*B2 *stop*

Figure 47. Examples of attB sequences used for LR reaction.

As mentioned, the multisite Gateway system relies on the different attB introduced to the DNA of interest. For cloning 2 different DNAs in one final vector, the first of them will be generated in an entry clone with the sequences attB1 and attB5R, whereas the second fragment will be introduced in an entry clone with the attB5 and attB2 sequences. The STOP codon of the first gene codified (attb1,5R) needs to be removed so that the final recombinant protein can be expressed. The generation of the Entry Clones follows the same protocol as the standard Gateway Cloning, that is listed below.

Entry clones can then be easily recombined into any destination vector (pDEST) of interest. Those vectors contain ampicillin resistance genes and the recombination sequences attR1 and attR2, which will recombine with the attL1/2 sequences flanking the gene of interest coming from the entry clone.

1.3.1 Generation of entry clones (BP reaction)

Once the DNA with these attBs is generated, the recombination reaction (called BP reaction) is performed between this fragment and a donor vector pDONR221, which contains attP1 and attP2 sequences. Those will recombine with the attB, introducing the target DNA into the vector.

MATERIAL

- BP clonase II enzyme mix
- PCR product
- pDONR221
- Milli-Q Water
- Eppendorf tubes
- Proteinase K
- Dry bath

PROTOCOL

1. Prepare the reaction mix in an individual Eppendorf tube. The final volume of each reaction is 5 µL:

   attB-PCR product (20-50 fmols): 3 µL
   pDONR (150 ng/µL): 1 µL
   BP Clonase II: 1 µL

   i. Vortex BP clonase II enzyme before pipetting
2. Vortex and centrifuge the total reaction volume
3. Incubate at 25 ºC for 2 hours
   a. Reaction can be left up to 12 hours
4. Stop the reaction
   a. Add 0,5 µL of Proteinase K
      i. Vortex Proteinase K before pipetting
   b. Vortex and centrifuge the total volume
   c. Incubate at 37 ºC for 10 minutes

1.3.2 Generation of expression clones (LR reaction)

The recombination between one entry clone (which has the gene of interested flanked with the attL1,2 sequences) and the destination vector (containing attR1,2 recombination sequences) is performed with the enzyme LR clonase II.

MATERIAL

- LR clonase II enzyme mix
- Entry clone
- Destination vector
- Milli-Q water
- Eppendorf tubes
- Proteinase K
- Dry thermal bath

PROTOCOL

1. Prepare the reaction mix in an individual Eppendorf tube. The final volume of each reaction is 5 µL:

Destination vector:	150ng (1-3 µL)
Entry clone:	150ng (1-3 µL)
LR clonase II:	1 µL
Milli-Q water	Up to 5 µL

2. Vortex and centrifuge the total reaction volume
3. Incubate at 25 ºC for 16 hours or O/N
4. Stop the reaction
    a. Add 0,5 µL of Proteinase K
        i. Vortex Proteinase K before pipetting
    b. Vortex and centrifuge the total volume
    c. Incubate at 37 ºC for 10 minutes

1.3.3 Generation of expression clones in the Multisite Gateway

In this work we used the Multisite Gateway System mostly to fuse molecular tags or fluorescent proteins to our genes of interest. In this case, the recombination will occur between two entry clones (the first one containing attL1,5R sequences, and the second one containing attL5,2 sequences) and the destination vector (containing attR1,2 recombination sequences). In this case the reaction is made with the enzyme LR clonase II^{+}

Destination vector:	20 fmol (≤1 µL)
Entry clone1:	10 fmol (≤1 µL)

Entry clone1:	10 fmol (≤1 µL)
LR Clonase II^{+}:	1 µL
Milli-Q water	Up to 5 µL

The DNA femtomoles (fmols) are converted to nanograms (ng) using the following formula:

$$\mathbf{ng = (x\ fmols)\ (N)\ (660\ fg\ /\ fmols)\ (1\ ng\ /\ 10^{6}\ fg)}$$

The protocol for Multisite Gateway LR reaction is the same for standard Gateway LR reaction. Volume adjustments depending on the number of plasmids to recombine (as well as the stock concentration) are the only changes to be made.

The whole Gateway system for DNA cloning is summarized in **Figure 48**:

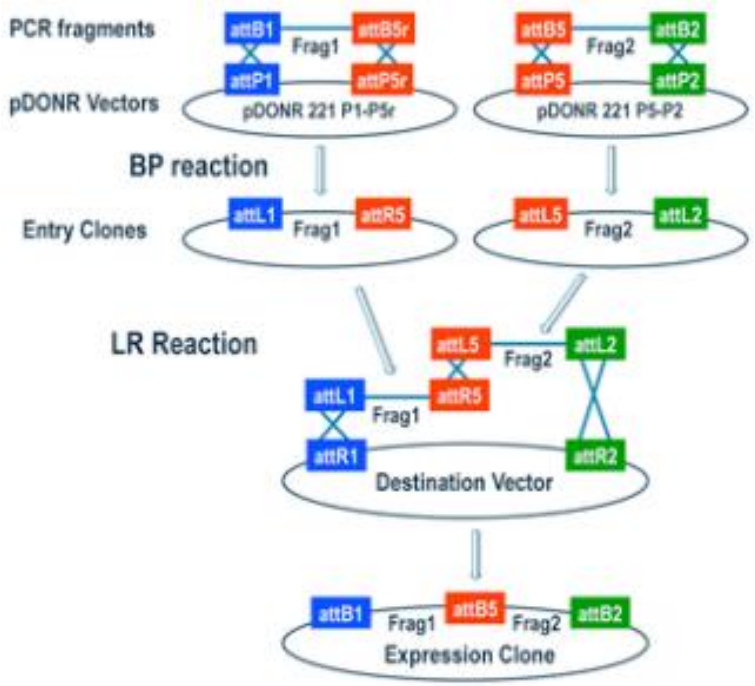

Figure 48. Schematic representation of BP and LR reactions to obtain expression plasmids. Genes of interest are cloned by PCR using the attB primers. These PCR products are recombined with pDONR vectors to give Entry Clones. Different entry clones can be later recombined in a destination vector obtaining the final expression plasmid.

1.4 PLASMID TRANSFORMATION IN ELECTROCOMPETENT BACTERIA

Cloned vectors generated with the Gateway system can be transformed and amplified in bacteria. Generated plasmids feature a replication origin or ORI that allows the vector to be self-replicative within bacterial cells. The process by which DNA is taken up by

bacterial cells is called transformation. It happens spontaneously in living bacteria, which are called competent. However, this phenomenon takes place at a low frequency.

At the same time, it can be reproduced in the lab for research purposes. Bacterial cell competence can be artificially induced, and bacterial strains have been optimized for artificial transformation. Thanks to this technology, we can obtain higher amounts of DNA molecules to work in the lab properly.

The bacteria used for this application were the *DH5α* strain of E. coli. These bacterial cells are transformed based on the generation of pores in the bacterial wall following an electric charge. Since these cells acquire competence through electricity, they are called electrocompetent. The procedure of pore generation by electric charge is known as electroporation.

The plasmid DNA displays a key feature in addition to the cloned insert and the forementioned ORI. Specifically, it contains an antibiotic resistance gene that allows for the selective growth of successfully electroporated bacterial cells in antibiotic-containing medium. Only cells positive for transformation will survive, which can be further seeded on LB-Agar petri dishes to form strains macroscopically visible.

1.4.1 Method for High Efficiency Electrocompetent Bacteria Obtention

MATERIALS

- 2 Erlenmeyer flasks (1 L capacity)
- 2 Centrifuge bottles (500 mL capacity)
- Spectrophotometer and spectrophotometer compatible cuvettes
- Refrigerated centrifuge
    - Rotor compatible with the 500 mL bottles
- Laminar flow hood (for bacteria)
- 50 mL Falcon tubes
- Sterile Pasteur pipettes
- Sterile Eppendorf tubes
- Liquid nitrogen within a tank
- *E.coli* (DH5α or DB3.1)
    - DB3.1 strain is used to amplify empty vectors. It is used because it contains gyrA462 allele, which makes these bacteria resistant to *ccdB* lethality gene

    - To seed pre-cultured DB3.1 bacteria transformed with empty vectors, we will use selective LB medium containing chloramphenicol and the antibiotic used for recombined vectors (Kanamycin for pDONR221 to generate entry clones, Ampicillin for vectors that are used to generate expression vectors)
- Sterile LB medium
    - Every 500 mL distilled water: NaCl 5 gr, yeast extract 2,5 gr, peptone 5 gr
- Glycerol 10 % (v/v) in Milli-Q water
    - Autoclaved and pre-chilled (incubated on ice)

PROTOCOL

When manipulating bacteria, we will work under the laminar flow hood to ensure sterility and avoid contamination

Day 1

1. Prepare starter cultures under the hood
    a. Pour 2 aliquots of 10 mL LB inside 50 mL Falcon tubes
    b. Inoculate aliquots with bacterial stock
        i. Using a sterile pipette yellow tip, scratch frozen bacterial stock and pipette inside the aliquot
    c. Incubate on an agitation platform at 250 rpm inside an incubator at 37ºC for 12-16 hours
2. Autoclave material (at 120ºC for 20 minutes)
    a. 2 Erlenmeyer flasks containing 500 mL of fresh LB each
    b. 1 L of glycerol 10%
    c. Centrifuge bottles

Day 2

3. Add one starter culture to each Erlenmeyer flask. Work under the hood
4. Incubate each flask on an agitation platform at 250 rpm inside an incubator at 37ºC for around 100 minutes
5. Transfer 1 mL from each culture to a separate spectrophotometer cuvette
6. Read OD (sigles) at a 600 nm wavelength. Use 1 mL of fresh LB as blank

    a. The goal is a value within 0,5-0,7 range. In case of value below threshold, continue culturing and repeat measurements every 15 minutes
        i. When OD is within the specified range, bacterial cells are amidst logarithmic phase of growth
7. Place the flasks on ice to stop bacterial growth. With this aim, all further steps must be performed on ice
8. Transfer flask contents to the centrifuge bottles
9. Centrifuge at 4 000 xg at 4ºC for 15 minutes
10. Discard SN by decantation
    a. It is important to get rid of all SN, even if it is at the expense of accidentally eliminating a little bit of bacterial pellet
11. Resuspend each pellet with the sterile Pasteur pipette using 2 mL of glycerol 10%
12. Combine the resuspended pellets in one of the bottles and add 300 mL of glycerol 10%
13. Repeat centrifuge as in step 9 of this protocol
    a. It is important to properly balance the centrifuge using the two bottles
14. Repeat steps 10 to 13 three times more, although with just one pellet now. Eventually we will have washed the bacterial pellet four times. The first two will be using 300 mL of glycerol 10%, but the last two will be using 150 mL of glycerol 10%
15. Resuspend pellet with the sterile Pasteur pipette using 2 mL of glycerol 10%
16. Prepare 50 µL aliquots in fresh Eppendorf tubes
17. Freeze immediately after pipetting each volume by placing the tubes in liquid nitrogen within a safe tank
18. Store at -80ºC

1.4.2 Bacterial Transformation and DNA Amplification

MATERIALS

- 50µL of DH5α strain of *E.Coli* bacteria

- LB medium with selection antibiotic (Tryptone 1%, Yeast Extract 0,5%, NaCl 1% in H_2O, sterilized). The antibiotic (Kanamycin or Ampicillin) is added at 100 µg/mL concentration.
- Micropulser™ electroporation cuvettes 0,1cm (Bio-Rad)
- Electroporator (Bio-Rad Micropulser)
- LB-agar Petri dishes with antibiotic for bacterial selection

PROTOCOL

For LB-agar Petri dishes with antibiotic for selection

1. Prepare LB containing Agar
    a. Peptone 5 gr, Yeast extract 2,5 gr, NaCl 5 gr, 7,5 gr agar in 500 mL Milli-Q water
2. Autoclave LB (at 120ºC for 20 minutes)
3. Bring solution temperature down in a water bath at 55ºC
4. Add antibiotic and mix (work in semi-sterile conditions next to a Bunsen burner)
    a. Kanamycin 50 µg/mL
    b. Ampicillin 100 µg/mL
5. Pour on Petri dishes and let undisturbed for 16 hours to allow solidification
6. Seal using parafilm, label and store at 4ºC

For DNA transformation

1. Add 0,5 µL of the DNA to thawed electrocompetent bacteria
    a. Bacteria should always be on ice once they leave -80ºC freezer
2. Mix the bacteria by gently tapping
3. Transfer the volume to the cuvette
4. Place the cuvette in the electroporator and apply a 375V electric charge
5. Collect the electroporated bacteria by adding 250 mL of fresh LB medium and transfer them to a 15 mL Falcon tube
6. Rest the bacteria by placing the Falcon tube in a table-top shaker at 37 ºC and 250 rpm
7. Seed 50-100 µL of the bacteria on the antibiotic-containing LB-agar Petri dish
    a. Seed just 5 µL if it is an expression vector plasmid amplification
8. Incubate the seeded dish at 37°C O/N in an incubator
    a. Bacterial colonies should appear the next day on the plate

9. Select isolated colonies of bacteria and grow them in 4 mL of a mixture of LB with antibiotic of selection at 37°C O/N
    a. Recommended: work within range of a Bunsen burner. Gently tap the colony of choice using a P20 pipette with the tip properly placed. Inoculate the LB 4 mL aliquot

1.5 PLASMID DNA PURIFICATION: MINIPREP

Some commercial kits are designed to extract and purify the DNA produced by transformed bacteria. In this work we used the QIAprep Spin Miniprep Kit (Qiagen). The protocol is based on the alkaline lysis of bacteria followed by DNA binding to an ionic resin. The miniprep kit can obtain small amounts (0,3-0,6µg/µL) of DNA from a small volume (4 mL) of bacteria.

MATERIALS

- 4 mL of precultured transformed bacteria.
- QIAprep Spin Miniprep Kit:
    - Resuspension Buffer (Tris-HCl 50 mM, pH 7,5; EDTA 10 mM; RNAse A 100 µg/ml)
    - Lysis Buffer (NaOH 200 mM, SDS 1%).
    - Neutralization Buffer (Potassium Acetate 2,55 M, pH 4,8).
    - Qiagen ionic columns with coupled collector tubes
    - Washing Buffer (NaCl 200 mM; Tris-HCl 20 mM, pH 7,5; EDTA 5 mM) mixed 1:1 with absolute EtOH.
- Milli-Q water
- Eppendorf tubes

PROTOCOL

1. Centrifuge at 4 000 rpm for 10 minutes at RT
2. Resuspend the bacterial pellet in 250 µL of resuspension buffer
3. Add 250 µL of lysis buffer and mix by inversion
    a. The solution should become blue
4. Add 350 µL of Neutralization buffer and mix by inversion
    a. The solution should become white
5. Centrifuge the homogenate solution at 13 000 rpm for 10 minutes at RT

6. Retrieve the SN by pipetting and transfer it to a column with the ionic resin from the kit
7. Incubate for 1 minute at RT and centrifuge at 13 000 rpm for 1 minute
    a. DNA binds to the resin in this step
8. Discard the SN
9. Wash the column by adding 750 µL of washing buffer and centrifuge at 13 000 rpm for 1 minute
10. Place the column over an Eppendorf tube (1,5 mL capacity)
11. Elute the DNA by adding 50 µL of Milli-Q water and incubating for 1 minute at RT before centrifuging at 13 000 rpm for 1 minute
12. Quantify DNA using Nanodrop
13. Store at -20°C

1.6 DNA Restriction Analysis

Restriction endonucleases are enzymes that were discovered in bacteria. Their use is very common in research, and they have several applications. Restriction endonucleases or restriction enzymes recognize a specific DNA sequence, and they cleave it.

Due to this feature, they are useful in DNA cloning as well as genetic engineering. Also, they can be used for diagnosis and DNA profiling. In this thesis, restriction enzymes have been mostly used in restriction analyses, aimed at validating the specificity of DNA. We can design a vector and create a map for it using computer software. Next, we can simulate the restriction pattern that the activity of a certain restriction enzyme would give out of cleaving our DNA. In the lab, we can validate this pattern reproducing the reaction and running an agarose gel for restricted DNA samples

MATERIALS

- Computer with Vector NTI software
- DNA to be restricted
- Restriction enzymes and buffers (NEB)
- Milli-Q water
- Eppendorf tubes
- Lab equipment and reagents for agarose gel electrophoresis (see chapter 1.2)

PROTOCOL

1. Design restriction using Vector NTI software
    a. Check that the restriction enzyme (or combination of two enzymes) cuts in the middle of the insert as well as in the middle of the insert-free area of the vector
    b. NEB supports an online website to check for compatibility of different restriction enzymes activity, as well as the optimal buffer for the reaction: Double Digest Finder (link)
2. Prepare reaction mix:
    a. 600 ng of DNA
    b. 1 µL of buffer
    c. 1 µL of enzyme mix
    d. Milli-Q water for a total volume of 10 µL
3. Incubate in a thermal dry bath at 37ºC for 90 minutes
4. Load the samples to an already prepared agarose gel

2. PROTEIN BIOLOGY TECHNIQUES

The purpose of cloning genes of interest to use in expression systems is to express proteins encoded by these genes and to perform biochemical studies on them. Several techniques have been used in this thesis to achieve this goal. Aside from the classical techniques to study protein localization and protein expression, several methodologies have been developed in this work that allow the study of protein-protein interactions and protein complexes.

2.1 IMMUNOCYTOCHEMISTRY

Immunohistochemistry assays are useful to study the subcellular localization of different proteins. Briefly, these assays allow the analysis of this behavior for our proteins of interest by detecting them with specific primary antibodies. Within immunocytochemistry, in this thesis we have applied immunofluorescence technique. In this protocol, the forementioned specific primary antibodies are detected in turn by fluorescence-labelled secondary antibodies. The fluorescent signal can be observed under the microscope. Our experiments feature immunofluorescence assays in either cell lines (HeLa) or primary cultured astrocytes.

MATERIALS AND REAGENTS

- Cultured cells on 10 mm coverslips
- 24-well culture plate
- Surgical tweezers
- Paraformaldehyde (PFA) 4%
- Sterile PBS 1X
- Blocking solution (PBS 1X, FBS 10%)
- Blocking and permeabilizing solution (PBS1X, 0,1% Triton-X100, 10%FBS)
- Primary antibodies (at 1/50 to 1/200 dilutions, depending on the antibody).
- Secondary antibodies (1/500 diluted)
- Mounting medium Vectashield (VECTOR); DAPI 1,5 μg/mL
- Glass micro slides (26 x 76 mm)

PROTOCOL

1. Wash cells with PBS 1X twice after discarding the medium of the cellular cultures
2. Fix cultured cells with PFA 4% at RT for 20 minutes
3. Wash cultured cells with PBS 1X 3 times
    - Fixed cells can be stored in 0,05% NaN_3-PBS 1X solution at 4ºC
4. Incubate cultured cells with the blocking and permeabilizing solution at RT for 2 hours
    - If the immunoassay does not require permeabilization, cells are incubated with the blocking solution (detergent-free) at RT for 2 hours
5. Incubate cultured cells with the primary antibodies diluted in blocking and permeabilizing solution at RT for 1 hour
    - Alternatively, primary antibodies can be incubated O/N at 4ºC.
6. Wash cultured cells with PBS 1X 3 times with blocking/permeabilizing solution for 10 minutes each wash
7. Incubate cultured cells with the primary antibodies diluted in blocking and permeabilizing solution at RT for 2 hours, protected from light
8. Wash cultured cells with PBS 1X 3 times for 10 minutes each wash
9. Mount the coverslips onto glass micro slides with *Vectashield* + DAPI mounting medium
10. Carefully remove excess mounting medium and seal with nail polish
11. Keep glass micro slides at 4ºC and protected from light
12. Acquire images using a Cell R Olympus DSU spinning-disk microscope

DATA ANALYSIS

Immunofluorescence experiments on HeLa cells are analysed manually using ImageJ software. Protein distribution across the plasma membrane together with enrichment in tight junctions are the main assays performed for these experiments in this thesis.

Pairs of immunostained cells are selected for intensity profile analysis. As seen in Figure 35, this is used to discern between junctional and plasma membrane localization. The analysis is based on the comparative quantification of the fluorescent signal between cell-cell contacts (FC) and the plasma membrane of each cell (F1, F2). When FC > F1 + F2, the analyzed protein is enriched at cell-cell junctions. This criterion is used to determine determines the percentage of localization of the respective proteins in junctions **Figure 49**.

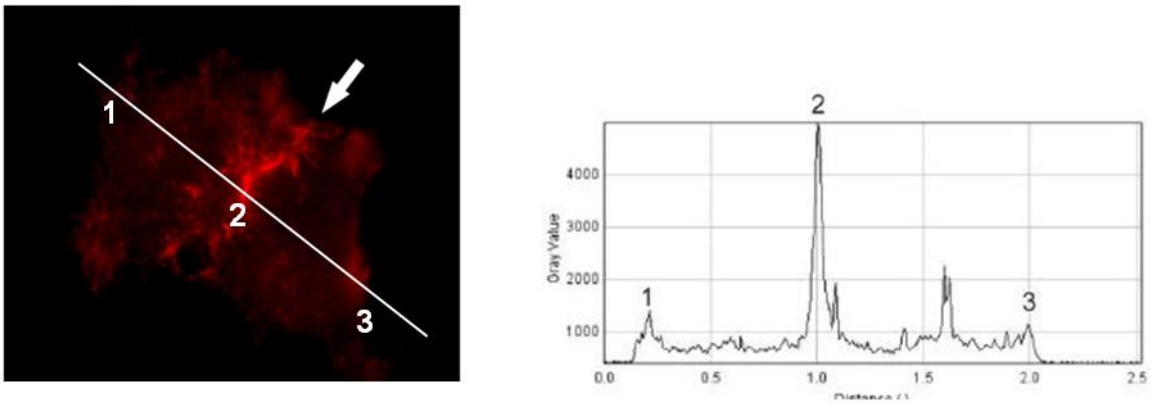

Figure 49. Analysis of cell-cell junction localization using ImageJ command.

MATERIAL

- Microscope images acquired using Cell R
- ImageJ software

PROTOCOL

1. Open images in ImageJ software
2. Select *Straight* box to draw a straight line across a pair of cells
3. Calculate the fluorescence profile across the line following the command *Analyze > Plot Profile*
    a. If FC > F1 + F2, the immunolabeled protein is enriched at cell-cell junctions.

2.2 Protein-Protein Interactions

2.2.1 Split-TEV Assays

The characterization of protein-protein interactions is of high relevance in molecular biology. A wide array of techniques has been developed with this aim. Protein complementation methodology features among the most used to determine the ability of two proteins to interact with each other. Within this array of methods, in our lab we work with the complementation of TEV protease protocol, also known as Split-TEV (as will be referred to in this manuscript).

In this technique, TEV protease is split in two halves. Following a DNA cloning approach, each of the split fragments is fused to either of the proteins we are assaying for interaction. Thus, one protein will be attached to TEV-N half along with TEV recognition site and

GV transcription factor. The second protein will be attached to TEV-C half of the protease. Upon effective interaction, the fused fragments reconstitute TEV protease activity and the transcription factor GV is released. This leads to the activation of *Gaussia luciferase,* which is a chemiluminescent reporter gene. The enzyme is released into the culture medium. Hence, the addition of a colenterazine substrate allows us to monitor the chemiluminescent signal with a luminometer. A summary of this process can be seen in Figure 50.

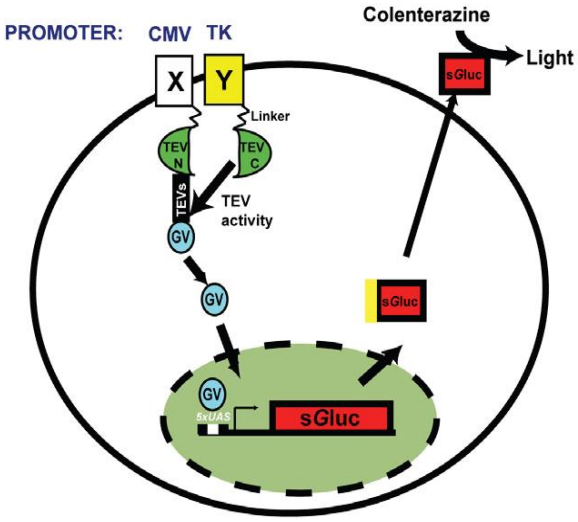

Figure 50. Schematic representation of the split-TEV method. Cells expressed a fusion of one protein of interest (X) by a flexible linker to the TEV N-terminal fragment, the TEV recognition site of normal affinity, and the transcription factor GV, under the control of a CMV promoter. The other protein of interest (Y) is fused by a flexible linker to the TEV C-terminal fragment, and its expression is controlled by the promoter TK. Interaction between the two proteins reconstitutes TEV protease activity, which releases a transcription factor (GV) that enters the nucleus and activates the expression of the reporter gene Gluc after binding to Gal4 responsive elements. The luciferase is released to the culture medium after peptide cleavage, and its activity is monitored by a luminometer after the addition of coelenterazine. Figure and description from (Capdevila-Nortes et al., 2012).

MATERIALS AND REAGENTS

- Cultured HeLa cells in 6-well plates
- Transfection Lipid Reagent (Bio-Rad)
- DNA constructs for Split-TEV assay
    - TEV-N and TEV-C fused constructs for our genes of interest and control groups
    - pNEBr-X1Gluc reporter gene
    - pCMV-β-Galactosidase vector for transfection normalization
- Sterile PBS 1X

- Native coelenterazine (Nanolight technology)
- Lysis solution (Triton X-100 1%, NaCl 150 mM, PMSF 1 mM, leupeptin/pepstatin 1mg/L and aprotinin 2mg/L in PBS 1X)
- Blocking and permeabilizing solution (PBS 1X, Triton X-100 0,1%, FBS 10%)
- β-Galactosidase Detection Kit II (Clontech)
- TD-20/20 Luminometer (Turner BioSystems)

PROTOCOL

For Split-TEV assay (chemiluminescent signal monitorization)

1. Seed HeLa cells on a 6 well plate the day before transfection
2. Transiently transfect each well with 1 µg of both plasmidic DNAs containing the proteins of interest fused to either TEV-N or TEV-C, respectively. 0,3 µg of reporter gene pNEBr-X1Gluc and 0,2 µg of pCMV-βGal vector are co-transfected. Transfection[1] is performed following the protocol *Transient Transfection in Cell Lines (see section 3.1 from these methods)*
3. Collect 20 µL of SN from each well and transfer to a fresh Eppendorf tube, at 48 hours after transfection
4. Add native coelenterazine to each tube at a final concentration of 20 µM
5. Read chemiluminescent signal immediately in a Luminometer

For transfection levels' monitorization

6. Wash cells with PBS 1X after discarding the medium of the cellular cultures
7. Add 100 µL of lysis solution to each well
8. Scrape cells vigorously and collect the final volume after resuspending with a pipette. Transfer to an Eppendorf tube
9. Incubate samples in a rotator at 4ºC for 1 hour
10. Centrifuge at 18 500 *xg* at 4ºC for 10 minutes
11. Transfer SN to fresh Eppendorf tube
12. Add 30 µL of SN to a reaction Eppendorf tube
13. Prepare β-galactosidase mix according to manufacturer's instructions

[1] It is also important to transfect one control group with only the protein fused to TEV-N and the GV transcription factor, since it may present certain degree of self-proteolysis and give background signal that needs to be subtracted.

a. Mix 196 µL reaction buffer with 4 µL of substrate for each sample group

14. Add 200 µL of the mix to each sample of cell lysate. Incubate the reaction at RT for 1 hour
    a. With the luminometer in our lab, the interval between machine reads is 25 seconds. Taking this into consideration, each volume is pipetted to the sample group with a delay of 25 seconds to the former. Thus, reaction times are equal across groups
15. Read luminescence values in the luminometer
16. β-galactosidase chemiluminescence values are subtracted from luciferase chemiluminescence values

2.2.2 NanoLuc Binary Technology (NanoBiT)

NanoBiT system is another protein complementation technique to reveal protein-protein interactions. This method is more recent in our lab than Split-TEV. It is based on NanoLuc (Nluc) protein, which is an engineered luciferase derived from *Oplophorus gacilirostris*. The enzyme has been optimized and it is characterized by its small molecular weight (19 kDa), its stability, sustained bright luminescence. For this system, Nluc is also divided in two fragments. This configuration is selected for high conformational stability but low intrinsic affinity, which allow for high sensitivity and specificity. This split reporter is known as NanoBiT, short for NanoLuc Binary Technology.

The two NanoBiT subunits that are attached to candidate proteins are LgBiT and SmBiT (for long and small NanoBiT, respectively). LgBiT is the big fragment and weighs 17,6 kDa. SmBiT consists of 11 amino acids and it weighs 1,3 kDa. Upon interaction, active luciferase is reconstituted. Only then the enzyme can emit luminescence in the presence of reaction substrate (Figure 51)

This technique offers some advantages compared to other protein complementation techniques like Split-TEV. Specifically, the luminescence response is fast as well as reversible. This property enables the study of protein interaction dynamics, including the effect of intracellular changes for a time span of up to 1 hour (duration of signal stability).

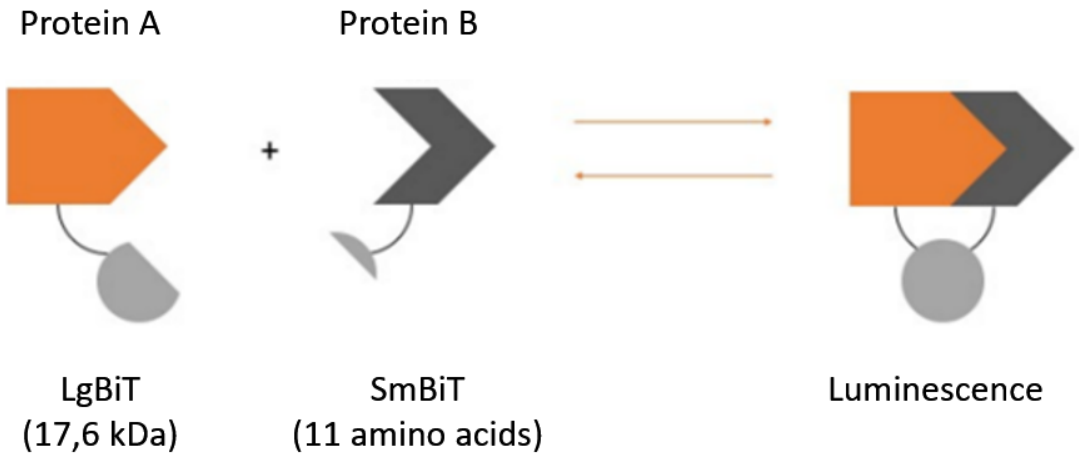

Figure 51. Schematic representation of NanoBiT interaction between two proteins. Each protein is fused to either a LgBiT fragment or a SmBiT fragment. The interaction between the two fusion proteins leads to complementation of the luciferase, restoring its function and eliciting reporter luminescent signal.

MATERIAL AND REAGENTS

- Cultured HEK293T cells
- Transfection Lipid Reagent (Bio-Rad)
- DNA constructs for NanoBiT assay
    - LgBiT and SmBiT fused constructs for our genes of interest and control groups
    - Venus construct for transfection efficiency normalization
- Sterile PBS 1X
- Dark-bottomed 96-well plates
- H coelenterazine (Nanolight technology)
- POLARstar Optima plate reader
- TD-20/20 Luminometer (Turner BioSystems)

PROTOCOL

1. Seed HEK293T cells on a 6 well plate the day before transfection
2. Transiently transfect each well with 1,4 µg of both plasmidic DNAs containing the proteins of interest fused to either LgBiT or SmBiT, respectively. 0,2 µg of Venus fluorescent protein are transfected. Transfection is performed following the protocol *Transient Transfection in Cell Lines (see chapter 3.1)*

3. Wash cells with PBS 1X after discarding the medium of the cellular cultures, at 48 hours after transfection
4. Detach cells using 1 mL of PBS 1X and transfer to an Eppendorf tube 1,5 mL
5. Centrifuge at 200 xg at RT for 5 minutes
6. Discard SN and resuspend pellet using 70 µL of PBS 1X
7. Add 10 µL of each cell suspension onto wells in dark-bottomed 96-well plated
    a. It is important to homogenize cells properly before pipetting
8. Read fluorescence (Venus) using excitation filter 485±12 nm and emission filter 535±30 using the POLARstar Optima plate reader
9. Add 40 µL of H-coelenterazine (final concentration of 1 mM, 1:50 from stock) to each Eppendorf tube
10. Incubate at RT for 1 minute
11. Read luminescence using TD-20/20 Luminometer (Turner BioSystems)
12. Normalize luminescence values using fluorescence values. Results are given as a Luminescence/Fluorescence ratio.
    a. A control group where we only transfect LgBiT-fused protein is important to determine the experimental background (unspecific signal)

2.2.3 NF-κB Activity Assay: Dual-Luciferase Reporter System

MATERIALS AND REAGENTS

- Cultured HEK293T cells
- Transfection Lipid Reagent (Bio-Rad)
- DNA constructs to test for NF-κB activity stimulation
    - NF-κB reporter vector (Promega, #E8491)
    - pCMV-β-Galactosidase vector for transfection normalization
- Sterile PBS 1X
- Dual-Luciferase Reporter Assay System (Promega, #E1910)
    - Luciferase Assay Buffer II
    - Luciferase Assay Substrate
    - Passive Lysis Buffer (PLB) 5X
- β-Galactosidase II detection kit (Clontech)
- TNFα 10mg/mL
- TD-20/20 Luminometer (Turner BioSystems)

PROTOCOL

1. Seed HEK293T cells on a 6 well plate the day before transfection
2. Transiently transfect each well with 1 µg of each plasmidic DNA encoding for the protein of interest for study. 0,8 µg of NF-κB reporter vector and 0,2 µg of pCMV-βGal vector are co-transfected. Transfection is performed following the protocol *Transient Transfection in Cell Lines (see section 3.1 from these methods)*
3. Wash cells with PBS 1X twice after discarding the medium of the cellular cultures, 24 hours after transfection
4. Add fresh serum-free DMEM, otherwise supplemented
5. Add TNFα 44 hours after transfection. Final working concentration is 10 ng/mL
6. Incubate cells for 4 hours

For cell lysate obtention

1. Remove medium from cultured cells
2. Wash cells using PBS 1X to remove detached cells and residual growth medium
3. Add 250 µL PLB 1X (dilution from stock in Milli-Q water)
4. Scrape cells vigorously and harvest them, tilting the plate and homogenizing using a pipette
5. Transfer cell lysate to a tube
6. Incubate cell lysates in agitation at RT for 30 minutes
7. Centrifuge samples at 13 000 *xg* for 10 minutes
8. Collect supernatant in a fresh tube

For NF-κB reporter activity assay

1. Add 50 µL of prepared Luciferase Assay Substrate (LAS) to a tube for each test we want to perform
    a. Blank
2. Add 50 µL of cell lysate to the tube already containing LAS. Mix by pipetting, avoid vortexing
3. Read luciferase activity in the luminometer
    a. Calibrate and adjust the sensitivity of the luminometer for each experiment using a positive control

For β-Gal activity assay (normalization)

1. Prepare a mix of 196 µL reaction buffer with 4 µL reaction substrate for each condition.
2. Add 30 µL of cell lysate to a tube

3. Add 200 µL of the mix to each tube
4. Incubate for 1 hour at RT
5. Read β-gal activity in the luminometer
    a. Set sensitivity at 30 %

2.3 TOTAL PROTEIN EXTRACTION AND QUANTIFICATION FROM CELLULAR CULTURES

Quantification of protein levels is the most direct measure of protein expression. This is one of the easiest and informative methods to determine the effects of various biochemical modifications (gene mutation, gene overexpression, lack or inhibition of certain protein, effect of drugs or chemical compounds) on our target proteins. In this thesis, these experiments were mostly carried out on transfected cell lines or primary cultures.

To successfully quantify protein levels, a previous protein extraction from our samples is necessary. This extraction consists in the lysis of cells expressing the proteins of interest, by chemical and mechanical means. Lysis solutions containing detergents are used with this aim. Detergent choice is relevant, because the solubilization level of our proteins will largely depend on this decision.

Once the protein extraction is complete, total protein levels present on our sample is necessary. When we talk about protein quantification, we always measure this expression levels relative to the total amount of protein that is present in our sample. Depending on the protein quantification assay to be further performed, the total protein quantification will vary. Nonetheless, in this thesis we have mostly quantified total protein levels using BCA commercial kit or Bradford assays.

MATERIALS

For protein extractions:

- Cellular cultures (cell lines or primary cultured astrocytes) seeded on cell culture plates
- PBS 1X
- Lysis buffer (Triton X-100 1%, NaCl 150 mM, Leupeptin 2 µM, Pepstatin 2 µM, PMSF 1 µM, Aprotinin 1 µM[2]; in PBS 1X)

[2] Leupeptin, Pepstatin, PMSF and Aprotinin are protease inhibitors. These compounds are necessary to avoid protein degradation during cell lysis and protein solubilization. Also, working on ice is recommended for the same reason.

- Cell scraper
- 1,5 mL Eppendorf tubes
- Centrifuge

For protein quantification:

- 96-well cell culture plate
- ELISA microplate reader (Biotek)
- BCA Protein assay kit (Thermofisher Pierce)
- BSA 2 mg/mL

PROTOCOL

For protein extraction and solubilization

1. Wash cells using sterile PBS 1X twice after removing cell culture medium
    - The solubilization process is made entirely on ice or at 4°C to avoid protein degradation.
2. Add 100 µL lysis buffer to the 6-well cell culture plate
3. Scrape cells vigorously and harvest them, tilting the plate and homogenizing using a pipette
4. Transfer cell lysates to a 1,5 mL Eppendorf tube
5. Incubate samples in agitation at 4ºC for 1 hour
6. Centrifuge samples at 13 000 *xg* at 4ºC for 10 minutes
7. Collect supernatant in a fresh tube

For BCA protein assay kit

8. Quantify protein lysates using BCA protein assay kit (Pierce) on a 96-well cell culture plate:
    - Set a standard calibration line with increasing amounts of protein. Duplicates are performed for each concentration point, as well as for each sample
        - Calibration line: 0, 1, 2, 5 and 10 mg of BSA stock diluted in Milli-Q water inside each well
    - Set experimental groups and add 1 µL of sample to each replicate
    - Adjust to a final volume of 10 µL per well
    - Add 200 µL of BCA reagent to all groups

        - Mix 1 µL of reagent B for every 50 µL of reagent A (contained inside Pierce BCA kit)
    - Incubated plate protected from light at 37 ºC for 15-20 minutes
    - Read the reaction at the ELISA microplate reader at a 595nm absorbance
    - Calculate sample concentration using the values obtained for the calibration line

2.3.1 Membrane protein extraction and quantification from brain tissue

For some experiments where the fraction of membrane proteins needed to be enriched, total membranes from mouse brain and cerebellum were extracted.

MATERIALS

For protein extractions:

- Mouse tissue (Brain or cerebellum)
- Homogenate buffer (PBS 1X containing HEPES 25 mM, EDTA 4 mM, Sucrose 250 mM, Leupeptin 2 µM, Pepstatin 2 µM, PMSF 1 µM and Aprotinin 1 µM)
- Polytron
- 15mL glass test tubes
- 15mL falcon
- 1,5 mL safe-lock Eppendorf tubes
- Beckman Coulter Ultracentrifuge with a 70Ti Rotor

For protein quantification:

- 96 well ELISA plate
- ELISA microplate reader (Biotek)
- Bradford reagent (BioRad Protein Assay) diluted 1/5 in H_2O.
- BSA 2 mg/mL

PROTOCOL

1. Place tissue in a 15 mL glass test tube already containing homogenate buffer
    - 8 mL of Buffer are required for every 1 gram of tissue
    - The extraction process is made entirely on ice to avoid protein degradation
2. Homogenize tissue with the polytron
3. Transfer the sample to a 15 mL Falcon tube
4. Centrifuge tissue homogenates at 4 000 *xg* at 4°C for 10 minutes

5. Transfer supernatant to 1,5 mL safe-lock Eppendorf tube
6. Centrifuge at 100 000 xg at 4ºC for 2 hours
7. Discard SN
8. Add 100-200 µL of homogenate buffer to resuspend the pellet, which contains the membrane proteins
9. Quantify protein lysates using the Bradford protein assay:
    - Set a standard calibration line with increasing amounts of protein. Duplicates are performed for each concentration point, as well as for each sample
        - Calibration line: 0, 1, 2, 5 and 10 mg of BSA stock diluted in Milli-Q water inside each well
    - Set experimental groups and add 1 µL of sample to each replicate
    - Adjust to a final volume of 10 µL per well
    - Add 200 µL of Bradford reagent diluted in Milli-Q water at a 1/5 ratio to the wells
    - Read at the ELISA microplate reader, at a 595 nm absorbance
    - Calculate sample concentration using the values obtained for the calibration line

2.4. WESTERN BLOT

The western blot is one of the most common techniques in molecular biology. Its main application is the detection of specific proteins from biological samples. It allows us to obtain information about protein presence and size, as well as several biochemical properties (expression levels, states of oligomerization or phosphorylation). The assay is divided in three major steps. First, an SDS-PAGE electrophoresis separates proteins within the sample based on their molecular weight. In this step, the use of SDS for both the gel and buffers keeps our polypeptides of study in a denatured state. Second, the transference of the proteins from the gel onto a polyvinylidenedifluoride (PVDF) membrane makes them accessible for the antibody detection. Last, the detection of specific epitopes using specific antibodies reveals the proteins of interest.

MATERIALS

For the SDS-Page electrophoresis

- Protein extracts
- Loading buffer LSB 4X (TrisHCl 0,4M pH 6,8, glycerol 80%, SDS 8%, Bromophenol Blue 0,005%)
- β-mercaptoethanol 5% or DTT 100 mM
- Mini–Protean Trans Blot system (BioRad)
- Power supply
- Electrophoresis buffer 10X (Tris Base 250 mM, Glycine 1,92 M, SDS 1%)
- Electrophoresis separation gel buffer (TrisHCl 1,5 M pH 8,8; SDS 0,1%)
- Electrophoresis stacking gel buffer (TrisHCl 0,5M pH6,8; SDS 0,1%)
- Acrylamide/Bis solution 40% (BioRad)
- APS 10%
- TEMED
- Page Ruler protein ladder (BioRad)

For the membrane transference

- Trans-Blot turbo transfer system (BioRad)
- Whatmann paper 3 mm
- Immobilon-P 0,45µm PVDF transfer membrane (Millipore)
- Anode Buffer (Tris-Base 0,3 M, Methanol 20% in H_2O)
- Cathode Buffer (Aminocaproic acid 40 mM, Methanol 20% in H_2O)
- Methanol

For the immunodetection

- Ponceau's solution (acetic acid 5%, Ponceau S 0,1% in H_2O)
- TTBS 1X washing solution (TBS 1X, Triton X-100 0,1%)
- Blocking solution (dry fat-free milk 5% in TTBS 1X)
- Primary antibodies diluted in blocking solution
- Secondary antibodies, HRP-conjugated and diluted 1:5 000 in blocking solution
- ECL western blotting substrate solution. Per each PVDF membrane, combine 1 mL of solution A with 20 µL of solution B
    - Solution A (5mL Tris 1M, 110 µL of Coumaric Acid 90 mM, 250 µL of Luminol 250 mM and 45mL Milli-Q H_2O)

- Solution B (100 µL of H_2O_2 30% and 900 µL of Milli-Q H_2O
- Hyperfilms (Amersham) and cassette
- AI680 machine

PROTOCOL

For SDS-Page electrophoresis

1. Dilute LSB 4X containing the reducing agent into the protein samples
2. Heat samples
    a. At 56°C for 3 minutes for membrane proteins. In this thesis, GlialCAM and VCAM-1 samples were heated at 65ºC
    b. At 95°C for 5 minutes for cytosolic proteins or very stable membrane proteins.
3. Prepare polyacrylamide gels inside 1,5 mm glass plate moulds according to the recipe found in the following table
    a. Separation gel is prepared first. When polymerized, stacking gel is added on top
    b. Isopropanol is added on top of separation gel during polymerization to ensure a smooth, flat edge. It needs to be removed before adding stacking gel solution by washing three times with Milli-Q water
    c. Either a 10-well or 15-well comb are added to the stacking gel in polymerization for proper lane formation

SEPARATION GEL (2X1.5mm gels, 20mL)	**7.5%**	**10%**	**STACKING GEL (2X1.5mm gels, 10mL)**	**4%**
Acrylamide	3.8mL	5mL	Acrylamide	1mL
Running Buffer	5.2mL	5.2mL	Stacking Buffer	2.5mL
Water	11mL	9.8mL	Water	6.5mL
APS	200µL	200µL	APS	200µL
TEMED	20µL	20µL	TEMED	20µL

4. Cast the desired gels at the mini buffer tank and fill with electrophoresis buffer 1X
    a. Electrophoresis buffer 1X is prepared by dilution of the stock buffer in Milli-Q H_2O.
5. Remove the well combs and load the samples into the wells
    a. A protein ladder is added at the first lane next to the samples
    b. Ideally, every well should contain liquid to avoid hydrostatic pressure. LSB 4X can be added into wells that do not contain sample
6. Place the lid on the tank and connect to the power supply
7. Set power at a constant voltage of 100-120V until the desired level of protein migration.
    a. Monitor protein separation based on the protein ladder. Stop when it matches the weight range of our protein or proteins of interest

For membrane transference

8. Hydrate PVDF membranes with methanol in agitation for 3 minutes
9. Assemble blotting cassettes. From the bottom of the box up to the cathode lid:
    a. 3 Whatmann papers, previously soaked in anode buffer
    b. The PVDF membrane, previously soaked in anode buffer
    c. The polyacrylamide gel, previously soaked in cathode buffer
        i. The stacking gel is removed using a plastic spatula
    d. 3 Whatmann papers, previously soaked in cathode buffer
10. Set the blotting cassettes inside the Trans-Blot Turbo blotting instrument. The protocol used is the Bio-Rad pre-programmed standard protocol for 1 or 2 mini gels (25 V, 1 A, 30 minutes)

For immunodetection[3]

11. Stain transferred membranes using Ponceau solution to validate correct protein transference
12. Wash stained membranes with TTBS 1X several times
    a. Ponceau's dye is reversible, and membranes should get back to former color
13. Block membranes with freshly prepared blocking solution at RT for 1 hour

[3] Each wash or incubation step is performed in agitation, excepte for O/N primary antibody incubation

14. Incubate membranes with the primary antibody for either 1 hour at RT or O/N at 4°C
15. Wash membranes with TTBS 1X three times for 10 minutes
16. Incubate membranes with the corresponding secondary antibody at RT for 1 hour
17. Wash membranes with TTBS1X three times for 10 minutes
18. Incubate the membranes with the final combined ECL solution
19. Develop signal using AI680 Imaging System (Amersham, GE)

DATA ANALYSIS

Quantification of protein levels obtained in Western Blot assay

The images acquired for each western blot membranes show protein detection and expression levels. This data is not fully quantitative. However, it is possible to transform this data into quantitative information thanks to software data analysis.

As it was the case for IHC, ImageJ is the software of choice. Using command lines within Image J we can measure the intensity of immunodetection and compare across samples upon normalization from total protein levels.

MATERIAL

- Western Blot images acquired using AI680
- ImageJ software

PROTOCOL

1. Create a rectangular selection around the widest lane within our image
2. Drag the selection to the first signal band from the membrane
3. Go to *Analyze > Gels > Select First Lane*
4. Move the selection onto the following band using keyboard's arrows
5. Go to *Analyze > Gels > Select Second Lane*
6. Repeat steps 4 and 5 for all bands
7. Go to *Analyze > Gels > Plot Lanes*
8. Create a straight line closing the area under the peak for each graph that the software will generate. Each graph equals one lane
    a. The graph will give back a bell-shaped curve. The idea is to connect the points at each end of the bell, once the curve flattens

9. Select the magical wand menu and click on each bell-shaped graph
10. Copy data to our numerical data analysis software
    a. With the aim of normalizing the protein levels of our protein of interest regarding total protein levels, this process should be repeated for either actin or tubulin. Thus, quantitative information should be plotted as a ratio. Otherwise, the obtained quantitative data is not scientifically relevant

2.4.1 Cross-Linking Assays With Cysteine Mutants And Oxidizing Reagents

In this thesis, some of our western blot experiments were aimed at assessing potential interaction between polypeptide chains through cysteine residues. In other words, we wanted to test for the formation of disulphide bonds that would lead to oligomeric structures. This study required several modifications to the standard protocol.

When processing samples following the standard SDS-PAGE protocol, we use reducing agents along with denaturation to ensure that proteins resolve exclusively according to molecular weight. However, when testing proteins that are candidate to establish disulphide bonds, it is important not to treat these samples with reducing agents that would eliminate this interaction. Thus, samples need to be prepared with LSB 4X without reducing agents.

Nonetheless, it is necessary to confirm that resolved structures are dimeric and specifically due to the formation of a disulphide bond. To that end, protein extracts were divided in two groups. The first one was treated with LSB 4X without reducing agents and the samples were heated at 56 ºC for 3 minutes. The second one was treated with the same LSB 4X, although complemented with DTT 100 mM and heated at 95ºC for 5 minutes. DTT is a strong reducing agent, so this treatment breaks the disulphide bonds that may be formed, eliminating its interactions on the protein visualization. Therefore, if the structure observed in the western blot without reducing conditions is specific, it will not be present in the western blot where samples have been treated with DTT.

CYSTEINE CROSS-LINKING ASSAYS USING OXIDIZING REAGENTS

At a structural level, some cysteine residues can be found close enough to form disulphide bonds, but the addition of a redox catalyst boosts the reaction. Hence, disulphide bonds can be induced by adding these compounds to cell cultures. At an experimental level, this technique is known as cysteine cross-linking.

In this work, cells have been treated with Cu(II)-(1,10-phenanthroline)(3) 500 μM in PBS 1X for 15 minutes before the preparation of protein extract as already detailed (see chapter 2.1).

3. CELL CULTURE

Cell cultures are relatively easy, largely accessible, and cost-efficient models for biomedical research. A big part of the experiments carried out in this thesis used cellular models, either commercially available cell lines or primary cultures. Most of the projects featured in this work involved transient expression of proteins in HeLa or HEK293 cells. In addition, we produced primary cultures of astrocytes from the rodent brain. These served as a more relevant model from a physiological standpoint since they allowed for the study of our proteins of interest in an environment where they were endogenously present. However, we developed adenoviral constructs to overexpress (or inhibit) our proteins of interest as well as introducing mutant variations of them to our experiments.

Manipulation of cell lines or primary cultures from animal models were always performed in conditions of sterility with fully equipped laminar flow cabinet. All materials used during these protocols were either disposable or previously sterilized. Cultured cells were kept at 37ºC inside 5% CO_2 sterile incubators.

3.1 TRANSIENT TRANSFECTION IN CELL LINES

To achieve transient protein expression in our cell lines, we performed transient transfection of cDNAs encoding our proteins of interest. With this aim we used Transfectin (Bio-Rad) as a lipid transfection reagent. We used mostly two different cell lines: HeLa and HEK293. On the one hand, HeLa cells are an immortalized epithelial cell line coming from human cervix adenocarcinoma. On the other hand, HEK293 cells are an established cell line derived from human embryonic kidney cells. Both cell lines are cultured in the same conditions: temperature 37°C, relative humidity 90% and CO_2 5%, in Dulbecco's Modified Eagle Medium (DMEM, Biological Industries) supplemented with inactivated FBS 10%, Penicillin/Streptomycin antibiotic solution 1% and Glutamine 1%.

MATERIALS

- Supplemented DMEM
- Opti-MEM Glutamax medium (Gibco).
- HeLa or HEK293 cells seeded on confluent cell culture petri dishes
- Sterile PBS1X
- Disposable sterile serological pipette tips
- 6 well culture plates

- Transfectin Lipid Reagent (Bio-Rad)
- Plasmid cDNAs (3 µg of total DNA per well)
- Trypsin-EDTA 1X (Biological Industries)
- Eppendorf tubes

PROTOCOL

1. Wash cells on confluent cell culture dish using sterile PBS 1X after removing supplemented DMEM for cell culture
2. Trypsinize cells by adding 1 mL of Trypsin-EDTA
3. Seed cells on a 6 well plate at a 35% confluence and add fresh supplemented DMEM
    a. Approximately 400 000 cells per well
    b. After 24 hours incubated, cells should divide and reach an optimal 70-80% confluence
4. Prepare transfection mix
    a. Add 3 µg of the cDNA into an Eppendorf tube containing 250 µL of OPTIMEM
    b. Add 3 µL of Transfectin lipid reagent into 250uL of OPTIMEM (following a 1:1 DNA in µg to lipid reagent ratio)
        i. Since all groups included in the experiment will require this mix, it is recommended to prepare a global working stock keeping this proportions
    c. Combine both volumes in the same Eppendorf tube
    d. Gently mix by inversion and short centrifuge
    e. Incubate at RT for 20 minutes
5. Wash cells to be transfected using sterile PBS 1X after removing supplemented DMEM for cell culture
6. Add 1 mL of OPTIMEM
7. Pipette the combined volume of OPTIMEM-Transfectin-DNA dropwise onto the well containing the cells
8. Gently agitate the plate in a circular motion and place the cells inside the incubator at 37ºC for 4 hours
9. Washed transfected cells using sterile PBS 1X after removing transfection medium

10. Add 2 mL of fresh, supplemented DMEM onto each well
11. Place cells inside the incubator until next experimental protocol

3.2 Generation of Primary Cultured Astrocytes

Primary cultured rat or mouse astrocytes have been the cellular model of choice to study the proteins involved in MLC disease. Since MLC1 protein displays an almost exclusive astrocytic expression, primary cultured astrocytes have been used to study the behavior of endogenously expressed proteins potentially exerting a role in MLC pathogenesis. The protocol to obtain primary cultured astrocytes was adapted from the gold-standard protocol by McCarthy and de Vellis, 1980. The animal handling procedures were approved by the ethic committee of the University of Barcelona and the animal facility of Bellvitge Health Campus.

MATERIALS

- Wistar Rats or C57bl6 *WT* and *Mlc1*$^{-/-}$ mouse P0-P3 pups
- Surgery tools (scissors, microsurgery forceps and surgical blades)
- 100 mm and 35 mm Petri dishes
- Dissection solution (sterile PBS1X containing Glucose 0,6%, BSA 0,3%)
- Sterile PBS 1X
- Sterile 15 mL and 50 mL Falcon tubes
- T25 or T75 tissue culture flasks
- Sterile 5 mL and 10 mL glass pipettes
- 100 μm filter
- Neubauer chamber
- Binocular loupe (Nikon)
- Supplemented DMEM (inactivated FBS 10%, Penicillin/Streptomycin antibiotic solution 1%, Glutamine 1%)
- Trypsine-EDTA 1X (Biological Industries)
- DNAse I (1000 U/ml in NaCl 150 mM)
- Ara C 4 mM (Sigma)

PROTOCOL

For pup dissection (perform everything on ice)

1. Anesthetize P0-P3 rat or mouse pups on ice
2. Euthanize by decapitation using scissors
3. Perform cuts to remove the head epidermis and skull brain
    a. Proceed from the posterior of the head to the anterior end right up to the ocular area
4. Remove the brain with surgery forceps
5. Place the piece on a Petri dish filled with pre-chilled dissection solution
6. Discard the cerebellum, olfactory bulbs and brainstem
7. Cut in half the two hemispheres with only the cortex and the hippocampus remaining
8. Remove all meninges and both thalamus with the help of surgical forceps

For primary culture

9. Transfer the cerebral cortices and hippocampi to a new 35 mm Petri dish
10. Incubated with Trypsin-EDTA at 37ºC for 10 minutes
    a. Proceed inside the culture hood
    b. Dispense 1 mL of Trypsin for every 5 to 6 brains
11. Transfer tissue to a 50 mL falcon tube containing 5 mL of fresh, supplemented DMEM and containing DNAse (stock diluted 1:100)
12. Homogenize by mechanical dispersion with the pipette, in a constant up-and-down motion
13. Centrifuge the sample at 1 000 rpm at RT for 5 minute and discard SN
14. Resuspend the cell pellet in 10mL of supplemented DMEM
15. Filter cell suspension through the µm filter set on top of a 50 mL Falcon tube
16. Seed on cell culture flasks, distributing cell suspension volume
    a. For rat pup brains, we use T75 flasks. We use one flask every three brains and bring cell culture to a final volume of 12 mL
    b. For mouse pup brains, we use T25 flasks. We use one flask every three brains and bring cell culture to a final volume of 4 mL
17. Change medium for the first time 24 hours after the production of the culture
18. Repeat every 2-3 days until the flask is confluent

For astrocyte culture purification

The cultured flasks in DMEM contain the three types of glial cells (astrocytes, oligodendrocytes and microglia). In order to purify the astrocytes, the flasks are subjected to a strong mechanical agitation that will detach any other cell types (250rpm) O/N at 37°C.

19. Cover the confluent flasks with three layers of parafilm to seal them from outer oxygen
20. Place the flasks on a shaker and attach them to the platform
21. Set the shaker to 250 rpm inside an incubator at 37ºC
22. Incubate 12-16 hours (O/N)
23. Discard the medium, containing now all microglial and oligodendrocyte cells in suspension
24. Wash the enriched astrocytes twice with sterile PBS 1X
25. Add Trypsin-EDTA to the cells and incubate at 37ºC for 10 minutes or until cells are detached
    a. 500 µL for T25, 2 mL for T75 flasks
26. Resuspend the detached astrocytes in supplemented DMEM. Mix gently but thoroughly and transfer to a 50 mL Falcon tube. Cells need to be perfectly disaggregated and individualized
27. Count cells in a Neubauer chamber
28. Seed on multi-well plates according to the following numbers:
    a. 60 000 cells in 24-well plates
    b. 200 000 cells in 6-well plates
    c. 1 000 000 cells in 100 mm Petri dishes
29. Replace the cell culture medium every 3-4 days
30. Start AraC treatment once the multi-well plates reach 80-90% confluence. AraC treatment consists in supplementing DMEM with 4 µM of AraC solution (1:1 000 dilution from stock)
    a. AraC inhibits the DNA synthesis, arresting the astrocytes at the G0/G1 phase of the cell cycle. After 3 weeks of AraC treatment the experiments are performed. This is the optimal situation to study MLC1 proper location at cellular junctions (Duarri et al., 2008, Duarri et al., 2011).

3.3 ASTROCYTE TREATMENTS WITH EXTRACELLULAR SOLUTIONS

In several experiments of this thesis, astrocytes have been treated with solutions that reproduce certain physiological conditions to observe the effects of these conditions on our proteins of interest (MLC1, GlialCAM and ClC-2 concretely).

MATERIALS

- Primary cultured rat or mouse astrocytes seeded on 24well plates with coverslips and differentiated with AraC for 3 weeks
- *Physiological solution*: NaCl 122 mM, KCl 3,3 mM, $MgSO_2$ 0,4 mM, $CaCl_2$ 1,3 mM, KH_2PO_4 1,2 mM, HEPES 25 mM, Glucose 10 mM, pH 7,2, 300 mOsm/kg in H_2O
- *Depolarizing or High K^+ solution*: NaCl 60 mM, KCl 60 mM, $MgSO_2$ 0,4 mM, $CaCl_2$ 1,3 mM, KH_2PO_4 1,2 mM, HEPES 25 mM, Glucose 10 mM, pH 7,2, 300 mOsm/kg in H_2O
- *TNFα:* 10 ng/mL

PROTOCOL

1. Wash cultured astrocytes using sterile PBS 1X
2. Add the treatment onto the cells
    a. 1,5 mL per well (6-well plates)
    b. 400 µL per well (24-well plates with cells seeded on coverslips)
3. Incubate for 3 to 6 hours depending on the treatment
4. Proceed with cell processing to perform WB, immunofluorescence, or electrophysiological studies

3.3 ADENOVIRAL PRODUCTION, AMPLIFICATION AND TITERING

Once primary cultured astrocytes are treated with AraC and arrested at G0/G1 phase of the cell cycle, transfection is not an efficient technique to obtain transient expression of the proteins we want to study. The chosen methodology in our lab to solve this problem is the use of an adenoviral expression system. This technology allows us to overexpress proteins or even inhibit protein expression (for instance, using miRNAs to generate knockdown models).

Adenoviruses (Adv) feature several advantages as a tool to express target proteins. While they are relatively easy to obtain and manipulate, both the infection efficiency and the protein expression levels achieved are extremely high.

In our research group we work with ViraPower Adenoviral Expression System (Invitrogen). One of the most interesting features of this ViraPower is that it is compatible with Gateway technology, already established in the lab. In this system, clonation of our genes of interest is targeted into the expression vector pAdV/CMV/V5-DEST. This means that the expression of our insert will be controlled by cytomegalovirus promoter. In addition, the vector contains the 5' and 3' ITRs as well as the encapsidation signal needed for the virion production. Generated adenoviral particles are non-replicative and non-integrative since the vector lacks E1 and E3 viral genes. However, the adenoviral constructs are then transfected into HEK293A cells. This cell line contains a stably integrated copy of E1 necessary for viral generation. These cells will facilitate initial production and amplification of adenoviruses.

MATERIALS

For adenoviral production and amplification

- Adenoviral DNA constructs (pAdV/CMV/V5-DEST vectors containing our inserts, generated by LR reaction)
- PacI enzyme + CutSmart Buffer (NEB)
- DNA purification kit
- Supplemented DMEM + Non-essential amino acids (NE-AA)
- HEK293A cells cultured in DMEM + NE-AA
    - For adenoviral production: cultured on 6-well plates, at a 70-80% confluence (ready to be transfected)
    - For adenoviral amplification: cultured on 100 mm culture plates, close to confluence
- Lipofectamine 3000 transfection reagent kit
- OptiMEM
- 6-well and 100 mm culture plates
- 15 mL and 50 mL Falcon tubes
- 0,2 µm sterile filters
- NUNC cryotubes for -80ºC storage

For adenoviral titering

- 96-well cultured HEK293A cells
- Methanol 100%
- PBS-CM
- Blocking solution (BSA 1% in PBS-CM)
- α-2Hx-2antibody (or any other primary antibody of interest)
- Alexa-conjugated secondary antibody of interest
- Olympus DSU microscope

PROTOCOL

For adenoviral production (perform under the hood and in sterile conditions from step 3 on)

1. Digest 10 µg[4] of verified adenoviral DNA with PacI enzyme, at 37°C for 12-16 hours
    a. This step is aimed at exposing the viral ITRs
2. Purify digested DNA (see chapter 1.2)
3. Transfect 1 µg of digested and purified DNA to HEK293A cells cultured on 6-well plates
    a. Dilute Lipofectamine 3000 reagent in 250 µL OptiMEM medium. A ratio of 3:1 is used as 3 µL of reagent to 1 µg of DNA to transfect. Mix by pipetting
    b. Add the DNA volume to 250 µL of OptiMEM combined with 3 µL of P3000 reagent (1:1 ratio Lipofectamine 3000 to P3000 reagent). Mix by pipetting and incubate at RT for 5 minutes
    c. Combine both volumes, mix by pipetting and centrifuge gently
    d. Incubate at RT for 20 minutes
        i. Wash HEK293A cells to be transfected using sterile PBS1X while transfection mix is incubating
        ii. Add 1 mL of OptiMEM
    e. Pipette the transfection mix dropwise onto the cells. Shake gently in a circular motion before placing the cells inside an incubator at 37ºC O/N

[4] The amount of digested DNA can be increased to 15 µg for constructs giving efficiency problems in the production phase

4. Remove transfection medium 24 hours after transfection
5. Add fresh supplemented DMEM + NE-AA
6. Pass cells onto a 100 mm culture plate 48 hours after transfection
    a. Normally, cells can be detached by gentle pipetting. If necessary, trypsin can be used to this end
7. Harvest medium containing cells when the cytopathic effect of the virus is observed across more than 80 % of the cells. We will detect cytopathic effect because cells swell, eventually round up and detach
    a. This takes around 7 to 10 days after transfection, although it is normal that some adenoviruses take up to 14 days
8. Proceed to put the adenoviral stock through 3 cycles of freezing (-80°C) and thawing in a water bath (37°C)
9. Centrifuge at 3 000 rpm at RT for 15 minutes to separate the cell lysates from the virus in suspension.
10. Retrieve the supernatant (containing the virus in suspension) and filter to obtain the adenoviral stock
11. Divide stock in aliquot cryotubes and store at -80°C

For adenoviral amplification

1. Inoculate 10 µL of the adenoviral stock to a 100 mm cell culture dish with confluent HEK293A cells
2. Harvest medium containing cells when the cytopathic effect of the virus is observed across more than 90 % of the cells
3. Transfer to a 15 mL Falcon tube
4. The viral medium is treated as described in *adenoviral production*, from steps 8 until the end of the protocol

For adenoviral titering by immunocytochemistry (α-hexon antibody or others)

1. Seed HEK293A cells on a 96-well plate (40 000 cells per well) at a final volume of 100 µL per well
2. Culture cells inside a cell incubator at 37ºC for 8-12 hours
3. Infect the viral stock in serial 1:10 dilutions at a final volume of 100 µL per well and incubate at 37ºC for at least and O/N and up to 24 hours
    a. Dispense 10 µL of viral stock to the first well by pipetting against the well wall with the plate tilted

b. Mix gently with the same pipette
c. Replace the tip and repeat the same step. However, this time the 10 µL come from the first well and are added to the second one. Thus, the first well is back to a final volume of 100 µL
d. Repeat these steps up until the last well

4. Remove the cellular medium from each well
5. Leave the cells to air dry for approximately 5 minutes
6. Fix cells with 100 µL of cold methanol 100%. Incubate cells in fixation at -20ºC for 15 minutes
7. Wash cells twice using PBS-CM
8. Block and permeabilize cells using 100 µL blocking solution per well, at RT for 15 minutes
9. Incubate cells with 50 µL primary antibody diluted in blocking solution, at 37°C for 1h
    a. If the adenovirus features an insert with no molecular tag or we lack a proper primary antibody, we use 1:5 of α-2Hx-2. This antibody recognizes a capsid protein of the adenovirus
    b. If we can use a primary antibody, dilution is 1:100
10. Wash cells three times using PBS-CM
11. Incubate cells with 50 µL secondary antibody diluted 1:500 in blocking solution at 37°C for 1 hour and light-protected
12. Wash cells three times using PBS-CM
13. Image cells using an Olympus DSU spinning disk microscope. Fluorescence-positive cells are counted for each dilution
14. Calculate the adenoviral titer in Transduction Units/milliliter (TU/mL) as follows:

$$TU/mL = \% \text{ positive cells counted in dilution X} \times 100$$

3.4 ADENOVIRAL INFECTION IN PRIMARY CULTURED ASTROCYTES

Two main types of adenoviral constructs have been used in this thesis. On the one hand, a few experiments have been based on the use of short hairpin RNA (shRNA) to suppress endogenous protein expression in astrocytes. On the other hand, in the great majority of experiments we aimed at obtaining the overexpression of proteins in astrocytes.

Regarding the first case, the infection of adenovirus containing shRNA for a specific protein requires preliminary optimization. Suppression of protein expression is accepted at a reduction of more than 80% of original protein levels. Therefore, it is necessary to validate what multiplicity of infection (MOI) as well as incubation time are needed to achieve that. In our lab, these conditions are typically set at MOI 1 for 5 days

The second case implies the introduction of these proteins in adenoviral vectors that are stably expressed in the primary cultured astrocytes. In this case, all adenoviruses are infected at MOI 2 for 48 hours before the experiment is carried out.

MATERIALS

- Primary cultured astrocytes, AraC-treated for 3 weeks
- Adenoviral stocks, sterile and titered
- Calibrated automatic pipettes

PROTOCOL

1. Calculate the total amount of adenoviral stock needed to infect the total amount of plated cells, using the titer
    a. TU equal the number of cells that the stock can infect using a mL. The obtained value is the necessary volume to infect cells at MOI 1
2. Replace DMEM containing AraC for the cell culture
3. Inoculate adenoviral stock using automatic pipettes
4. Shake gently and incubate cells as specified for each application
    a. Overexpression: MOI 2, 48 hours
    b. Knockdown: MOI 1, 5 day

RESULTS

1. STUDIES OF THE ROLE OF GPRC5B IN THE REGULATION OF VCAM-1. CHARACTERIZATION OF THE EFFECT OF MLC1 ON THIS REGULATION

1.1 Identification of GPRC5B as a Relevant Protein in MLC Pathophysiology

The first gene that was described to be involved in MLC disease was *MLC1* (Leegwater et al., 2002). Hence, our research group has studied the protein that it encodes, also known as MLC1, since its beginning. Unfortunately, the function for MLC1 is not known. This has been an issue for our study of this protein. To overcome this problem, our group started the study of MLC1 through the identification of its interacting proteins.

Our experimental approach consisted in several proteomic studies. In a first project, we used brain membrane fractions from rat and mice samples. Affinity purifications were conducted using polyclonal anti-MLC1 antibodies, and the purified proteins were analyzed by means of Mass Spectrometry (MS). Using this methodology, we could obtain quantitative results in terms of protein abundance of purified proteins. In the final work, the affinity purifications of two anti-MLC1 antibodies were evaluated. Only proteins enriched more than 10-fold over the obtained amount in the corresponding IgG control were considered. In the two experiments, the Pearson correlation of one protein and MLC1 was r = 0,96. This protein was GlialCAM, and these experiments allowed for the identification of *GLIALCAM* as the second gene involved in MLC disease (López-Hernández et al., 2011a).

The second effort by our research group in these proteomic studies was directed at the identification of GlialCAM partners. Therefore, two anti-GlialCAM antibodies were used in affinity purification experiments. Samples used were also obtained from adult WT rat and WT mice. This time, quantitative MS identified peptides belonging to ClC-2 chloride channel in addition to GlialCAM and MLC1 within the proteins consistently and specifically copurified (Jeworutzki et al., 2012). In this published article, we showed that ClC-2 is present in myelin by immunogold experiments. Interestingly, we also characterized a regulation of ClC-2 by GlialCAM. Indeed, GlialCAM could induce changes in the subcellular localization of ClC-2 and target the channel to cell-cell junctions, both in cell lines and primary astrocytes. Moreover, GlialCAM changed the gating properties of the channel: currents were increased, and the channel switched from inwardly rectifying to conducting almost ohmic currents. This study confirmed GlialCAM as an auxiliary subunit of ClC-2, but we could not provide a detailed molecular mechanism for this regulation.

The most recent published study in this research line featured a refinement of GlialCAM proteomic studies, which led to a detailed GlialCAM interactome. The biggest optimization that was featured in these experiments was the inclusion of samples obtained from *Glialcam*$^{-/-}$ mice. Proteins identified by MS were evaluated based on their abundance, consistency across different antibodies used, and correlated with the purified GlialCAM protein. The used criteria allowed for the identification of 21 proteins constituents of the GlialCAM interactome (Figure 52):

Identified proteins	MLC1 IP
HECAM: Hepatocyte cell adhesion molecule	yes
MLC1: Membrane protein MLC1	yes
Transport/Ion channels	
CLCN2: Chloride channel protein 2 (Clc-2)	yes
CXA1: Connexin 43	no
EAA1: Excitatory amino acid transporter 1 (Glast)	yes
EAA2: Excitatory amino acid transporter 2 (Glt-1)	yes
AT1A2: Sodium/potassium-transporting ATPase subunit alpha-2	yes
S4A4: Electrogenic sodium bicarbonate cotransporter 1 (Nbce1)	yes
TTYH1: Protein tweety homolog1	yes
AT1B2: Sodium/potassium-transporting ATPase subunit beta-2	yes
GTR1: Solute carrier family 2, facilitated glucose transporter member 1 (Glut1)	no
NAC1: Sodium/calcium exchanger 1 (Ncx1)	no
Signalling	
GPR37: Prosaposin receptor GPR37	no
GPR37L1: G-protein coupled receptor 37-like 1	no
GPRC5B: G-protein coupled receptor family C group 5 member B	yes*
Adhesion/Junctions/Trafficking	
TSN9: Tetraspanin-9 (CD9)	no*
GPM6A: Neuronal membrane glycoprotein M6-a	yes
GPM6B: Neuronal membrane glycoprotein M6-b	yes
STX1B: Syntaxin-1B	no
STX1A: Syntaxin-1A	no
SNP25: Synaptosomal-associated protein 25	no

* Identified in MYTH screenings using human MLC1 as bait.

Figure 52. List of proteins belonging to the GlialCAM interactome. Classification according to the protein function is provided. Also, the table features whether the proteins identified in the GlialCAM interactome have also been purified using anti-MLC1 antibodies, as well as whether they have been detected in a MLC1 MYTH screening. Modified from (Alonso-Gardón et al., 2021).

For the first time, GPCRs were retrieved as components of the GlialCAM interactome. These receptors were GPRC5B, GPR37, and GPR37L1. On the one hand, GPRC5B belongs to group IV, family C of GPCRs (Hirabayashi and Kim, 2020). This GPCR displays ubiquitous expression, but it is enriched in the brain, where it has been described to be important for motor learning (Sano et al., 2011, Sano et al., 2018). At a subcellular

level, it is located in the plasma membrane, exosomes and the Golgi apparatus (Kwon et al., 2014). On the other hand, the last two are also orphan receptors that belong to family A of rhodopsin-like GPCRs, also known for being linked to endothelin B receptors (Marazziti et al., 1997, Marazziti et al., 1998). These two GPCRs are highly expressed in the CNS. GPR37 has been observed to negatively regulate oligodendrocyte differentiation (Yang et al., 2016), whereas GPR37L1 would be important for the regulation of neuronal and glial development in the cerebellum (Marazziti et al., 2013). Among the three GPCRs, GPRC5B was also identified both in membrane yeast two-hybrid (MYTH) studies and AP experiments for MLC1. Thus, GPRC5B was considered a bona fide interactor (Alonso-Gardón et al., 2021). Several experiments indicated that GPRC5B regulates GlialCAM and MLC1 expression.

In summary, this study supported the idea of a protein scaffold modulated by GlialCAM/MLC1 involving transporters and ion channels participating in neuronal homeostasis. The identification of GPRC5B within this protein network was consistent with the previously observed role of GlialCAM/MLC1 in signaling pathways controlling astrocyte activation and proliferation. To give an example, MLC1 overexpression has been linked to reduced activation of IL-1β-induced inflammatory signals (pERK, pNF-κB), pathways that are activated by GPRC5B (Elorza-Vidal et al., 2018, Lanciotti et al., 2016). Consistently, the opposing effect was observed in primary astrocytes lacking Mlc1 expression (Alonso-Gardón et al., 2021).

1.2 A Novel GlialCAM Interactor that Depends on MLC1 Presence: VCAM-1

Other previous findings by our group showed that ClC-2 interaction with GlialCAM was significantly reduced in the absence of MLC1, as seen by comparison between co-immunoprecipitation studies in solubilized brain membranes from WT mice vs *Mlc1*$^{-/-}$ animals. This was consistent with the lack of ClC-2 enrichment at cell-cell junctions in primary astrocytes obtained from *Mlc1*$^{-/-}$ animals, together with a lack of changes in gating properties for ClC-2 in the same conditions (Sirisi et al., 2017). As mentioned above, the incubation of WT primary astrocytes in high extracellular potassium concentrations leads to a GlialCAM-mediated targeting of ClC-2 to cell-cell junctions and a change in its electrophysiological properties. Taking this into consideration, we were interested in determining whether there could be more interactors of GlialCAM that were dependent on MLC1 presence.

Thus, in the last project regarding proteomic studies for MLC-related proteins we added *Mlc1*$^{-/-}$ samples in the control groups of these experiments. Comparative affinity purifications were performed on these samples using either anti-GlialCAM antibodies or a new monoclonal anti-MLC1 antibody, which was the only MLC1 antibody that was able to immunoprecipitated ClC-2. **Figure 53** shows the relative abundance of those proteins interacting with GlialCAM in the WT samples compared to the *Mlc1*$^{-/-}$ samples. Noteworthy, only proteins validated for immunoprecipitation with MLC1 are included in the final graph.

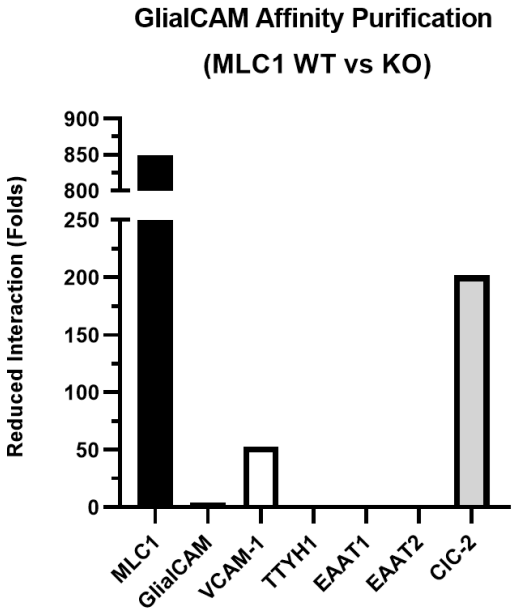

Figure 53. GlialCAM interaction with VCAM-1 and ClC-2 depends on MLC1. The figure shows comparative AP studies using antibodies against GlialCAM in both Mlc1 WT and Mlc1 KO samples. ClC-2 and VCAM-1 were the only two proteins that showed a strong reduction in the quantitative interaction with GlialCAM in the absence of Mlc1. Data represents the interaction folds provided by Logopharm.

Since ClC-2 was retrieved as a protein showing significant differences in its ability to interact with GlialCAM comparing presence and absence of MLC1, we considered that the analysis was robust. Thus, this project enabled the identification of VCAM-1 as a GlialCAM interacting protein that was dependent on MLC1 presence.

Vascular Cell Adhesion Molecule 1 or VCAM-1 is a cell adhesion molecule found in endothelial cells in the brain. The main ligand for VCAM-1 is integrin α4β1, also known as VLA-4, which is present in inflammatory leukocytes (Elices et al., 1990). Indeed, while

its expression is minimal in the normal brain (Miyamoto et al., 2016), VCAM-1 is upregulated in inflammatory conditions. For instance, it is the case for multiple sclerosis (Gimenez et al., 2004). At a physiological level, VCAM-1 participates in leukocyte rolling and transmigration from the bloodstream to tissue. It also regulates T cell activity. Indeed, VCAM-1 is expressed in cytokine-activated astrocytes, both in animal models and primary cultures. The main cytokines inducing VCAM-1 expression are TNF-α, IFN-γ, or IL-1β (Gimenez et al., 2004, Rosenman et al., 1995). Briefly, TNF-α binding to its receptor leads to downstream NF-κB pathway activity, being VCAM-1 among the induced genes by this pathway (Yang and Li, 2000). However, the exact role for VCAM-1 in astrocytes remains unknown.

Unpublished preliminary results from our research group validated the proteomic results (experiments by Dr Xabier Elorza Vidal and Dr Marta Alonso Gardón). First, in brain membranes obtained from WT mice, VCAM-1 could be successfully immunoprecipitated using monoclonal antibodies against MLC1 or GlialCAM. Also, when comparing immunoprecipation using GlialCAM monoclonal antibody in brain membranes obtained from *Mlc1* WT mice vs membranes obtained from *Mlc1*$^{-/-}$ animals, the detected IP levels of VCAM-1 decreased in the second group **Figure 54**.

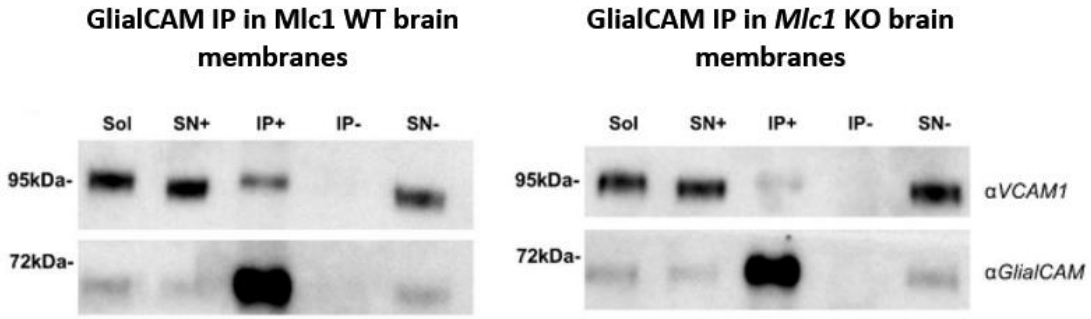

Figure 54. The interaction between GlialCAM and VCAM-1 depends on MLC1 presence. Immunoprecipitation of GlialCAM using the anti-GlialCAM monoclonal antibody in brain membrane fractions obtained from either WT mice or *Mlc1*$^{-/-}$ animals shows that detected levels of VCAM-1 are significantly decreased in KO samples. Data shown comes from three independent experiments. Data obtained by Dr Xabi Elorza Vidal.

Next, we wanted to reproduce VCAM-1 upregulation described in the literature (Gimenez et al., 2004) in our model of primary cultured astrocytes after inflammation stimuli. Indeed, a TNF-α treatment (48h, 10 ng/mL) could induce VCAM-1 protein level upregulation as revealed by WB (Figure 55**A**). Also, the same treatment revealed a shift

in the subcellular localization of VCAM-1 in primary astrocytes: IF assays of control astrocytes showed internalization of VCAM-1 in basal conditions. However, the treatment led to a redistribution of VCAM-1, which reached the plasma membrane and cell-cell junctions **(**Figure 55**B).** Last, the interaction between GlialCAM/MLC1 and VCAM-1 also increased in inflammatory conditions, as revealed by Proximity Ligation Assays (PLA) (**Figure 55**C).

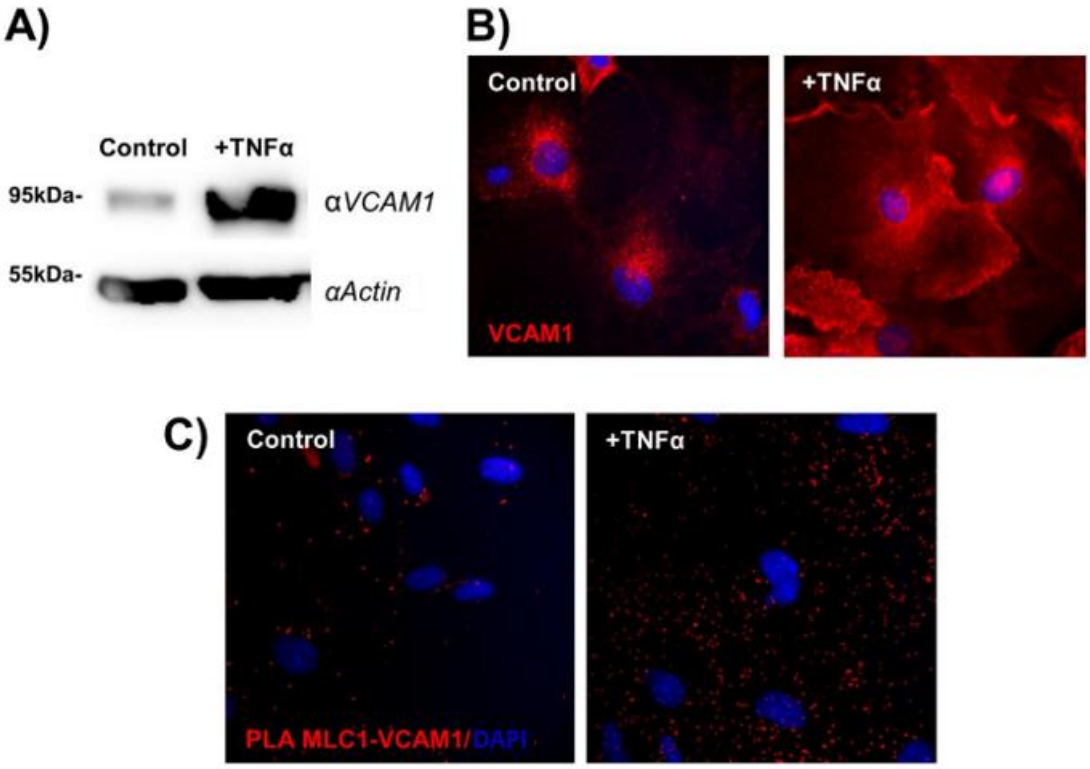

Figure 55. The GlialCAM/MLC1 complex interacts with VCAM-1 in primary astrocytes in inflammatory conditions. A Treatment of rat primary astrocytes with TNFα (10 ng/mL, 48h) leads to the upregulation of VCAM-1 as revealed by western blot. **B** VCAM-1 is enriched at cell-cell junctions in the same TNFα-treated astrocytes. In control conditions, VCAM-1 is internalized and displays a weaker signal. **C** Interaction between VCAM-1 and MLC1 is boosted in primary astrocytes treated with TNFα, as revealed by PLA assay. Preliminary results from Dr Xabi Elorza Vidal and Dr Marta Alonso Gardón.

Afterwards, we worked with the *Glialcam*$^{-/-}$ model to obtain primary astrocytes from these animals. We validated that total protein extracts from *Glialcam*$^{-/-}$ primary astrocytes showed upregulation of VCAM-1 after TNF-α treatment, consistent with what had been observed in WT primary astrocytes. In addition, we addressed VCAM-1 plasma membrane localization by surface biotinylation assays. Interestingly, the surface levels of

VCAM-1 were found lower in *Glialcam*$^{-/-}$ astrocytes, despite showing equal total VCAM-1 expression to WT cells (data not shown). These results indicated that the interaction between GlialCAM and VCAM-1 is somehow important for the proper localization and function of VCAM-1 in inflammatory conditions in astrocytes.

1.3 GPRC5B IN THE REGULATION OF VCAM-1 EXPRESSION

As described in the introduction of this thesis (*see section 3.2.3.1*) the binding of TNF-α to TNFR triggers a signaling pathway that results in NF-κB phosphorylation, which further leads to the induction of VCAM-1 expression.

Alternatively, some researchers saw evidence of a functional link between GPRC5B constitutive signaling and NF-κB activity in the vascular wall that was dependent on Fyn, a downstream effector of GPRC5B signaling. These authors noticed an upregulation of GPRC5B in a context of inflammation (TNF-α stimulation) or high glucose concentrations in cultured immortalized endothelial cells. Consistently, overexpression of GPRC5B in these cells resulted in increased levels of phosphorylation of ERK1/2 and increased activation of NF-κB signaling, responsible for enhanced VCAM-1 protein levels. Furthermore, these effects were Fyn-dependent, since overexpression of GPRC5B that was accompanied by suppression of Fyn showed no effects on NF-κB signaling (Freundt et al., 2022). Complementarily, a study by Kim and colleagues (Kim et al., 2012) identified a mutation in patients suffering from obesity that inhibited the phosphorylation of a Tyrosine residue in the cytosolic C-terminal end of GPRC5B that resulted essential for Fyn activation. The authors showed that SH2 domains of Fyn specifically recognized the Tyrosine residue 383 (referred as Y383) for the kinase activation, since the patient-derived variant (p.Tyr383>Phe, Y383F) was not recognized by Fyn.

The combination of all the evidence available in the literature with both our proteomic results and the obtained preliminary results raised a hypothesis. We reasoned that the VCAM-1 induction by NF-κB signaling modulated by GPRC5B/Fyn could be important in astrocytes. If that were true, we thought that MLC1 could be modulating this pathway somehow. To proceed with this study, we generated both plasmids and adenoviral constructs for GPRC5B WT and Y383F mutant.

First, we tested whether GPRC5B could upregulate VCAM-1 in our system **Figure 56**. Also, we wanted to assess whether GPRC5B is necessary for this upregulation by

depleting endogenous Gprc5b in our cultured cells. We could observe VCAM-1 upregulation after GPRC5B overexpression using adenoviral constructs. Interestingly, these protein levels did not differ from those detected in samples obtained from astrocytes overexpressing GPRC5B while being treated with TNF-α. Last, we repeated this design for Gprc5b depletion, which was achieved using specific shRNA targeting Gprc5b translation. For this group, the evoked VCAM-1 upregulation was lower, reinforcing the idea of the contribution of GPCR signaling in this pathway that results in VCAM-1 expression. Nonetheless, the observed response was the same for untreated astrocytes, where we would have expected VCAM-1 levels like control, untreated astrocytes. Here, we thought that the protocol for adenoviral transduction of miRNA (five days) could result in a unspecific stimulation of NF-κB, maybe due to cell stress and potential inflammatory responses. For this reason, we did not take this group into consideration. The development of a more specific, controlled tool could prove insightful in this experiment.

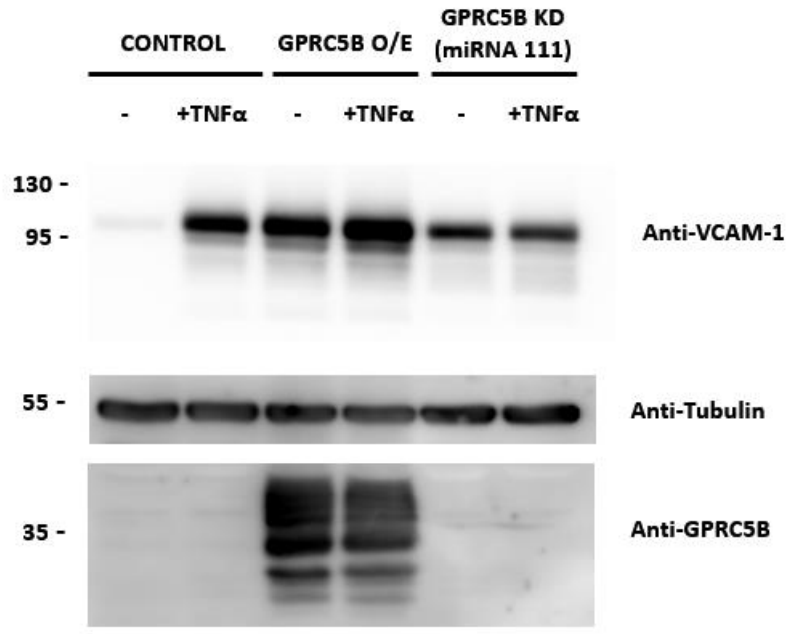

Figure 56. GPRC5B upregulates VCAM-1 in primary astrocytes. Overexpression of GPRC5B using adenoviral particles leads to increased VCAM-1 signal compared to untreated control astrocytes, as revealed by western blot experiments. Elicited VCAM-1 levels corresponded to the obtained levels in TNFα-treated (10 ng/mL, 48h) control astrocytes. Knockdown of Gprc5b lowered VCAM-1 upregulation in TNFα-treated astrocytes. 30 µg of total protein extracts from each group were loaded in 10 % gels. Data is representative of two independent experiments.

1.3.1 GPRC5B Upregulation of VCAM-1 is Dependent on Fyn Kinase

Next, we wanted to analyze whether the increase of VCAM-1 expression induced by GPRC5B signaling was effectively mediated by Fyn activity. With this aim, we repeated the experiments on primary astrocytes. We overexpressed either GPRC5B WT or the mutant GPRC5B Y383F previously described, which Fyn does not recognize (Kim et al., 2012). We repeated both conditions in combination with TNF-α treatment.

The obtained results are featured in Figure 57. Consistent with the preliminary hypothesis, astrocytes overexpressing the mutant variant of GPRC5B did not show VCAM-1 increased levels, contrarily to what happened in astrocytes overexpressing the WT version. Thus, our data supported the idea of a Fyn-dependency of the mechanism by which GPRC5B induces VCAM-1.

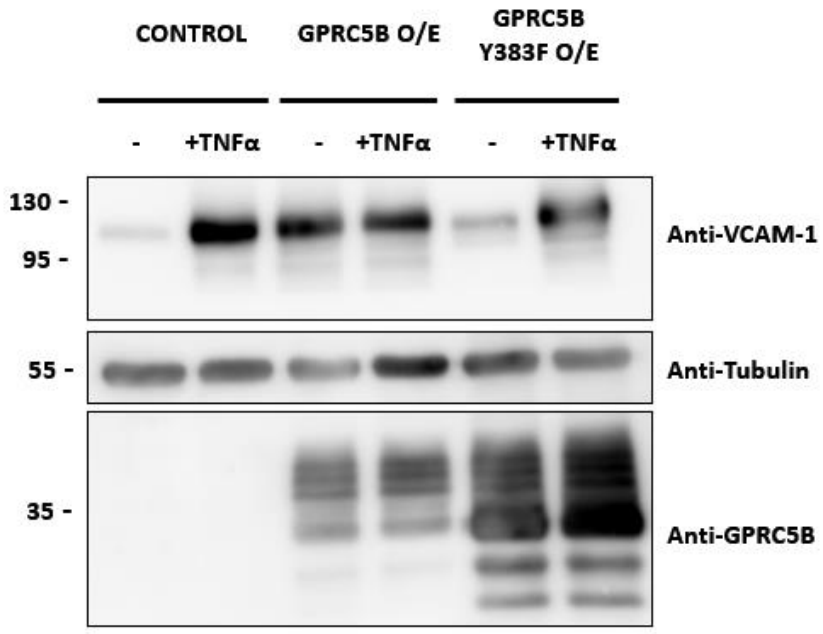

Figure 57. VCAM-1 upregulation induced by GPRC5B is dependent on Fyn activity. Overexpression of GPRC5B Y383F variant using adenoviral particles does not upregulate VCAM-1 signal compared to the effect of the overexpression of WT GPRC5B, as revealed by western blot experiments. Elicited VCAM-1 levels in Y383F overexpression corresponded to the obtained levels in untreated control astrocytes. 30 µg of total protein extracts from each group were loaded in 10 % gels. Data is representative of three independent experiments.

1.3.2 MLC1 Modulates GPRC5B-Mediated VCAM-1 Upregulation

Once we showed that results available in the literature for immortalized endothelial cells are valid for primary astrocytes, we wanted to address whether MLC1 and/or GlialCAM are involved or affect this signaling pathway. In this regard, previous works by our

research group pointed out that ERK signaling is downregulated in astrocytes by the overexpression of human MLC1, while ERK phosphorylation is enhanced in MLC1 KO cells (Elorza-Vidal et al., 2018). Furthermore, MLC1 was found to be inhibiting of NF-κB and ERK phosphorylation in astrocytoma (Brignone et al., 2019). Therefore, we hypothesized that MLC1 would be having a negative modulatory effect on GPRC5B activity. Taking all these data into account, we hypothesized that MLC1 would likely be bound to GPRC5B in the plasma membrane, clustering the receptor and thus hampering its ability to initiate downstream signaling. In turn, this would reduce GPRC5B induction of VCAM-1 upregulation.

To evaluate this hypothesis, we continued working with our astrocytic primary culture system. Thus, we incorporated the test groups of combined overexpression of GPRC5B and human MLC1. The results for this experiment appear on Figure 58. In these experiments, we saw a reduction of VCAM-1 upregulation in untreated astrocytes that were overexpressing the combination of human MLC1 and GPRC5B.

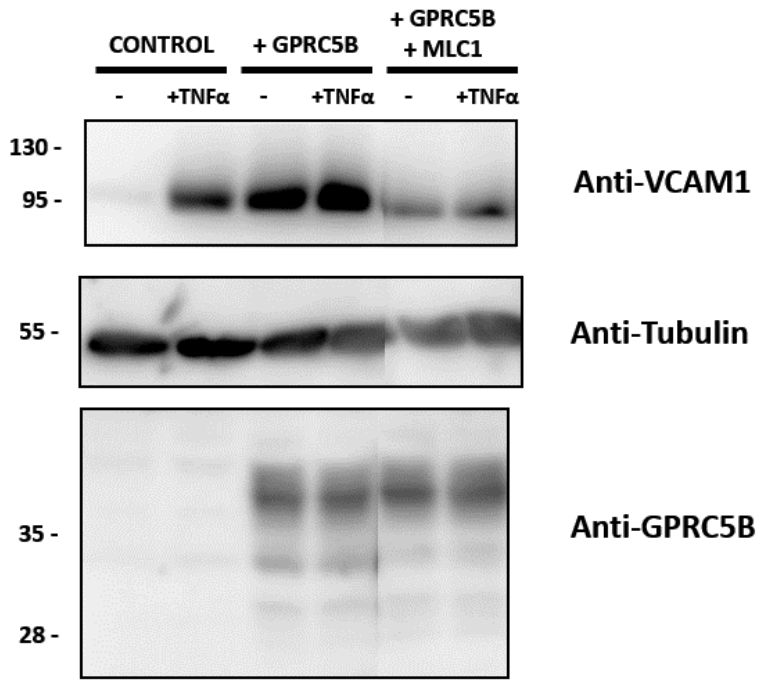

Figure 58. MLC1 modulates GPRC5B-induced VCAM-1 overexpression in primary astrocytes. Combined overexpression of GPRC5B and MLC1 using adenoviral particles results in lower VCAM-1 upregulation compared to the effect of the overexpression of WT GPRC5B alone, as revealed by western blot experiments. 30 µg of total protein extracts from each group were loaded in 10 % gels. Data is representative of three independent experiments.

To further analyze this experiment, we measured the elicited VCAM-1 protein levels for the obtained groups. Using ImageJ software, we measured relative intensity of VCAM-1 WB bands, together with the corresponding Tubulin signal as loading controls. We established a ratio between the two measurements to normalize the obtained values for each group.

The results of this analysis are shown in Figure 59**.** With this quantification we were able to validate the statistical significance of VCAM-1 upregulation in TNF-α-treated cells, the induced upregulation by GPRC5B overexpression, and the lack of expression provoked by the Y383F GPRC5B mutant. This latter observation would confirm that the upregulation is dependent on Fyn activity. Last, we could validate at a quantitative level the negative modulatory effect of MLC1 on GPRC5B-induced of VCAM-1 upregulation. Evoked VCAM-1 levels were around half of VCAM-1 levels induced with TNF-α treatments on rat primary astrocytes. At the same time, observed differences between control VCAM-1 levels and those showed in this group were not statistically significant.

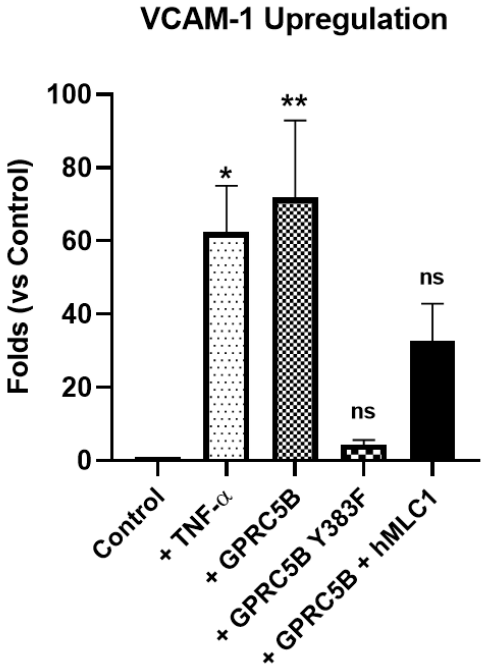

Figure 59. MLC1 exerts negative modulation on GPRC5B induction of VCAM-1 expression. As revealed by ImageJ software analysis for protein quantification, numeric protein abundance data corresponded to what was observed at a qualitative level. GPRC5B overexpression elicited similar VCAM-1 expression levels compared to TNF-α treatment in control astrocytes. On the other hand, GPRC5B Y383F mutant resembled the phenotyp observed for untreated control astrocytes. Combined overexpression of GPRC5B and hMLC1 decreased the induced VCAM-1 levels. Represented data is the intensity folds of normalized VCAM-1 signal respect control levels. Data comes from three independent experiments.

Statistical analysis was assessed using One-way ANOVA with Tukey's Multiple Comparisons Test. * $p < 0.05$, ** $p < 0.01$. Statistical significance corresponds to the comparison with control VCAM-1 levels.

1.4 G-PROTEIN-ALFA-12/13 AND G-PROTEIN-ALFA-I ARE INVOLVED IN GPRC5B DOWNSTREAM SIGNALING

Our experiments seemed to support a modulatory effect of MLC1 on GPRC5B signaling via Fyn, but we reasoned that GPRC5B could be displaying signaling activities through other pathways relevant to astrocyte homeostasis. In fact, some authors had published a study that linked GPRC5B downstream activity to G-protein-12/13, which also highlighted its relevance in neuronal differentiation occurring in the developing mouse neocortex (Kurabayashi et al., 2013).

With the aim of better understanding signaling activities performed by GPRC5B, we engaged in the *in vitro* characterization of several pathways that had previously been related to the receptor. In this project, we worked together with my PhD student colleague Laura Ferigle.

A first line of research tried to reproduce *in vitro* what had been observed for NF-κB pathway and GPRC5B described in the previous sections (Freundt et al., 2022). In the experiments within this project, we used luc2P Reporter Vector with NF-κB Response element from Promega (#E8491) in assays on HEK293T cells. The idea was to achieve successful monitorization of NF-κB stimulation by GPRC5B through transient transfection of the cells, to afterwards replicate *in vitro* the modulatory effect by MLC1 on this GPRC5B stimulation of NF-κB pathway. Having established that, this assay would serve as a screening system for potential signaling partners or proteins participating in these processes linked to MLC pathophysiology. Unfortunately, we could not make this system work because we suffered technical difficulties. In our experiments, we observed that this sensitive was extremely sensitive to cell state, background activity was very high, and negative controls / empty vectors already elicited even higher responses. Hence, we were forced to give up this project.

The second *in vitro* model we tested was the monitorization of this $G_{12/13}$ downstream activity of GPRC5B. To this end, we used specific G-protein constructs for NanoBiT system, in HEK293T cells. Additionally, we were interested in analyzing potential impacts of GlialCAM/MLC1 on the modulation of these signaling processes.

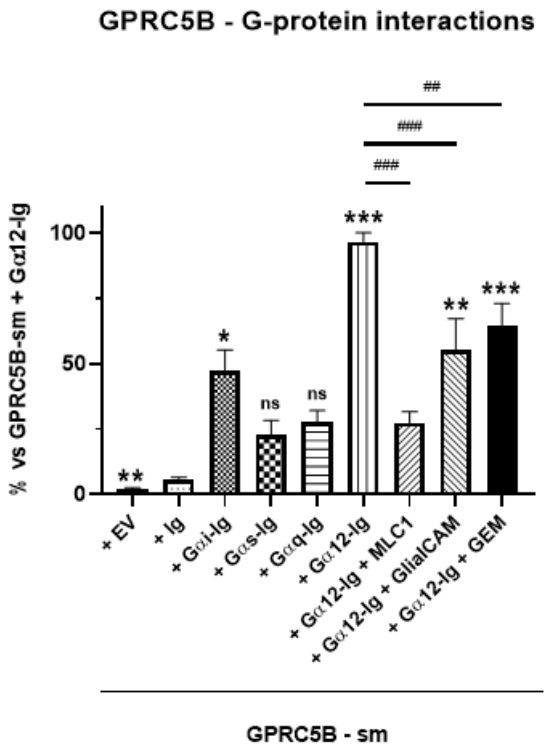

Figure 60. MLC1 modulates GPRC5B interacion with G12/13 in vitro. GPRC5B interacts with G_{12} (but not other G-proteins) in vitro, as revealed by NanoBiT experiments performed on transfected HEK293T cells. However, this interaction is decreased to baseline levels upon co-transfection of NanoBiT constructs and MLC1. This effect is partially observed for GlialCAM and a bit less in GlialCAM/MLC1 at equimolar expression using E2A plasmids. Data comes from three independent experiments. Statistical analysis was assessed using One-way ANOVA with Bonferroni Multiple Comparisons Test. * $p < 0.05$, **/## $p < 0.01$, ***/### $p < 0.001$. * Statistical significance corresponds to the comparison with GPRC5B-smallBiT + longBiT group, # Statistical significance corresponds to the comparison with GPRC5B-smallBiT + $G_{\alpha 12}$ longBiT group. EV = empty vector, GEM = GlialCAM E2A MLC1, sm = smallBiT.

As shown in the experiment depicted in Figure 60, we confirmed that NanoBiT system could reproduce specific $G_{\alpha 12}$ binding to GPRC5B. We used G_i, G_s, and G_q as controls. The unexpected results were that G_i also interacted with GPRC5B. Moreover, we tested whether MLC1 or GlialCAM were interfering with this interaction. We observed that the binding of GPRC5B and $G_{\alpha 12}$ was largely reduced when MLC1 was co-expressed. The differences observed were much lower in the groups of GPRC5B – $G_{\alpha 12}$ co-expression with GlialCAM, and even less pronounced for the co-expression with GlialCAM/MLC1 at equimolar concentrations. However, in all cases the differences regarding GPRC5B-$G_{\alpha 12}$ binding were statistically significant. In conclusion, this experiment supported our hypothesis for the ability of MLC1 to cluster GPRC5B and disrupt its signaling activity via $G_{\alpha 12/13}$.

2. MOLECULAR BASIS FOR THE PATHOGENICITY OF PATIENT-DERIVED MUTATIONS LOCATED IN GLIALCAM IGC2 DOMAIN INVOLVE GPRC5B. ESTABLISHMENT OF GLIALCAM HOMOPHILIC LATERAL INTERACTIONS

As already developed in the introduction of this thesis, Megalencephalic Leukoencephalopathy with Subcortical Cysts (MLC) is a rare genetic disorder. 25 % of the patients bear mutations in the *GLIALCAM* gene (López-Hernández et al., 2011a, Ridder et al., 2011). From a clinical standpoint, two different phenotypes can be observed in MLC patients: the classic phenotype (responsible for MLC2A subvariant if the affected gene is *GLIALCAM*), and the benign or remitting phenotype (responsible for MLC2B subvariant if the affected gene is *GLIALCAM*).

The classic phenotype is due to recessive mutations, whereas the remitting phenotype is due to dominant mutations. Most missense mutations do not alter protein expression, but rather the subcellular localization of GlialCAM at cell-cell junctions (Arnedo et al., 2014a, López-Hernández et al., 2011b).

Among the identified disease-causing mutations in *GLIALCAM*, the only two missense mutations that affect residues located at GlialCAM IgC2 domain are p.Ser196>Tyr and p.Asp211>Gln. However, biochemical characterization of these GlialCAM variants showed that their phenotype differs from the mentioned for most missense mutations. These mutant proteins do not show reductions in protein expression, nor localization defects at cell-cell junctions (López-Hernández et al., 2011a, López-Hernández et al., 2011b). In addition, they interact with both MLC1 and ClC-2. Regarding their interaction with ClC-2, they keep the ability of the WT protein to induce changes in the gating of the channel when the two proteins interact at cell-cell junctions in depolarizing conditions (Arnedo et al., 2014b). We were not able to observe a pathologic phenotype for these mutations.

Other ongoing projects from our group showed that the lack of MLC1 leads to GlialCAM mislocalization, both in *Mlc1*$^{-/-}$ mice (Hoegg-Beiler et al., 2014) and in an MLC patient (Sirisi et al., 2014). However, we had also been unable to replicate this phenotype in our *in vitro* model of primary astrocytes from *Mlc1*$^{-/-}$ mice, where GlialCAM protein was localized at the plasma membrane. At this point, we hypothesized that we lacked the stimulus that is present *in vivo* that could trigger the phenotype. With this aim, former researchers from our group treated these primary cultures with a potassium-enriched solution that would mimic the context of high neuronal activity found *in vivo*. These experiments were successful and the mislocalization of GlialCAM was shown (Sirisi et al., 2014).

Thus, we tried to characterize GlialCAM variants S196Y and D211N for this internalization phenotype in *Mlc1*$^{-/-}$-derived primary astrocytes upon incubation in high extracellular potassium concentrations. These experiments showed that the localization of both variants was not altered in these conditions (**Figure 61**). For the first time, we could see a defective phenotype for these mutations. These variants showed resistance to internalization in the absence of Mlc1 expression.

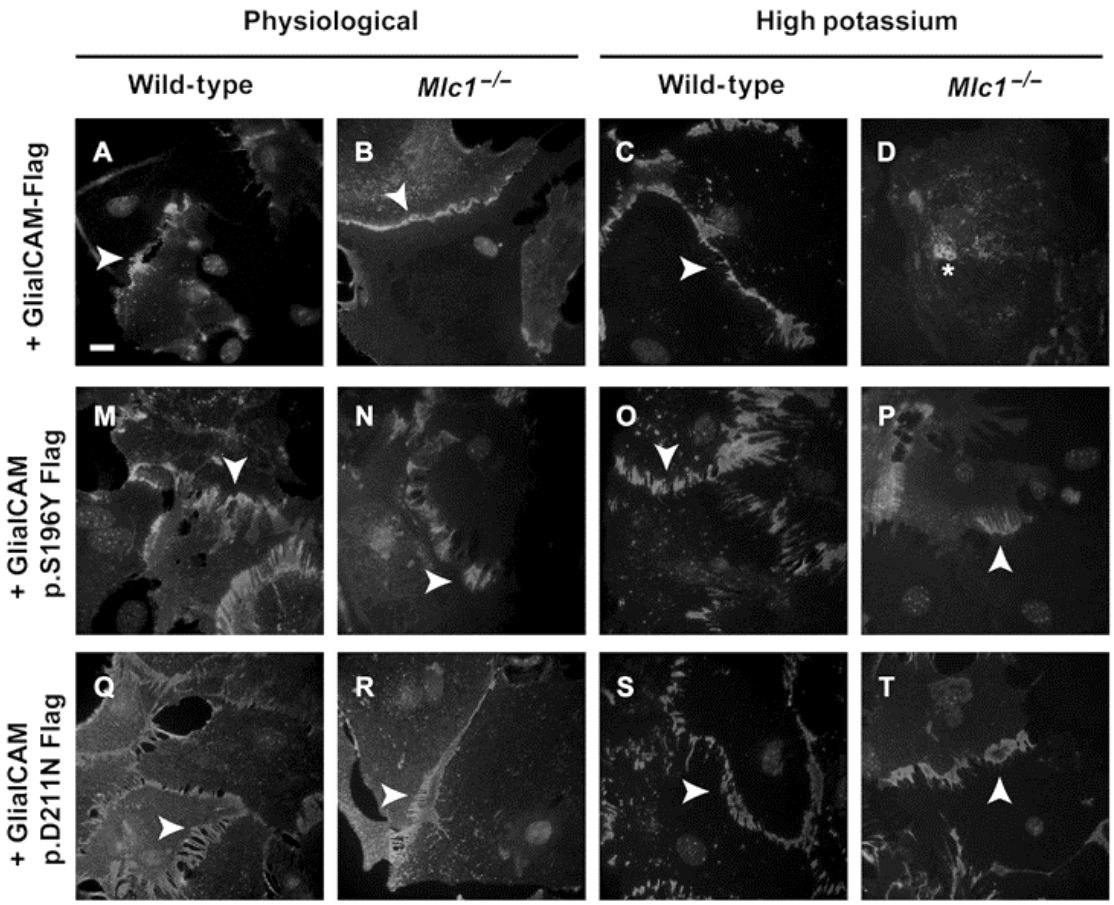

Figure 61. Patient-derived MLC-causing mutations in GlialCAM IgC2 domains always localize at cell-cell junctions. Overexpression of p.S196Y and p.D211N GlialCAM variants in mouse WT astrocytes or *Mlc1*$^{-/-}$ astrocytes reveals proper localization of both variants at cell-cell junctions (marked with arrowheads), which show WT-like behavior. However, both variants are defective for internalization upon conditions of increased potassium concentrations. While WT protein is internalized (labeled with an asterisk), both GlialCAM IgC2 mutants maintain their subcellular localization in depolarizing conditions. Modified from (Arnedo et al., 2014b).

However, we did not know how this phenotype led to disease. Our information up to this point indicated that GlialCAM IgC2 domain was not essential for the intracellular traffic of GlialCAM. At the same time, the domain did not seem to be involved in the interaction

with GlialCAM molecular partners. In this thesis, we tried to understand the mechanism by which this 'gain-of-function' MLC-causing mutations are pathogenic.

2.1 GLIALCAM IGC2 DOMAIN IS RELEVANT FOR PROTEIN LOCALIZATION

First, we wanted to confirm that IgC2 domain is indeed not important in the normal traffic of GlialCAM. We assessed that by heterologous expression of the Flag-tagged WT protein and modifications of the GlialCAM protein lacking IgV or IgC2 domain (**Figure 62**). While the WT protein appeared concentrated at cell-cell junctions with a proportion of 60 %, both the lack of IgV domain or the lack of IgC2 domain compromised this property and reduced it to almost 0. The experiment was carried out by Flag-immunolabeling in transiently transfected HeLa cells. The Flag tag from each protein was detected by means of ICC.

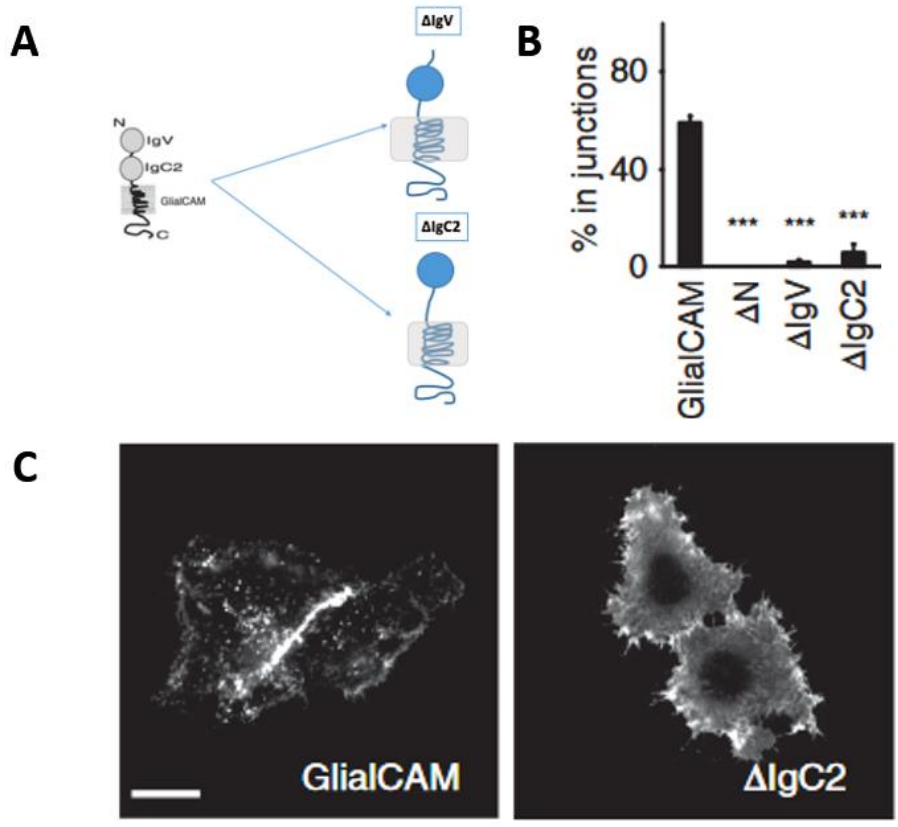

Figure 62. IgC2 is necessary for the localization of GlialCAM protein at cell-cell junctions. A Schematic representation of the DNA constructs lacking either IgV (ΔIgV construct) or IgC2 (ΔIgC2) domain used in ICC assays. **B** Graph showing the proportion of cells displaying each of the analyzed GlialCAM constructs at cell-cell junctions. **C** Representative IF images of HeLa cells expressing WT GlialCAM or ΔIgC2 GlialCAM protein. *Left* GlialCAM at cell-cell junctions, *right* diffuse GlialCAM pattern. Detection of the protein was directed against the Flag tag. Data comes from 3 independent experiments. Unpaired Student's multiple comparison tests were used for statistical analysis. *** $p < 0{,}001$. Scale bar = 20 µm. Modified from (Capdevila-Nortes et al., 2015)

Contrary to what we had hypothesized, IgC2 domain is essential for proper GlialCAM function and behavior. Thus, we wanted to characterize more GlialCAM mutations encoding for amino acids within IgC2 domain, to improve our understanding of IgC2 function. However, very few mutations identified in patients for GLIALCAM encode for residues located at GlialCAM IgC2 domain. Since GlialCAM had been described to be altered in some cancers (Moh et al., 2008), we decided to look up for candidate residues in the COSMIC (Catalogue of Somatic Mutations in Cancer) database. There, we retrieved a list of all described mutations for *HEPACAM* in cancer. Based on the properties of the mutated residues, we selected four candidate mutations/residues of interest (Figure 63).

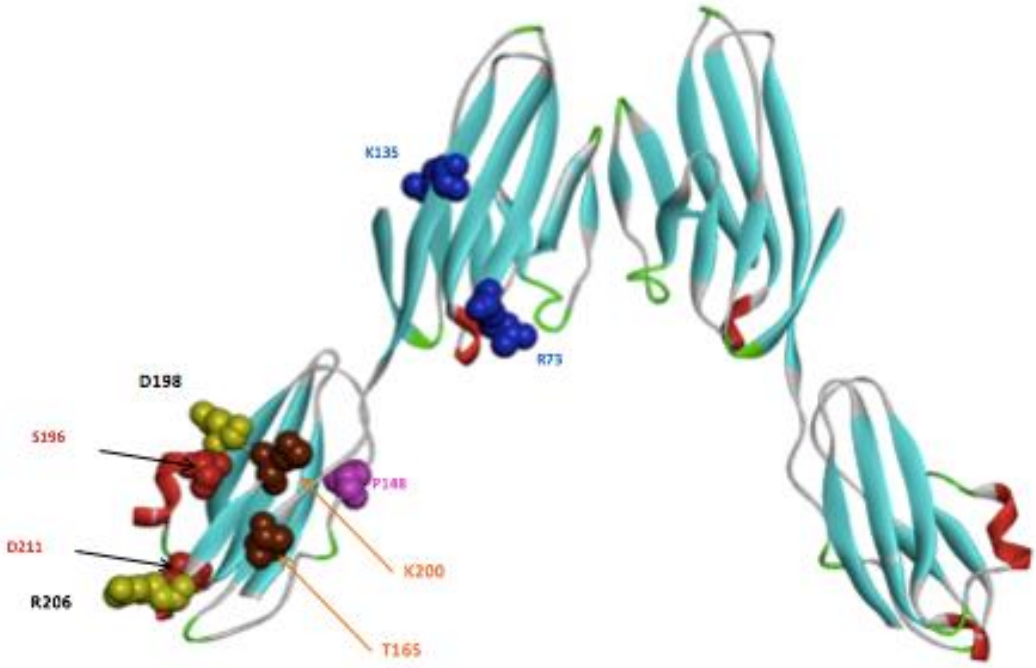

Figure 63. Selected COSMIC mutants for GlialCAM IgC2 domain Residues T165, D198, K200, and R206 were featured in COSMIC database. We selected these residues based on the biochemical properties of the amino acid encoded by the mutant codon. The figure also features residues that are involved in patient-derived mutations (R73, K135, P148, S196).

The selected mutations were p.Thr165>Ile (also T165I in this work), p.Asp198>Lys (also D198K), p.Lys200>Asn (also K200N), and p.Arg206>Cys (also R206C). We designed and cloned *GLIALCAM* coding sequences for each of them, to be able to express them in HeLa cells and characterise the variants. The final constructs included a Flag molecular tag. We expressed them in HeLa cells and performed the same ICC assays against Flag epitope. Results are depicted in Figure 64.

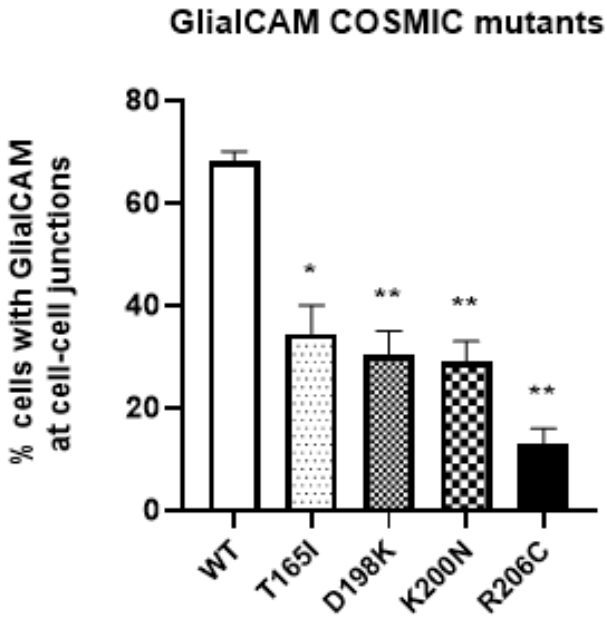

Figure 64. Biochemical characterization of GlialCAM IgC2 COSMIC mutants. COSMIC mutants were defective for localization at cell-cell junctions compared to the WT protein, as revealed by Immunofluorescence assays detecting the FLAG molecular tag attached to GlialCAM variants. Data is representative of two to three independent experiments. Ordinarye One-way ANOVA with Tukey's Multiple comparisons test was carried out for statistical analysis. * $p < 0.05$, ** $p < 0.01$.

GlialCAM WT protein locates at cell-cell junctions with a rate of close to 60 % out of the total amount of analyzed cells. All mutants were defective for this phenotype, being the mutant R206C the one suffering the biggest decrease.

These results confirmed that IgC2 is important for the localization of GlialCAM at cell-cell junctions. Nonetheless, GlialCAM variants for patient-derived mutations did not show a phenotype of mislocalization *in vitro*. Hence, we decided to generate a Knock-in (KI) mouse model for one of these mutations, GlialCAM p.Ser196>Tyr. The model would allow us to decipher whether *in vivo* this variant is properly localized. On the long term, we would also be able to confirm whether the mutation leads to a vacuolizing phenotype in KI animals.

2.2 Generation of an Animal Model of GlialCAM IgC2 Patient-Derived Mutation: p.Ser196Tyr Knock-in Mouse Model

To develop the mouse model for p.Ser196>Tyr KI, we worked with the Transgenic Animal Unit (UAT, *Unitat d'Animals Transgènic*) in Autonomous University of Barcelona (UAB, *Universitat Autònoma de Barcelona*). Our goal was to establish it using

CRISPR/Cas9 technology. Also, for the animal housing, as well as histological and future behavioural studies on these animals, we collaborated with the research group led by Dr Assumpció Bosch.

The general workflow of this facility for KI generation consists in the microinjection of DNA in Embryonic Stem Cells (ESCs) plus injection of blastocysts using CRISPR/Cas9 system. The technique requires the design of short guide RNA (sgRNA), single-stranded oligodeoxynucleotides (ssODNs), and the election of the Cas9 protein. Briefly, sgRNA is the specific RNA sequence necessary for the binding for Cas9 activity while it contains the nucleotide spacer that defines the genomic target to be modified. This spacer is around 20 nucleotides long, usually. On the other hand, ssODNs are the homology-directed repair (HDR) template DNA sequence that we design to be introduced after the targeted double strand break by Cas9. The advantage of ssODNs is that they have been reported to be one of the most efficient donor systems for successful recombination in mammalian cells (Yoshimi et al., 2016, Wu et al., 2013). A visual and schematic summary of the procedure is featured in Figure 65.

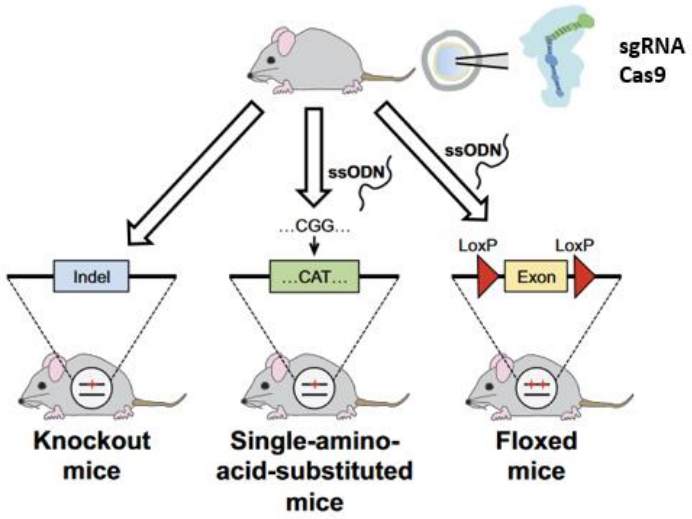

Figure 65. Generation of a Knock-in (KI) mouse model by CRISPR/Cas9 mediated by Homology-directed repair (HDR). The guide RNA is injected in the embryo, together with the Cas9 and ssODNs. The combination of the three elements allows for a non-mosaic mutant model with directed amino-acid substitution. Extracted from (Ma et al., 2017).

The sgRNA needed to be designed considering that *HEPACAM* p.Ser196>Tyr mutation is located in the exon 3. Its sequence is listed below:

*5'*TGCCCATTTCAAGGCCGCAGGTATTAGTGGCTTCAACCACTGTGCTGGAG
CTCAGTGAGGCCTTCACCCTCAACTGCTCCCATGAGAATGGCACCAAGCCTA
GCTACACGTGGCTGAAGGATGGCAAACCCCTCCTCAATGACTCCCGAATGC
TCCTG**TCC**CCTGACCAAAAGGTGCTCACCATCACCCGAGTACTCATGGAAG
ATGACGACCTGTACAGCTGTGTGGTGGAGAACCCCATCAGCCAGGTCCGCA
GCCTGCCTGTCAAGATCACTGTGTATA*3'*

Among the different possibilities, in collaboration with UAT service we decided to design an antisense sgRNA to the underlined sequence. The sequence was the following: *5'*GTGAGCACCTTTTGGTCAG*3'*. Also, to design the ssODN, the whole exomic information was relevant. The codon highlighted in bold within the sequence (TCC) was changed to TAC to confirm the missense mutation and encode for Tyrosine.

With this design, UAT facility injected this CRISPR/Cas9 system into ESCs and blastocytes for the generation of non-mosaic animals (F0). Then, animals were to be genotyped in search of homozygous animals that would allow for the establishment of a homozygous line.

Genotyping of the animals was performed by PCR amplification of DNA extracted from the tail of the animals. The amplified DNA fragment was 540 bp long. To screen for homozygous animals for the KI missense mutation, RsaI restriction enzyme was used. In Figure 66, we see a first round of screened animals. While the whole DNA was 540 bp, digested WT DNA would give a pattern of fragments consisting of three bands (268 bp, 249 bp, 23 bp), and digested KI DNA would give a pattern of four bands (268 bp, 215 bp, 34 bp, 23 bp). The agarose gel with the extracted DNA further digested with the enzyme revealed only one clear candidate for being homozygous for the KI (animal 90), whereas two animals seem to be heterozygous (animals 91 and 95) **Figure 66**. Complementary gels were prepared to better decipher the low molecular weight bands (not shown).

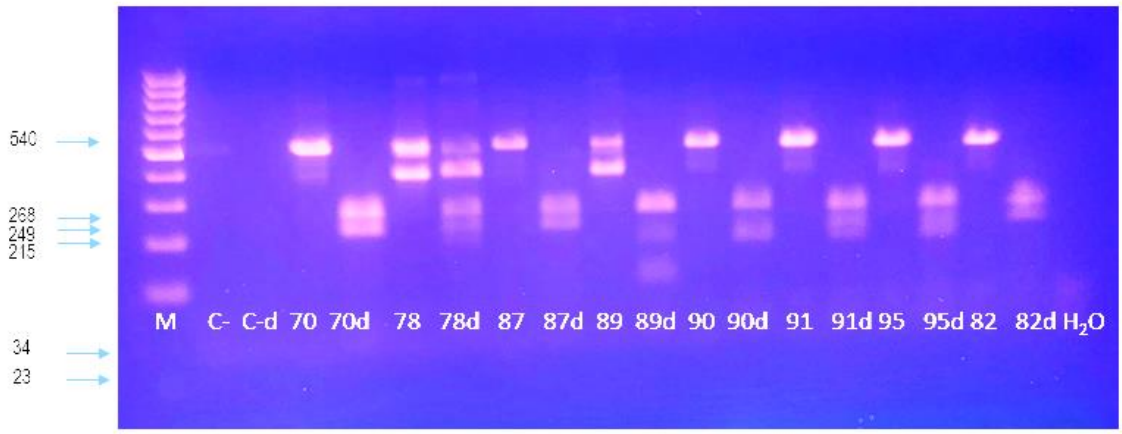

Figure 66. Screening of F0 animals for GlialCAM KI generated by CRISPR/Cas9. RsaI-digested DNA samples obtained from the animals were loaded in an agarose gel for low molecular weight samples. DNA coming from a homozygous KI animal would give a pattern of 268 bp, 215 bp, 34 bp, and 23 bp. Only animal 90 fits the pattern. 91 and 95 are candidate for heterozygous carriers. Samples for each animal were loaded undigested and digested (lanes represented as *X* and *Xd*, where *X* stands for animal number and *d* for digested).

Animal 90 was confirmed to be heterozygous after DNA sequencing. This animal would be further bred to establish the animal line. Analyzing the offspring between putative homozygous KI animals with WT animals also leads to confirmation of the animals being bred, based on the percentage of animals displaying each phenotype.

At the time this thesis is being written, the line has been successfully established and it is fertile, giving enough homozygous offspring. We still do not have animals old enough to proper screen for vacuole formation, which is developed at an animal age of around 12 months. Nonetheless, we performed Hematoxylin-Eosin stainings (HE) on cerebellar slices from KI animals at 6,5 months of age, as an intermediate timepoint. The results of the histological analysis are depicted in **Figure 67**.

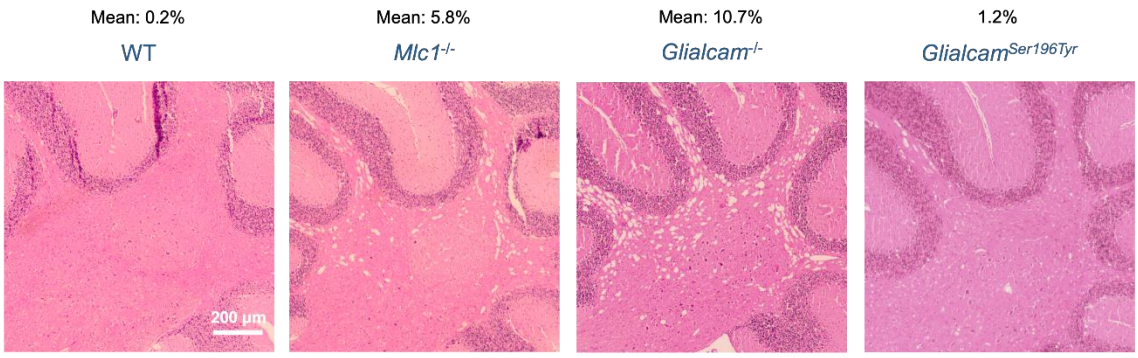

Figure 67. Glialcam KI mouse seems to develop vacuoles in slices of the cerebellum. HE stainings performed on slices of WT, *Mlc1*$^{-/-}$, *Glialcam*$^{-/-}$, and *Glialcam*^{Ser196Tyr} animals at 14 months of age, except

for KI mice which were 6,5 months old. Animals lacking *Glialcam* display the most vacuole formation, whereas animals lacking *Mlc1* display barely half the number of vacuoles. The analyzed animal for KI genotype already displayed vacuoles, but the percentage is still not comparable to the other groups due to lack of age equivalence. Experiments performed in collaboration with Alejandro Brao, PhD student from Dr Assumpció Bosch group.

Although it is important to highlight that only one animal was analyzed, it did show observable and clear vacuoles already formed. We would expect this phenotype to be even more progressed had the animal arrived at the year of age. Nonetheless, we cannot predict the percentage of white matter affected at 12 months of age based on these results. If they were to be repeated, we would confirm that the KI animal is a proper model for the study of the phenotype and pathophysiologic mechanisms underlying MLC disease.

Furthermore, we used the cerebellar slices for KI animals at this time point of 6,5 months of age to analyze the potential effect of the KI mutation on the physiology and biology of MLC-related proteins can be assessed before this timepoint. To do that, we performed immunofluorescence (IF) assays. In this regard, the localization of MLC1, ClC-2 and GlialCAM in Bergmann Glia in the cerebellum of a KI animal are featured in Figure 68. The experiment reveals proper localization for all proteins. Therefore, they support the idea that GlialCAM patient-derived IgC2 mutations are not defective for protein localization at cell-cell junctions, and the pathogenic mechanism does not include the mislocalization of any of the proteins within the ternary complex we described in previous publications (Sirisi et al., 2017).

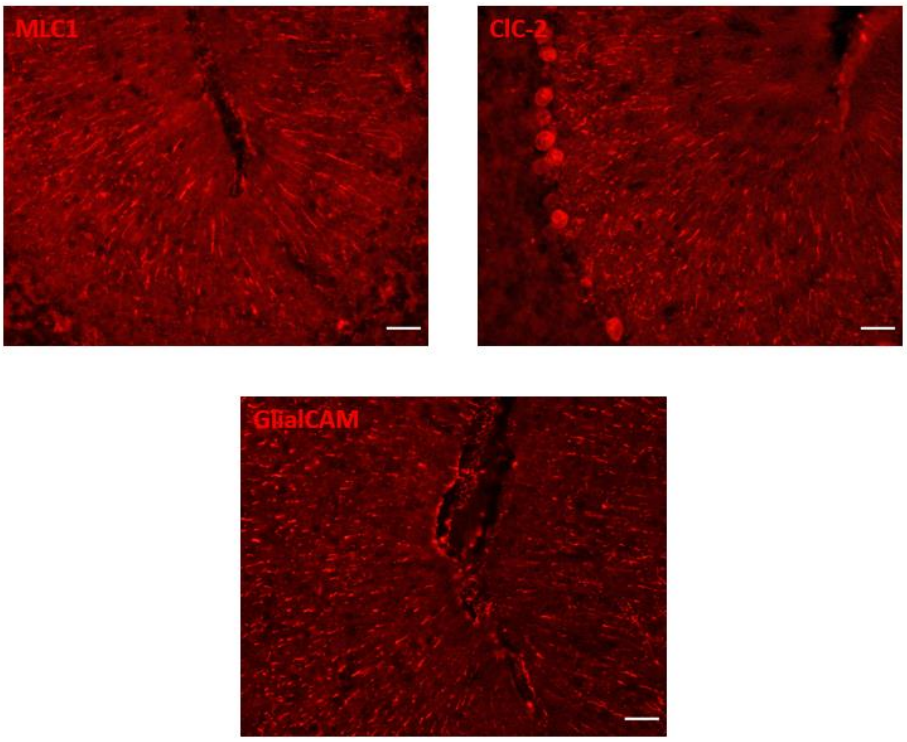

Figure 68. MLC1, ClC-2 and GlialCAM are properly localized in the Bergmann Glia of KI animals. Inmunofluorescence assays on cerebellar slices from GlialCAM p.Ser196>Tyr KI mice at 6,5 months of age reveal that all three proteins display the same localization in Bergmann Glia as happens in WT animals, as previously published (Hoegg-Beiler et al., 2014, López-Hernández et al., 2011a). Thickness of tissue sections = 12 µm. Scale bar = 100 µm. Experiments performed in collaboration with Alejandro Brao, PhD student from Dr Assumpció Bosch group.

2.3 GPRC5B Activity Modulates GlialCAM Endocytosis

Previously in this section, we reviewed the GlialCAM phenotype observed in primary astrocytes: WT GlialCAM protein is mislocalized upon incubation in depolarizing conditions in cells obtained from *Mlc1*$^{-/-}$ animals. In line with these results, simultaneous ongoing experiments carried out by Dr Xabier Elorza Vidal made uncovered that GPRC5B overexpression induces GlialCAM endocytosis in the absence of MLC1 in depolarizing conditions, in primary astrocytes obtained from *Mlc1*$^{-/-}$ animals (**Figure 69**). Since the observed phenotype for GlialCAM matched in the two situations, we reasoned that these two processes might be connected. Thus, we hypothesized that GPRC5B could be participating in the induction of GlialCAM endocytosis. Moreover, we thought that GPRC5B could be interacting with GlialCAM, and that this complex would be endocytosed for signaling.

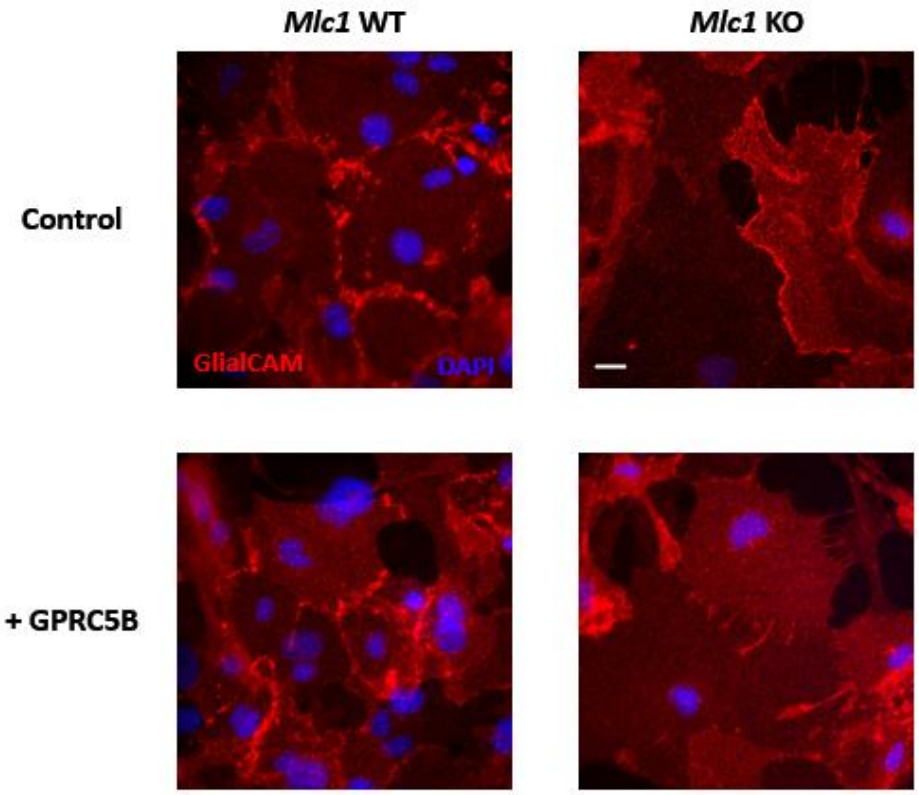

Figure 69. GPRC5B leads to GlialCAM endocytosis in the absence of MLC1. WT GlialCAM is localized at cell-cell junctions in primary astrocytes, both in WT astrocytes (*upper left panel*) and in *Mlc1*$^{-/-}$ astrocytes (*upper right panel*). When GPRC5B is overexpressed using adenoviral constructs, however, GlialCAM is internalized in the absence of MLC1 (*lower right panel*), but not in WT cells (*lower left panel*). Images are representative of three independent experiments. Scale bar = 20 µm. Experiments performed by Dr Xabi Elorza Vidal.

We tested this hypothesis *in vitro*. We expressed the patient-derivad GlialCAM variants in HeLa cells, both alone and in combination with GPRC5B. We analyzed the cells by ICC detecting the Flag tag attached to each GlialCAM construct. As we can see in the results plotted in Figure 70**,** the internalization of neither of the GlialCAM mutated proteins could be induced by GPRC5B, unlike what happened for the GlialCAM WT protein. Importantly, the experiments confirm that all proteins reach the plasma membrane and behave normally. The only observed difference in phenotype was this resistance to endocytosis.

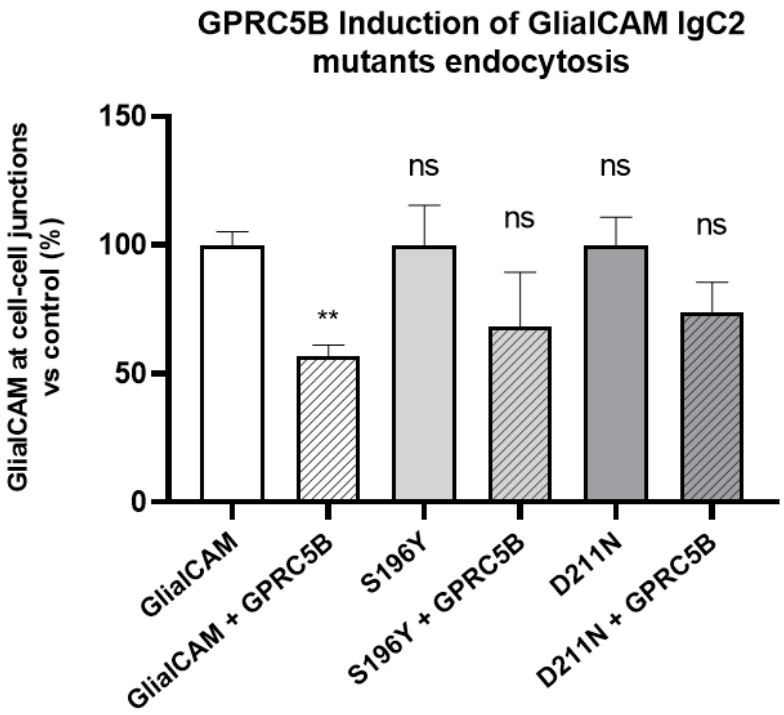

Figure 70. GPRC5B does not induce internalization of GlialCAM IgC2 variants. Immunofluorescence assays on transfected HeLa cells showed that GPRC5B induces the internalization of WT GlialCAM protein, but not of patient-derived GlialCAM IgC2 mutant variants. The graph shows the phenotype of GlialCAM enrichment at cell-cell junctions for each variant, either alone or in co-expression with GPRC5B. The values expressed are percentage of localization in relation to the control WT GlialCAM protein. Data comes from three independent 4 to 7 independent experiments. Statistical analysis was performed as One-way ANOVA with paired comparisons (Sidak's multiple comparisons test) between the two conditions for each variant. ** $p < 0.01$, ns = not significant. Experiments performed in collaboration with Laura Ferigle.

One interpretation to these results could have been a lack of interaction between the tested GlialCAM variants and GPRC5B we analyzed whether GlialCAM S196Y and D211N variants can interact with GPRC5B, to confirm the specificity of the obtained information. We approached this idea by means of Split-TEV assays, which are summarized in **Figure 71**.

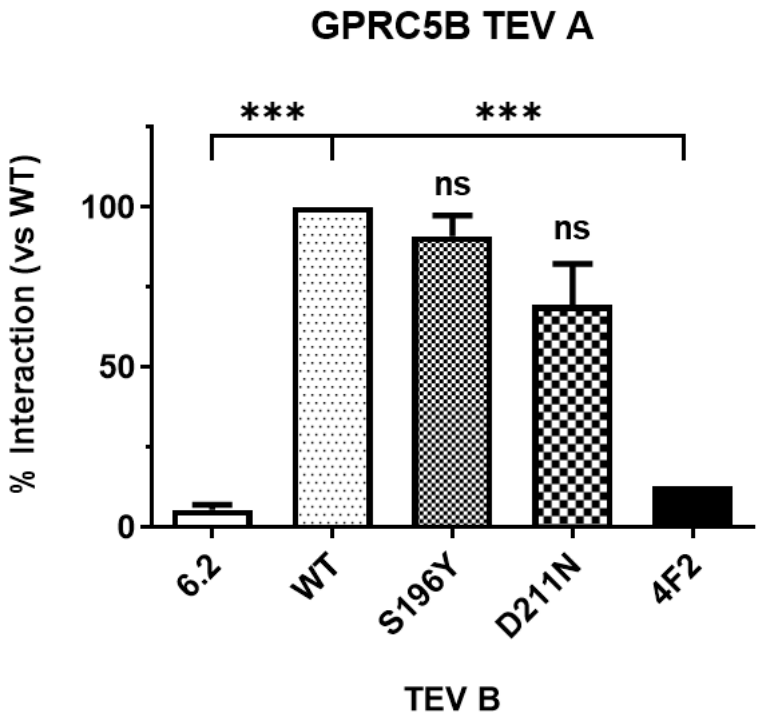

Figure 71. GlialCAM S196Y and D211N variants are not defective for their ability to interact with GPRC5B. Split-TEV assays analyzing the ability of GlialCAM IgC2 patient-derived variants to interact with GPRC5B in transfected HeLa cells. Data indicates the average percentage of interaction shown by each protein related to the interaction showm by GlialCAM WT protein. Empty vector 'pcDNA6.2TK' and 4F2 were used as control groups. Data comes from three independent experiments. Statistical significance was addressed by One-way ANOVA with Bonferroni post-test. ns = not significant, *** $p < 0,001$. Experiments performed by Dr Marta Alonso Gardón.

Since GlialCAM IgC2 mutants maintain direct interactions with GPRC5B, our data supports the idea of GPRC5B actively playing a role in the endocytosis of GlialCAM protein. In this regard, GlialCAM IgC2 patient-derived mutants would be resistant to the induction of GPRC5B-mediated internalization. However, we wanted to understand how these mutations confer resistance to endocytosis to GlialCAM protein.

2.4 Lateral Interactions Between Adjacent GlialCAM IgC2 Domains Lead To GlialCAM Oligomerization

As a result of our established collaboration with Dr Juan Fernández-Recio, a bioinformatic model of the extracellular region of the GlialCAM dimer was available in our lab. This model was obtained in two stages. First, a monomer model was genereated by homology modeling based on CAR protein due to its homology with GlialCAM. Then, a docking modeling was applied using the monomer model. After both processes, biochemical experiments were performed to validate the models. This allowed for the

optimized final GlialCAM homo-dimerization model, featured it in one of our published works (Elorza-Vidal et al., 2020).

A closer examination of this model for this thesis made us realize that the residues encoded by both patient-derived mutations are located in each of the two outward-facing α-helices contained in GlialCAM IgC2 domain. In the literature, some authors described the property of other similar IgCAMs to form zipper-like structures through lateral interactions between IgC2 domains (Kamiguchi and Lemmon, 2000). Based on this feature together with the importance of *cis*- and *trans*- interactions for GlialCAM (Elorza-Vidal et al., 2020), we hypothesized that IgC2 domain in GlialCAM could also be responsible for lateral interactions essential for GlialCAM oligomerization, necessary for the correct function of the protein. Hence, we reasoned that these α-helix motifs might be involved in these putative lateral interactions.

To address whether GlialCAM IgC2 domains show lateral interactions to form oligomeric structures, we engaged in mutagenesis studies. The first of the two helices will be referred in this manuscript as α-helix 1. It comprises residues from 191 to 196. The second, referred to as α-helix 2, is smaller and comprises residues from 209 to 211. The detailed list of the residues that conform these two motifs is in Figure 72**,** whereas the models for predicted lateral interactions and the position of the residues conforming both α-helices are featured in **Figure 73.**

α-helix 1		α-helix 2
Serine 191	Leucine 194	Methionine 209
Arginine 192	Leucine 195	Glutamic acid 210
Methionine 193	Serine 196	Aspartic acid 211

Figure 72. List of residues candidate for lateral interactions from the two outward-facing IgC2 α-helices.

Specifically, our experimental approach was to design individual GlialCAM mutants for each amino acid to replace it with a cysteine. The idea was to assess whether any of the newly introduced residue is close enough to its counterpart in the adjacent IgC2 domain to establish disulfide bonds. These experiments are also known as cross-linking assays.

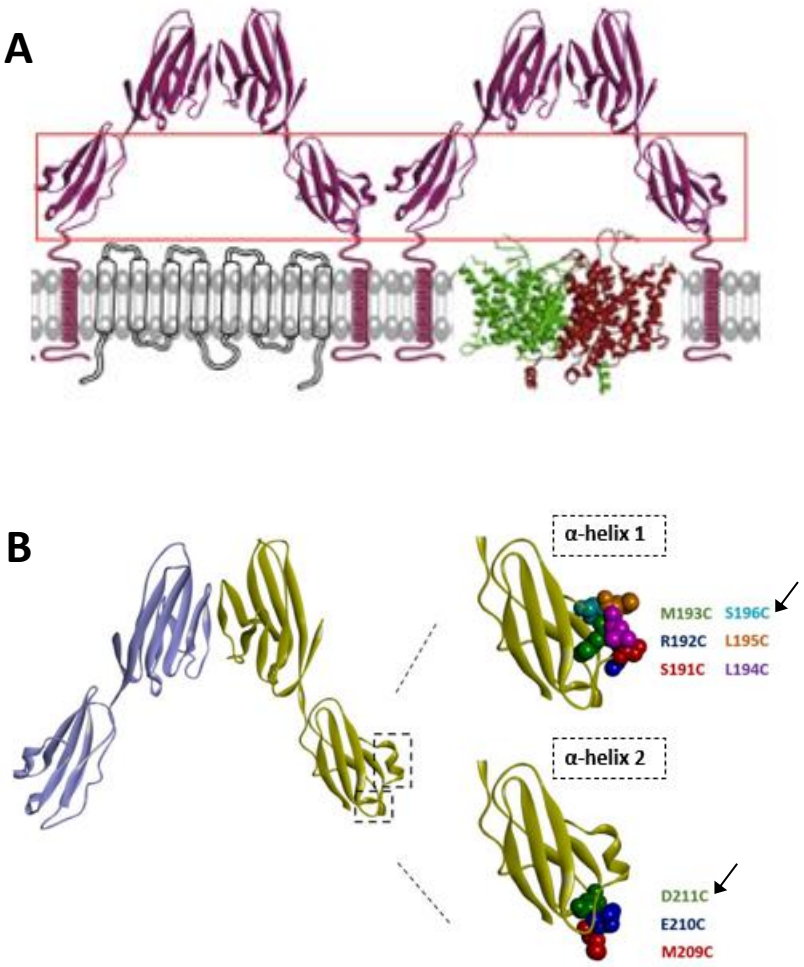

Figure 73. GlialCAM IgC2 motifs hypothesized to be establishing lateral interactions. A Model for GlialCAM zipper-like structures and oligomer formation via IgC2 lateral interactions (red box). **B** Zoom of the two α-helices displaying the selected residues as colored spheres. Arrows point at residues that are originally affected in patient-derived mutations (S196Y, D211N).

Our aim was to characterize the phenotype for these GlialCAM mutants by means of ICC and WB. WB experiments were also carried out in the absence of reducing conditions to ensure integrity of putative disulfide bonds. In addition, protein extracts were split in two groups and loaded in separate polyacrylamide gels. In one of the groups samples were treated with DTT as a strong reducing agent, in order to determine the specificity of dimers that could appear in the untreated samples provided that cysteine mutants formed lateral interactions as hypothesized. Interestingly, specific dimers appeared in cysteine mutants in both helices. Among them, the more evident residues were Ser191, Arg192 (α-helix 1) and Glu210 (α-helix 2). However, almost all cysteine mutants suggested to be establishing disulfide bonds as revealed by the membrane in which untreated protein was detected (Figure 74).

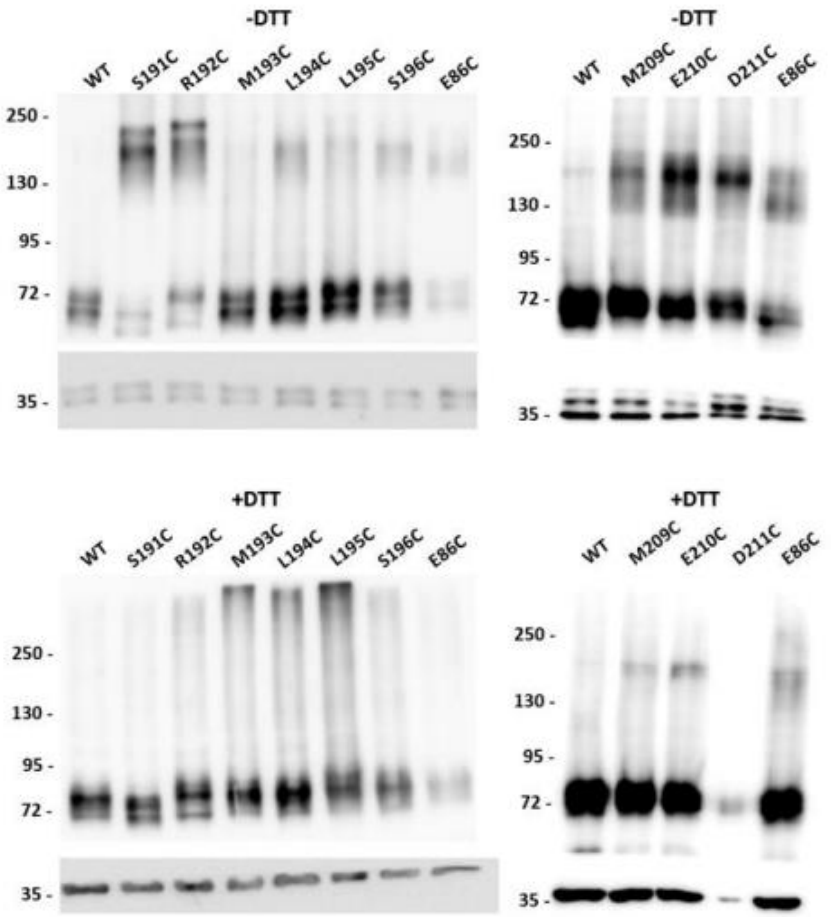

Figure 74. GlialCAM IgC2 cysteine mutants from α-helix 1 and α-helix 2 form cross-links. Dimeric structures could be observed for most of the cysteine mutants transfected in HeLa cells, as revealed by western blot experiments. 30 µg of cell protein samples were loaded in a 7,5 % gel. Samples were split in two groups, one of which further treated with DTT 100 mM and heated at 95ºC. This step was aimed at ensuring specificity of dimeric structures. E86C variant was used as positive control for specific cross-link formation, as it had been previously validated in the lab. Dimer formation (ca. 145 kDa) was confirmed for variants S191C, R192C, E210C, and D211C. For all experiments, detection was directed against the FLAG tag of the variants. Actin (35 kDa) was used as a loading control. Data comes from three independent experiments. Experiments performed in collaboration with Dr Efren Xicoy Espaulella.

Interestingly, this had a moderate correlation with what we could observe in immunofluorescence assays. GlialCAM mutants S191C, R192C, E210C and D211C showed an increase in the proportion of cells displaying the phenotype of enrichment at cell-cell junctions for the Flag-tagged protein detected in transiently transfected HeLa cells. However, only the mutant S191C did so in a statistically significant manner, with over 90 % of the cells displaying the GlialCAM protein targeted at junctions (**Figure 75**).

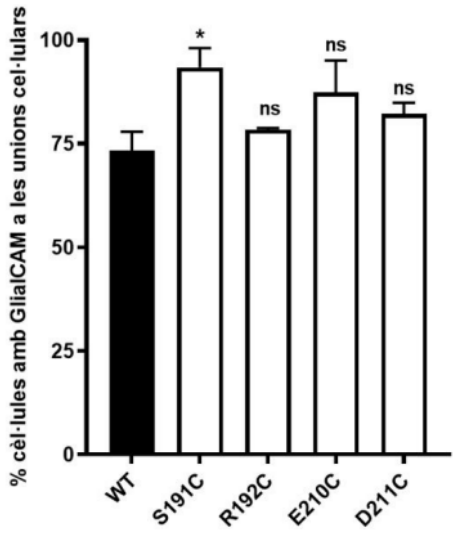

Figure 75. GlialCAM Cysteine-mutants that show dimerization appear enriched at cell-cell junctions. The graph shows the percentage of cells displaying each of the tested GlialCAM variants at cell-cell junctions, as revealed by Immunofluorescence assays detecting the FLAG molecular tag attached to GlialCAM mutants. Data corresponds to the mean for each group, together with SEM. Statistical significance was addressed by One-way ANOVA with Bonferroni post-test. Data comes from three independent experiments. $p<0,05$. Experiments performed in collaboration with Dr Efren Xicoy Espaulella.

2.5 Resistance To Endocytosis As a Proposed Mechanism For GlialCAM IgC2 Mutations Pathogenicity

Next, we wanted to find out whether this phenotype was accompanied by resistance to internalization in primary astrocytes, as occurring with disease-related GlialCAM variants. We generated adenoviral constructs for the GlialCAM variants that were more evidently forming dimeric structures, as revealed by WB experiments. Indeed, we generated the constructs for GlialCAM S191C and GlialCAM E210C and used them to infect primary cultured astrocytes. We wanted to address whether these mutants were perfectly localized at cell-cell junctions even after treatment with a potassium-enriched solution, as was described to happen in the constructs for the patient-derived GlialCAM variants.

The results confirmed such functional link. As Figure 76 shows, the control group of WT-Infected *Mlc1*$^{-/-}$ primary astrocytes showed GlialCAM internalization after treatment with depolarizing solution. Mutant S196Y was used as a control, and it was observed to be resistant to this internalization, as expected. Interestingly, the same occurred for the two cysteine-mutants. Therefore, these experiments confirmed that an abnormal/gain-of-

function-like stabilization of oligomeric structures at the plasma membrane is linked to the phenotype of the disease.

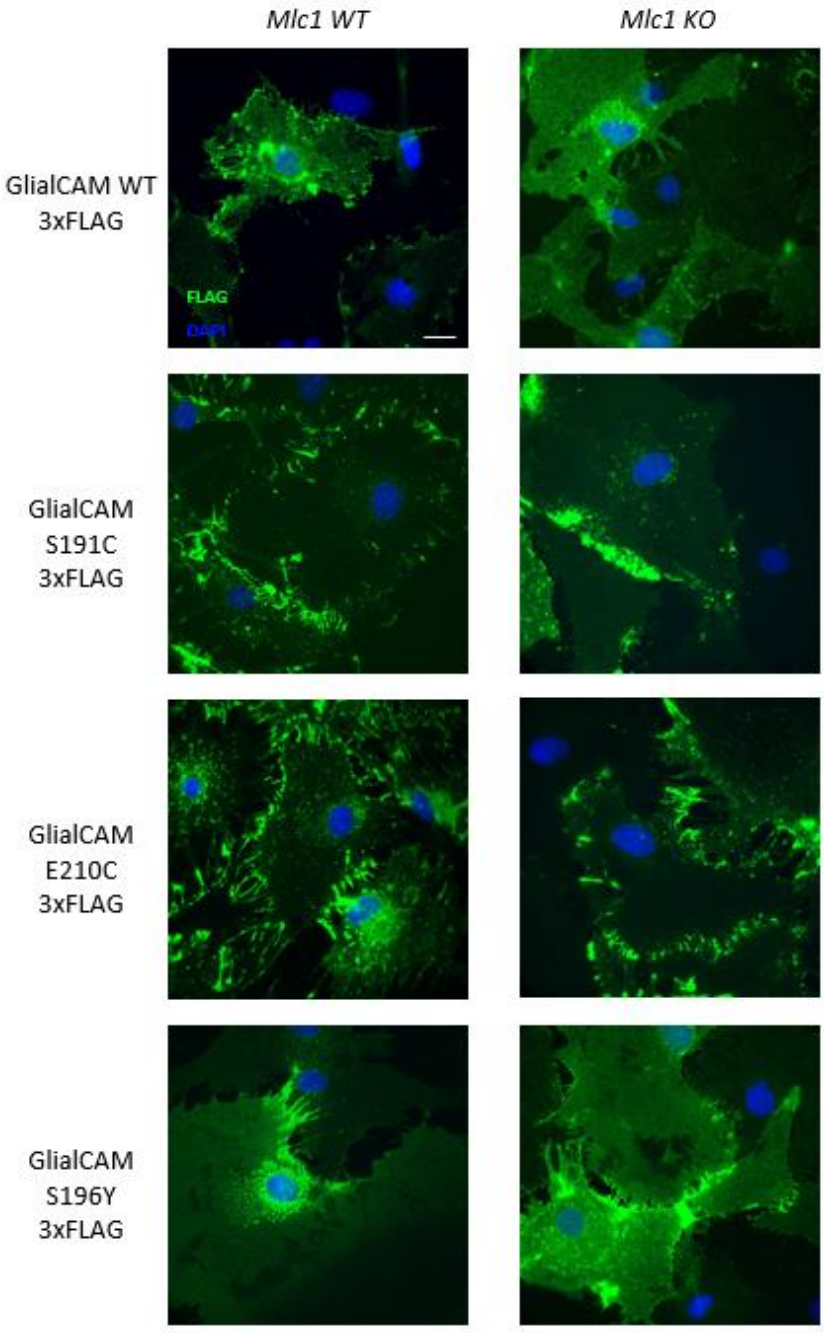

Figure 76. GlialCAM IgC2 α-helix Cysteine-mutants behave like MLC-derived mutant variants. GlialCAM variants S191C and E210C were overexpressed in mouse primary WT astrocytes or *Mlc1*$^{-/-}$ astrocytes. In a context of high potassium concentration, both variants were defective for internalization. This behavior corresponded to what had been observed for S196Y patient-derived mutant, here used as a control. In these conditions, WT protein is internalized in KO astrocytes, while GlialCAM IgC2 mutants maintain their subcellular localization. Images are representative of three independent experiments.

Combined, all the new information on cysteine-mutants in IgC2 was a big advance in our understanding of the role of IgC2 domain since it seemed to indicate that our hypothesis of GlialCAM IgC2 forming lateral interactions with adjacent molecules would be correct. At the same time, the experiments with these mutants in our *in vitro* model of primary astrocytes established that the cross-linked, oligomeric variants of GlialCAM show the same phenotype that patient-derived mutations confer to GlialCAM.

We collaborated again with Dr Juan Fernández-Recio to further refine a model for GlialCAM interactions in the plasma membrane that considered these new experimental restrictions (lateral IgC2 interactions through the identified structural proximity of residues of adjacent α-helices). We hoped to obtain a model that would optimize our understanding of the pathogenicity of the patient-derived mutations at a structural/functional level. The results of this approach are depicted in Figure 77**.**

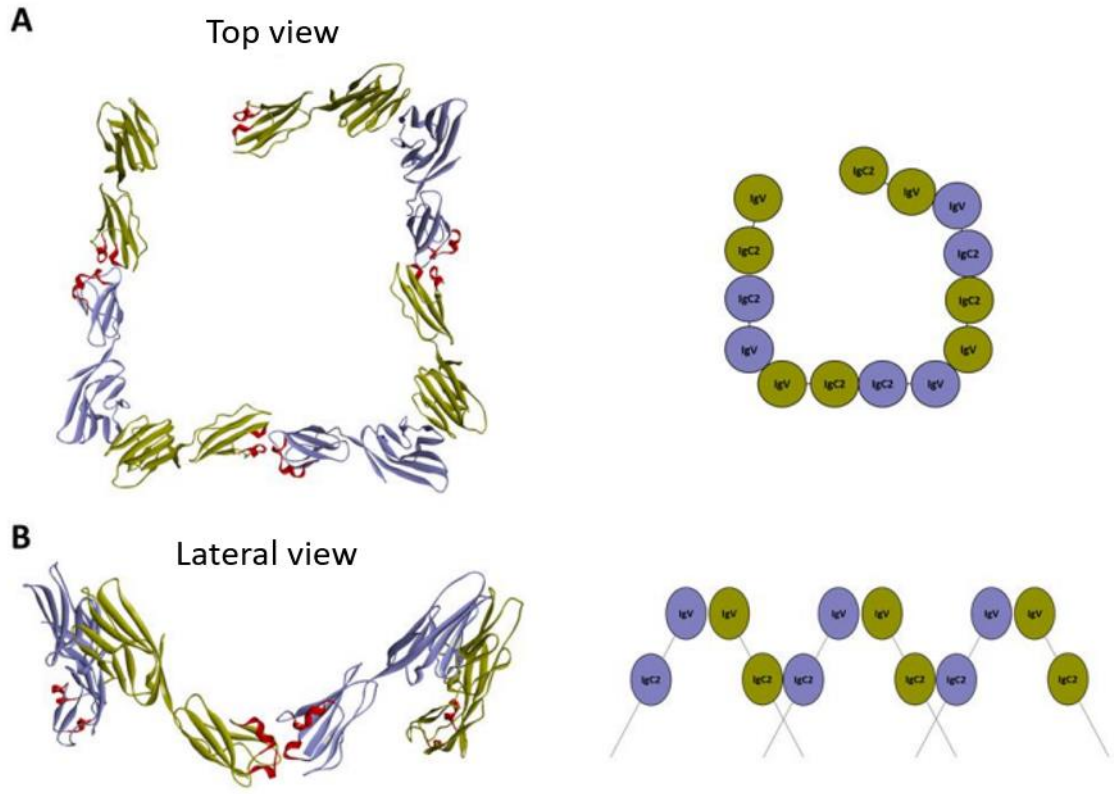

Figure 77. Model for GlialCAM oligomerization at the plasma membrane considering IgV cis- and trans- interactions, as well as IgC2 lateral interactions.

The analysis of this model revealed that both mutant residues have a characteristic in common regarding their structural localization within the GlialCAM oligomerization surface. While S196Y residue is pointing at K185, D211N finds itself in a region of negative charges. Therefore, the replacement of a serine for a tyrosine residue is likely creating a *de novo* cation-pi bond. On the other hand, the loss of a negative charge in when Aspartate is substituted by Asparagine could be having a similar effect by a reduction of electrostatic repulsion forces. A model representing this hypothesis is represented in the following **Figure 78**.

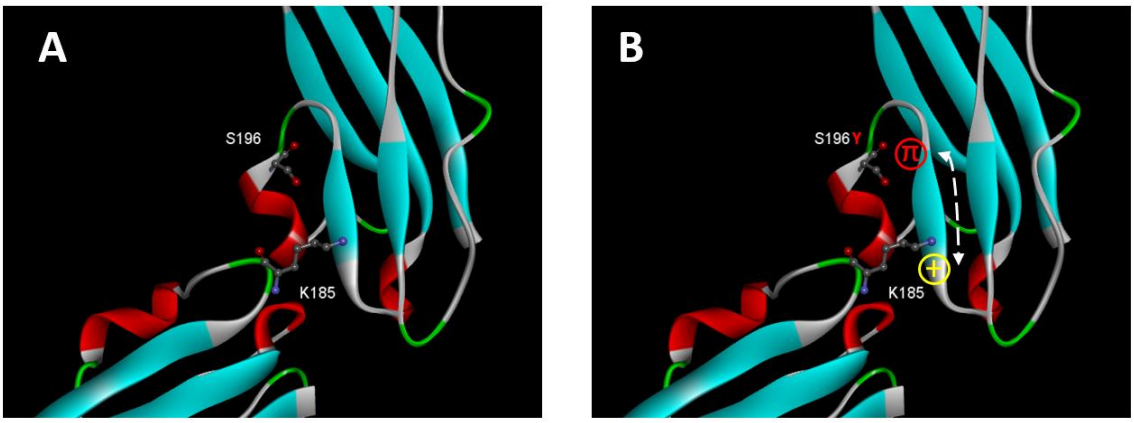

Figure 78. Proposed mechanism underlying pathogenicity of MLC-causing GlialCAM IgC2 mutations. A interaction interface between adjacent α-helix motifs from oligomerizing GlialCAM molecules. Serine residue 196 (S196) is in close proximity with Lysine residue 185 (K185). **B** Since Lysine is a positively charged amino acid, the replacement of S196 for Tyrosine provides negative electrostatic potential to the residue. Hence, a cation-pi bond would be established between the abnormal Tyrosine residue and the Lysine residue, thus resulting in the stabilization of the structure. This gain of function would be preventing the physiological lability of GlialCAM oligomeric structures, which would be necessary for its signaling-related endocytosis.

3. PHOSPHORYLATION EVENTS AND SIGNALING PATHWAYS MODULATE MLC-RELATED CHLORIDE CHANNELS VRAC AND CLC-2

3.1 GPRC5B MODULATES VRAC ACTIVITY VIA FYN KINASE

Brain biopsies of MLC patients reveal white matter vacuolation (Duarri et al., 2011). Consistently, MRI studies in patients show increased water content (De Stefano et al., 2001). In addition, both primary astrocytes and oligodendrocytes from *Glialcam*$^{-/-}$ and *Mlc1*$^{-/-}$ mice are swollen and vacuolated (Bugiani et al., 2017, Capdevila-Nortes et al., 2013, Hoegg-Beiler et al., 2014). This data suggested that MLC patients suffer defects in fluid homeostasis (Elorza-Vidal et al., 2018). Related, several studies reported that the MLC1/GlialCAM complex is related to proteins that are relevant to these processes (Estévez et al., 2018). In the literature, works by various authors show that VRAC activity is compromised in patient-derived lymphocytes or monocytes, as well as primary rat astrocytes with MLC1 or GlialCAM reduced expression (Capdevila-Nortes et al., 2013, Dubey et al., 2015, Petrini et al., 2013).

As a research group, we were interested in assessing whether GlialCAM/MLC1 complex could be modulating VRAC activity via phosphorylation, since GlialCAM/MLC1 do not show direct interaction with VRAC. Indeed, we proved that MLC1 is correlated with two phosphorylation events in VRAC accessory subunit LRRC8C. Also, we observed a negative modulatory role for MLC1 on molecular pathways like ERK signaling in primary astrocytes (Elorza-Vidal et al., 2018). The same was observed in astrocytoma, together with the inhibition of NF-κB signaling (Brignone et al., 2019). These findings are relevant because ERK has been involved in the activation of VRAC (Pedersen et al., 2016). Thus, GlialCAM/MLC1 would be modulating signaling pathways that result in regulation of VRAC.

Furthermore, one of the latest studies published by our group identified GPRC5B as a member of the GlialCAM interactome (Alonso-Gardón et al., 2021). Specifically, we found that the last experiments from this work aimed at establishing a functional relationship between GPRC5B activity and VRAC currents. What we found was that the Gprc5b is essential for VRAC activation induced by hypotonicity in rat-derived primary astrocytes (Figure 79**)**. Indeed, patch-clamp experiments were performed in these cells with or without Gprc5b expression. Depletion of Gprc5b expression was obtained by degradation of Gprcb5 mRNA using specific short hairpin RNA (sh Gprc5b).

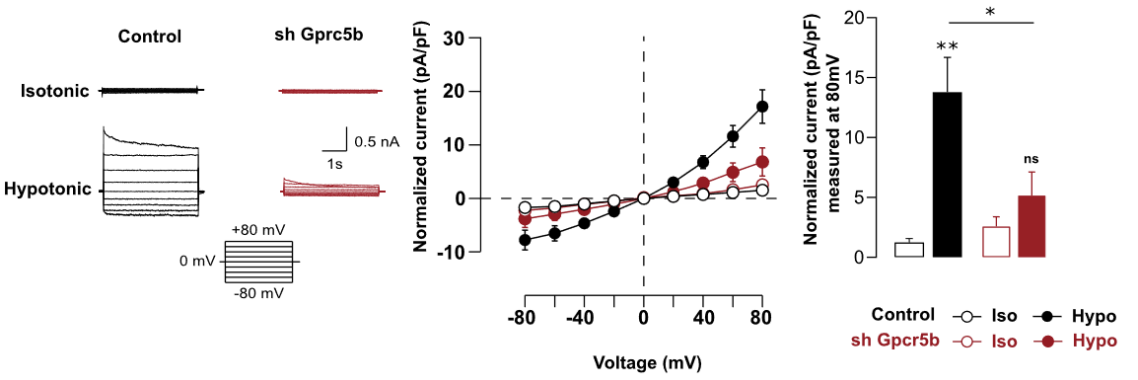

Figure 79. Gprc5b activity is necessary for hypotonicity-induced VRAC activations in rat primary astrocytes. *Left panel* Representative whole-cell recordings from control and GPRC5B-depleted rat astrocytes showing VRAC currents evoked by voltage pulses (from −80 to +80 mV) before and after 5 min of hypotonic stimulation. The protocol applied is depicted in between recordings. *Middle panel* Current-voltage relationships from the same recordings. The curves show that current activation upon hypotonicity was not statistically significant in GPRC5B-depleted astrocytes. Also, VRAC currents from these cells were much smaller when compared with those of control astrocytes incubated in a hypotonic solution. *Right panel* Quantification of the current measured at +80 mV for all groups. All featured whole-cell currents are normalized by cell capacitance. ns, not significant, ∗P < 0,05, ∗∗P < 0,01. The number of experiments is Control = 12, sh Gprc5b = 8.

Next, we wanted to elucidate the molecular mechanism by which GPRC5B regulation of VRAC was taking place. We came across an article by Trouet and colleagues (Trouet et al., 2001) that proposed that VRAC activity would be modulated by c-Src tyrosine kinase targeted to caveolae. In this paper, the authors claimed that this inhibition is mediated by direct interaction between SH domains from the kinase with VRAC. Interestingly, GPRC5B is known to signal via Fyn kinase (Kim et al., 2012), which is another Src tyrosine-kinase. Therefore, we hypothesized that Fyn might be involved in the GPRC5B-mediated modulation of hypotonicity-induced VRAC activity.

In this case, our hypothesis was that the lack of Fyn activation was responsible for the lack of VRAC activation after a hypotonic stimulus in the absence of GPRC5B. We intended to prove that using this GPRC5B mutant. If our hypothesis were true, the heterologous expression of GPRC5B Y383F variant (*see section 1.3 of the results of this thesis*) would lead to the same effect as the lack of GPRC5B.

Again, we carried out patch-clamp experiments on rat-derived primary astrocytes to test this hypothesis (Figure 80**).** A first surprise was that we could observe that the overexpression of GPRC5B WT protein reduced VRAC currents. However, this effect

was not seen for the overexpression of Y383F mutant. In conclusion, these results support the idea that Fyn would be regulating the observed effect by GPRC5B on VRAC activity.

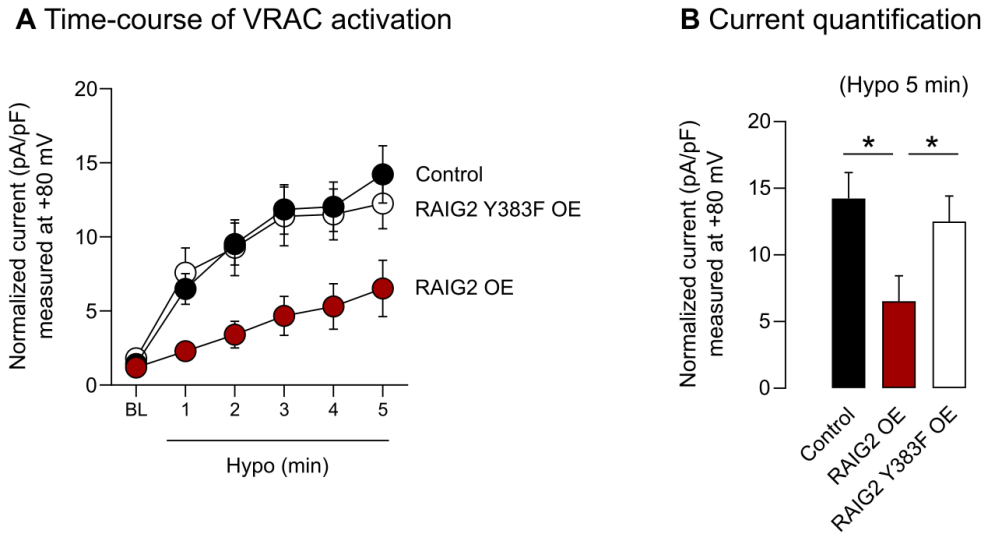

Figure 80. The overexpression of WT GPRC5B, but not Y383F mutant, reduces VRAC currents after hypotonic stimuli. A Time-course of VRAC activation. The graph features elicited VRAC currents at +80 mV in hypotonic conditions for 5 minutes, in one-minute intervals, for all experimental groups: control uninfected astrocytes, GPRC5B overexpression (RAIG2 OE), GPRC5B Y383F overexpression (RAIG2 Y383F OE). **B** Comparison of the quantification of the currents measured at +80 mV after the first 5 minutes after hypotonic stimulation for the same experimental groups All whole-cell currents shown are normalized by cell capacitance. * $p < 0,05$. N = 11 (Control), 7 (RAIG2 OE), 8 (RAIG2 Y383F OE). Experiments performed by Dr Aida Castellanos Esparraguera.

We reasoned that one possibility to explain these results would be the lack of interaction of GPRC5B Y383F mutant with VRAC. Therefore, we measured the ability of this variant to interact with the main VRAC subunit, LRRC8A. To this end, we performed Split-TEV experiments (Figure 81**).**

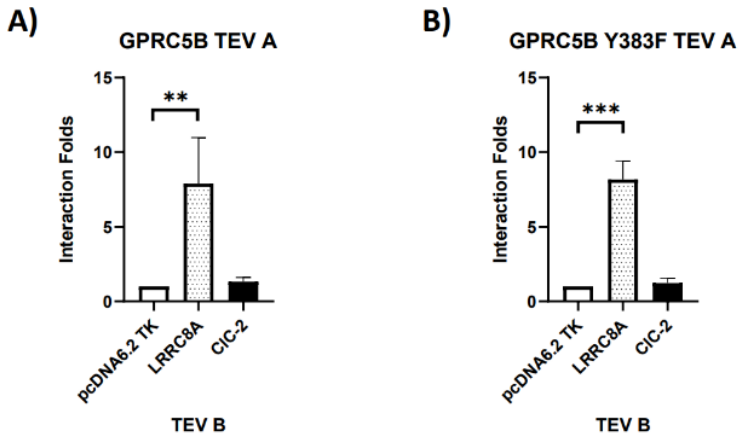

Figure 81. GPRC5B mutant Y383F conserves the ability to interact with LRRC8A, the main VRAC subunit. A, B Split-TEV assays assessing the ability of GPRC5B Y383F to interact with LRRC8A in transfected HeLa cells. Data indicates the average interaction folds for GPCR5B or GPRC5B Y383F related to the baseline (interaction with the empty vector 'pcDNA6.2TK') from three independent experiments. ClC-2 was used as a negative control. Statistical significance was addressed by One-way ANOVA with Bonferroni post-test. ** $p < 0,01$, *** $p < 0,001$.

We observed that the mutant variant does not lose WT GPRC5B ability to interact with VRAC. In the future, we will complement these experiments using Fyn inhibitors as well as adenoviral constructs for the overexpression of two new mutants. One will be a Fyn variant lacking enzymatic activity (K299M variant, (Kim et al., 2018), whereas the other will be a GPRC5B variant designed to enhance Fyn activity. Specifically, we cloned Y383D variant to mimic a constitutive phosphorylated state of GPRC5B, that would in turn be activating Fyn in a constitutive manner. This approach will allow us to determine whether the effect of Fyn on VRAC activity is via phosphorylation or it is by direct interaction, as described for c-Src (Trouet et al., 2001).

3.2 Phosphorylation/Dephosphorylation Events Modulate ClC-2 Activity

Our group has been studying ClC-2 since GlialCAM was discovered to be its auxiliary subunit (Jeworutzki et al., 2012). In that published work, it was shown that the association between GlialCAM and ClC-2 leads to changes in the localization and functional properties of ClC-2 *in vitro*. Specifically, the electrophysiological properties of the channel switch from inward rectification to ohmic behavior upon interaction with GlialCAM. Further *in vivo* studies in *Mlc1*$^{-/-}$ and *Glialcam*$^{-/-}$ models highlighted the importance of GlialCAM in proper function and localization of ClC-2 in

oligodendrocytes. However, ClC-2 properties were not altered in recordings from Bergmann Glia in *Glialcam*$^{-/-}$ mice (Hoegg-Beiler et al., 2014). At first, studies in primary astrocytes expressing both MLC1 and GlialCAM still could not replicate the reported changes in ClC-2 properties (Jeworutzki et al., 2012, Sirisi et al., 2017).

Nonetheless, former works carried out in our lab observed that incubation of these primary astrocytes using potassium-enriched solutions induced these functional changes in ClC-2 channel. These solutions, also referred to depolarizing solutions or High K^+ in this thesis, mimicked the context of high neuronal activity found in the brain. The observed changes were consistent both at low potassium concentrations as well as high potassium concentrations (ranging from 12,5 mM to 60 mM). Importantly, this behavior was observed both for the endogenous protein and for Flag-tagged ClC-2 overexpressed using adenoviral constructs. Along with the changes in the electrophysiological changes, depolarizing conditions lead to a shift in the subcellular localization of ClC-2. When detecting ClC-2 in IF assays, the protein concentrated at cell-cell junctions in potassium-enriched conditions (Figure 82). This phenotype was not observed in primary astrocytes in which Glialcam was depleted (data not shown, experiments performed by Dr. Xabi Elorza-Vidal). Additional GlialCAM expression in *Glialcam*$^{-/-}$ astrocytes using adenoviral particles rescued the ability of ClC-2 to switch its properties in these cells. In *Mlc1*$^{-/-}$ astrocytes, depolarizing conditions did not lead to the reported changes in ClC-2 activity. Also, in samples obtained from the brain of *Mlc1*$^{-/-}$ animals, the immunoprecipitation of ClC-2 and GlialCAM was abolished. Indeed, our group suggested that some ternary complex between GlialCAM/MLC1 and ClC-2 was being formed in depolarizing conditions, as revealed in cultured astrocytes and *in vivo* (Sirisi et al., 2017).

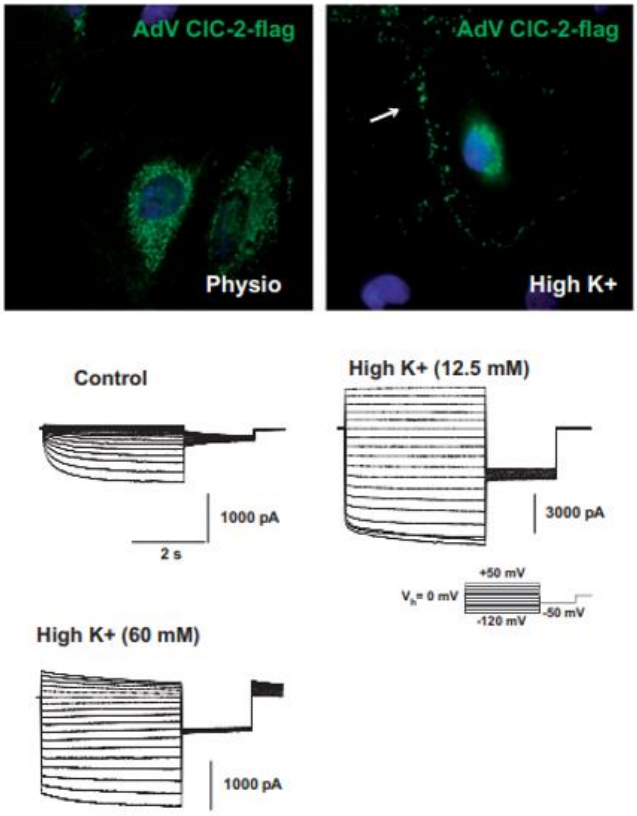

Figure 82. GlialCAM induces changes in ClC-2 localization and electrophysiological properties. Upon incubation with a depolarizing solution, overexpressed FLAG-tagged ClC-2 concentrates at cell-cell junctions in primary astrocytes, as revealed by immunofluorescence (*upper panels*). Consistently, high potassium concentrations lead to increased currents and disappearance of inward rectification of the channel (*lower panels*).

Finally, this work also proved that the formation of this ternary complex is dependent on both calcium flux through L-type calcium channels and calcium-dependent calpain proteases, which are typically activated as a response to high concentrations of potassium in the extracellular compartment (Yaguchi and Nishizaki, 2010). Indeed, the addition of calcium chelators or calcium channel blockers prevented the localization of ClC-2 at cell-cell junctions as well as its gating modifications under depolarizing conditions (Sirisi et al., 2017). However, preliminary data using a calcium ionophore seemed to indicate that the single addition of calcium to astrocytes is not sufficient to trigger these changes.

Other ongoing projects in the lab linked ClC-2 function and GPCR activity. Specifically, we showed that the lack of Gprc5b in rat primary astrocytes leads to defective ClC-2 activity. In the absence of Gprc5b, the channel is not enriched at cell-cell junctions after cells are incubated in depolarizing conditions **Figure 83**.

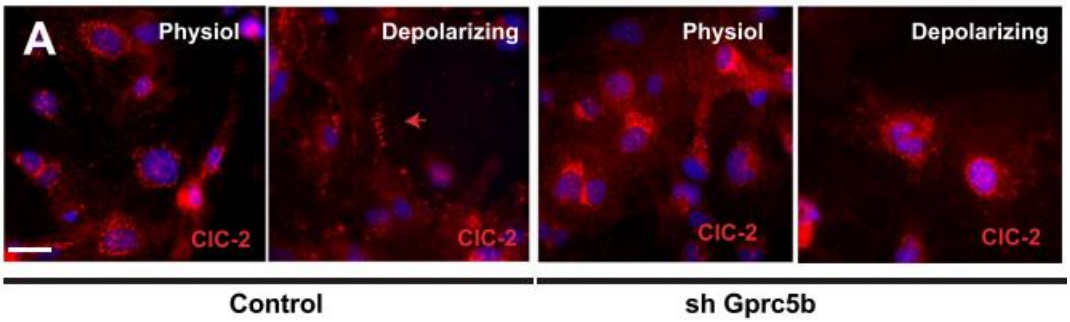

Figure 83. Lack of Gprc5b affects ClC-2 localization at cell-cell junctions after incubation in depolarizing conditions. A Immunostainings of ClC-2 in Control or Gprc5b-depleted primary astrocytes treated with physiological or depolarizing conditions. ClC-2 enrichment at cell-cell junctions is not observed in Gprc5b-depleted astrocytes in depolarizing conditions, a phenotype that is observed in control astrocytes (red arrows). Adapted from (Alonso-Gardón et al., 2021).

Therefore, we wanted to know the mechanism behind this apparent modulation of ClC-2 activity by GPRC5B. Indeed, we were interested in addressing whether the channel is regulated by phosphorylation. Together with our proposed hypothesis of the observed changes in calcium levels activating kinase or phosphatase activity, we decided to perform phosphorylation-proteomic analyses in rat primary astrocytes, comparing control conditions and potassium-enriched conditions. A selection of the obtained results is summarized in Figure 84.

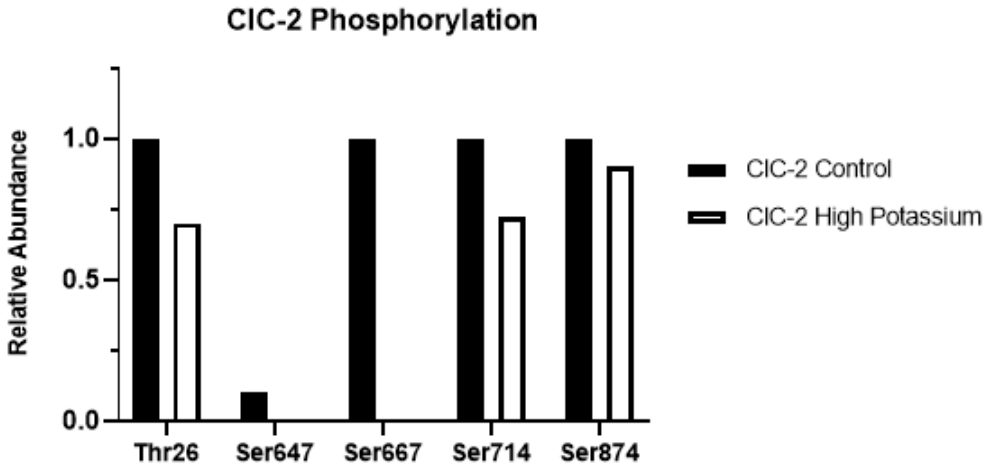

Figure 84. Analysis of ClC-2 phosphorylation status in rat primary astrocytes. Proteomic data obtained in rat primary astrocytes, both in high potassium concentrations and in control conditions. Results come from two independent experiments.

The most interesting piece of information from these results was that Serine residue 667 is completely phosphorylated in control conditions, but this post-translational modification is completely reverted in depolarizing conditions. Serine residue 647 was also completely dephosphorylated in potassium-enriched conditions, although phosphorylation levels for this amino acid were already low in control conditions. However, we thought that these dephosphorylation events could be linked to the signaling activity that we hypothesized to be taking place together with calcium fluxes, as suggested by our previous works.

3.2.1 Development of a Molecular Tool to Study ClC-2 Phosphorylation: Phospho-Specific Antibody Against Serine 667

To begin the study of the role of phosphorylation in the regulation of ClC-2 activity, we decided to develop a tool to monitor the changes in the phosphorylation status of ClC-2 predicted in our proteomic studies of ClC-2 phosphorylation. With this aim, we developed a phosphorylation-specific (or phosphor-specific, or P-specific) antibody for Serine residue 667, based on our preliminary phosphor-proteomic data.

We ordered the production of this antibody to Eurogentec company. We designed the antibody to be responsive to a selected peptide featuring the desired phosphorylated residue. The 13 amino acid sequence of the peptide was the following:

N-terminal CQMSPP**S**DQESPP C-terminal (Underlined 'S' represents Serine 667)

In the production process, two variants of this peptide were synthesized. The first variant featured the Serine with an attached phosphate group, whereas the second one was unmodified Serine. Therefore, we obtained the Specific Peptide and the Unspecific Peptide. These peptides were used for rabbit immunizations to eventually obtain purified antibodies (IgG) against either the phosphorylated (specific peptide) form or the non-phosphorylated (unspecific peptide) form of the protein.

We further tested the antibody in our working environment using an ELISA protocol. We aimed at comparing the affinity and the detection window of the Phospho-specific antibody to our total ClC-2 antibody (Ct New antibody). We used an antibody dilution series for both antibodies. Regarding the plate coating, we tested both specific peptide and unspecific peptide for our phospho-specific antibody. The use of Ct New antibody on its own peptide served as experimental control. The results are featured in Figure 85.

Phospho-specific antibody was able to detect the specific peptide with good sensitivity and showed little background binding reaction to the unspecific peptide. As expected, elicited ELISA signal for specific reaction decreased the more diluted the antibody. As for the control group, The Ct New antibody perfectly validated the experiment, giving great epitope detection.

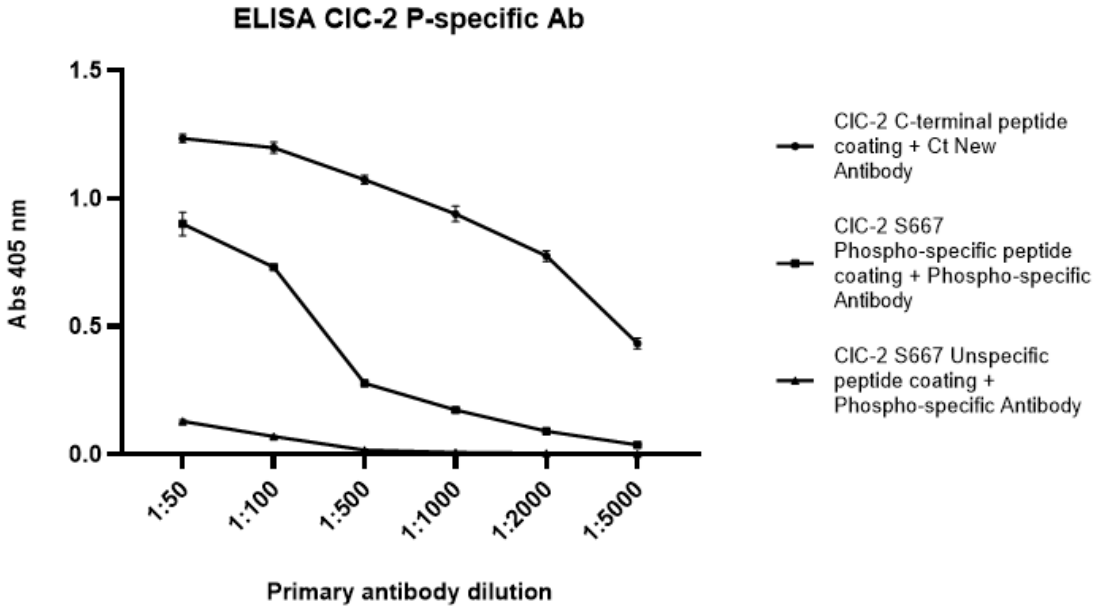

Figure 85. ELISA assay revealed good sensitivity and specificity for phospho-specific antibody. Purified phosphorylation-specific antibody could detect a coating of the phosphorylated (specific) peptide on an ELISA plate (squared dots), but not a non-phosphorylated peptide coating (triangle dots). Regular ClC-2 (Ct New) antibody (circle dots) was used as a control using its own peptide coating.

These tests confirmed that the developed antibody was a good tool to monitor phosphorylation activity for ClC-2. Thus, we proceeded to characterize whether this tool served to replicate the expected results from the preliminary phospho-proteomic studies. Indeed, we wanted to address whether we could see this dephosphorylation of Serine 667 in our primary astrocyte system in WB experiments using the developed antibody. To this end, we overexpressed FLAG-tagged ClC-2 WT protein using adenoviral constructs in rat astrocytes. We subsequently treated incubated those cells in a physiologic solution or in a potassium-enriched solution.

Importantly, during the obtaining of the total protein extracts for WB analysis, we used PHOSTOP reagent to ensure that phosphorylation modifications were maintained in the final sample.

What we expected to see was that samples belonging to cells treated with a depolarizing solution would elicit a band of lower intensity compared to the same cells treated with a physiologic solution, whereas total ClC-2 detection would be comparable across the two groups. Indeed, Figure 86 shows a representative experiment confirming these forementioned results.

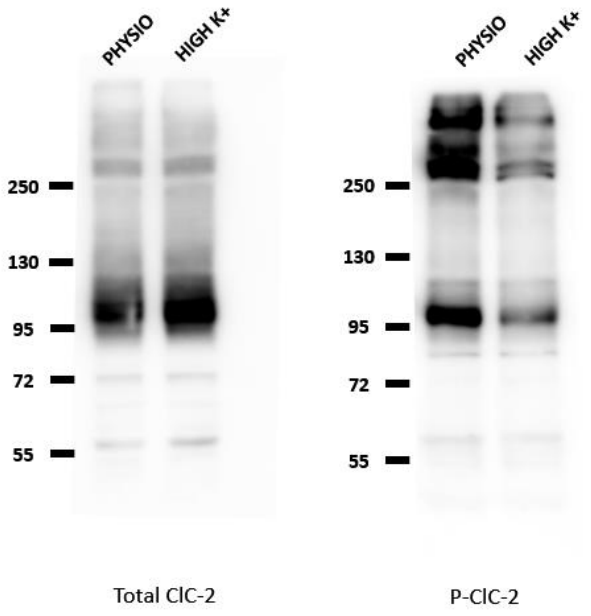

Figure 86. The developed P-specific antibody is a good tool to monitor phosphorylation and dephosphorylation events in protein extracts from rat primary astrocytes. Increased phosphorylated ClC-2 was observed in protein extracts obtained from astrocytes at physiological conditions (labeled as PHYSIO) compared to the same cells incubated with potassium-enriched solutions (60 mM). Total ClC-2 levels were equal across groups. This meant that the antibody monitored ClC-2 dephosphorylation in depolarizing conditions. Protein extracts were obtained using lysis buffer containing PHOSTOP to ensure phosphate groups were preserved in the final protein extract. 30 µg of total protein extracts from each group were loaded in 10 % gels.

Interestingly, we also measured the quantitative signal from these membranes using ImageJ software. The results can be observed in **Figure 87**, and they showed that the designed antibody can be applied in quantitative studies of phosphorylation changes in ClC-2.

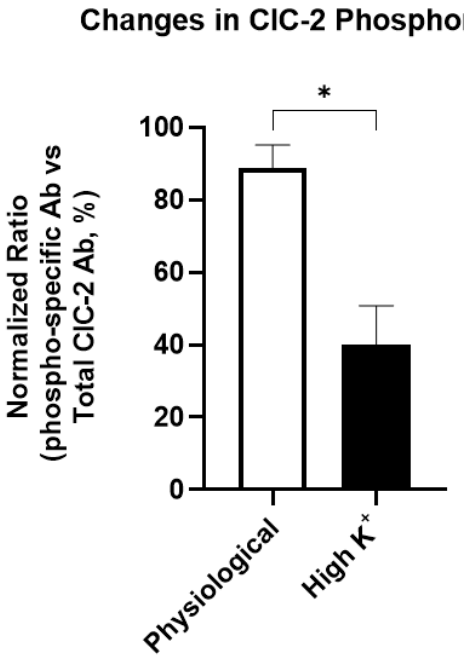

Figure 87. Phospho-specific anti-ClC-2 allows for quantitative analysis of ClC-2 phosphorylation changes. ImageJ software analysis for protein quantification validates the observed changes for ClC-2 dephosphorylation after incubation in high extracellular potassium concentrations in rat primary astrocytes. As revealed by ImageJ software analysis for protein quantification, numeric protein abundance data corresponded to what was observed at a qualitative level. Represented data corresponds to ratios between phosphorylated ClC-2 and total ClC-2, expressed as a percentage and normalized using the highest signal ratio. Data comes from three independent experiments. Statistical analysis was assessed using standard t-test. * $p < 0.05$.

3.2.2 Dephosphorylation is Necessary for ClC-2 Activity Changes

Once we confirmed that P-antibody is a good tool to study ClC-2 activity regulation by phosphorylation, we began tackling a validation of the importance of the phosphorylation status of these residues at the functional level. Considering the reported results on the changes of the phosphorylation status that ClC-2 undergoes when switching from control conditions to depolarizing conditions, we decided to conduct mutagenesis studies to verify that these modifications are directly linked to the change in behavior previously reported for ClC-2 in depolarizing conditions.

Specifically, we generated constructs aimed at the production of adenoviral particles to overexpress the distinct ClC-2 variants in rat primary astrocytes. We generated ClC-2 double mutants for both Serine residues found dephosphorylated in depolarizing conditions. We designed constructs featuring Alanine residues and Aspartic Acid residues, that we named p.Ser647>Ala; p.Ser667>Ala (from here on referred to as

S647A/S667A), and p.Ser647>Asp; p.Ser667>Asp (from here on referred to as S647D/S667D). The reason that we did these directed mutations is that Alanine residues mimic the dephosphorylated status of these Serine residues, whereas Aspartic acid residues mimic the phosphorylated status of the same amino acids.

Our first experiment within these studies was to express both S647A/S667A and S647D/S667D in our model system using rat primary astrocytes, using the expression of WT ClC-2 as a control. In addition, we conducted these studies in control conditions as well as in potassium-enriched conditions. Our hypothesis was that the mutant mimicking constitutive dephosphorylation of these residues would be localized at cell-cell junctions independent of the extracellular osmolarity, while we expected the 'phosphorylated' mutants to be internalized or reaching the plasma membrane displaying a diffuse pattern. Instead of detecting total ClC-2 protein in the cells, we performed these tests against the molecular Flag tag that was added to each construct. With this approach we only were to monitor the overexpressed protein, giving us a clearer picture of the phenotype of each variant.

The results obtained for these experiments confirmed our hypothesis. A visual summary of the observed phenotype in each group is provided in Figure 88**A**. The detailed quantification of the results appears in Figure 88**B**. The mutant mimicking for constitutive dephosphorylation showed constant enrichment at cell-cell junctions, like was the case for the WT ClC-2 incubated using a high-potassium solution. This phenotype was not observed for ClC-2 S647D/S667D variant.

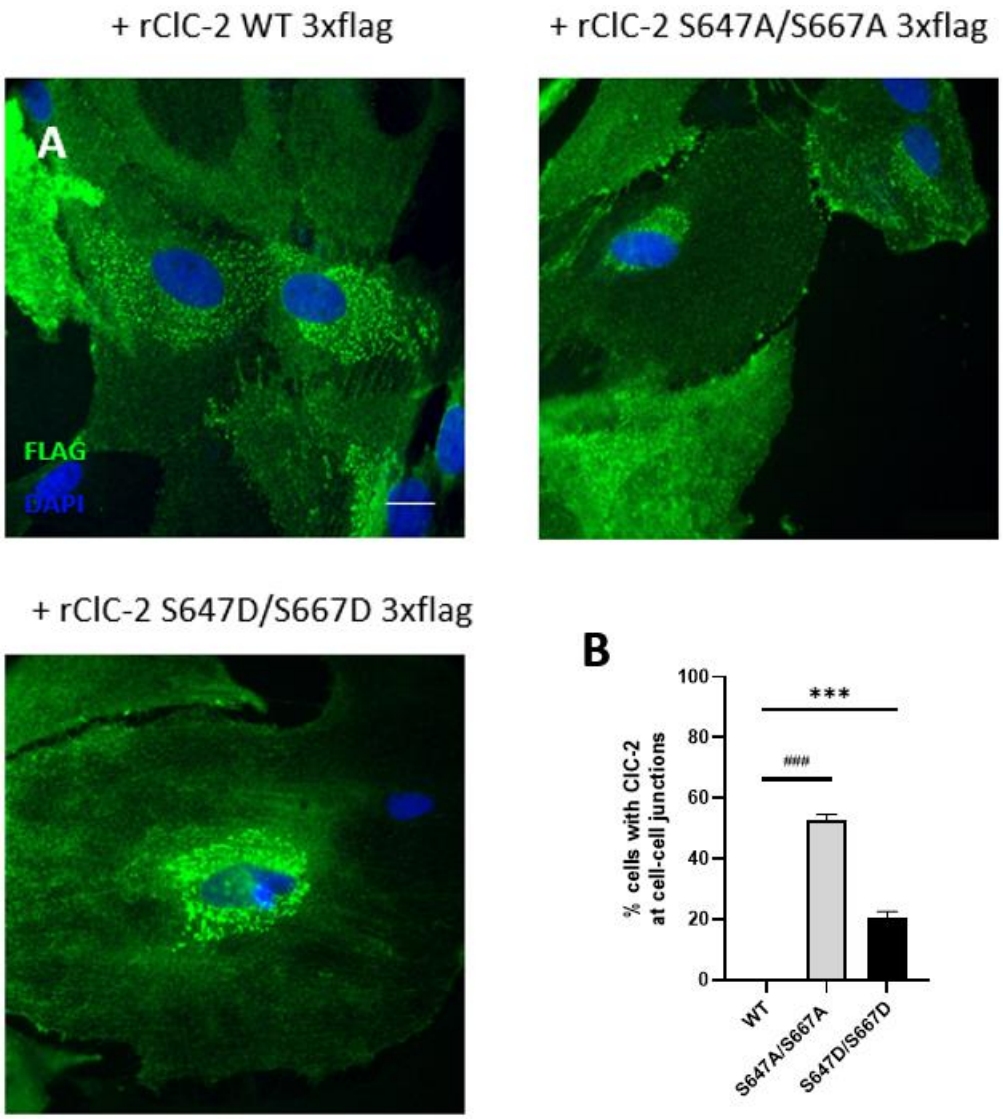

Figure 88. ClC-2 dephosphorylation is linked to the localization of the channel at cell-cell junctions. **A** IF assays were performed on rat primary astrocytes, directed against the FLAG tag of overexpressed ClC-2 variants. Experiments showed that ClC-2 variant S647A/S667A is localized at cell-cell without increased extracellular potassium concentration. Groups overexpressing WT ClC-2 showed the normal diffuse and internalized localization of the protein, whereas the overexpression of the S647D/S667D variant resulted in some ClC-2 at cell-cell junctions, but less than half of the dephosphorylated variant. The quantitative results can be observed in the graph in **B**. Images are representative of three independent experiments. Scale bar = 20 µm. Statistical analysis was performed using One-way ANOVA with Bonferroni post-test. ***, ### $p < 0.001$.

After the confirmation of these results, we checked whether the dephosphorylation of these Serine residues also led to the shift of the electrophysiological properties of ClC-2 observed in depolarizing conditions.

We continued with the functional assessment of the effect of dephosphorylation on ClC-2 activity using rat primary astrocytes. We performed whole-cell patch-clamp to analyze cells overexpressing either WT ClC-2 or the S647A/S667A double mutant. Uninfected astrocytes were recorded as background control group. Also, we used YFP to detect infected cells, since our adenoviral constructs for ClC-2 overexpression were not fluorescent **Figure 89**.

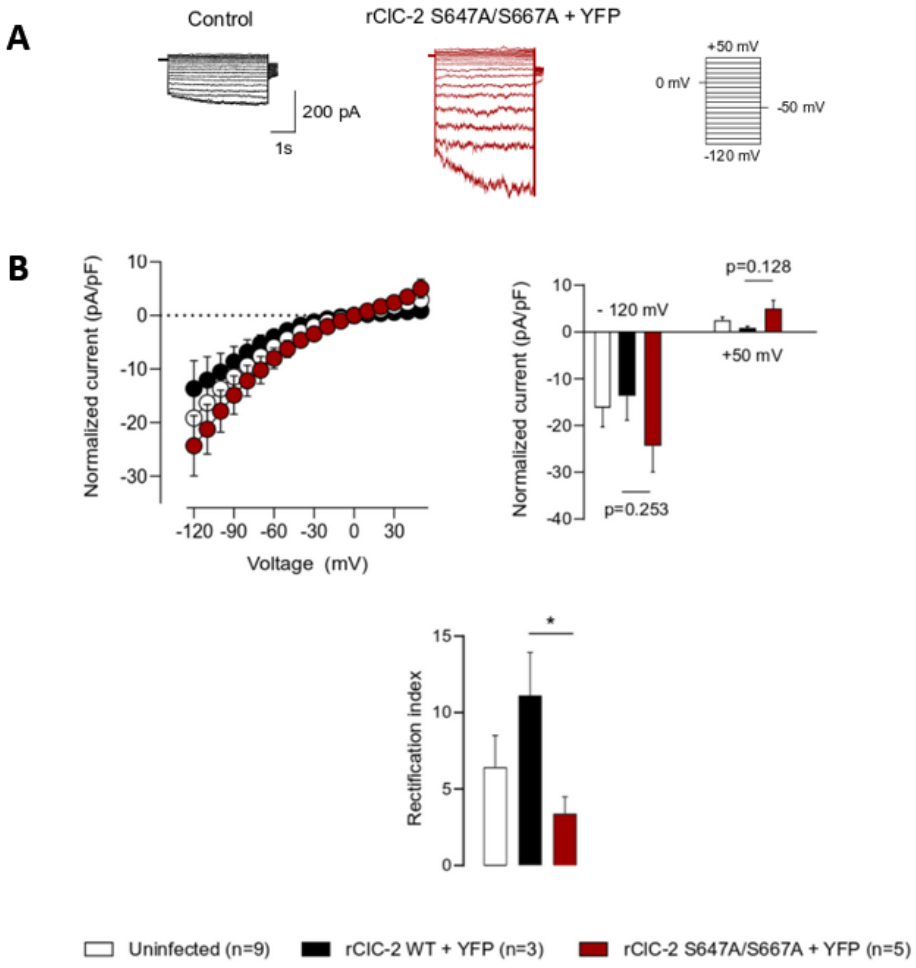

Figure 89. Dephosphorylation alters ClC-2 gating. A Representative whole-cell recordings from uninfected cells and rat astrocytes overexpressing rClC-2 S647A/S667A (+ YFP). Starting from a holding potential of 0 mV, ClC-2 currents were evoked by 10 mV-voltage pulses from -120 mV to +50 mV. The protocol applied is depicted on the right and the scale applies to all traces. **B** *Left panel* Steady-state current-voltage relationships show an increase in current density in astrocytes overexpressing rClC-2 S647A/S667A (+ YFP) when compared to the control group and uninfected astrocytes (in red, black and white, respectively). *Right panel* Quantification of the current measured at -120 and +50 mV in both uninfected and rClC-2 S647A/S667A (+YFP) - expressing astrocytes. *Lower panel* Rectification index for all groups. Whole-cell currents shown in B are normalized by cell capacitance. *** p <0.001. Experiments performed in collaboration with Dr Aida Castellanos Esparraguera.

Consistent to what was observed for Immunofluorescence assays, these experiments confirmed that ClC-2 variant mimicking constitutive dephosphorylation of the Serine residues conducted bigger currents in response to our protocol of applied voltage pulses, compared to the WT channel and uninfected astrocytes, and in physiological conditions. Also, when assessing the rectification pattern of the channel, the double mutant showed a statistically significant reduction in the rectification index than the WT, indicating electrophysiological properties closer to an ohmic behavior.

Together, this data strongly supported the functional link between dephosphorylation events in ClC-2 Serine residues 647 and 667 and the altered gating observed *in vivo* upon interaction with GlialCAM.

DISCUSSION

Megalencephalic Leukoencephalopathy with subcortical Cysts (MLC) is a rare type of genetic leukodystrophy caused by mutations in either *MLC1* or *GLIALCAM* genes. Both genes encode for membrane proteins expressed almost exclusively in glial cells (Leegwater et al., 2002, López-Hernández et al., 2011a). While the etiology of the disease is properly characterized, the pathophysiological mechanisms underlying MLC are still not fully understood. The exact physiological roles of MLC1 and GlialCAM remain unclear. However, several studies using animal and cellular models, together with some histological studies on patient-derived brain samples, allowed to determine myelin and astrocyte vacuolation as the main hallmark in MLC pathology (Duarri et al., 2011).

These findings indicated that ion and water homeostasis are compromised in the disease. Several published works by our research group are dedicated to investigating the role of the GlialCAM/MLC1 complex in the regulation of these processes. In these studies, the complex has been related to the modulation of the activity of ion channels such as VRAC and ClC-2, among other partners. Specifically, one of these studies showed that MLC1 and VRAC are functionally linked, despite not showing direct interaction nor co-localization. In this regard, we showed that overexpression of MLC1 leads to reduced phosphorylation of extracellular signal-regulated kinases (ERK) (Elorza-Vidal et al., 2018). Thus, a connection between GlialCAM/MLC1 and signaling processes was proved for the first time. The following figure **Figure 90** summarizes our model for the regulation of physiological processes carried out by the GlialCAM/MLC1 complex, involving signaling events:

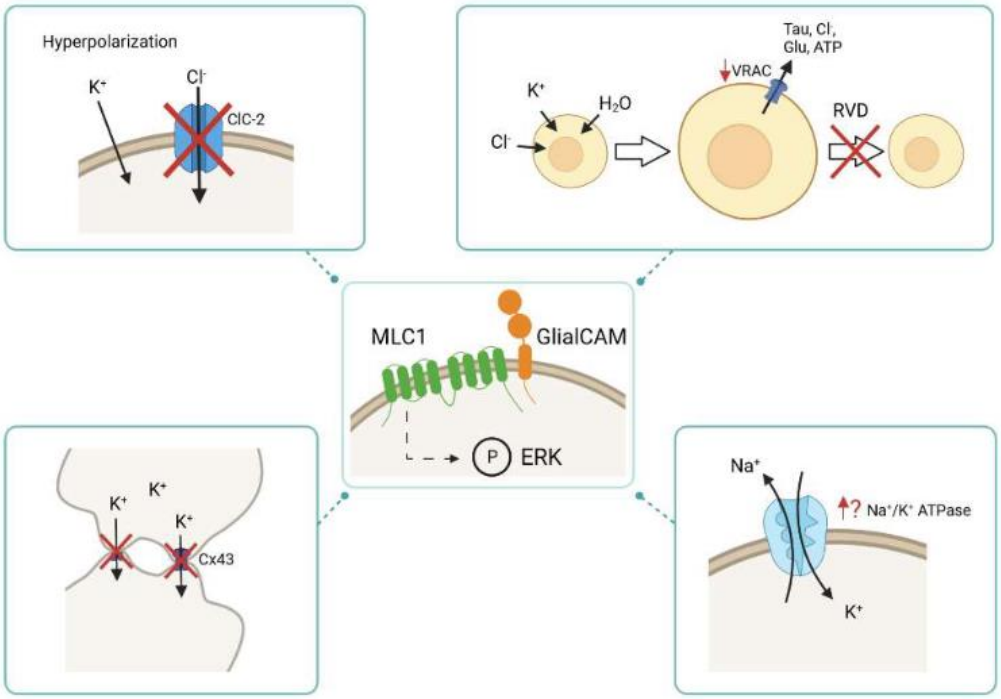

Figure 90. Physiological processes involving the activity of GlialCAM/MLC1 complex. The absence of GlialCAM/MLC1 alters the activity of different transporters and ion channels, such as ClC-2, VRAC, Cx43, and Na^+/K^+ ATPase (red crosses). Hence, GlialCAM/MLC1 participate in the modulation of hyperpolarization phase of the neuronal action potential (ClC-2), regulatory volume decrease or RVD (VRAC), potassium siphoning (Cx43), and restoring membrane potential (Na^+/K^+ ATPase). Our previous working hypotheses to explain the regulation of these processes by GlialCAM/MLC1 was via ERK signaling cascade, as we observed that it was upregulated in the absence of MLC1. Modified from (Pla-Casillanis et al., 2022).

This remark was consistent with what we could later observe in proteomic studies for MLC1 and GlialCAM interactome. Indeed, several GPCRs were identified to be molecular partners of this complex. Among them, GPRC5B was the receptor that showed a stronger functional relationship with GlialCAM/MLC1, ClC-2 and VRAC. When we characterized the interplay between this GPRC and MLC-related proteins, we found out that a reduction of GPRC5B expression levels in cellular models (primary astrocytes) led to the downregulation of GlialCAM/MLC1. This translated into an impaired activation of ClC-2 and VRAC (Alonso-Gardón et al., 2021).

Also, we obtained quantitative results within our proteomic data that aimed at comparing GlialCAM co-immunoprecipitated partners in WT samples vs *Mlc1*$^{-/-}$ samples. Such experiments revealed that two proteins interacted significantly less with GlialCAM when Mlc1 was not present. The proteins were ClC-2 and VCAM-1.

MLC1 modulates GPRC5B/Fyn-mediated VCAM-1 upregulation via NF-κB signaling

In the literature, we came across a published work by some authors who observed that GPRC5B leads to increased activation of NF-κB through direct interaction with Fyn kinase. These results were obtained in immortalized Endothelial cells (iECs) (Freundt et al., 2022). In this project, we validated that this process is also occurring in mature primary astrocytes obtained from rat pups, our experimental model. Moreover, we showed that MLC1 is somehow exerting a negative modulatory effect on this signaling pathway, since we demonstrated that induced upregulation of VCAM-1 after GPRC5B overexpression is diminished upon co-expression with MLC1 protein.

GPRC5B is an orphan receptor belonging to family C of metabotropic glutamate receptors, with 7 TMD and a short N-terminal domain. As orphan receptors, no ligand has been linked to the activation of the receptor. At the same time, no specific mechanism for its activation has been confirmed. However, it is described that class C GPCRs typically require dimerization or heteromerization to transduce signaling in response to agonists (Kniazeff et al., 2011, Vischer et al., 2015). The most studied case is $GABA_B$ receptor, in which case the functional receptor consists of heterodimers of $GABA_{B1}$ and $GABA_{B2}$. Both subunits undergo allosteric transactivation upon binding of GABA to the N-terminal domain of $GABA_{B1}$ (Kniazeff et al., 2002).

Here, we hypothesize that a similar need for multimerization would be necessary for GPRC5B signaling activity. Also, with this project we have observed that MLC1 interferes with GPRC5B signaling activity, while previous results from our lab showed that GPRC5B stabilized MLC1 at the plasma membrane (Alonso-Gardón et al., 2021). In this regard, we propose that the interaction of GPRC5B with MLC1 prevents its multimerization, thus modulating the cellular response that leads to the upregulation of VCAM-1 via NF-κB in inflammatory conditions. This hypothesis would also be consistent with the previously described role of MLC1 in the restoration of astrocyte homeostasis after inflammation (Brignone et al., 2019). The summarized model for this process is featured in **Figure 91**.

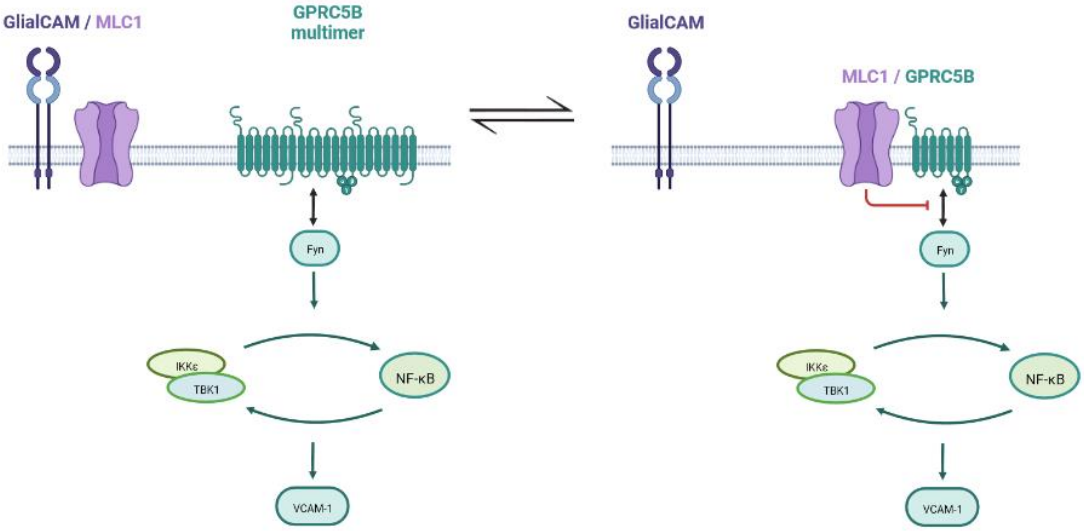

Figure 91. Proposed model for MLC1 modulation of GPRC5B/Fyn-mediated activation of NF-κB signaling pathway, which regulates VCAM-1 expression. We validated in primary astrocytes that GPRC5B displays signaling activity via Fyn that leads to the activation of the positive feedback loop established between IKKε/TBK1 and NF-κB. When this loop is stimulated, NF-κB translocates to the nucleus and induces VCAM-1 expression. In this regard, our results indicate that MLC1 exerts a negative modulatory effect on this downstream signaling of GPRC5B. Here, we propose a model to explain the observed effects. We believe that active GPRC5B could require formation of multimers (left), which would be disrupted by the binding of MLC1 to GPRC5B monomers (right). This interaction would be hampering the activation of NF-κB pathway, downregulating VCAM-1 induced expression.

Pathogenicity of GlialCAM IgC2 patient-derived mutations

One of the main goals of our research group is to understand the pathophysiologic mechanisms underlying MLC disease. Despite the progress made in this direction, some questions are not yet resolved. Among these unanswered questions lies the pathogenicity mechanism of *GLIALCAM* mutations that encode for residues located at the IgC2 domain of GlialCAM protein.

Previous works had been dedicated to the study of mutations in the IgV domain of GlialCAM since it is where most missense mutations are found. These studies showed that the pathogenicity of dominant GlialCAM IgV mutations was linked to the disruption of interaction surfaces between GlialCAM proteins, either in *cis*- or in *trans* (dimerization interfaces and interaction with molecules from neighbouring cells, respectively).

Related, the results from this thesis confirm that GlialCAM forms oligomeric structures through the lateral interactions of GlialCAM IgC2 domains from adjacent proteins, as seen by cross-linking experiments. In addition, we report that this interaction between

GlialCAM monomers is mediated by outward-facing α-helices. Interestingly, the residues encoded by patient-derived GlialCAM IgC2 mutations are located within these motifs.

Our former works already established that mutants p.Ser196>Tyr and p.Asp211>Asn showed a lack of endocytosis phenotype. Specifically, experiments carried out in primary astrocytes showed that GlialCAM variants bearing those mutations were resistant to endocytosis upon incubation in potassium-enriched conditions in the absence of Mlc1. A similar phenotype was observed for GlialCAM upon GPRC5B overexpression: whereas GPRC5B induced GlialCAM endocytosis in physiological conditions in primary astrocytes, this internalization is not induced in the absence of MLC1. Thus, our experimental data allows us to propose a mechanism to explain the pathogenicity of GlialCAM IgC2 mutations. Here, we report that the observed abnormal phenotype of the mutant variants is due to the stabilization of GlialCAM oligomeric structures provided by the mutation that prevent its physiological endocytosis. This endocytosis would be mediated by GPRC5B, so that an internalized GPRC5B/GlialCAM complex would be involved in signaling pathways yet to be characterized. We believe that our observations could also be explained by a signaling activity from endosomes as it has been reported to happen for some GPCRs like β2-adrenoceptor (Irannejad et al., 2013). The visual summary of our proposed model is featured in Figure 92**.**

Last, in **Figure 78** from chapter 2.5 of this thesis Results section, we proposed the mechanism by which IgC2 mutations achieve the stabilization of GlialCAM oligomeric structures. Specifically, we hypothesized that p.Ser196>Tyr would favor the formation of a *de novo* cation pi interaction with a neighboring Lysine residue (K185), whereas p.Asp>211Asn would be removing electrostatic repulsion through the loss of a negative charge in the oligomerization interface. Therefore, future mutagenesis experiments could be useful to further confirm this mechanism. In the case of K185 – Y196 (mutant residue) cation- pi formation, we could clone a GlialCAM variant replacing K185 for a small, apolar amino acid like Alanine. We would expect the double mutant K185A/S196Y to rescue the WT phenotype by removal of the *de novo* cation-pi interaction that we hypothesize the mutation is originating.

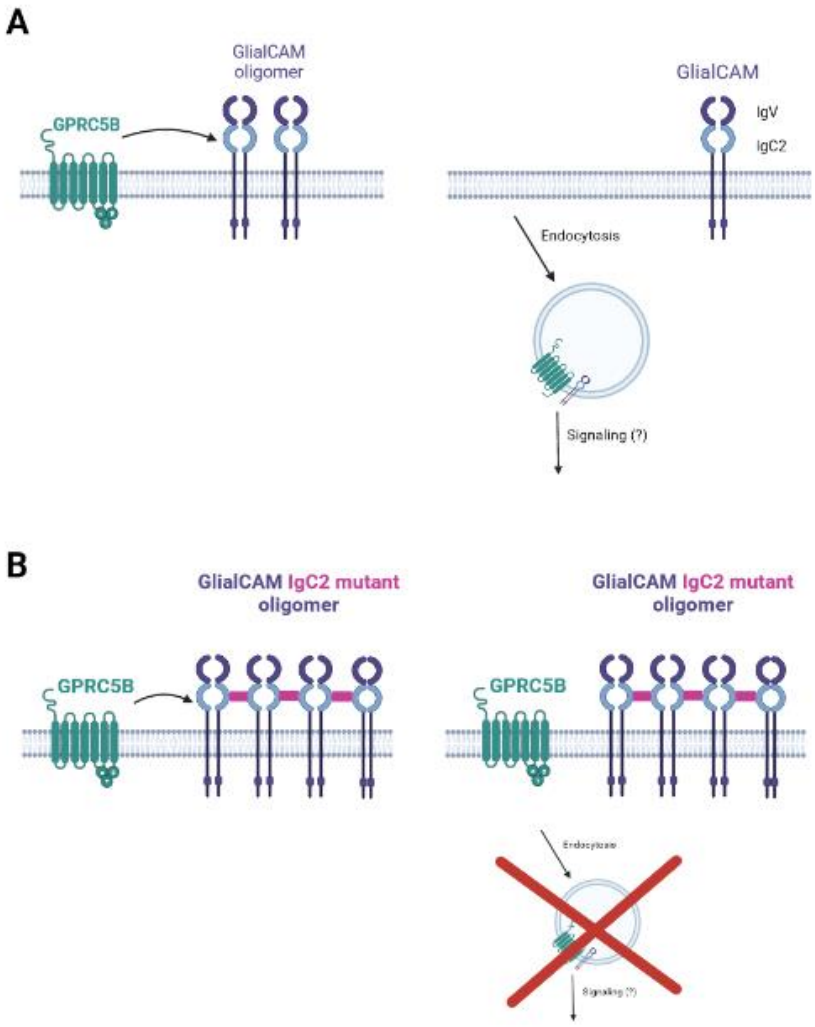

Figure 92. MLC-causing GLIALCAM mutations encoding for residues located at IgC2 domain abnormally stabilize GlialCAM oligomeric structures. A Our proposed model is that GPRC5B interacts with GlialCAM at the plasma membrane of astrocytes, leading to the endocytosis of both proteins. We believe that the complex formed by GPRC5B/GlialCAM could be important for signal transduction from the resulting endosomes. **B** GlialCAM mutant variants would be abnormally stabilized at the plasma membrane, preventing the dissociation of the oligomeric structure. Thus, no GlialCAM would be released to interact and bind GPRC5B. Hence, potential downstream signaling of this complex regulating homeostasic processes would not occur, leading to disease.

Signaling events in MLC-related chloride channels regulation

In the past, several signaling pathways have been associated with MLC1 activity, being ERK phosphorylation one of the most studied (Elorza-Vidal et al., 2018). Also, GlialCAM/MLC1 have been shown to be involved with the regulation of chloride channel activity, especially VRAC and ClC-2 (Alonso-Gardón et al., 2021, Capdevila-Nortes et al., 2013, Dubey et al., 2015).

Published results from our grup demonstrated that GPRC5B is important for VRAC function and for ClC-2 localization (Alonso-Gardón et al., 2021). From those results, we continued to study how signaling processes affect MLC-related chloride channels at a functional level.

Tyrosine phosphorylation had been proposed as an activation mechanism for VRAC (Bertelli et al., 2021). Specifically, PKC downstream signaling was suggested as the mechanism underlying this phosphorylation events regulating VRAC activity (König et al., 2019). With this thesis, we intended to figure out whether GPRC5B was involved in activation of VRAC through phosphorylation. On the one hand, our results indicated that GPRC5B is indeed modulating VRAC activity via Fyn kinase. However, we also showed that Fyn effect would be kinase-independent, since inhibitors of its enzymatic activity did not influence VRAC activation mediated by GPRC5B. Interestingly, some researchers observed a similar effect on the modulation of VRAC activity in caveolae regarding c-Src kinase. For that case, the authors of the study showed that it was direct interaction between c-Src and VRAC that led to the observed modulation of the channel activity (Trouet et al., 2001). On the other hand, within our work in this thesis we also identified that GPRC5B would be acting downstream with $G_{\alpha 12/\alpha 13}$ proteins. Related to that finding, other published studies connect the activity of such G-proteins to Rho and Rho associated kinase (ROCK) signaling pathway, that are necessary for VRAC currents (Carton et al., 2002).

Therefore, our results are compatible with two independent modulatory mechanisms of VRAC activity mediated by GPRC5B. A summarized model integrating the two pathways is featured in **Figure 93**.

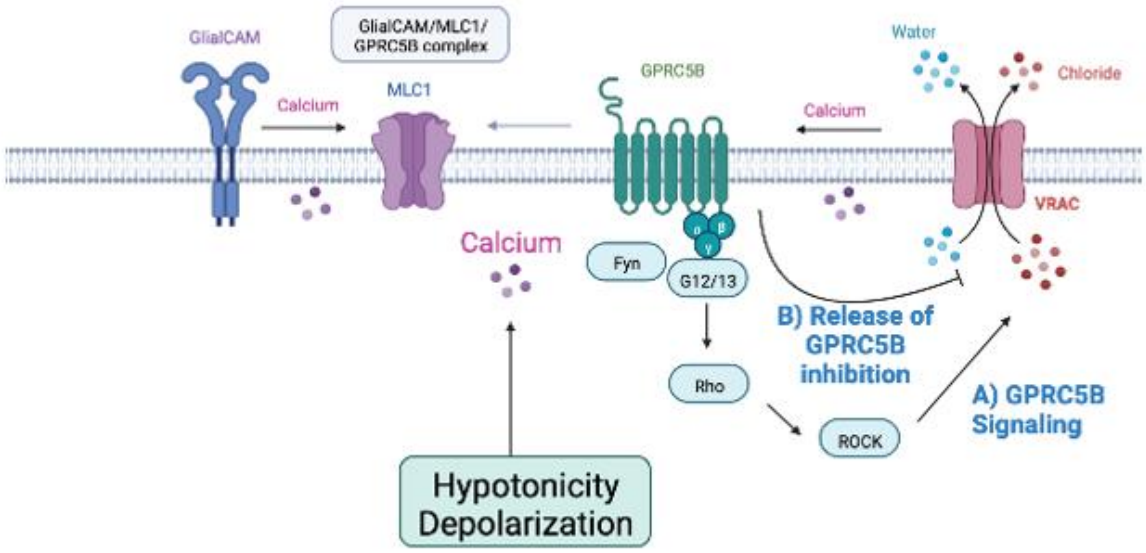

Figure 93. Hypothetical scheme of VRAC channel activity regulation by GPRC5B and the GlialCAM/MLC1 complex. As indicated, two mechanisms are postulated: **A** Hypotonicity and/or depolarization leads to an increase of intracellular calcium, which leads to an increase in the formation of the GlialCAM/MLC1/GPRC5B complex. Activated GPRC5B would signal through $G_{\alpha 12}/G_{\alpha 13}$ release, resulting in the activitation of the GTPase Rho and the Rho associated kinase (ROCK), which have been shown to activate the VRAC channel. **B** Fyn, downstream effector of GPRC5B, interacts directly with the LRRC8A subunit and it inactivates the channel. The release of GPRC5B from VRAC through its interaction with the GlialCAM/MLC1 complex might end VRAC inhibition.

Alternatively, we analyzed the effect of phosphorylation on ClC-2 activity. We observed that dephosphorylation events in key residues, especially residue Serine 647, was necessary for subcellular localization of the channel and its gating alteration characteristic of a context of high neuronal activity. In the future, it will be interesting to identify which are the molecular partners that specifically phosphorylate and dephosphorylate ClC-2 at this residue. Dr Kevin Strange and colleagues work with the ClC-2 ortholog in *C.elegans,* which is CLH-3b. Using oocytes from these animals as a model, they have shown that inhibitors of PP2A (Calyculin A) reduce current activation in up to 90 % (Rutledge et al., 2002).

Concluding remarks of the relevance of our findings in MLC disease and in glial physiology

This thesis has served to obtain valuable new knowledge of the pathophysiological events responsible for MLC disease that could help develop novel therapies for patients in the

future. We hope that the focus on the interplay between GlialCAM/MLC1, chloride channels, and especially GPRC5B/signaling pathways will provide a new therapeutic outlook that will lead to novel treatments to improve the condition of patients suffering from MLC and other pathologies that involve these pathophysiologic processes.

CONCLUSIONS

1. GPRC5B overexpression in rat primary astrocytes is able to induce VCAM-1 upregulation like TNF-α treatments. This effect is mediated by a downstream effector of GPRC5B, Fyn kinase. The activity of this enzyme leads to the activation of NF-κB signaling pathway, that results in enhanced VCAM-1 expression. MLC1 has a negative modulatory effect on this process.
2. GlialCAM IgC2 domain is involved in the formation of oligomeric GlialCAM structures through the interaction with other IgC2 domains from adjacent GlialCAM molecules. Specifically, two outward facing α-helices conform the interaction surfaces responsible for this oligomerization.
3. Patient-derived *GLIALCAM* mutations encoding for residues located at GlialCAM IgC2 domain result in a gain-of-function-like stabilization of oligomeric structures. This phenotype hampers the internalization ability of GlialCAM, which is mediated by GPRC5B.
4. GPRC5B modulates VRAC activity in rat primary astrocytes in a Fyn-dependent manner.
5. Dephosphorylation changes on specific ClC-2 serine residues are responsible for the change of both the subcellular localization of the channel and its gating properties, in a context of depolarizing conditions in rat primary astrocytes.

BIBLIOGRAPHY

ABASCAL, F. & ZARDOYA, R. 2012. LRRC8 proteins share a common ancestor with pannexins, and may form hexameric channels involved in cell-cell communication. *Bioessays,* 34**,** 551-60.

ABBOTT, N. J., RÖNNBÄCK, L. & HANSSON, E. 2006. Astrocyte-endothelial interactions at the blood-brain barrier. *Nat Rev Neurosci,* 7**,** 41-53.

ABRAMS, C. K. & SCHERER, S. S. 2012. Gap junctions in inherited human disorders of the central nervous system. *Biochim Biophys Acta,* 1818**,** 2030-47.

ACCARDI, A. & PUSCH, M. 2000. Fast and slow gating relaxations in the muscle chloride channel CLC-1. *J Gen Physiol,* 116**,** 433-44.

AFSHARI, F. S., CHU, A. K. & SATO-BIGBEE, C. 2001. Effect of cyclic AMP on the expression of myelin basic protein species and myelin proteolipid protein in committed oligodendrocytes: differential involvement of the transcription factor CREB. *J Neurosci Res,* 66**,** 37-45.

AKITA, T. & OKADA, Y. 2014. Characteristics and roles of the volume-sensitive outwardly rectifying (VSOR) anion channel in the central nervous system. *Neuroscience,* 275**,** 211-31.

ALBAYRAK, Ö., PÜTTER, C., VOLCKMAR, A. L., CICHON, S., HOFFMANN, P., NÖTHEN, M. M., JÖCKEL, K. H., SCHREIBER, S., WICHMANN, H. E., FARAONE, S. V., NEALE, B. M., HERPERTZ-DAHLMANN, B., LEHMKUHL, G., SINZIG, J., RENNER, T. J., ROMANOS, M., WARNKE, A., LESCH, K. P., REIF, A., SCHIMMELMANN, B. G., SCHERAG, A., HEBEBRAND, J., HINNEY, A. & SUBGROUP, P. G. C. A. 2013. Common obesity risk alleles in childhood attention-deficit/hyperactivity disorder. *Am J Med Genet B Neuropsychiatr Genet,* 162B**,** 295-305.

ALEXANDER, S. P., BENSON, H. E., FACCENDA, E., PAWSON, A. J., SHARMAN, J. L., SPEDDING, M., PETERS, J. A., HARMAR, A. J. & COLLABORATORS, C. 2013. The Concise Guide to PHARMACOLOGY 2013/14: G protein-coupled receptors. *Br J Pharmacol,* 170**,** 1459-581.

ALLEN, N. J. & BARRES, B. A. 2005. Signaling between glia and neurons: focus on synaptic plasticity. *Curr Opin Neurobiol,* 15**,** 542-8.

ALON, R., KASSNER, P. D., CARR, M. W., FINGER, E. B., HEMLER, M. E. & SPRINGER, T. A. 1995. The integrin VLA-4 supports tethering and rolling in flow on VCAM-1. *J Cell Biol,* 128**,** 1243-53.

ALONSO-GARDÓN, M., ELORZA-VIDAL, X., CASTELLANOS, A., LA SALA, G., ARMAND-UGON, M., GILBERT, A., DI PIETRO, C., PLA-CASILLANIS, A., CIRUELA, F., GASULL, X., NUNES, V., MARTÍNEZ, A., SCHULTE, U., COHEN-SALMON, M., MARAZZITI, D. & ESTÉVEZ, R. 2021. Identification of the GlialCAM interactome: the G protein-coupled receptors GPRC5B and GPR37L1 modulate megalencephalic leukoencephalopathy proteins. *Hum Mol Genet,* 30**,** 1649-1665.

ALTEVOGT, B. M. & PAUL, D. L. 2004. Four classes of intercellular channels between glial cells in the CNS. *J Neurosci,* 24**,** 4313-23.

AMBROSINI, E., SERAFINI, B., LANCIOTTI, A., TOSINI, F., SCIALPI, F., PSAILA, R., RAGGI, C., DI GIROLAMO, F., PETRUCCI, T. C. & ALOISI, F. 2008. Biochemical characterization of MLC1 protein in astrocytes and its association with the dystrophin-glycoprotein complex. *Mol Cell Neurosci,* 37**,** 480-93.

AMIRY-MOGHADDAM, M., OTSUKA, T., HURN, P. D., TRAYSTMAN, R. J., HAUG, F. M., FROEHNER, S. C., ADAMS, M. E., NEELY, J. D., AGRE, P., OTTERSEN, O. P. & BHARDWAJ, A. 2003a. An alpha-syntrophin-dependent pool of AQP4 in astroglial

end-feet confers bidirectional water flow between blood and brain. *Proc Natl Acad Sci U S A,* 100**,** 2106-11.

AMIRY-MOGHADDAM, M., WILLIAMSON, A., PALOMBA, M., EID, T., DE LANEROLLE, N. C., NAGELHUS, E. A., ADAMS, M. E., FROEHNER, S. C., AGRE, P. & OTTERSEN, O. P. 2003b. Delayed K+ clearance associated with aquaporin-4 mislocalization: phenotypic defects in brains of alpha-syntrophin-null mice. *Proc Natl Acad Sci U S A,* 100**,** 13615-20.

ARNEDO, T., AIELLO, C., JEWORUTZKI, E., DENTICI, M. L., UZIEL, G., SIMONATI, A., PUSCH, M., BERTINI, E. & ESTÉVEZ, R. 2014a. Expanding the spectrum of megalencephalic leukoencephalopathy with subcortical cysts in two patients with GLIALCAM mutations. *Neurogenetics,* 15**,** 41-8.

ARNEDO, T., LÓPEZ-HERNÁNDEZ, T., JEWORUTZKI, E., CAPDEVILA-NORTES, X., SIRISI, S., PUSCH, M. & ESTÉVEZ, R. 2014b. Functional analyses of mutations in HEPACAM causing megalencephalic leukoencephalopathy. *Hum Mutat,* 35**,** 1175-8.

ATANES, P., RUZ-MALDONADO, I., HAWKES, R., LIU, B., PERSAUD, S. J. & AMISTEN, S. 2018. Identifying Signalling Pathways Regulated by GPRC5B in β-Cells by CRISPR-Cas9-Mediated Genome Editing. *Cell Physiol Biochem,* 45**,** 656-666.

AURRAND-LIONS, M., JOHNSON-LEGER, C., WONG, C., DU PASQUIER, L. & IMHOF, B. A. 2001. Heterogeneity of endothelial junctions is reflected by differential expression and specific subcellular localization of the three JAM family members. *Blood,* 98**,** 3699-707.

BAIG, D. N., YANAGAWA, T. & TABUCHI, K. 2017. Distortion of the normal function of synaptic cell adhesion molecules by genetic variants as a risk for autism spectrum disorders. *Brain Res Bull,* 129**,** 82-90.

BALDWIN, K. T., TAN, C. X., STRADER, S. T., JIANG, C., SAVAGE, J. T., ELORZA-VIDAL, X., CONTRERAS, X., RÜLICKE, T., HIPPENMEYER, S., ESTÉVEZ, R., JI, R. R. & EROGLU, C. 2021. HepaCAM controls astrocyte self-organization and coupling. *Neuron,* 109**,** 2427-2442.e10.

BARNETT, S. C. & LININGTON, C. 2013. Myelination: do astrocytes play a role? *Neuroscientist,* 19**,** 442-50.

BARRALLO-GIMENO, A., GRADOGNA, A., ZANARDI, I., PUSCH, M. & ESTÉVEZ, R. 2015. Regulatory-auxiliary subunits of CLC chloride channel-transport proteins. *J Physiol,* 593**,** 4111-27.

BEAUDOIN, G. M. 2006. Con-nectin axons and dendrites. *J Cell Biol,* 174**,** 7-9.

BEKAR, L. K. & NEDERGAARD, M. 2013. Is potassium a ubiquitous mediator of vasodilation in the central nervous system? *Biophys J,* 105**,** 2238-9.

BEN-ZEEV, B., LEVY-NISSENBAUM, E., LAHAT, H., ANIKSTER, Y., SHINAR, Y., BRAND, N., GROSS-TZUR, V., MACGREGOR, D., SIDI, R., KLETA, R., FRYDMAN, M. & PRAS, E. 2002. Megalencephalic leukoencephalopathy with subcortical cysts; a founder effect in Israeli patients and a higher than expected carrier rate among Libyan Jews. *Hum Genet,* 111**,** 214-8.

BENARROCH, E. E. 2005. Neuron-astrocyte interactions: partnership for normal function and disease in the central nervous system. *Mayo Clin Proc,* 80**,** 1326-38.

BENFENATI, V., AMIRY-MOGHADDAM, M., CAPRINI, M., MYLONAKOU, M. N., RAPISARDA, C., OTTERSEN, O. P. & FERRONI, S. 2007. Expression and functional characterization of transient receptor potential vanilloid-related channel 4 (TRPV4) in rat cortical astrocytes. *Neuroscience,* 148**,** 876-92.

BENFENATI, V., CAPRINI, M., DOVIZIO, M., MYLONAKOU, M. N., FERRONI, S., OTTERSEN, O. P. & AMIRY-MOGHADDAM, M. 2011. An aquaporin-4/transient receptor potential vanilloid 4 (AQP4/TRPV4) complex is essential for cell-volume control in astrocytes. *Proc Natl Acad Sci U S A,* 108**,** 2563-8.

BENFENATI, V. & FERRONI, S. 2010. Water transport between CNS compartments: functional and molecular interactions between aquaporins and ion channels. *Neuroscience,* 168**,** 926-40.

BERGELSON, J. M., CUNNINGHAM, J. A., DROGUETT, G., KURT-JONES, E. A., KRITHIVAS, A., HONG, J. S., HORWITZ, M. S., CROWELL, R. L. & FINBERG, R. W. 1997. Isolation of a common receptor for Coxsackie B viruses and adenoviruses 2 and 5. *Science,* 275**,** 1320-3.

BERTELLI, S., REMIGANTE, A., ZUCCOLINI, P., BARBIERI, R., FERRERA, L., PICCO, C., GAVAZZO, P. & PUSCH, M. 2021. Mechanisms of Activation of LRRC8 Volume Regulated Anion Channels. *Cell Physiol Biochem,* 55**,** 41-56.

BIGNAMI, A., ENG, L. F., DAHL, D. & UYEDA, C. T. 1972. Localization of the glial fibrillary acidic protein in astrocytes by immunofluorescence. *Brain Res,* 43**,** 429-35.

BLACKBURN, D., SARGSYAN, S., MONK, P. N. & SHAW, P. J. 2009. Astrocyte function and role in motor neuron disease: a future therapeutic target? *Glia,* 57**,** 1251-64.

BLANZ, J., SCHWEIZER, M., AUBERSON, M., MAIER, H., MUENSCHER, A., HÜBNER, C. A. & JENTSCH, T. J. 2007. Leukoencephalopathy upon disruption of the chloride channel ClC-2. *J Neurosci,* 27**,** 6581-9.

BLATTNER, R., VON MOERS, A., LEEGWATER, P. A., HANEFELD, F. A., VAN DER KNAAP, M. S. & KÖHLER, W. 2003. Clinical and genetic heterogeneity in megalencephalic leukoencephalopathy with subcortical cysts (MLC). *Neuropediatrics,* 34**,** 215-8.

BOOR, I., NAGTEGAAL, M., KAMPHORST, W., VAN DER VALK, P., PRONK, J. C., VAN HORSSEN, J., DINOPOULOS, A., BOVE, K. E., PASCUAL-CASTROVIEJO, I., MUNTONI, F., ESTÉVEZ, R., SCHEPER, G. C. & VAN DER KNAAP, M. S. 2007. MLC1 is associated with the dystrophin-glycoprotein complex at astrocytic endfeet. *Acta Neuropathol,* 114**,** 403-10.

BOOR, P. K., DE GROOT, K., WAISFISZ, Q., KAMPHORST, W., OUDEJANS, C. B., POWERS, J. M., PRONK, J. C., SCHEPER, G. C. & VAN DER KNAAP, M. S. 2005. MLC1: a novel protein in distal astroglial processes. *J Neuropathol Exp Neurol,* 64**,** 412-9.

BORK, P., HOLM, L. & SANDER, C. 1994. The immunoglobulin fold. Structural classification, sequence patterns and common core. *J Mol Biol,* 242**,** 309-20.

BORTOLATO, A., DORÉ, A. S., HOLLENSTEIN, K., TEHAN, B. G., MASON, J. S. & MARSHALL, F. H. 2014. Structure of Class B GPCRs: new horizons for drug discovery. *Br J Pharmacol,* 171**,** 3132-45.

BOSCH, A. & ESTÉVEZ, R. 2020. Megalencephalic Leukoencephalopathy: Insights Into Pathophysiology and Perspectives for Therapy. *Front Cell Neurosci,* 14**,** 627887.

BOURQUE, C. W. & OLIET, S. H. 1997. Osmoreceptors in the central nervous system. *Annu Rev Physiol,* 59**,** 601-19.

BOVOLENTA, P., LIEM, R. K. & MASON, C. A. 1984. Development of cerebellar astroglia: transitions in form and cytoskeletal content. *Dev Biol,* 102**,** 248-59.

BRENNER, D., BLASER, H. & MAK, T. W. 2015. Regulation of tumour necrosis factor signalling: live or let die. *Nat Rev Immunol,* 15**,** 362-74.

BRIGNONE, M. S., LANCIOTTI, A., CAMERINI, S., DE NUCCIO, C., PETRUCCI, T. C., VISENTIN, S. & AMBROSINI, E. 2015. MLC1 protein: a likely link between leukodystrophies and brain channelopathies. *Front Cell Neurosci,* 9**,** 66.

BRIGNONE, M. S., LANCIOTTI, A., MACIOCE, P., MACCHIA, G., GAETANI, M., ALOISI, F., PETRUCCI, T. C. & AMBROSINI, E. 2011. The beta1 subunit of the Na,K-ATPase pump interacts with megalencephalic leucoencephalopathy with subcortical cysts protein 1 (MLC1) in brain astrocytes: new insights into MLC pathogenesis. *Hum Mol Genet,* 20**,** 90-103.

BRIGNONE, M. S., LANCIOTTI, A., SERAFINI, B., MALLOZZI, C., SBRICCOLI, M., VERONI, C., MOLINARI, P., ELORZA-VIDAL, X., PETRUCCI, T. C., ESTÉVEZ, R. & AMBROSINI, E. 2019. Megalencephalic Leukoencephalopathy with Subcortical Cysts Protein-1 (MLC1) Counteracts Astrocyte Activation in Response to Inflammatory Signals. *Mol Neurobiol,* 56**,** 8237-8254.

BRIGNONE, M. S., LANCIOTTI, A., VISENTIN, S., DE NUCCIO, C., MOLINARI, P., CAMERINI, S., DIOCIAIUTI, M., PETRINI, S., MINNONE, G., CRESCENZI, M., LAUDIERO, L. B., BERTINI, E., PETRUCCI, T. C. & AMBROSINI, E. 2014. Megalencephalic leukoencephalopathy with subcortical cysts protein-1 modulates endosomal pH and protein trafficking in astrocytes: relevance to MLC disease pathogenesis. *Neurobiol Dis,* 66**,** 1-18.

BROCKMANN, K., FINSTERBUSCH, J., TERWEY, B., FRAHM, J. & HANEFELD, F. 2003. Megalencephalic leukoencephalopathy with subcortical cysts in an adult: quantitative proton MR spectroscopy and diffusion tensor MRI. *Neuroradiology,* 45**,** 137-42.

BRÄUNER-OSBORNE, H., WELLENDORPH, P. & JENSEN, A. A. 2007. Structure, pharmacology and therapeutic prospects of family C G-protein coupled receptors. *Curr Drug Targets,* 8**,** 169-84.

BRÜMMENDORF, T. & RATHJEN, F. G. 1996. Structure/function relationships of axon-associated adhesion receptors of the immunoglobulin superfamily. *Curr Opin Neurobiol,* 6**,** 584-93.

BUGIANI, M., DUBEY, M., BREUR, M., POSTMA, N. L., DEKKER, M. P., TER BRAAK, T., BOSCHERT, U., ABBINK, T. E. M., MANSVELDER, H. D., MIN, R., VAN WEERING, J. R. T. & VAN DER KNAAP, M. S. 2017. Megalencephalic leukoencephalopathy with cysts: the. *Ann Clin Transl Neurol,* 4**,** 450-465.

BUTT, A. M. & KALSI, A. 2006. Inwardly rectifying potassium channels (Kir) in central nervous system glia: a special role for Kir4.1 in glial functions. *J Cell Mol Med,* 10**,** 33-44.

BÖSL, M. R., STEIN, V., HÜBNER, C., ZDEBIK, A. A., JORDT, S. E., MUKHOPADHYAY, A. K., DAVIDOFF, M. S., HOLSTEIN, A. F. & JENTSCH, T. J. 2001. Male germ cells and photoreceptors, both dependent on close cell-cell interactions, degenerate upon ClC-2 Cl(-) channel disruption. *EMBO J,* 20**,** 1289-99.

CAO, B., YAN, H., GUO, M., XIE, H., WU, Y., GU, Q., XIAO, J., SHANG, J., YANG, Y., XIONG, H., NIU, Z., WU, X., JIANG, Y. & WANG, J. 2016. Ten Novel Mutations in Chinese Patients with Megalencephalic Leukoencephalopathy with Subcortical Cysts and a Long-Term Follow-Up Research. *PLoS One,* 11**,** e0157258.

CAO, X. & TABUCHI, K. 2017. Functions of synapse adhesion molecules neurexin/neuroligins and neurodevelopmental disorders. *Neurosci Res,* 116**,** 3-9.

CAPDEVILA-NORTES, X., JEWORUTZKI, E., ELORZA-VIDAL, X., BARRALLO-GIMENO, A., PUSCH, M. & ESTÉVEZ, R. 2015. Structural determinants of interaction, trafficking and function in the ClC-2/MLC1 subunit GlialCAM involved in leukodystrophy. *J Physiol,* 593**,** 4165-80.

CAPDEVILA-NORTES, X., LÓPEZ-HERNÁNDEZ, T., APAJA, P. M., LÓPEZ DE HEREDIA, M., SIRISI, S., CALLEJO, G., ARNEDO, T., NUNES, V., LUKACS, G. L., GASULL, X. & ESTÉVEZ, R. 2013. Insights into MLC pathogenesis: GlialCAM is an MLC1 chaperone required for proper activation of volume-regulated anion currents. *Hum Mol Genet,* 22**,** 4405-16.

CAPDEVILA-NORTES, X., LÓPEZ-HERNÁNDEZ, T., CIRUELA, F. & ESTÉVEZ, R. 2012. A modification of the split-tobacco etch virus method for monitoring interactions between membrane proteins in mammalian cells. *Anal Biochem,* 423**,** 109-18.

CARTON, I., TROUET, D., HERMANS, D., BARTH, H., AKTORIES, K., DROOGMANS, G., JORGENSEN, N. K., HOFFMANN, E. K., NILIUS, B. & EGGERMONT, J. 2002. RhoA exerts a permissive effect on volume-regulated anion channels in vascular endothelial cells. *Am J Physiol Cell Physiol,* 283**,** C115-25.

CATALÁN, M. A., FLORES, C. A., GONZÁLEZ-BEGNE, M., ZHANG, Y., SEPÚLVEDA, F. V. & MELVIN, J. E. 2012. Severe defects in absorptive ion transport in distal colons of mice that lack ClC-2 channels. *Gastroenterology,* 142**,** 346-54.

CAVALLARO, U. & DEJANA, E. 2011. Adhesion molecule signalling: not always a sticky business. *Nat Rev Mol Cell Biol,* 12**,** 189-97.

CECCHELLI, R., BEREZOWSKI, V., LUNDQUIST, S., CULOT, M., RENFTEL, M., DEHOUCK, M. P. & FENART, L. 2007. Modelling of the blood-brain barrier in drug discovery and development. *Nat Rev Drug Discov,* 6**,** 650-61.

CERUTTI, C. & RIDLEY, A. J. 2017. Endothelial cell-cell adhesion and signaling. *Exp Cell Res,* 358**,** 31-38.

CHATZANTONI, K. & MOUZAKI, A. 2006. Anti-TNF-alpha antibody therapies in autoimmune diseases. *Curr Top Med Chem,* 6**,** 1707-14.

CHENG, Y. & LOTAN, R. 1998. Molecular cloning and characterization of a novel retinoic acid-inducible gene that encodes a putative G protein-coupled receptor. *J Biol Chem,* 273**,** 35008-15.

CHENG, Z., GARVIN, D., PAGUIO, A., STECHA, P., WOOD, K. & FAN, F. 2010. Luciferase Reporter Assay System for Deciphering GPCR Pathways. *Curr Chem Genomics,* 4**,** 84-91.

CHEVER, O., DJUKIC, B., MCCARTHY, K. D. & AMZICA, F. 2010. Implication of Kir4.1 channel in excess potassium clearance: an in vivo study on anesthetized glial-conditional Kir4.1 knock-out mice. *J Neurosci,* 30**,** 15769-77.

CHMELOVA, M., SUCHA, P., BOCHIN, M., VORISEK, I., PIVONKOVA, H., HERMANOVA, Z., ANDEROVA, M. & VARGOVA, L. 2019. The role of aquaporin-4 and transient receptor potential vaniloid isoform 4 channels in the development of cytotoxic edema and associated extracellular diffusion parameter changes. *Eur J Neurosci,* 50**,** 1685-1699.

CHOW, B. W. & GU, C. 2015. The molecular constituents of the blood-brain barrier. *Trends Neurosci,* 38**,** 598-608.

CHUN, L., ZHANG, W. H. & LIU, J. F. 2012. Structure and ligand recognition of class C GPCRs. *Acta Pharmacol Sin,* 33**,** 312-23.

CHUNG MOH, M., HOON LEE, L. & SHEN, S. 2005. Cloning and characterization of hepaCAM, a novel Ig-like cell adhesion molecule suppressed in human hepatocellular carcinoma. *J Hepatol,* 42**,** 833-41.

CLAING, A., LAPORTE, S. A., CARON, M. G. & LEFKOWITZ, R. J. 2002. Endocytosis of G protein-coupled receptors: roles of G protein-coupled receptor kinases and beta-arrestin proteins. *Prog Neurobiol,* 66**,** 61-79.

CLAUSEN, T. 1992. Potassium and sodium transport and pH regulation. *Can J Physiol Pharmacol,* 70 Suppl**,** S219-22.

COHEN, C. J., GAETZ, J., OHMAN, T. & BERGELSON, J. M. 2001. Multiple regions within the coxsackievirus and adenovirus receptor cytoplasmic domain are required for basolateral sorting. *J Biol Chem,* 276**,** 25392-8.

CONNORS, B. W., RANSOM, B. R., KUNIS, D. M. & GUTNICK, M. J. 1982. Activity-dependent K+ accumulation in the developing rat optic nerve. *Science,* 216**,** 1341-3.

COOK-MILLS, J. M., MARCHESE, M. E. & ABDALA-VALENCIA, H. 2011. Vascular cell adhesion molecule-1 expression and signaling during disease: regulation by reactive oxygen species and antioxidants. *Antioxid Redox Signal,* 15**,** 1607-38.

CORNEJO, I., NIEMEYER, M. I., ZÚÑIGA, L., YUSEF, Y. R., SEPÚLVEDA, F. V. & CID, L. P. 2009. Rapid recycling of ClC-2 chloride channels between plasma membrane and endosomes: role of a tyrosine endocytosis motif in surface retrieval. *J Cell Physiol,* 221**,** 650-7.

CORTEZ, M. A., LI, C., WHITEHEAD, S. N., DHANI, S. U., D'ANTONIO, C., HUAN, L. J., BENNETT, S. A., SNEAD, O. C. & BEAR, C. E. 2010. Disruption of ClC-2 expression is associated with progressive neurodegeneration in aging mice. *Neuroscience,* 167**,** 154-62.

COTRINA, M. L., KANG, J., LIN, J. H., BUENO, E., HANSEN, T. W., HE, L., LIU, Y. & NEDERGAARD, M. 1998. Astrocytic gap junctions remain open during ischemic conditions. *J Neurosci,* 18**,** 2520-37.

CRÉPEL, V., PANENKA, W., KELLY, M. E. & MACVICAR, B. A. 1998. Mitogen-activated protein and tyrosine kinases in the activation of astrocyte volume-activated chloride current. *J Neurosci,* 18**,** 1196-206.

D'AGOSTINO, D., BERTELLI, M., GALLO, S., CECCHIN, S., ALBIERO, E., GAROFALO, P. G., GAMBARDELLA, A., ST HILAIRE, J. M., KWIECINSKI, H., ANDERMANN, E. & PANDOLFO, M. 2004. Mutations and polymorphisms of the CLCN2 gene in idiopathic epilepsy. *Neurology,* 63**,** 1500-2.

D'AMBROSIO, R., GORDON, D. S. & WINN, H. R. 2002. Differential role of KIR channel and Na(+)/K(+)-pump in the regulation of extracellular K(+) in rat hippocampus. *J Neurophysiol,* 87**,** 87-102.

DAVENPORT, A. P., ALEXANDER, S. P., SHARMAN, J. L., PAWSON, A. J., BENSON, H. E., MONAGHAN, A. E., LIEW, W. C., MPAMHANGA, C. P., BONNER, T. I., NEUBIG, R. R., PIN, J. P., SPEDDING, M. & HARMAR, A. J. 2013. International Union of Basic and Clinical Pharmacology. LXXXVIII. G protein-coupled receptor list: recommendations for new pairings with cognate ligands. *Pharmacol Rev,* 65**,** 967-86.

DAVIES, M. N., SECKER, A., FREITAS, A. A., MENDAO, M., TIMMIS, J. & FLOWER, D. R. 2007. On the hierarchical classification of G protein-coupled receptors. *Bioinformatics,* 23**,** 3113-8.

DE SANTIAGO, J. A., NEHRKE, K. & ARREOLA, J. 2005. Quantitative analysis of the voltage-dependent gating of mouse parotid ClC-2 chloride channel. *J Gen Physiol,* 126**,** 591-603.

DE STEFANO, N., BALESTRI, P., DOTTI, M. T., GROSSO, S., MORTILLA, M., MORGESE, G. & FEDERICO, A. 2001. Severe metabolic abnormalities in the white matter of patients with vacuolating megalencephalic leukoencephalopathy with subcortical cysts. A proton MR spectroscopic imaging study. *J Neurol,* 248**,** 403-9.

DEEM, T. L., ABDALA-VALENCIA, H. & COOK-MILLS, J. M. 2007. VCAM-1 activation of endothelial cell protein tyrosine phosphatase 1B. *J Immunol,* 178**,** 3865-73.

DENG, J., FUJIMOTO, J., YE, X. F., MEN, T. Y., VAN PELT, C. S., CHEN, Y. L., LIN, X. F., KADARA, H., TAO, Q., LOTAN, D. & LOTAN, R. 2010. Knockout of the tumor suppressor gene Gprc5a in mice leads to NF-kappaB activation in airway epithelium and promotes lung inflammation and tumorigenesis. *Cancer Prev Res (Phila),* 3**,** 424-37.

DEPIENNE, C., BUGIANI, M., DUPUITS, C., GALANAUD, D., TOUITOU, V., POSTMA, N., VAN BERKEL, C., POLDER, E., TOLLARD, E., DARIOS, F., BRICE, A., DE DIE-SMULDERS, C. E., VLES, J. S., VANDERVER, A., UZIEL, G., YALCINKAYA, C., FRINTS, S. G., KALSCHEUER, V. M., KLOOSTER, J., KAMERMANS, M., ABBINK, T. E., WOLF, N. I., SEDEL, F. & VAN DER KNAAP, M. S. 2013. Brain white matter oedema due to ClC-2 chloride channel deficiency: an observational analytical study. *Lancet Neurol,* 12**,** 659-68.

DEV, K. K., VAN DER PUTTEN, H., SOMMER, B. & ROVELLI, G. 2003. Part I: parkin-associated proteins and Parkinson's disease. *Neuropharmacology,* 45**,** 1-13.

DEWA, K. I. & ARIMURA, N. 2022. Neuronal and astrocytic protein connections and associated adhesion molecules. *Neurosci Res*.

DEWIRE, S. M., AHN, S., LEFKOWITZ, R. J. & SHENOY, S. K. 2007. Beta-arrestins and cell signaling. *Annu Rev Physiol,* 69**,** 483-510.

DHANI, S. U., KIM CHIAW, P., HUAN, L. J. & BEAR, C. E. 2008. ATP depletion inhibits the endocytosis of ClC-2. *J Cell Physiol,* 214**,** 273-80.

DI BELLA, D., PAREYSON, D., SAVOIARDO, M., FARINA, L., CIANO, C., CALDARAZZO, S., SAGNELLI, A., BONATO, S., NAVA, S., BRESOLIN, N., TEDESCHI, G., TARONI, F. & SALSANO, E. 2014. Subclinical leukodystrophy and infertility in a man with a novel homozygous CLCN2 mutation. *Neurology,* 83**,** 1217-8.

DOMINGUES, H. S., PORTUGAL, C. C., SOCODATO, R. & RELVAS, J. B. 2016. Corrigendum: Oligodendrocyte, Astrocyte and Microglia Crosstalk in Myelin Development, Damage, and Repair. *Front Cell Dev Biol,* 4**,** 79.

DONOHUE, P. J., SHAPIRA, H., MANTEY, S. A., HAMPTON, L. L., JENSEN, R. T. & BATTEY, J. F. 1998. A human gene encodes a putative G protein-coupled receptor highly expressed in the central nervous system. *Brain Res Mol Brain Res,* 54**,** 152-60.

DORNER, A. A., WEGMANN, F., BUTZ, S., WOLBURG-BUCHHOLZ, K., WOLBURG, H., MACK, A., NASDALA, I., AUGUST, B., WESTERMANN, J., RATHJEN, F. G. & VESTWEBER, D. 2005. Coxsackievirus-adenovirus receptor (CAR) is essential for early embryonic cardiac development. *J Cell Sci,* 118**,** 3509-21.

DOSSI, E., VASILE, F. & ROUACH, N. 2018. Human astrocytes in the diseased brain. *Brain Res Bull,* 136**,** 139-156.

DRAKE, M. T., SHENOY, S. K. & LEFKOWITZ, R. J. 2006. Trafficking of G protein-coupled receptors. *Circ Res,* 99**,** 570-82.

DUARRI, A., LOPEZ DE HEREDIA, M., CAPDEVILA-NORTES, X., RIDDER, M. C., MONTOLIO, M., LÓPEZ-HERNÁNDEZ, T., BOOR, I., LIEN, C. F., HAGEMANN, T., MESSING, A., GORECKI, D. C., SCHEPER, G. C., MARTÍNEZ, A., NUNES, V., VAN DER KNAAP, M. S. & ESTÉVEZ, R. 2011. Knockdown of MLC1 in primary astrocytes causes cell vacuolation: a MLC disease cell model. *Neurobiol Dis,* 43**,** 228-38.

DUARRI, A., TEIJIDO, O., LÓPEZ-HERNÁNDEZ, T., SCHEPER, G. C., BARRIERE, H., BOOR, I., AGUADO, F., ZORZANO, A., PALACÍN, M., MARTÍNEZ, A., LUKACS, G. L., VAN DER KNAAP, M. S., NUNES, V. & ESTÉVEZ, R. 2008. Molecular pathogenesis of megalencephalic leukoencephalopathy with subcortical cysts: mutations in MLC1 cause folding defects. *Hum Mol Genet,* 17**,** 3728-39.

DUBEY, M., BROUWERS, E., HAMILTON, E. M. C., STIEDL, O., BUGIANI, M., KOCH, H., KOLE, M. H. P., BOSCHERT, U., WYKES, R. C., MANSVELDER, H. D., VAN DER KNAAP, M. S. & MIN, R. 2018. Seizures and disturbed brain potassium dynamics in the leukodystrophy megalencephalic leukoencephalopathy with subcortical cysts. *Ann Neurol,* 83**,** 636-649.

DUBEY, M., BUGIANI, M., RIDDER, M. C., POSTMA, N. L., BROUWERS, E., POLDER, E., JACOBS, J. G., BAAYEN, J. C., KLOOSTER, J., KAMERMANS, M., AARDSE, R., DE KOCK, C. P., DEKKER, M. P., VAN WEERING, J. R., HEINE, V. M., ABBINK, T. E., SCHEPER, G. C., BOOR, I., LODDER, J. C., MANSVELDER, H. D. & VAN DER KNAAP, M. S. 2015. Mice with megalencephalic leukoencephalopathy with cysts: a developmental angle. *Ann Neurol,* 77**,** 114-31.

DUNHAM, J. H., MEYER, R. C., GARCIA, E. L. & HALL, R. A. 2009. GPR37 surface expression enhancement via N-terminal truncation or protein-protein interactions. *Biochemistry,* 48**,** 10286-97.

DUTZLER, R. 2007. A structural perspective on ClC channel and transporter function. *FEBS Lett,* 581**,** 2839-44.

DUTZLER, R., CAMPBELL, E. B., CADENE, M., CHAIT, B. T. & MACKINNON, R. 2002. X-ray structure of a ClC chloride channel at 3.0 A reveals the molecular basis of anion selectivity. *Nature,* 415**,** 287-94.

EBNET, K., AURRAND-LIONS, M., KUHN, A., KIEFER, F., BUTZ, S., ZANDER, K., MEYER ZU BRICKWEDDE, M. K., SUZUKI, A., IMHOF, B. A. & VESTWEBER, D. 2003. The junctional adhesion molecule (JAM) family members JAM-2 and JAM-3 associate with the cell polarity protein PAR-3: a possible role for JAMs in endothelial cell polarity. *J Cell Sci,* 116**,** 3879-91.

EDWARDS, M. M., MARÍN DE EVSIKOVA, C., COLLIN, G. B., GIFFORD, E., WU, J., HICKS, W. L., WHITING, C., VARVEL, N. H., MAPHIS, N., LAMB, B. T., NAGGERT, J. K., NISHINA, P. M. & PEACHEY, N. S. 2010. Photoreceptor degeneration, azoospermia, leukoencephalopathy, and abnormal RPE cell function in mice expressing an early stop mutation in CLCN2. *Invest Ophthalmol Vis Sci,* 51**,** 3264-72.

EGLEN, R. M., BOSSE, R. & REISINE, T. 2007. Emerging concepts of guanine nucleotide-binding protein-coupled receptor (GPCR) function and implications for high throughput screening. *Assay Drug Dev Technol,* 5**,** 425-51.

ELICES, M. J., OSBORN, L., TAKADA, Y., CROUSE, C., LUHOWSKYJ, S., HEMLER, M. E. & LOBB, R. R. 1990. VCAM-1 on activated endothelium interacts with the leukocyte integrin VLA-4 at a site distinct from the VLA-4/fibronectin binding site. *Cell,* 60**,** 577-84.

ELORZA-VIDAL, X., SIRISI, S., GAITÁN-PEÑAS, H., PÉREZ-RIUS, C., ALONSO-GARDÓN, M., ARMAND-UGÓN, M., LANCIOTTI, A., BRIGNONE, M. S., PRAT, E., NUNES, V., AMBROSINI, E., GASULL, X. & ESTÉVEZ, R. 2018. GlialCAM/MLC1 modulates LRRC8/VRAC currents in an indirect manner: Implications for megalencephalic leukoencephalopathy. *Neurobiol Dis,* 119**,** 88-99.

ELORZA-VIDAL, X., XICOY-ESPAULELLA, E., PLA-CASILLANIS, A., ALONSO-GARDÓN, M., GAITÁN-PEÑAS, H., ENGEL-PIZCUETA, C., FERNÁNDEZ-RECIO, J. & ESTÉVEZ, R. 2020. Structural basis for the dominant or recessive character of GLIALCAM mutations found in leukodystrophies. *Hum Mol Genet,* 29**,** 1107-1120.

ERNEST, N. J., WEAVER, A. K., VAN DUYN, L. B. & SONTHEIMER, H. W. 2005. Relative contribution of chloride channels and transporters to regulatory volume decrease in human glioma cells. *Am J Physiol Cell Physiol,* 288**,** C1451-60.

ESTÉVEZ, R., ELORZA-VIDAL, X., GAITÁN-PEÑAS, H., PÉREZ-RIUS, C., ARMAND-UGÓN, M., ALONSO-GARDÓN, M., XICOY-ESPAULELLA, E., SIRISI, S., ARNEDO, T., CAPDEVILA-NORTES, X., LÓPEZ-HERNÁNDEZ, T., MONTOLIO, M., DUARRI, A., TEIJIDO, O., BARRALLO-GIMENO, A., PALACÍN, M. & NUNES, V. 2018. Megalencephalic leukoencephalopathy with subcortical cysts: A personal biochemical retrospective. *Eur J Med Genet,* 61**,** 50-60.

ESTÉVEZ, R. & JENTSCH, T. J. 2002. CLC chloride channels: correlating structure with function. *Curr Opin Struct Biol,* 12**,** 531-9.

ESTÉVEZ, R., PUSCH, M., FERRER-COSTA, C., OROZCO, M. & JENTSCH, T. J. 2004. Functional and structural conservation of CBS domains from CLC chloride channels. *J Physiol,* 557**,** 363-78.

FANNING, A. S. & ANDERSON, J. M. 2009. Zonula occludens-1 and -2 are cytosolic scaffolds that regulate the assembly of cellular junctions. *Ann N Y Acad Sci,* 1165**,** 113-20.

FAVRE-KONTULA, L., ROLLAND, A., BERNASCONI, L., KARMIRANTZOU, M., POWER, C., ANTONSSON, B. & BOSCHERT, U. 2008. GlialCAM, an immunoglobulin-like cell adhesion molecule is expressed in glial cells of the central nervous system. *Glia,* 56**,** 633-45.

FERNANDES-ROSA, F. L., DANIIL, G., OROZCO, I. J., GÖPPNER, C., EL ZEIN, R., JAIN, V., BOULKROUN, S., JEUNEMAITRE, X., AMAR, L., LEFEBVRE, H., SCHWARZMAYR, T., STROM, T. M., JENTSCH, T. J. & ZENNARO, M. C. 2018. A gain-of-function mutation in the CLCN2 chloride channel gene causes primary aldosteronism. *Nat Genet,* 50**,** 355-361.

FOORD, S. M., BONNER, T. I., NEUBIG, R. R., ROSSER, E. M., PIN, J. P., DAVENPORT, A. P., SPEDDING, M. & HARMAR, A. J. 2005. International Union of Pharmacology. XLVI. G protein-coupled receptor list. *Pharmacol Rev,* 57**,** 279-88.

FOORD, S. M., JUPE, S. & HOLBROOK, J. 2002. Bioinformatics and type II G-protein-coupled receptors. *Biochem Soc Trans,* 30**,** 473-9.

FRANCO, R., RODRÍGUEZ, R. & PASANTES-MORALES, H. 2004. Mechanisms of the ATP potentiation of hyposmotic taurine release in Swiss 3T3 fibroblasts. *Pflugers Arch,* 449**,** 159-69.

FREDRIKSSON, R., LAGERSTRÖM, M. C., LUNDIN, L. G. & SCHIÖTH, H. B. 2003. The G-protein-coupled receptors in the human genome form five main families. Phylogenetic analysis, paralogon groups, and fingerprints. *Mol Pharmacol,* 63**,** 1256-72.

FREIMUTH, P., PHILIPSON, L. & CARSON, S. D. 2008. The coxsackievirus and adenovirus receptor. *Curr Top Microbiol Immunol,* 323**,** 67-87.

FREUNDT, G. V., VON SAMSON-HIMMELSTJERNA, F. A., NITZ, J. T., LUEDDE, M., WALTENBERGER, J., WIELAND, T., FREY, N., PREUSCH, M. & HIPPE, H. J. 2022. The orphan receptor GPRC5B activates pro-inflammatory signaling in the vascular wall via Fyn and NFκB. *Biochem Biophys Res Commun,* 592**,** 60-66.

GAITÁN-PEÑAS, H., APAJA, P. M., ARNEDO, T., CASTELLANOS, A., ELORZA-VIDAL, X., SOTO, D., GASULL, X., LUKACS, G. L. & ESTÉVEZ, R. 2017. Leukoencephalopathy-causing CLCN2 mutations are associated with impaired Cl. *J Physiol,* 595**,** 6993-7008.

GAITÁN-PEÑAS, H., GRADOGNA, A., LAPARRA-CUERVO, L., SOLSONA, C., FERNÁNDEZ-DUEÑAS, V., BARRALLO-GIMENO, A., CIRUELA, F.,

LAKADAMYALI, M., PUSCH, M. & ESTÉVEZ, R. 2016. Investigation of LRRC8-Mediated Volume-Regulated Anion Currents in Xenopus Oocytes. *Biophys J,* 111**,** 1429-1443.

GARCIA-OLIVARES, J., ALEKOV, A., BOROUMAND, M. R., BEGEMANN, B., HIDALGO, P. & FAHLKE, C. 2008. Gating of human ClC-2 chloride channels and regulation by carboxy-terminal domains. *J Physiol,* 586**,** 5325-36.

GARIN, N. & ESCHER, G. 2001. The development of inhibitory synaptic specializations in the mouse deep cerebellar nuclei. *Neuroscience,* 105**,** 431-41.

GARRETT, A. M. & WEINER, J. A. 2009. Control of CNS synapse development by {gamma}-protocadherin-mediated astrocyte-neuron contact. *J Neurosci,* 29**,** 11723-31.

GARROD, D. & CHIDGEY, M. 2008. Desmosome structure, composition and function. *Biochim Biophys Acta,* 1778**,** 572-87.

GAUDRY, J. P., AROD, C., SAUVAGE, C., BUSSO, S., DUPRAZ, P., PANKIEWICZ, R. & ANTONSSON, B. 2008. Purification of the extracellular domain of the membrane protein GlialCAM expressed in HEK and CHO cells and comparison of the glycosylation. *Protein Expr Purif,* 58**,** 94-102.

GEORGE, S. R., O'DOWD, B. F. & LEE, S. P. 2002. G-protein-coupled receptor oligomerization and its potential for drug discovery. *Nat Rev Drug Discov,* 1**,** 808-20.

GIDDENS, M. M., WONG, J. C., SCHROEDER, J. P., FARROW, E. G., SMITH, B. M., OWINO, S., SODEN, S. E., MEYER, R. C., SAUNDERS, C., LEPICHON, J. B., WEINSHENKER, D., ESCAYG, A. & HALL, R. A. 2017. GPR37L1 modulates seizure susceptibility: Evidence from mouse studies and analyses of a human GPR37L1 variant. *Neurobiol Dis,* 106**,** 181-190.

GIMENEZ, M. A., SIM, J. E. & RUSSELL, J. H. 2004. TNFR1-dependent VCAM-1 expression by astrocytes exposes the CNS to destructive inflammation. *J Neuroimmunol,* 151**,** 116-25.

GIORGIO, E., VAULA, G., BENNA, P., LO BUONO, N., EANDI, C. M., DINO, D., MANCINI, C., CAVALIERI, S., DI GREGORIO, E., POZZI, E., FERRERO, M., GIORDANA, M. T., DEPIENNE, C. & BRUSCO, A. 2017. A novel homozygous change of. *J Neurol Neurosurg Psychiatry,* 88**,** 894-896.

GOROSPE, J. R., SINGHAL, B. S., KAINU, T., WU, F., STEPHAN, D., TRENT, J., HOFFMAN, E. P. & NAIDU, S. 2004. Indian Agarwal megalencephalic leukodystrophy with cysts is caused by a common MLC1 mutation. *Neurology,* 62**,** 878-82.

GREENHOUGH, A., BAGLEY, C., HEESOM, K. J., GUREVICH, D. B., GAY, D., BOND, M., COLLARD, T. J., PARASKEVA, C., MARTIN, P., SANSOM, O. J., MALIK, K. & WILLIAMS, A. C. 2018. Cancer cell adaptation to hypoxia involves a HIF-GPRC5A-YAP axis. *EMBO Mol Med,* 10.

GRÜNDER, S., THIEMANN, A., PUSCH, M. & JENTSCH, T. J. 1992. Regions involved in the opening of CIC-2 chloride channel by voltage and cell volume. *Nature,* 360**,** 759-62.

GUTNICK, M. J., HEINEMANN, U. & LUX, H. D. 1979. Stimulus induced and seizure related changes in extracellular potassium concentration in cat thalamus (VPL). *Electroencephalogr Clin Neurophysiol,* 47**,** 329-44.

HAJ-YASEIN, N. N., JENSEN, V., ØSTBY, I., OMHOLT, S. W., VOIPIO, J., KAILA, K., OTTERSEN, O. P., HVALBY, Ø. & NAGELHUS, E. A. 2012. Aquaporin-4 regulates extracellular space volume dynamics during high-frequency synaptic stimulation: a gene deletion study in mouse hippocampus. *Glia,* 60**,** 867-74.

HANAGASI, H. A., BILGIÇ, B., ABBINK, T. E., HANAGASI, F., TÜFEKÇIOĞLU, Z., GÜRVIT, H., BAŞAK, N., VAN DER KNAAP, M. S. & EMRE, M. 2015. Secondary

paroxysmal kinesigenic dyskinesia associated with CLCN2 gene mutation. *Parkinsonism Relat Disord,* 21**,** 544-6.

HASHIMOTO, Y. & CAMPBELL, M. 2020. Tight junction modulation at the blood-brain barrier: Current and future perspectives. *Biochim Biophys Acta Biomembr,* 1862**,** 183298.

HEACOCK, A. M., FOSTER, D. J. & FISHER, S. K. 2006. Prostanoid receptors regulate the volume-sensitive efflux of osmolytes from murine fibroblasts via a cyclic AMP-dependent mechanism. *J Pharmacol Exp Ther,* 319**,** 963-71.

HEINEMANN, U. & LUX, H. D. 1977. Ceiling of stimulus induced rises in extracellular potassium concentration in the cerebral cortex of cat. *Brain Res,* 120**,** 231-49.

HENDRIKS-BALK, M. C., PETERS, S. L., MICHEL, M. C. & ALEWIJNSE, A. E. 2008. Regulation of G protein-coupled receptor signalling: focus on the cardiovascular system and regulator of G protein signalling proteins. *Eur J Pharmacol,* 585**,** 278-91.

HERTZ, L., CHEN, Y. & SPATZ, M. 2000. Involvement of non-neuronal brain cells in AVP-mediated regulation of water space at the cellular, organ, and whole-body level. *J Neurosci Res,* 62**,** 480-90.

HEWETT, J. A. 2009. Determinants of regional and local diversity within the astroglial lineage of the normal central nervous system. *J Neurochem,* 110**,** 1717-36.

HIGASHI, K., FUJITA, A., INANOBE, A., TANEMOTO, M., DOI, K., KUBO, T. & KURACHI, Y. 2001. An inwardly rectifying K(+) channel, Kir4.1, expressed in astrocytes surrounds synapses and blood vessels in brain. *Am J Physiol Cell Physiol,* 281**,** C922-31.

HINZPETER, A., LIPECKA, J., BROUILLARD, F., BAUDOIN-LEGROS, M., DADLEZ, M., EDELMAN, A. & FRITSCH, J. 2006. Association between Hsp90 and the ClC-2 chloride channel upregulates channel function. *Am J Physiol Cell Physiol,* 290**,** C45-56.

HIRABAYASHI, S., TAJIMA, M., YAO, I., NISHIMURA, W., MORI, H. & HATA, Y. 2003. JAM4, a junctional cell adhesion molecule interacting with a tight junction protein, MAGI-1. *Mol Cell Biol,* 23**,** 4267-82.

HIRABAYASHI, Y. & KIM, Y. J. 2020. Roles of GPRC5 family proteins: focusing on GPRC5B and lipid-mediated signalling. *J Biochem,* 167**,** 541-547.

HO, K. S. & SCOTT, M. P. 2002. Sonic hedgehog in the nervous system: functions, modifications and mechanisms. *Curr Opin Neurobiol,* 12**,** 57-63.

HOEGG-BEILER, M. B., SIRISI, S., OROZCO, I. J., FERRER, I., HOHENSEE, S., AUBERSON, M., GÖDDE, K., VILCHES, C., DE HEREDIA, M. L., NUNES, V., ESTÉVEZ, R. & JENTSCH, T. J. 2014. Disrupting MLC1 and GlialCAM and ClC-2 interactions in leukodystrophy entails glial chloride channel dysfunction. *Nat Commun,* 5**,** 3475.

HOFFMANN, E. K., LAMBERT, I. H. & PEDERSEN, S. F. 2009. Physiology of cell volume regulation in vertebrates. *Physiol Rev,* 89**,** 193-277.

HOLLMANN, M. W., STRUMPER, D., HERROEDER, S. & DURIEUX, M. E. 2005. Receptors, G proteins, and their interactions. *Anesthesiology,* 103**,** 1066-78.

HONDA, T., SAITOH, H., MASUKO, M., KATAGIRI-ABE, T., TOMINAGA, K., KOZAKAI, I., KOBAYASHI, K., KUMANISHI, T., WATANABE, Y. G., ODANI, S. & KUWANO, R. 2000. The coxsackievirus-adenovirus receptor protein as a cell adhesion molecule in the developing mouse brain. *Brain Res Mol Brain Res,* 77**,** 19-28.

HORNG, S., THERATTIL, A., MOYON, S., GORDON, A., KIM, K., ARGAW, A. T., HARA, Y., MARIANI, J. N., SAWAI, S., FLODBY, P., CRANDALL, E. D., BOROK, Z., SOFRONIEW, M. V., CHAPOULY, C. & JOHN, G. R. 2017. Astrocytic tight junctions control inflammatory CNS lesion pathogenesis. *J Clin Invest,* 127**,** 3136-3151.

HOSSEINZADEH, Z., BHAVSAR, S. K. & LANG, F. 2012. Downregulation of ClC-2 by JAK2. *Cell Physiol Biochem,* 29**,** 737-42.

HOWARTH, C. 2014. The contribution of astrocytes to the regulation of cerebral blood flow. *Front Neurosci,* 8**,** 103.

HU, G. M., MAI, T. L. & CHEN, C. M. 2017. Visualizing the GPCR Network: Classification and Evolution. *Sci Rep,* 7**,** 15495.

HUANGFU, D., LIU, A., RAKEMAN, A. S., MURCIA, N. S., NISWANDER, L. & ANDERSON, K. V. 2003. Hedgehog signalling in the mouse requires intraflagellar transport proteins. *Nature,* 426**,** 83-7.

HUXLEY, A. F. & STÄMPFLI, R. 1949. Evidence for saltatory conduction in peripheral myelinated nerve fibres. *J Physiol,* 108**,** 315-39.

HWANG, J., PARK, K., LEE, G. Y., YOON, B. Y., KIM, H., ROH, S. H., LEE, B. C., KIM, K. & LIM, H. H. 2021. Transmembrane topology and oligomeric nature of an astrocytic membrane protein, MLC1. *Open Biol,* 11**,** 210103.

HYZINSKI-GARCÍA, M. C., RUDKOUSKAYA, A. & MONGIN, A. A. 2014. LRRC8A protein is indispensable for swelling-activated and ATP-induced release of excitatory amino acids in rat astrocytes. *J Physiol,* 592**,** 4855-62.

IADECOLA, C. & NEDERGAARD, M. 2007. Glial regulation of the cerebral microvasculature. *Nat Neurosci,* 10**,** 1369-76.

ILIFF, J. J. & NEDERGAARD, M. 2013. Is there a cerebral lymphatic system? *Stroke,* 44**,** S93-5.

ILIFF, J. J., WANG, M., LIAO, Y., PLOGG, B. A., PENG, W., GUNDERSEN, G. A., BENVENISTE, H., VATES, G. E., DEANE, R., GOLDMAN, S. A., NAGELHUS, E. A. & NEDERGAARD, M. 2012. A paravascular pathway facilitates CSF flow through the brain parenchyma and the clearance of interstitial solutes, including amyloid β. *Sci Transl Med,* 4**,** 147ra111.

ILJA BOOR, P. K., DE GROOT, K., MEJASKI-BOSNJAK, V., BRENNER, C., VAN DER KNAAP, M. S., SCHEPER, G. C. & PRONK, J. C. 2006. Megalencephalic leukoencephalopathy with subcortical cysts: an update and extended mutation analysis of MLC1. *Hum Mutat,* 27**,** 505-12.

IMAI, Y., SODA, M., INOUE, H., HATTORI, N., MIZUNO, Y. & TAKAHASHI, R. 2001. An unfolded putative transmembrane polypeptide, which can lead to endoplasmic reticulum stress, is a substrate of Parkin. *Cell,* 105**,** 891-902.

INOUE, S., NAMBU, T. & SHIMOMURA, T. 2004. The RAIG family member, GPRC5D, is associated with hard-keratinized structures. *J Invest Dermatol,* 122**,** 565-73.

IRANNEJAD, R., TOMSHINE, J. C., TOMSHINE, J. R., CHEVALIER, M., MAHONEY, J. P., STEYAERT, J., RASMUSSEN, S. G., SUNAHARA, R. K., EL-SAMAD, H., HUANG, B. & VON ZASTROW, M. 2013. Conformational biosensors reveal GPCR signalling from endosomes. *Nature,* 495**,** 534-8.

JACOBY, E., BOUHELAL, R., GERSPACHER, M. & SEUWEN, K. 2006. The 7 TM G-protein-coupled receptor target family. *ChemMedChem,* 1**,** 761-82.

JAYAKUMAR, A. R. & NORENBERG, M. D. 2010. The Na-K-Cl Co-transporter in astrocyte swelling. *Metab Brain Dis,* 25**,** 31-8.

JAYAKUMAR, A. R., PANICKAR, K. S., CURTIS, K. M., TONG, X. Y., MORIYAMA, M. & NORENBERG, M. D. 2011. Na-K-Cl cotransporter-1 in the mechanism of cell swelling in cultured astrocytes after fluid percussion injury. *J Neurochem,* 117**,** 437-48.

JENTSCH, T. J. 2016. VRACs and other ion channels and transporters in the regulation of cell volume and beyond. *Nat Rev Mol Cell Biol,* 17**,** 293-307.

JENTSCH, T. J., FRIEDRICH, T., SCHRIEVER, A. & YAMADA, H. 1999. The CLC chloride channel family. *Pflugers Arch,* 437**,** 783-95.

JENTSCH, T. J., STEIN, V., WEINREICH, F. & ZDEBIK, A. A. 2002. Molecular structure and physiological function of chloride channels. *Physiol Rev,* 82**,** 503-68.

JEWORUTZKI, E., LÓPEZ-HERNÁNDEZ, T., CAPDEVILA-NORTES, X., SIRISI, S., BENGTSSON, L., MONTOLIO, M., ZIFARELLI, G., ARNEDO, T., MÜLLER, C. S., SCHULTE, U., NUNES, V., MARTÍNEZ, A., JENTSCH, T. J., GASULL, X., PUSCH, M. & ESTÉVEZ, R. 2012. GlialCAM, a protein defective in a leukodystrophy, serves as a ClC-2 Cl(-) channel auxiliary subunit. *Neuron,* 73**,** 951-61.

JIE, P., TIAN, Y., HONG, Z., LI, L., ZHOU, L. & CHEN, L. 2015. Blockage of transient receptor potential vanilloid 4 inhibits brain edema in middle cerebral artery occlusion mice. *Front Cell Neurosci,* 9**,** 141.

JO, A. O., RYSKAMP, D. A., PHUONG, T. T., VERKMAN, A. S., YARISHKIN, O., MACAULAY, N. & KRIŽAJ, D. 2015. TRPV4 and AQP4 Channels Synergistically Regulate Cell Volume and Calcium Homeostasis in Retinal Müller Glia. *J Neurosci,* 35**,** 13525-37.

JORDT, S. E. & JENTSCH, T. J. 1997. Molecular dissection of gating in the ClC-2 chloride channel. *EMBO J,* 16**,** 1582-92.

JUMPER, J., EVANS, R., PRITZEL, A., GREEN, T., FIGURNOV, M., RONNEBERGER, O., TUNYASUVUNAKOOL, K., BATES, R., ŽÍDEK, A., POTAPENKO, A., BRIDGLAND, A., MEYER, C., KOHL, S. A. A., BALLARD, A. J., COWIE, A., ROMERA-PAREDES, B., NIKOLOV, S., JAIN, R., ADLER, J., BACK, T., PETERSEN, S., REIMAN, D., CLANCY, E., ZIELINSKI, M., STEINEGGER, M., PACHOLSKA, M., BERGHAMMER, T., BODENSTEIN, S., SILVER, D., VINYALS, O., SENIOR, A. W., KAVUKCUOGLU, K., KOHLI, P. & HASSABIS, D. 2021. Highly accurate protein structure prediction with AlphaFold. *Nature,* 596**,** 583-589.

KAJANDER, T., CORTAJARENA, A. L. & REGAN, L. 2006. Consensus design as a tool for engineering repeat proteins. *Methods Mol Biol,* 340**,** 151-70.

KALLIOLIAS, G. D. & IVASHKIV, L. B. 2016. TNF biology, pathogenic mechanisms and emerging therapeutic strategies. *Nat Rev Rheumatol,* 12**,** 49-62.

KALSI, A. S., GREENWOOD, K., WILKIN, G. & BUTT, A. M. 2004. Kir4.1 expression by astrocytes and oligodendrocytes in CNS white matter: a developmental study in the rat optic nerve. *J Anat,* 204**,** 475-85.

KAMHOLZ, J. A. 1996. Regulation of myelin development. *Mult Scler,* 2**,** 236-40.

KAMIGUCHI, H. & LEMMON, V. 2000. IgCAMs: bidirectional signals underlying neurite growth. *Curr Opin Cell Biol,* 12**,** 598-605.

KARIMINEJAD, A., RAJAEE, A., ASHRAFI, M. R., ALIZADEH, H., TONEKABONI, S. H., MALAMIRI, R. A., GHOFRANI, M., KARIMZADEH, P., MOHAMMADI, M. M., BAGHALSHOOSHTARI, A., BOZORGMEHR, B., KARIMINEJAD, M. H., POSTMA, N., ABBINK, T. E. & VAN DER KNAAP, M. S. 2015. Eight novel mutations in MLC1 from 18 Iranian patients with megalencephalic leukoencephalopathy with subcortical cysts. *Eur J Med Genet,* 58**,** 71-4.

KESHET, Y. & SEGER, R. 2010. The MAP kinase signaling cascades: a system of hundreds of components regulates a diverse array of physiological functions. *Methods Mol Biol,* 661**,** 3-38.

KETTENMANN, H. & VERKHRATSKY, A. 2011. [Neuroglia--living nerve glue]. *Fortschr Neurol Psychiatr,* 79**,** 588-97.

KIM, J., LEE, J. E., HEYNEN-GENEL, S., SUYAMA, E., ONO, K., LEE, K., IDEKER, T., AZA-BLANC, P. & GLEESON, J. G. 2010. Functional genomic screen for modulators of ciliogenesis and cilium length. *Nature,* 464**,** 1048-51.

KIM, Y. J., GREIMEL, P. & HIRABAYASHI, Y. 2018. GPRC5B-Mediated Sphingomyelin Synthase 2 Phosphorylation Plays a Critical Role in Insulin Resistance. *iScience,* 8**,** 250-266.

KIM, Y. J., SANO, T., NABETANI, T., ASANO, Y. & HIRABAYASHI, Y. 2012. GPRC5B activates obesity-associated inflammatory signaling in adipocytes. *Sci Signal,* 5**,** ra85.

KIMELBERG, H. K. 2004. The problem of astrocyte identity. *Neurochem Int,* 45**,** 191-202.

KIMELBERG, H. K. 2005. Astrocytic swelling in cerebral ischemia as a possible cause of injury and target for therapy. *Glia,* 50**,** 389-397.

KIMELBERG, H. K., GODERIE, S. K., HIGMAN, S., PANG, S. & WANIEWSKI, R. A. 1990. Swelling-induced release of glutamate, aspartate, and taurine from astrocyte cultures. *J Neurosci,* 10**,** 1583-91.

KIMELBERG, H. K., MACVICAR, B. A. & SONTHEIMER, H. 2006. Anion channels in astrocytes: biophysics, pharmacology, and function. *Glia,* 54**,** 747-757.

KLEEFUSS-LIE, A., FRIEDL, W., CICHON, S., HAUG, K., WARNSTEDT, M., ALEKOV, A., SANDER, T., RAMIREZ, A., POSER, B., MALJEVIC, S., HEBEISEN, S., KUBISCH, C., REBSTOCK, J., HORVATH, S., HALLMANN, K., DULLINGER, J. S., RAU, B., HAVERKAMP, F., BEYENBURG, S., SCHULZ, H., JANZ, D., GIESE, B., MÜLLER-NEWEN, G., PROPPING, P., ELGER, C. E., FAHLKE, C. & LERCHE, H. 2009. CLCN2 variants in idiopathic generalized epilepsy. *Nat Genet,* 41**,** 954-5.

KNIAZEFF, J., GALVEZ, T., LABESSE, G. & PIN, J. P. 2002. No ligand binding in the GB2 subunit of the GABA(B) receptor is required for activation and allosteric interaction between the subunits. *J Neurosci,* 22**,** 7352-61.

KNIAZEFF, J., PRÉZEAU, L., RONDARD, P., PIN, J. P. & GOUDET, C. 2011. Dimers and beyond: The functional puzzles of class C GPCRs. *Pharmacol Ther,* 130**,** 9-25.

KOFUJI, P., CEELEN, P., ZAHS, K. R., SURBECK, L. W., LESTER, H. A. & NEWMAN, E. A. 2000. Genetic inactivation of an inwardly rectifying potassium channel (Kir4.1 subunit) in mice: phenotypic impact in retina. *J Neurosci,* 20**,** 5733-40.

KOFUJI, P. & NEWMAN, E. A. 2004. Potassium buffering in the central nervous system. *Neuroscience,* 129**,** 1045-56.

KOHYAMA-KOGANEYA, A., KIM, Y. J., MIURA, M. & HIRABAYASHI, Y. 2008. A Drosophila orphan G protein-coupled receptor BOSS functions as a glucose-responding receptor: loss of boss causes abnormal energy metabolism. *Proc Natl Acad Sci U S A,* 105**,** 15328-33.

KOLAKOWSKI, L. F. 1994. GCRDb: a G-protein-coupled receptor database. *Recept Channels,* 2**,** 1-7.

KONG, D. H., KIM, Y. K., KIM, M. R., JANG, J. H. & LEE, S. 2018. Emerging Roles of Vascular Cell Adhesion Molecule-1 (VCAM-1) in Immunological Disorders and Cancer. *Int J Mol Sci,* 19.

KOSTREWA, D., BROCKHAUS, M., D'ARCY, A., DALE, G. E., NELBOECK, P., SCHMID, G., MUELLER, F., BAZZONI, G., DEJANA, E., BARTFAI, T., WINKLER, F. K. & HENNIG, M. 2001. X-ray structure of junctional adhesion molecule: structural basis for homophilic adhesion via a novel dimerization motif. *EMBO J,* 20**,** 4391-8.

KOZLOVA, I., SAH, S., KEABLE, R., LESHCHYNS'KA, I., JANITZ, M. & SYTNYK, V. 2020. Cell Adhesion Molecules and Protein Synthesis Regulation in Neurons. *Front Mol Neurosci,* 13**,** 592126.

KUMAR, L., CHOU, J., YEE, C. S., BORZUTZKY, A., VOLLMANN, E. H., VON ANDRIAN, U. H., PARK, S. Y., HOLLANDER, G., MANIS, J. P., POLIANI, P. L. & GEHA, R. S. 2014. Leucine-rich repeat containing 8A (LRRC8A) is essential for T lymphocyte development and function. *J Exp Med,* 211**,** 929-42.

KUME-KICK, J., MAZEL, T., VORISEK, I., HRABĚTOVÁ, S., TAO, L. & NICHOLSON, C. 2002. Independence of extracellular tortuosity and volume fraction during osmotic challenge in rat neocortex. *J Physiol,* 542**,** 515-27.

KURABAYASHI, N., NGUYEN, M. D. & SANADA, K. 2013. The G protein-coupled receptor GPRC5B contributes to neurogenesis in the developing mouse neocortex. *Development,* 140**,** 4335-46.

KWON, S. H., LIU, K. D. & MOSTOV, K. E. 2014. Intercellular transfer of GPRC5B via exosomes drives HGF-mediated outward growth. *Curr Biol,* 24**,** 199-204.

KÖNIG, B., HAO, Y., SCHWARTZ, S., PLESTED, A. J. & STAUBER, T. 2019. A FRET sensor of C-terminal movement reveals VRAC activation by plasma membrane DAG signaling rather than ionic strength. *Elife,* 8.

LA SALA, G., DI PIETRO, C., MATTEONI, R., BOLASCO, G., MARAZZITI, D. & TOCCHINI-VALENTINI, G. P. 2020. Gpr37l1/prosaposin receptor regulates Ptch1 trafficking, Shh production, and cell proliferation in cerebellar primary astrocytes. *J Neurosci Res*.

LAFRENAYE, A. D. & SIMARD, J. M. 2019. Bursting at the Seams: Molecular Mechanisms Mediating Astrocyte Swelling. *Int J Mol Sci,* 20.

LAGERSTRÖM, M. C. & SCHIÖTH, H. B. 2008. Structural diversity of G protein-coupled receptors and significance for drug discovery. *Nat Rev Drug Discov,* 7**,** 339-57.

LANCIOTTI, A., BRIGNONE, M. S., CAMERINI, S., SERAFINI, B., MACCHIA, G., RAGGI, C., MOLINARI, P., CRESCENZI, M., MUSUMECI, M., SARGIACOMO, M., ALOISI, F., PETRUCCI, T. C. & AMBROSINI, E. 2010. MLC1 trafficking and membrane expression in astrocytes: role of caveolin-1 and phosphorylation. *Neurobiol Dis,* 37**,** 581-95.

LANCIOTTI, A., BRIGNONE, M. S., VISENTIN, S., DE NUCCIO, C., CATACUZZENO, L., MALLOZZI, C., PETRINI, S., CARAMIA, M., VERONI, C., MINNONE, G., BERNARDO, A., FRANCIOLINI, F., PESSIA, M., BERTINI, E., PETRUCCI, T. C. & AMBROSINI, E. 2016. Megalencephalic leukoencephalopathy with subcortical cysts protein-1 regulates epidermal growth factor receptor signaling in astrocytes. *Hum Mol Genet,* 25**,** 1543-58.

LAPPANO, R. & MAGGIOLINI, M. 2011. G protein-coupled receptors: novel targets for drug discovery in cancer. *Nat Rev Drug Discov,* 10**,** 47-60.

LARSEN, B. R., ASSENTOFT, M., COTRINA, M. L., HUA, S. Z., NEDERGAARD, M., KAILA, K., VOIPIO, J. & MACAULAY, N. 2014. Contributions of the Na^+/K^+-ATPase, NKCC1, and Kir4.1 to hippocampal K^+ clearance and volume responses. *Glia,* 62**,** 608-22.

LEE, S., YOON, B. E., BERGLUND, K., OH, S. J., PARK, H., SHIN, H. S., AUGUSTINE, G. J. & LEE, C. J. 2010. Channel-mediated tonic GABA release from glia. *Science,* 330**,** 790-6.

LEEGWATER, P. A., BOOR, P. K., YUAN, B. Q., VAN DER STEEN, J., VISSER, A., KÖNST, A. A., OUDEJANS, C. B., SCHUTGENS, R. B., PRONK, J. C. & VAN DER KNAAP, M. S. 2002. Identification of novel mutations in MLC1 responsible for megalencephalic leukoencephalopathy with subcortical cysts. *Hum Genet,* 110**,** 279-83.

LENG, N., GU, G., SIMERLY, R. B. & SPINDEL, E. R. 1999. Molecular cloning and characterization of two putative G protein-coupled receptors which are highly expressed in the central nervous system. *Brain Res Mol Brain Res,* 69**,** 73-83.

LI, Y., SERWANSKI, D. R., MIRALLES, C. P., FIONDELLA, C. G., LOTURCO, J. J., RUBIO, M. E. & DE BLAS, A. L. 2010. Synaptic and nonsynaptic localization of protocadherin-gammaC5 in the rat brain. *J Comp Neurol,* 518**,** 3439-63.

LIANG, T. W., DEMARCO, R. A., MRSNY, R. J., GURNEY, A., GRAY, A., HOOLEY, J., AARON, H. L., HUANG, A., KLASSEN, T., TUMAS, D. B. & FONG, S. 2000. Characterization of huJAM: evidence for involvement in cell-cell contact and tight junction regulation. *Am J Physiol Cell Physiol,* 279**,** C1733-43.

LIEDTKE, W., EDELMANN, W., BIERI, P. L., CHIU, F. C., COWAN, N. J., KUCHERLAPATI, R. & RAINE, C. S. 1996. GFAP is necessary for the integrity of CNS white matter architecture and long-term maintenance of myelination. *Neuron,* 17**,** 607-15.

LIU, B., MOSIENKO, V., VACCARI CARDOSO, B., PROKUDINA, D., HUENTELMAN, M., TESCHEMACHER, A. G. & KASPAROV, S. 2018. Glio- and neuro-protection by prosaposin is mediated by orphan G-protein coupled receptors GPR37L1 and GPR37. *Glia,* 66**,** 2414-2426.

LIU, H. T., TASHMUKHAMEDOV, B. A., INOUE, H., OKADA, Y. & SABIROV, R. Z. 2006. Roles of two types of anion channels in glutamate release from mouse astrocytes under ischemic or osmotic stress. *Glia,* 54**,** 343-57.

LUNDGAARD, I., OSÓRIO, M. J., KRESS, B. T., SANGGAARD, S. & NEDERGAARD, M. 2014. White matter astrocytes in health and disease. *Neuroscience,* 276**,** 161-73.

LUTTER, D., ULLRICH, F., LUECK, J. C., KEMPA, S. & JENTSCH, T. J. 2017. Selective transport of neurotransmitters and modulators by distinct volume-regulated LRRC8 anion channels. *J Cell Sci,* 130**,** 1122-1133.

LÓPEZ-HERNÁNDEZ, T., RIDDER, M. C., MONTOLIO, M., CAPDEVILA-NORTES, X., POLDER, E., SIRISI, S., DUARRI, A., SCHULTE, U., FAKLER, B., NUNES, V., SCHEPER, G. C., MARTÍNEZ, A., ESTÉVEZ, R. & VAN DER KNAAP, M. S. 2011a. Mutant GlialCAM causes megalencephalic leukoencephalopathy with subcortical cysts, benign familial macrocephaly, and macrocephaly with retardation and autism. *Am J Hum Genet,* 88**,** 422-32.

LÓPEZ-HERNÁNDEZ, T., SIRISI, S., CAPDEVILA-NORTES, X., MONTOLIO, M., FERNÁNDEZ-DUEÑAS, V., SCHEPER, G. C., VAN DER KNAAP, M. S., CASQUERO, P., CIRUELA, F., FERRER, I., NUNES, V. & ESTÉVEZ, R. 2011b. Molecular mechanisms of MLC1 and GLIALCAM mutations in megalencephalic leukoencephalopathy with subcortical cysts. *Hum Mol Genet,* 20**,** 3266-77.

MA, X., CHEN, C., VEEVERS, J., ZHOU, X., ROSS, R. S., FENG, W. & CHEN, J. 2017. CRISPR/Cas9-mediated gene manipulation to create single-amino-acid-substituted and floxed mice with a cloning-free method. *Sci Rep,* 7**,** 42244.

MALARKEY, E. B., NI, Y. & PARPURA, V. 2008. Ca2+ entry through TRPC1 channels contributes to intracellular Ca2+ dynamics and consequent glutamate release from rat astrocytes. *Glia,* 56**,** 821-35.

MANDELL, K. J., BABBIN, B. A., NUSRAT, A. & PARKOS, C. A. 2005. Junctional adhesion molecule 1 regulates epithelial cell morphology through effects on beta1 integrins and Rap1 activity. *J Biol Chem,* 280**,** 11665-74.

MANDELL, K. J., MCCALL, I. C. & PARKOS, C. A. 2004. Involvement of the junctional adhesion molecule-1 (JAM1) homodimer interface in regulation of epithelial barrier function. *J Biol Chem,* 279**,** 16254-62.

MARAZZITI, D., DI PIETRO, C., GOLINI, E., MANDILLO, S., LA SALA, G., MATTEONI, R. & TOCCHINI-VALENTINI, G. P. 2013. Precocious cerebellum development and improved motor functions in mice lacking the astrocyte cilium-, patched 1-associated Gpr37l1 receptor. *Proc Natl Acad Sci U S A,* 110**,** 16486-91.

MARAZZITI, D., GALLO, A., GOLINI, E., MATTEONI, R. & TOCCHINI-VALENTINI, G. P. 1998. Molecular cloning and chromosomal localization of the mouse Gpr37 gene encoding an orphan G-protein-coupled peptide receptor expressed in brain and testis. *Genomics,* 53**,** 315-24.

MARAZZITI, D., GOLINI, E., GALLO, A., LOMBARDI, M. S., MATTEONI, R. & TOCCHINI-VALENTINI, G. P. 1997. Cloning of GPR37, a gene located on chromosome 7 encoding a putative G-protein-coupled peptide receptor, from a human frontal brain EST library. *Genomics,* 45**,** 68-77.

MATTHÄUS, C., LANGHORST, H., SCHÜTZ, L., JÜTTNER, R. & RATHJEN, F. G. 2017. Cell-cell communication mediated by the CAR subgroup of immunoglobulin cell adhesion molecules in health and disease. *Mol Cell Neurosci,* 81**,** 32-40.

MCCARTY, N. A. & O'NEIL, R. G. 1992. Calcium signaling in cell volume regulation. *Physiol Rev,* 72**,** 1037-61.

MENICHELLA, D. M., GOODENOUGH, D. A., SIRKOWSKI, E., SCHERER, S. S. & PAUL, D. L. 2003. Connexins are critical for normal myelination in the CNS. *J Neurosci,* 23**,** 5963-73.

MENICHELLA, D. M., MAJDAN, M., AWATRAMANI, R., GOODENOUGH, D. A., SIRKOWSKI, E., SCHERER, S. S. & PAUL, D. L. 2006. Genetic and physiological evidence that oligodendrocyte gap junctions contribute to spatial buffering of potassium released during neuronal activity. *J Neurosci,* 26**,** 10984-91.

MEYER, R. C., GIDDENS, M. M., SCHAEFER, S. A. & HALL, R. A. 2013. GPR37 and GPR37L1 are receptors for the neuroprotective and glioprotective factors prosaptide and prosaposin. *Proc Natl Acad Sci U S A,* 110**,** 9529-34.

MILLIGAN, G. & KOSTENIS, E. 2006. Heterotrimeric G-proteins: a short history. *Br J Pharmacol,* 147 Suppl 1**,** S46-55.

MIYAMOTO, Y., TORII, T., TANOUE, A. & YAMAUCHI, J. 2016. VCAM1 acts in parallel with CD69 and is required for the initiation of oligodendrocyte myelination. *Nat Commun,* 7**,** 13478.

MIYATA, M., MANDAI, K., MARUO, T., SATO, J., SHIOTANI, H., KAITO, A., ITOH, Y., WANG, S., FUJIWARA, T., MIZOGUCHI, A., TAKAI, Y. & RIKITAKE, Y. 2016. Localization of nectin-2δ at perivascular astrocytic endfoot processes and degeneration of astrocytes and neurons in nectin-2 knockout mouse brain. *Brain Res,* 1649**,** 90-101.

MOH, M. C., ZHANG, C., LUO, C., LEE, L. H. & SHEN, S. 2005. Structural and functional analyses of a novel ig-like cell adhesion molecule, hepaCAM, in the human breast carcinoma MCF7 cells. *J Biol Chem,* 280**,** 27366-74.

MOH, M. C., ZHANG, T., LEE, L. H. & SHEN, S. 2008. Expression of hepaCAM is downregulated in cancers and induces senescence-like growth arrest via a p53/p21-dependent pathway in human breast cancer cells. *Carcinogenesis,* 29**,** 2298-305.

MOLA, M. G., SPARANEO, A., GARGANO, C. D., SPRAY, D. C., SVELTO, M., FRIGERI, A., SCEMES, E. & NICCHIA, G. P. 2016. The speed of swelling kinetics modulates cell

volume regulation and calcium signaling in astrocytes: A different point of view on the role of aquaporins. *Glia,* 64**,** 139-54.

MOLOFSKY, A. V., KRENCIK, R., KRENICK, R., ULLIAN, E. M., ULLIAN, E., TSAI, H. H., DENEEN, B., RICHARDSON, W. D., BARRES, B. A. & ROWITCH, D. H. 2012. Astrocytes and disease: a neurodevelopmental perspective. *Genes Dev,* 26**,** 891-907.

MONGIN, A. A. 2016. Volume-regulated anion channel--a frenemy within the brain. *Pflugers Arch,* 468**,** 421-41.

MONGIN, A. A. & KIMELBERG, H. K. 2002. ATP potently modulates anion channel-mediated excitatory amino acid release from cultured astrocytes. *Am J Physiol Cell Physiol,* 283**,** C569-78.

MONGIN, A. A. & KIMELBERG, H. K. 2005. ATP regulates anion channel-mediated organic osmolyte release from cultured rat astrocytes via multiple Ca2+-sensitive mechanisms. *Am J Physiol Cell Physiol,* 288**,** C204-13.

MONTAGNA, G., TEIJIDO, O., EYMARD-PIERRE, E., MURAKI, K., COHEN, B., LOIZZO, A., GROSSO, P., TEDESCHI, G., PALACÍN, M., BOESPFLUG-TANGUY, O., BERTINI, E., SANTORELLI, F. M. & ESTÉVEZ, R. 2006. Vacuolating megalencephalic leukoencephalopathy with subcortical cysts: functional studies of novel variants in MLC1. *Hum Mutat,* 27**,** 292.

MORI, S. & LEBLOND, C. P. 1969. Electron microscopic features and proliferation of astrocytes in the corpus callosum of the rat. *J Comp Neurol,* 137**,** 197-225.

MURAKAMI, T., SHOJI, M., IMAI, Y., INOUE, H., KAWARABAYASHI, T., MATSUBARA, E., HARIGAYA, Y., SASAKI, A., TAKAHASHI, R. & ABE, K. 2004. Pael-R is accumulated in Lewy bodies of Parkinson's disease. *Ann Neurol,* 55**,** 439-42.

MÉTAYÉ, T., GIBELIN, H., PERDRISOT, R. & KRAIMPS, J. L. 2005. Pathophysiological roles of G-protein-coupled receptor kinases. *Cell Signal,* 17**,** 917-28.

NAGELHUS, E. A., MATHIISEN, T. M. & OTTERSEN, O. P. 2004. Aquaporin-4 in the central nervous system: cellular and subcellular distribution and coexpression with KIR4.1. *Neuroscience,* 129**,** 905-13.

NAGY, J. I., DUDEK, F. E. & RASH, J. E. 2004. Update on connexins and gap junctions in neurons and glia in the mammalian nervous system. *Brain Res Brain Res Rev,* 47**,** 191-215.

NAIDU, S. 1999. Clinical delineation of leukodystrophies. *J Mol Neurosci,* 12**,** 185-192.

NASH, B., IOANNIDOU, K. & BARNETT, S. C. 2011. Astrocyte phenotypes and their relationship to myelination. *J Anat,* 219**,** 44-52.

NEDERGAARD, M., RANSOM, B. & GOLDMAN, S. A. 2003. New roles for astrocytes: redefining the functional architecture of the brain. *Trends Neurosci,* 26**,** 523-30.

NEWMAN, E. & REICHENBACH, A. 1996. The Müller cell: a functional element of the retina. *Trends Neurosci,* 19**,** 307-12.

NEWMAN, E. A. 1984. Regional specialization of retinal glial cell membrane. *Nature,* 309**,** 155-7.

NEWMAN, E. A. 1985. Membrane physiology of retinal glial (Müller) cells. *J Neurosci,* 5**,** 2225-39.

NICCHIA, G. P., SRINIVAS, M., LI, W., BROSNAN, C. F., FRIGERI, A. & SPRAY, D. C. 2005. New possible roles for aquaporin-4 in astrocytes: cell cytoskeleton and functional relationship with connexin43. *FASEB J,* 19**,** 1674-6.

NICHOLSON, C. & SYKOVÁ, E. 1998. Extracellular space structure revealed by diffusion analysis. *Trends Neurosci,* 21**,** 207-15.

NIEMEYER, M. I., CID, L. P., SEPÚLVEDA, F. V., BLANZ, J., AUBERSON, M. & JENTSCH, T. J. 2010. No evidence for a role of CLCN2 variants in idiopathic generalized epilepsy. *Nat Genet,* 42**,** 3.

NIEMEYER, M. I., CID, L. P., YUSEF, Y. R., BRIONES, R. & SEPÚLVEDA, F. V. 2009. Voltage-dependent and -independent titration of specific residues accounts for complex gating of a ClC chloride channel by extracellular protons. *J Physiol,* 587**,** 1387-400.

NIEMEYER, M. I., YUSEF, Y. R., CORNEJO, I., FLORES, C. A., SEPÚLVEDA, F. V. & CID, L. P. 2004. Functional evaluation of human ClC-2 chloride channel mutations associated with idiopathic generalized epilepsies. *Physiol Genomics,* 19**,** 74-83.

NILIUS, B. & DROOGMANS, G. 2003. Amazing chloride channels: an overview. *Acta Physiol Scand,* 177**,** 119-47.

NILIUS, B., EGGERMONT, J., VOETS, T., BUYSE, G., MANOLOPOULOS, V. & DROOGMANS, G. 1997. Properties of volume-regulated anion channels in mammalian cells. *Prog Biophys Mol Biol,* 68**,** 69-119.

NILIUS, B., VOETS, T., PRENEN, J., BARTH, H., AKTORIES, K., KAIBUCHI, K., DROOGMANS, G. & EGGERMONT, J. 1999. Role of Rho and Rho kinase in the activation of volume-regulated anion channels in bovine endothelial cells. *J Physiol,* 516 (Pt 1)**,** 67-74.

NUALART-MARTI, A., SOLSONA, C. & FIELDS, R. D. 2013. Gap junction communication in myelinating glia. *Biochim Biophys Acta,* 1828**,** 69-78.

OBERHEIM, N. A., WANG, X., GOLDMAN, S. & NEDERGAARD, M. 2006. Astrocytic complexity distinguishes the human brain. *Trends Neurosci,* 29**,** 547-53.

OFFERMANNS, S. 2003. G-proteins as transducers in transmembrane signalling. *Prog Biophys Mol Biol,* 83**,** 101-30.

OGITA, H., RIKITAKE, Y., MIYOSHI, J. & TAKAI, Y. 2010. Cell adhesion molecules nectins and associating proteins: Implications for physiology and pathology. *Proc Jpn Acad Ser B Phys Biol Sci,* 86**,** 621-9.

OH, S. J. & LEE, C. J. 2017. Distribution and Function of the Bestrophin-1 (Best1) Channel in the Brain. *Exp Neurobiol,* 26**,** 113-121.

OLSEN, M. L., HIGASHIMORI, H., CAMPBELL, S. L., HABLITZ, J. J. & SONTHEIMER, H. 2006. Functional expression of Kir4.1 channels in spinal cord astrocytes. *Glia,* 53**,** 516-28.

ORKAND, R. K., NICHOLLS, J. G. & KUFFLER, S. W. 1966. Effect of nerve impulses on the membrane potential of glial cells in the central nervous system of amphibia. *J Neurophysiol,* 29**,** 788-806.

PALCZEWSKI, K., KUMASAKA, T., HORI, T., BEHNKE, C. A., MOTOSHIMA, H., FOX, B. A., LE TRONG, I., TELLER, D. C., OKADA, T., STENKAMP, R. E., YAMAMOTO, M. & MIYANO, M. 2000. Crystal structure of rhodopsin: A G protein-coupled receptor. *Science,* 289**,** 739-45.

PARK, P. S., LODOWSKI, D. T. & PALCZEWSKI, K. 2008. Activation of G protein-coupled receptors: beyond two-state models and tertiary conformational changes. *Annu Rev Pharmacol Toxicol,* 48**,** 107-41.

PASANTES-MORALES, H., LEZAMA, R. A., RAMOS-MANDUJANO, G. & TUZ, K. L. 2006. Mechanisms of cell volume regulation in hypo-osmolality. *Am J Med,* 119**,** S4-11.

PASANTES-MORALES, H. & MORALES MULIA, S. 2000. Influence of calcium on regulatory volume decrease: role of potassium channels. *Nephron,* 86**,** 414-27.

PASANTES-MORALES, H. & VÁZQUEZ-JUÁREZ, E. 2012. Transporters and channels in cytotoxic astrocyte swelling. *Neurochem Res,* 37**,** 2379-87.

PATZKE, C., MAX, K. E., BEHLKE, J., SCHREIBER, J., SCHMIDT, H., DORNER, A. A., KRÖGER, S., HENNING, M., OTTO, A., HEINEMANN, U. & RATHJEN, F. G. 2010. The coxsackievirus-adenovirus receptor reveals complex homophilic and heterophilic interactions on neural cells. *J Neurosci,* 30**,** 2897-910.

PEDERSEN, S. F., BEISNER, K. H., HOUGAARD, C., WILLUMSEN, B. M., LAMBERT, I. H. & HOFFMANN, E. K. 2002. Rho family GTP binding proteins are involved in the regulatory volume decrease process in NIH3T3 mouse fibroblasts. *J Physiol,* 541**,** 779-96.

PEDERSEN, S. F., HOFFMANN, E. K. & MILLS, J. W. 2001. The cytoskeleton and cell volume regulation. *Comp Biochem Physiol A Mol Integr Physiol,* 130**,** 385-99.

PEDERSEN, S. F., KLAUSEN, T. K. & NILIUS, B. 2015. The identification of a volume-regulated anion channel: an amazing Odyssey. *Acta Physiol (Oxf),* 213**,** 868-81.

PEDERSEN, S. F., OKADA, Y. & NILIUS, B. 2016. Biophysics and Physiology of the Volume-Regulated Anion Channel (VRAC)/Volume-Sensitive Outwardly Rectifying Anion Channel (VSOR). *Pflugers Arch,* 468**,** 371-83.

PETERS, A. 2007. Golgi, Cajal, and the fine structure of the nervous system. *Brain Res Rev,* 55**,** 256-63.

PETRINI, S., MINNONE, G., COCCETTI, M., FRANK, C., AIELLO, C., CUTARELLI, A., AMBROSINI, E., LANCIOTTI, A., BRIGNONE, M. S., D'ORIA, V., STRIPPOLI, R., DE BENEDETTI, F., BERTINI, E. & BRACCI-LAUDIERO, L. 2013. Monocytes and macrophages as biomarkers for the diagnosis of megalencephalic leukoencephalopathy with subcortical cysts. *Mol Cell Neurosci,* 56**,** 307-21.

PLA-CASILLANIS, A., FERIGLE, L., ALONSO-GARDÓN, M., XICOY-ESPAULELLA, E., ERRASTI-MURUGARREN, E., MARAZZITI, D. & ESTÉVEZ, R. 2022. GPR37 Receptors and Megalencephalic Leukoencephalopathy with Subcortical Cysts. *Int J Mol Sci,* 23.

PLANELLS-CASES, R., LUTTER, D., GUYADER, C., GERHARDS, N. M., ULLRICH, F., ELGER, D. A., KUCUKOSMANOGLU, A., XU, G., VOSS, F. K., REINCKE, S. M., STAUBER, T., BLOMEN, V. A., VIS, D. J., WESSELS, L. F., BRUMMELKAMP, T. R., BORST, P., ROTTENBERG, S. & JENTSCH, T. J. 2015. Subunit composition of VRAC channels determines substrate specificity and cellular resistance to Pt-based anti-cancer drugs. *EMBO J,* 34**,** 2993-3008.

PONTING, C. P. 1997. CBS domains in CIC chloride channels implicated in myotonia and nephrolithiasis (kidney stones). *J Mol Med (Berl),* 75**,** 160-3.

POROCA, D. R., PELIS, R. M. & CHAPPE, V. M. 2017. ClC Channels and Transporters: Structure, Physiological Functions, and Implications in Human Chloride Channelopathies. *Front Pharmacol,* 8**,** 151.

PRICE, D. L., LUDWIG, J. W., MI, H., SCHWARZ, T. L. & ELLISMAN, M. H. 2002. Distribution of rSlo Ca2+-activated K+ channels in rat astrocyte perivascular endfeet. *Brain Res,* 956**,** 183-93.

PROTA, A. E., CAMPBELL, J. A., SCHELLING, P., FORREST, J. C., WATSON, M. J., PETERS, T. R., AURRAND-LIONS, M., IMHOF, B. A., DERMODY, T. S. & STEHLE, T. 2003. Crystal structure of human junctional adhesion molecule 1: implications for reovirus binding. *Proc Natl Acad Sci U S A,* 100**,** 5366-71.

QIU, Z., DUBIN, A. E., MATHUR, J., TU, B., REDDY, K., MIRAGLIA, L. J., REINHARDT, J., ORTH, A. P. & PATAPOUTIAN, A. 2014. SWELL1, a plasma membrane protein, is an essential component of volume-regulated anion channel. *Cell,* 157**,** 447-458.

QUINTANA, F. J. 2017. Astrocytes to the rescue! Glia limitans astrocytic endfeet control CNS inflammation. *J Clin Invest,* 127**,** 2897-2899.

RAJKUMAR, P., CHA, B., YIN, J., AREND, L. J., PĂUNESCU, T. G., HIRABAYASHI, Y., DONOWITZ, M. & PLUZNICK, J. L. 2018. Identifying the localization and exploring a functional role for Gprc5c in the kidney. *FASEB J,* 32**,** 2046-2059.

RAMOS-MANDUJANO, G., VÁZQUEZ-JUÁREZ, E., HERNÁNDEZ-BENÍTEZ, R. & PASANTES-MORALES, H. 2007. Thrombin potently enhances swelling-sensitive glutamate efflux from cultured astrocytes. *Glia,* 55**,** 917-25.

RASH, J. E. 2010. Molecular disruptions of the panglial syncytium block potassium siphoning and axonal saltatory conduction: pertinence to neuromyelitis optica and other demyelinating diseases of the central nervous system. *Neuroscience,* 168**,** 982-1008.

RATTÉ, S. & PRESCOTT, S. A. 2011. ClC-2 channels regulate neuronal excitability, not intracellular chloride levels. *J Neurosci,* 31**,** 15838-43.

REN, G., ROBERTS, A. I. & SHI, Y. 2011. Adhesion molecules: key players in Mesenchymal stem cell-mediated immunosuppression. *Cell Adh Migr,* 5**,** 20-2.

REZGAOUI, M., SÜSENS, U., IGNATOV, A., GELDERBLOM, M., GLASSMEIER, G., FRANKE, I., URNY, J., IMAI, Y., TAKAHASHI, R. & SCHALLER, H. C. 2006. The neuropeptide head activator is a high-affinity ligand for the orphan G-protein-coupled receptor GPR37. *J Cell Sci,* 119**,** 542-9.

RIDDER, M. C., BOOR, I., LODDER, J. C., POSTMA, N. L., CAPDEVILA-NORTES, X., DUARRI, A., BRUSSAARD, A. B., ESTÉVEZ, R., SCHEPER, G. C., MANSVELDER, H. D. & VAN DER KNAAP, M. S. 2011. Megalencephalic leucoencephalopathy with cysts: defect in chloride currents and cell volume regulation. *Brain,* 134**,** 3342-54.

RINKE, I., ARTMANN, J. & STEIN, V. 2010. ClC-2 voltage-gated channels constitute part of the background conductance and assist chloride extrusion. *J Neurosci,* 30**,** 4776-86.

ROBBINS, E. M., KRUPP, A. J., PEREZ DE ARCE, K., GHOSH, A. K., FOGEL, A. I., BOUCARD, A., SÜDHOF, T. C., STEIN, V. & BIEDERER, T. 2010. SynCAM 1 adhesion dynamically regulates synapse number and impacts plasticity and learning. *Neuron,* 68**,** 894-906.

ROBBINS, M. J., MICHALOVICH, D., HILL, J., CALVER, A. R., MEDHURST, A. D., GLOGER, I., SIMS, M., MIDDLEMISS, D. N. & PANGALOS, M. N. 2000. Molecular cloning and characterization of two novel retinoic acid-inducible orphan G-protein-coupled receptors (GPRC5B and GPRC5C). *Genomics,* 67**,** 8-18.

ROSENBAUM, D. M., RASMUSSEN, S. G. & KOBILKA, B. K. 2009. The structure and function of G-protein-coupled receptors. *Nature,* 459**,** 356-63.

ROSENMAN, S. J., SHRIKANT, P., DUBB, L., BENVENISTE, E. N. & RANSOHOFF, R. M. 1995. Cytokine-induced expression of vascular cell adhesion molecule-1 (VCAM-1) by astrocytes and astrocytoma cell lines. *J Immunol,* 154**,** 1888-99.

ROY, M. L., SAAL, D., PERNEY, T., SONTHEIMER, H., WAXMAN, S. G. & KACZMAREK, L. K. 1996. Manipulation of the delayed rectifier Kv1.5 potassium channel in glial cells by antisense oligodeoxynucleotides. *Glia,* 18**,** 177-84.

RUAT, M., ROUDAUT, H., FERENT, J. & TRAIFFORT, E. 2012. Hedgehog trafficking, cilia and brain functions. *Differentiation,* 83**,** S97-104.

RUTLEDGE, E., DENTON, J. & STRANGE, K. 2002. Cell cycle- and swelling-induced activation of a Caenorhabditis elegans ClC channel is mediated by CeGLC-7alpha/beta phosphatases. *J Cell Biol,* 158**,** 435-44.

RYSKAMP, D. A., IUSO, A. & KRIŽAJ, D. 2015. TRPV4 links inflammatory signaling and neuroglial swelling. *Channels (Austin),* 9**,** 70-2.

RÜBSAM, M., BROUSSARD, J. A., WICKSTRÖM, S. A., NEKRASOVA, O., GREEN, K. J. & NIESSEN, C. M. 2018. Adherens Junctions and Desmosomes Coordinate Mechanics and Signaling to Orchestrate Tissue Morphogenesis and Function: An Evolutionary Perspective. *Cold Spring Harb Perspect Biol,* 10.

SAIJO, H., NAKAYAMA, H., EZOE, T., ARAKI, K., SONE, S., HAMAGUCHI, H., SUZUKI, H., SHIROMA, N., KANAZAWA, N., TSUJINO, S., HIRAYAMA, Y. & ARIMA, M. 2003. A case of megalencephalic leukoencephalopathy with subcortical cysts (van der Knaap disease): molecular genetic study. *Brain Dev,* 25**,** 362-6.

SAKISAKA, T. & TAKAI, Y. 2004. Biology and pathology of nectins and nectin-like molecules. *Curr Opin Cell Biol,* 16**,** 513-21.

SANO, T., KIM, Y. J., OSHIMA, E., SHIMIZU, C., KIYONARI, H., ABE, T., HIGASHI, H., YAMADA, K. & HIRABAYASHI, Y. 2011. Comparative characterization of GPRC5B and GPRC5CLacZ knockin mice; behavioral abnormalities in GPRC5B-deficient mice. *Biochem Biophys Res Commun,* 412**,** 460-5.

SANO, T., KOHYAMA-KOGANEYA, A., KINOSHITA, M. O., TATSUKAWA, T., SHIMIZU, C., OSHIMA, E., YAMADA, K., LE, T. D., AKAGI, T., TOHYAMA, K., NAGAO, S. & HIRABAYASHI, Y. 2018. Loss of GPRC5B impairs synapse formation of Purkinje cells with cerebellar nuclear neurons and disrupts cerebellar synaptic plasticity and motor learning. *Neurosci Res,* 136**,** 33-47.

SAVIANE, C., CONTI, F. & PUSCH, M. 1999. The muscle chloride channel ClC-1 has a double-barreled appearance that is differentially affected in dominant and recessive myotonia. *J Gen Physiol,* 113**,** 457-68.

SAWADA, A., TAKIHARA, Y., KIM, J. Y., MATSUDA-HASHII, Y., TOKIMASA, S., FUJISAKI, H., KUBOTA, K., ENDO, H., ONODERA, T., OHTA, H., OZONO, K. & HARA, J. 2003. A congenital mutation of the novel gene LRRC8 causes agammaglobulinemia in humans. *J Clin Invest,* 112**,** 1707-13.

SCHEPER, G. C., VAN BERKEL, C. G., LEISLE, L., DE GROOT, K. E., ERRAMI, A., JENTSCH, T. J. & VAN DER KNAAP, M. S. 2010. Analysis of CLCN2 as candidate gene for megalencephalic leukoencephalopathy with subcortical cysts. *Genet Test Mol Biomarkers,* 14**,** 255-7.

SCHIÖTH, H. B. & FREDRIKSSON, R. 2005. The GRAFS classification system of G-protein coupled receptors in comparative perspective. *Gen Comp Endocrinol,* 142**,** 94-101.

SCHLESINGER, M. & BENDAS, G. 2015. Vascular cell adhesion molecule-1 (VCAM-1)--an increasing insight into its role in tumorigenicity and metastasis. *Int J Cancer,* 136**,** 2504-14.

SCHMITT, A., GOFFERJE, V., WEBER, M., MEYER, J., MÖSSNER, R. & LESCH, K. P. 2003. The brain-specific protein MLC1 implicated in megalencephalic leukoencephalopathy with subcortical cysts is expressed in glial cells in the murine brain. *Glia,* 44**,** 283-95.

SCHOBER, A. L., WILSON, C. S. & MONGIN, A. A. 2017. Molecular composition and heterogeneity of the LRRC8-containing swelling-activated osmolyte channels in primary rat astrocytes. *J Physiol,* 595**,** 6939-6951.

SCHOLL, U. I., STÖLTING, G., SCHEWE, J., THIEL, A., TAN, H., NELSON-WILLIAMS, C., VICHOT, A. A., JIN, S. C., LORING, E., UNTIET, V., YOO, T., CHOI, J., XU, S., WU, A., KIRCHNER, M., MERTINS, P., RUMP, L. C., ONDER, A. M., GAMBLE, C., MCKENNEY, D., LASH, R. W., JONES, D. P., CHUNE, G., GAGLIARDI, P., CHOI, M., GORDON, R., STOWASSER, M., FAHLKE, C. & LIFTON, R. P. 2018. CLCN2

chloride channel mutations in familial hyperaldosteronism type II. *Nat Genet,* 50**,** 349-354.

SENER, R. N. 2003. Proton MR spectroscopy demonstration of taurine peaks in megalencephalic leukoencephalopathy with cysts. *Comput Med Imaging Graph,* 27**,** 23-6.

SHAPIRO, L., LOVE, J. & COLMAN, D. R. 2007. Adhesion molecules in the nervous system: structural insights into function and diversity. *Annu Rev Neurosci,* 30**,** 451-74.

SHIMURA, H., HATTORI, N., KUBO, S., MIZUNO, Y., ASAKAWA, S., MINOSHIMA, S., SHIMIZU, N., IWAI, K., CHIBA, T., TANAKA, K. & SUZUKI, T. 2000. Familial Parkinson disease gene product, parkin, is a ubiquitin-protein ligase. *Nat Genet,* 25**,** 302-5.

SIMARD, M. & NEDERGAARD, M. 2004. The neurobiology of glia in the context of water and ion homeostasis. *Neuroscience,* 129**,** 877-96.

SINGHAL, B. S. 2005. Leukodystrophies: Indian scenario. *Indian J Pediatr,* 72**,** 315-8.

SIRISI, S., ELORZA-VIDAL, X., ARNEDO, T., ARMAND-UGÓN, M., CALLEJO, G., CAPDEVILA-NORTES, X., LÓPEZ-HERNÁNDEZ, T., SCHULTE, U., BARRALLO-GIMENO, A., NUNES, V., GASULL, X. & ESTÉVEZ, R. 2017. Depolarization causes the formation of a ternary complex between GlialCAM, MLC1 and ClC-2 in astrocytes: implications in megalencephalic leukoencephalopathy. *Hum Mol Genet,* 26**,** 2436-2450.

SIRISI, S., FOLGUEIRA, M., LÓPEZ-HERNÁNDEZ, T., MINIERI, L., PÉREZ-RIUS, C., GAITÁN-PEÑAS, H., ZANG, J., MARTÍNEZ, A., CAPDEVILA-NORTES, X., DE LA VILLA, P., ROY, U., ALIA, A., NEUHAUSS, S., FERRONI, S., NUNES, V., ESTÉVEZ, R. & BARRALLO-GIMENO, A. 2014. Megalencephalic leukoencephalopathy with subcortical cysts protein 1 regulates glial surface localization of GLIALCAM from fish to humans. *Hum Mol Genet,* 23**,** 5069-86.

SMITH, N. J. 2015. Drug Discovery Opportunities at the Endothelin B Receptor-Related Orphan G Protein-Coupled Receptors, GPR37 and GPR37L1. *Front Pharmacol,* 6**,** 275.

SMITH, R. L., CLAYTON, G. H., WILCOX, C. L., ESCUDERO, K. W. & STALEY, K. J. 1995. Differential expression of an inwardly rectifying chloride conductance in rat brain neurons: a potential mechanism for cell-specific modulation of postsynaptic inhibition. *J Neurosci,* 15**,** 4057-67.

SOMJEN, G. G. 2002. Ion regulation in the brain: implications for pathophysiology. *Neuroscientist,* 8**,** 254-67.

SONG, Y. & GUNNARSON, E. 2012. Potassium dependent regulation of astrocyte water permeability is mediated by cAMP signaling. *PLoS One,* 7**,** e34936.

SOWA, G. 2012. Caveolae, caveolins, cavins, and endothelial cell function: new insights. *Front Physiol,* 2**,** 120.

SPELIOTES, E. K., WILLER, C. J., BERNDT, S. I., MONDA, K. L., THORLEIFSSON, G., JACKSON, A. U., LANGO ALLEN, H., LINDGREN, C. M., LUAN, J., MÄGI, R., RANDALL, J. C., VEDANTAM, S., WINKLER, T. W., QI, L., WORKALEMAHU, T., HEID, I. M., STEINTHORSDOTTIR, V., STRINGHAM, H. M., WEEDON, M. N., WHEELER, E., WOOD, A. R., FERREIRA, T., WEYANT, R. J., SEGRÈ, A. V., ESTRADA, K., LIANG, L., NEMESH, J., PARK, J. H., GUSTAFSSON, S., KILPELÄINEN, T. O., YANG, J., BOUATIA-NAJI, N., ESKO, T., FEITOSA, M. F., KUTALIK, Z., MANGINO, M., RAYCHAUDHURI, S., SCHERAG, A., SMITH, A. V., WELCH, R., ZHAO, J. H., ABEN, K. K., ABSHER, D. M., AMIN, N., DIXON, A. L., FISHER, E., GLAZER, N. L., GODDARD, M. E., HEARD-COSTA, N. L., HOESEL, V., HOTTENGA, J. J., JOHANSSON, A., JOHNSON, T., KETKAR, S., LAMINA, C., LI, S., MOFFATT, M. F., MYERS, R. H., NARISU, N., PERRY, J. R., PETERS, M. J.,

PREUSS, M., RIPATTI, S., RIVADENEIRA, F., SANDHOLT, C., SCOTT, L. J., TIMPSON, N. J., TYRER, J. P., VAN WINGERDEN, S., WATANABE, R. M., WHITE, C. C., WIKLUND, F., BARLASSINA, C., CHASMAN, D. I., COOPER, M. N., JANSSON, J. O., LAWRENCE, R. W., PELLIKKA, N., PROKOPENKO, I., SHI, J., THIERING, E., ALAVERE, H., ALIBRANDI, M. T., ALMGREN, P., ARNOLD, A. M., ASPELUND, T., ATWOOD, L. D., BALKAU, B., BALMFORTH, A. J., BENNETT, A. J., BEN-SHLOMO, Y., BERGMAN, R. N., BERGMANN, S., BIEBERMANN, H., BLAKEMORE, A. I., BOES, T., BONNYCASTLE, L. L., BORNSTEIN, S. R., BROWN, M. J., BUCHANAN, T. A., et al. 2010. Association analyses of 249,796 individuals reveal 18 new loci associated with body mass index. *Nat Genet,* 42**,** 937-48.

SPIEGEL, I., ADAMSKY, K., EISENBACH, M., ESHED, Y., SPIEGEL, A., MIRSKY, R., SCHERER, S. S. & PELES, E. 2006. Identification of novel cell-adhesion molecules in peripheral nerves using a signal-sequence trap. *Neuron Glia Biol,* 2**,** 27-38.

SRIRAM, S. R., LI, X., KO, H. S., CHUNG, K. K., WONG, E., LIM, K. L., DAWSON, V. L. & DAWSON, T. M. 2005. Familial-associated mutations differentially disrupt the solubility, localization, binding and ubiquitination properties of parkin. *Hum Mol Genet,* 14**,** 2571-86.

STAGI, M., FOGEL, A. I. & BIEDERER, T. 2010. SynCAM 1 participates in axo-dendritic contact assembly and shapes neuronal growth cones. *Proc Natl Acad Sci U S A,* 107**,** 7568-73.

STOTZ, S. C. & CLAPHAM, D. E. 2012. Anion-sensitive fluorophore identifies the Drosophila swell-activated chloride channel in a genome-wide RNA interference screen. *PLoS One,* 7**,** e46865.

STRANGE, K., EMMA, F. & JACKSON, P. S. 1996. Cellular and molecular physiology of volume-sensitive anion channels. *Am J Physiol,* 270**,** C711-30.

STÖLTING, G., FISCHER, M. & FAHLKE, C. 2014. CLC channel function and dysfunction in health and disease. *Front Physiol,* 5**,** 378.

SÍK, A., SMITH, R. L. & FREUND, T. F. 2000. Distribution of chloride channel-2-immunoreactive neuronal and astrocytic processes in the hippocampus. *Neuroscience,* 101**,** 51-65.

TAKAHASHI, R. & IMAI, Y. 2003. Pael receptor, endoplasmic reticulum stress, and Parkinson's disease. *J Neurol,* 250 Suppl 3**,** III25-9.

TAKEICHI, M. 2007. The cadherin superfamily in neuronal connections and interactions. *Nat Rev Neurosci,* 8**,** 11-20.

TAO, Q., FUJIMOTO, J., MEN, T., YE, X., DENG, J., LACROIX, L., CLIFFORD, J. L., MAO, L., VAN PELT, C. S., LEE, J. J., LOTAN, D. & LOTAN, R. 2007. Identification of the retinoic acid-inducible Gprc5a as a new lung tumor suppressor gene. *J Natl Cancer Inst,* 99**,** 1668-82.

TAS, P. W., KRESS, H. G. & KOSCHEL, K. 1989. Volatile anesthetics inhibit the ion flux through Ca2+-activated K+ channels of rat glioma C6 cells. *Biochim Biophys Acta,* 983**,** 264-8.

TEIJIDO, O., CASAROLI-MARANO, R., KHARKOVETS, T., AGUADO, F., ZORZANO, A., PALACÍN, M., SORIANO, E., MARTÍNEZ, A. & ESTÉVEZ, R. 2007. Expression patterns of MLC1 protein in the central and peripheral nervous systems. *Neurobiol Dis,* 26**,** 532-45.

TEIJIDO, O., MARTÍNEZ, A., PUSCH, M., ZORZANO, A., SORIANO, E., DEL RÍO, J. A., PALACÍN, M. & ESTÉVEZ, R. 2004. Localization and functional analyses of the MLC1

protein involved in megalencephalic leukoencephalopathy with subcortical cysts. *Hum Mol Genet,* 13**,** 2581-94.

TEKOLA-AYELE, F., LEE, A., WORKALEMAHU, T. & SÁNCHEZ-POZOS, K. 2019. Shared genetic underpinnings of childhood obesity and adult cardiometabolic diseases. *Hum Genomics,* 13**,** 17.

THEODOSIS, D. T., POULAIN, D. A. & OLIET, S. H. 2008. Activity-dependent structural and functional plasticity of astrocyte-neuron interactions. *Physiol Rev,* 88**,** 983-1008.

THIEMANN, A., GRÜNDER, S., PUSCH, M. & JENTSCH, T. J. 1992. A chloride channel widely expressed in epithelial and non-epithelial cells. *Nature,* 356**,** 57-60.

TIKHONOVA, I. G. & COSTANZI, S. 2009. Unraveling the structure and function of G protein-coupled receptors through NMR spectroscopy. *Curr Pharm Des,* 15**,** 4003-16.

TILLY, B. C., EDIXHOVEN, M. J., TERTOOLEN, L. G., MORII, N., SAITOH, Y., NARUMIYA, S. & DE JONGE, H. R. 1996. Activation of the osmo-sensitive chloride conductance involves P21rho and is accompanied by a transient reorganization of the F-actin cytoskeleton. *Mol Biol Cell,* 7**,** 1419-27.

TOGASHI, H., SAKISAKA, T. & TAKAI, Y. 2009. Cell adhesion molecules in the central nervous system. *Cell Adh Migr,* 3**,** 29-35.

TOMITA, H., ZIEGLER, M. E., KIM, H. B., EVANS, S. J., CHOUDARY, P. V., LI, J. Z., MENG, F., DAI, M., MYERS, R. M., NEAL, C. R., SPEED, T. P., BARCHAS, J. D., SCHATZBERG, A. F., WATSON, S. J., AKIL, H., JONES, E. G., BUNNEY, W. E. & VAWTER, M. P. 2013. G protein-linked signaling pathways in bipolar and major depressive disorders. *Front Genet,* 4**,** 297.

TOPCU, M., SAATCI, I., TOPCUOGLU, M. A., KOSE, G. & KUNAK, B. 1998. Megalencephaly and leukodystrophy with mild clinical course: a report on 12 new cases. *Brain Dev,* 20**,** 142-53.

TROUET, D., CARTON, I., HERMANS, D., DROOGMANS, G., NILIUS, B. & EGGERMONT, J. 2001. Inhibition of VRAC by c-Src tyrosine kinase targeted to caveolae is mediated by the Src homology domains. *Am J Physiol Cell Physiol,* 281**,** C248-56.

ULRICH, C. D., HOLTMANN, M. & MILLER, L. J. 1998. Secretin and vasoactive intestinal peptide receptors: members of a unique family of G protein-coupled receptors. *Gastroenterology,* 114**,** 382-97.

VAILLANT, C. & MONARD, D. 2009. SHH pathway and cerebellar development. *Cerebellum,* 8**,** 291-301.

VALDENAIRE, O., GILLER, T., BREU, V., ARDATI, A., SCHWEIZER, A. & RICHARDS, J. G. 1998. A new family of orphan G protein-coupled receptors predominantly expressed in the brain. *FEBS Lett,* 424**,** 193-6.

VAN DER KNAAP, M., ABBINK, T. & MIN, R. 2003. Megalencephalic Leukoencephalopathy with Subcortical Cysts. GeneReviews [Internet].

VAN DER KNAAP, M. S., BARTH, P. G., VRENSEN, G. F. & VALK, J. 1996. Histopathology of an infantile-onset spongiform leukoencephalopathy with a discrepantly mild clinical course. *Acta Neuropathol,* 92**,** 206-12.

VAN DER KNAAP, M. S., BOOR, I. & ESTÉVEZ, R. 2012. Megalencephalic leukoencephalopathy with subcortical cysts: chronic white matter oedema due to a defect in brain ion and water homoeostasis. *Lancet Neurol,* 11**,** 973-85.

VAN DER KNAAP, M. S. & BUGIANI, M. 2017. Leukodystrophies: a proposed classification system based on pathological changes and pathogenetic mechanisms. *Acta Neuropathol,* 134**,** 351-382.

VAN DER KNAAP, M. S., LAI, V., KÖHLER, W., SALIH, M. A., FONSECA, M. J., BENKE, T. A., WILSON, C., JAYAKAR, P., AINE, M. R., DOM, L., LYNCH, B., KÁLMÁNCHEY, R., PIETSCH, P., ERRAMI, A. & SCHEPER, G. C. 2010. Megalencephalic leukoencephalopathy with cysts without MLC1 defect. *Ann Neurol,* 67**,** 834-7.

VAN RAAIJ, M. J., CHOUIN, E., VAN DER ZANDT, H., BERGELSON, J. M. & CUSACK, S. 2000. Dimeric structure of the coxsackievirus and adenovirus receptor D1 domain at 1.7 A resolution. *Structure,* 8**,** 1147-55.

VARADI, M., ANYANGO, S., DESHPANDE, M., NAIR, S., NATASSIA, C., YORDANOVA, G., YUAN, D., STROE, O., WOOD, G., LAYDON, A., ŽÍDEK, A., GREEN, T., TUNYASUVUNAKOOL, K., PETERSEN, S., JUMPER, J., CLANCY, E., GREEN, R., VORA, A., LUTFI, M., FIGURNOV, M., COWIE, A., HOBBS, N., KOHLI, P., KLEYWEGT, G., BIRNEY, E., HASSABIS, D. & VELANKAR, S. 2022. AlphaFold Protein Structure Database: massively expanding the structural coverage of protein-sequence space with high-accuracy models. *Nucleic Acids Res,* 50**,** D439-D444.

VASILE, F., DOSSI, E. & ROUACH, N. 2017. Human astrocytes: structure and functions in the healthy brain. *Brain Struct Funct,* 222**,** 2017-2029.

VENKATAKRISHNAN, A. J., DEUPI, X., LEBON, G., TATE, C. G., SCHERTLER, G. F. & BABU, M. M. 2013. Molecular signatures of G-protein-coupled receptors. *Nature,* 494**,** 185-94.

VERDINO, P., WITHERDEN, D. A., HAVRAN, W. L. & WILSON, I. A. 2010. The molecular interaction of CAR and JAML recruits the central cell signal transducer PI3K. *Science,* 329**,** 1210-4.

VISCHER, H. F., CASTRO, M. & PIN, J. P. 2015. G Protein-Coupled Receptor Multimers: A Question Still Open Despite the Use of Novel Approaches. *Mol Pharmacol,* 88**,** 561-71.

VOLKMER, H., SCHREIBER, J. & RATHJEN, F. G. 2013. Regulation of adhesion by flexible ectodomains of IgCAMs. *Neurochem Res,* 38**,** 1092-9.

VON SAMSON-HIMMELSTJERNA, F. A., FREUNDT, G., NITZ, J. T., STELTER, F., LUEDDE, M., WIELAND, T., FREY, N. & HIPPE, H. J. 2019. The orphan receptor GPRC5B modulates inflammatory and fibrotic pathways in cardiac fibroblasts and mice hearts. *Biochem Biophys Res Commun,* 514**,** 1198-1203.

VOSS, F. K., ULLRICH, F., MÜNCH, J., LAZAROW, K., LUTTER, D., MAH, N., ANDRADE-NAVARRO, M. A., VON KRIES, J. P., STAUBER, T. & JENTSCH, T. J. 2014. Identification of LRRC8 heteromers as an essential component of the volume-regulated anion channel VRAC. *Science,* 344**,** 634-8.

VYSKOCIL, F., KRITZ, N. & BURES, J. 1972. Potassium-selective microelectrodes used for measuring the extracellular brain potassium during spreading depression and anoxic depolarization in rats. *Brain Res,* 39**,** 255-9.

VÁZQUEZ-JUÁREZ, E., RAMOS-MANDUJANO, G., HERNÁNDEZ-BENÍTEZ, R. & PASANTES-MORALES, H. 2008. On the role of G-protein coupled receptors in cell volume regulation. *Cell Physiol Biochem,* 21**,** 1-14.

WALLRAFF, A., KÖHLING, R., HEINEMANN, U., THEIS, M., WILLECKE, K. & STEINHÄUSER, C. 2006. The impact of astrocytic gap junctional coupling on potassium buffering in the hippocampus. *J Neurosci,* 26**,** 5438-47.

WALSH, F. S. & DOHERTY, P. 1997. Neural cell adhesion molecules of the immunoglobulin superfamily: role in axon growth and guidance. *Annu Rev Cell Dev Biol,* 13**,** 425-56.

WANG, D. D. & BORDEY, A. 2008. The astrocyte odyssey. *Prog Neurobiol,* 86**,** 342-67.

WANG, F., SMITH, N. A., XU, Q., FUJITA, T., BABA, A., MATSUDA, T., TAKANO, T., BEKAR, L. & NEDERGAARD, M. 2012. Astrocytes modulate neural network activity by Ca^{2}+-dependent uptake of extracellular K+. *Sci Signal,* 5**,** ra26.

WANG, Y. F. & PARPURA, V. 2018. Astroglial Modulation of Hydromineral Balance and Cerebral Edema. *Front Mol Neurosci,* 11**,** 204.

WASHBOURNE, P., DITYATEV, A., SCHEIFFELE, P., BIEDERER, T., WEINER, J. A., CHRISTOPHERSON, K. S. & EL-HUSSEINI, A. 2004. Cell adhesion molecules in synapse formation. *J Neurosci,* 24**,** 9244-9.

WEBER, C., FRAEMOHS, L. & DEJANA, E. 2007. The role of junctional adhesion molecules in vascular inflammation. *Nat Rev Immunol,* 7**,** 467-77.

WEINREICH, F. & JENTSCH, T. J. 2001. Pores formed by single subunits in mixed dimers of different CLC chloride channels. *J Biol Chem,* 276**,** 2347-53.

WITTCHEN, E. S. 2009. Endothelial signaling in paracellular and transcellular leukocyte transmigration. *Front Biosci (Landmark Ed),* 14**,** 2522-45.

WU, Y., LIANG, D., WANG, Y., BAI, M., TANG, W., BAO, S., YAN, Z., LI, D. & LI, J. 2013. Correction of a genetic disease in mouse via use of CRISPR-Cas9. *Cell Stem Cell,* 13**,** 659-62.

XIE, L., KANG, H., XU, Q., CHEN, M. J., LIAO, Y., THIYAGARAJAN, M., O'DONNELL, J., CHRISTENSEN, D. J., NICHOLSON, C., ILIFF, J. J., TAKANO, T., DEANE, R. & NEDERGAARD, M. 2013. Sleep drives metabolite clearance from the adult brain. *Science,* 342**,** 373-7.

YAGUCHI, T. & NISHIZAKI, T. 2010. Extracellular high K+ stimulates vesicular glutamate release from astrocytes by activating voltage-dependent calcium channels. *J Cell Physiol,* 225**,** 512-8.

YANG, H. J., VAINSHTEIN, A., MAIK-RACHLINE, G. & PELES, E. 2016. G protein-coupled receptor 37 is a negative regulator of oligodendrocyte differentiation and myelination. *Nat Commun,* 7**,** 10884.

YANG, Y. L. & LI, X. M. 2000. The IAP family: endogenous caspase inhibitors with multiple biological activities. *Cell Res,* 10**,** 169-77.

YOSHIMI, K., KUNIHIRO, Y., KANEKO, T., NAGAHORA, H., VOIGT, B. & MASHIMO, T. 2016. ssODN-mediated knock-in with CRISPR-Cas for large genomic regions in zygotes. *Nat Commun,* 7**,** 10431.

YUDIN, Y. & ROHACS, T. 2018. Inhibitory G. *Mol Pain,* 14**,** 1744806918763646.

ZENG, Z., SU, K., KYAW, H. & LI, Y. 1997. A novel endothelin receptor type-B-like gene enriched in the brain. *Biochem Biophys Res Commun,* 233**,** 559-67.

ZEYDAN, B., UYGUNOGLU, U., ALTINTAS, A., SAIP, S., SIVA, A., ABBINK, T. E. M., VAN DER KNAAP, M. S. & YALCINKAYA, C. 2017. Identification of 3 Novel Patients with CLCN2-Related Leukoencephalopathy due to CLCN2 Mutations. *Eur Neurol,* 78**,** 125-127.

ZHANG, H. & VERKMAN, A. S. 2008. Aquaporin-4 independent Kir4.1 K+ channel function in brain glial cells. *Mol Cell Neurosci,* 37**,** 1-10.

ZHANG, Y., GAO, J., CHUNG, K. K., HUANG, H., DAWSON, V. L. & DAWSON, T. M. 2000. Parkin functions as an E2-dependent ubiquitin- protein ligase and promotes the degradation of the synaptic vesicle-associated protein, CDCrel-1. *Proc Natl Acad Sci U S A,* 97**,** 13354-9.

ZHOU, M., XU, G., XIE, M., ZHANG, X., SCHOOLS, G. P., MA, L., KIMELBERG, H. K. & CHEN, H. 2009. TWIK-1 and TREK-1 are potassium channels contributing significantly to astrocyte passive conductance in rat hippocampal slices. *J Neurosci,* 29**,** 8551-64.

ZÚÑIGA, L., NIEMEYER, M. I., VARELA, D., CATALÁN, M., CID, L. P. & SEPÚLVEDA, F. V. 2004. The voltage-dependent ClC-2 chloride channel has a dual gating mechanism. *J Physiol,* 555**,** 671-82.

ANNEX:

PUBLICATIONS

Human Molecular Genetics, 2020, Vol. 29, No. 7 1107–1120

doi: 10.1093/hmg/ddaa009
Advance Access Publication Date: 21 January 2020
General Article

GENERAL ARTICLE

Structural basis for the dominant or recessive character of *GLIALCAM* mutations found in leukodystrophies

Xabier Elorza-Vidal[1,2], Efren Xicoy-Espaulella[1], Adrià Pla-Casillanis[1], Marta Alonso-Gardón[1], Héctor Gaitán-Peñas[1,2], Carolyn Engel-Pizcueta[1], Juan Fernández-Recio[3,4,5] and Raúl Estévez[1,2,*]

[1]Unitat de Fisiologia, Departament de Ciències Fisiològiques, Genes Disease and Therapy Program IDIBELL-Institute of Neurosciences, Universitat de Barcelona, L'Hospitalet de Llobregat, Spain, [2]Centro de Investigación en red de enfermedades raras (CIBERER), ISCIII, Madrid, Spain, [3]Barcelona Supercomputing Center (BSC), Barcelona, Spain, [4]Institut de Biologia Molecular de Barcelona, CSIC, Barcelona, Spain and [5]Instituto de Ciencias de la Vid y del Vino (ICVV), CSIC- Universidad de La Rioja- Gobierno de la Rioja, Logroño, Spain

*To whom correspondence should be addressed at: Raúl Estévez, Facultat de Medicina, Departament de Ciències Fisiològiques, Universitat de Barcelona-IDIBELL, C/Feixa Llarga s/n 08907 L'Hospitalet de Llobregat, Barcelona, Spain. Tel: (+34) 93 403 9781; Fax: (+34) 93 402 4268; Email: restevez@ub.edu

Abstract

Megalencephalic leukoencephalopathy with subcortical cysts (MLC) is a type of leukodystrophy characterized by white matter edema, and it is caused mainly by recessive mutations in *MLC1* and *GLIALCAM* genes. These variants are called MLC1 and MLC2A with both types of patients sharing the same clinical phenotype. In addition, dominant mutations in *GLIALCAM* have also been identified in a subtype of MLC patients with a remitting phenotype. This variant has been named MLC2B. *GLIALCAM* encodes for an adhesion protein containing two immunoglobulin (Ig) domains and it is needed for MLC1 targeting to astrocyte–astrocyte junctions. Most mutations identified in *GLIALCAM* abolish GlialCAM targeting to junctions. However, it is unclear why some mutations behave as recessive or dominant. Here, we used a combination of biochemistry methods with a new developed anti-GlialCAM nanobody, double-mutants and cysteine cross-links experiments, together with computer docking, to create a structural model of GlialCAM homo-interactions. Using this model, we suggest that dominant mutations affect different GlialCAM–GlialCAM interacting surfaces in the first Ig domain, which can occur between GlialCAM molecules present in the same cell (*cis*) or present in neighbouring cells (*trans*). Our results provide a framework that can be used to understand the molecular basis of pathogenesis of all identified *GLIALCAM* mutations.

Introduction

Leukodystrophies constitute a large group of genetic disorders primarily affecting CNS white matter (1). Within these, Megalencephalic leukoencephalopathy with subcortical cysts (MLC) is characterized by early-onset macrocephaly, epilepsy and cerebral white matter edema (2). It can be caused by mutations in two

Received: December 12, 2019. **Revised:** January 10, 2020. **Accepted:** January 15, 2020

different genes: *MLC1*, which is more frequent (3), and *GLIALCAM* (4). Detailed characterization of MLC patients with *GLIALCAM* mutations revealed two different phenotypes: MLC2A, caused by two recessive mutations and which is indistinguishable from patients containing mutations in MLC1, and MLC2B, caused by one dominant mutation and which shows a remitting, more benign MLC phenotype (2,5).

MLC1 is a membrane protein of unknown functions (6), while GlialCAM is an adhesion molecule that belongs to the immunoglobulin superfamily (7). GlialCAM works as an obligatory subunit of MLC1, being required for MLC1 endoplasmic reticulum exit and targeting to astrocyte–astrocyte junctions (8–10). In addition, GlialCAM is further characterized as an auxiliary subunit of the ClC-2 chloride channel (11), targeting it to cell–cell junctions and modifying its functional properties (12).

Mutagenesis studies determined that the extracellular domain of GlialCAM is required for cell junction targeting, as well as for mediating interactions with itself or with MLC1 and ClC-2 (13). Accordingly, all MLC missense mutations in *GLIALCAM* have been identified in the extracellular domain (2). Within this domain, most missense mutations are located in the first Ig domain (IgV type) and affect GlialCAM localization at cell–cell junctions, observing the same phenotype for mutations identified in MLC2A or MLC2B patients (4,14,15). In contrast, the remaining mutations, which are located in the second Ig domain (IgC2 type), do not affect GlialCAM localization (14).

In order to understand what was the biochemical basis of the genetic character of these mutations, co-expression experiments in primary astrocytes were performed (4). These experiments revealed that the co-expression of GlialCAM wild-type (WT) with GlialCAM containing an MLC2B mutation affected the targeting of GlialCAM WT. In contrast, no effect was observed in GlialCAM WT upon co-expression with GlialCAM containing MLC2A mutations. These effects have been recently validated *in vivo* after the characterization of a knock-in *Glialcam* mice containing the mutation G89S identified in MLC2B patients (9). This mutation affected the targeting of the protein to cell–cell junctions in Bergmann glia, showed vacuoles in the cerebellum in homozygous mice and the heterozygous mice for this mutation showed also a partially altered GlialCAM localization.

All *GLIALCAM* missense mutations studied to date in the first IgV domain reduce the ability of the mutant to interact with GlialCAM WT in the same cell. However, the mutation p.D128N, identified in MLC2B patients, showed an equal ability to interact with GlialCAM WT (14). Thus, a reduced interaction with GlialCAM WT does not sufficiently explain why some mutations behave in a dominant or in a recessive manner. Furthermore, none of the *GLIALCAM* MLC2A or MLC2B mutations identified to date show a decrease in the interaction of GlialCAM with MLC1 or ClC-2, and all GlialCAM mutants are still able to change the functional properties of ClC-2, although its targeting to cell junctions is abolished (14).

So far, there is no evidence to suggest molecular clues that could be used to predict the genetic behaviour of GlialCAM mutants. One puzzling example is that some amino acids have been found containing recessive (the mutation p.R92Q was identified in MLC2A patients) or dominant mutations (the mutation p.R92W was identified in MLC2B patients) (4). Therefore, the molecular basis explaining why a mutation in *GLIALCAM* is recessive or dominant is completely unknown.

In this work, we aimed to understand the biochemical basis that determines why some *GLIALCAM* mutations behave as recessive or as dominant. Using a combination of computational and biochemical approaches, we provide a model for GlialCAM homo-interactions that explains the genetic behaviour of *GLIALCAM* mutations.

Results

Biochemical characterization of newly identified MLC2B GLIALCAM mutations

Previous studies (14) characterized most missense *GLIALCAM* mutations identified in MLC2A and MLC2B patients located in the first IgV domain. These studies indicated that nearly all IgV mutations caused a reduction of the targeting of GlialCAM to cell–cell junctions as well as a reduced ability to interact with GlialCAM WT (as measured by split-TEV assays). An exception was the mutation p.D128N that, despite having a targeting defect, maintained its ability to interact with WT GlialCAM (14).

We characterized in more detail two newly identified MLC2B *GLIALCAM* mutations, p.S59N (2) and p.Q56P (16). Both mutations showed a targeting defect to cell–cell junctions (Fig. 1A and B). Then, we analyzed their ability to interact with GlialCAM WT using split-TEV assays. The experiments showed that mutants p.Q56P and p.S59N maintained the ability to interact with GlialCAM WT, as the mutant p.D128N (14) (Fig. 1C).

Taking these new results into account, we classified mutations affecting residues into the first IgV domain of GlialCAM into three different groups (Fig. 1D): 1) mutants found in MLC2A patients (in green: p.R98C, p.R92Q) that show a reduced ability to interact with GlialCAM WT; 2) a subset of mutants (Dominant 1, D1) found in MLC2B patients (in red: p.G89S/D, p.R92W) with a reduced ability to interact with GlialCAM WT; and 3) a subset of mutants (Dominant 2, D2) found in MLC2B patients (in blue: p.Q56P, p.S59N, p.D128N) which display a normal ability to interact with GlialCAM WT. In a homology model of GlialCAM monomer (see Materials and Methods) (Fig. 1E), D2 mutants were in predicted loops within the same region of the IgV domain, very close in space, despite some of them being far in sequence.

In vitro biochemical assays of the dominant behaviour of MLC2B mutants

To systematically analyze the dominant behaviour of MLC2B mutations, we developed a simple test to determine whether a mutation was acting as dominant in terms of altered trafficking of the WT protein. To achieve this, we transfected HeLa cells with pCDNA3 GlialCAM (WT or containing an MLC2 mutation)-E2A-flag-tagged WT GlialCAM, which allowed the stoichiometric expression of untagged WT/mutant GlialCAM and flag-tagged WT (Fig. 1F, inset). We also co-transfected with MLC1 in order to maximize the cells containing GlialCAM at cell–cell junctions, as previously described (15). We then evaluated the percentage of cells where the flag tagged GlialCAM protein was located at cell–cell junctions by immunofluorescence experiments. These experiments indicated that GlialCAM containing an MLC2A mutation (p.R92Q) did not influence the localization at cell–cell junctions of the flag-tagged WT GlialCAM, whereas GlialCAM containing two different types of MLC2B mutations (p.R92W and p.D128N) reduced the localization of flag-tagged GlialCAM at cell–cell junctions (Fig. 1F). Thus, this newly developed assay was suitable to elucidate whether a GlialCAM mutant was affecting in a dominant manner, the junctional trafficking of the WT protein.

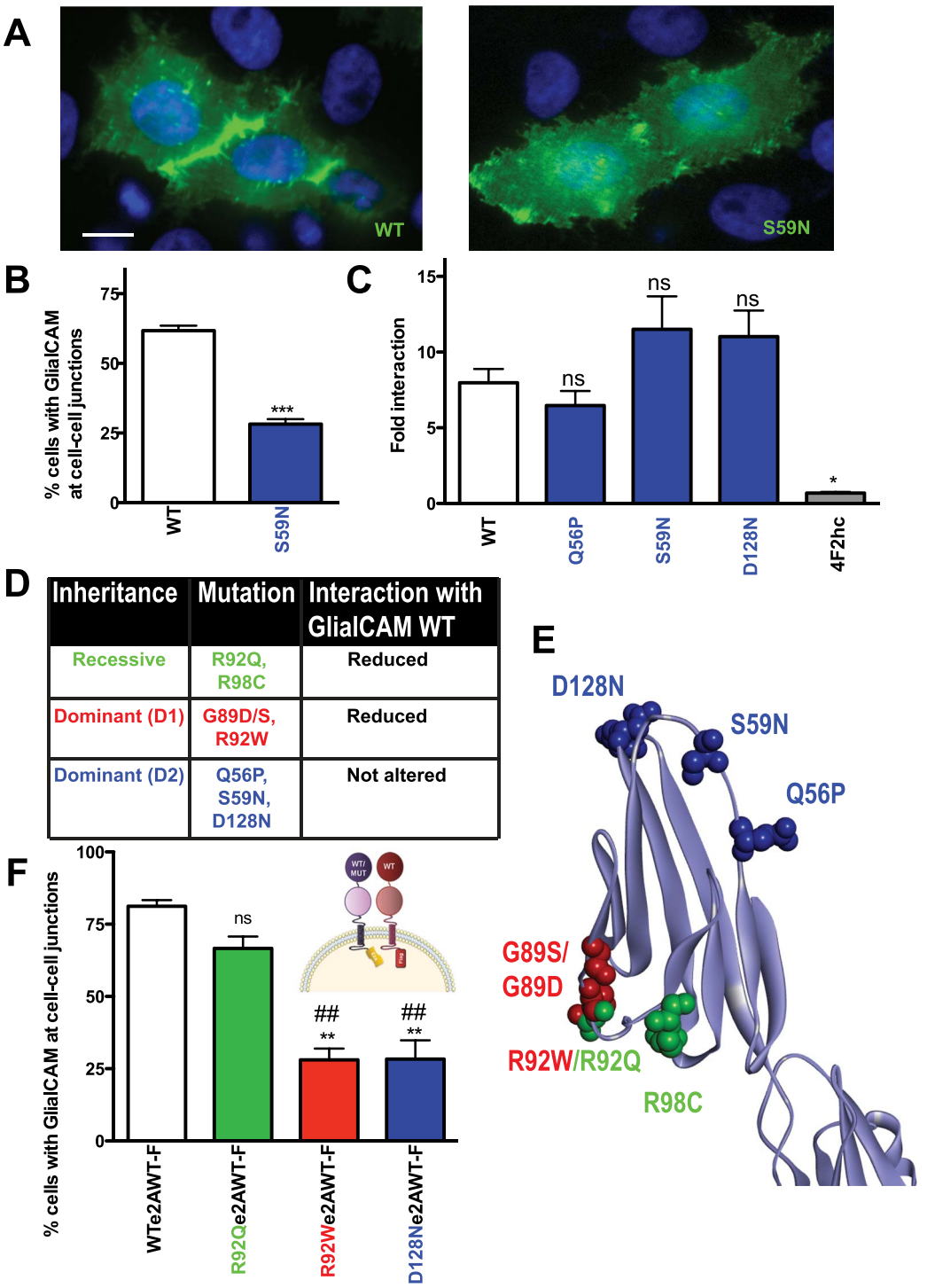

Figure 1. Dominant and recessive MLC2 mutations in *GLIALCAM*. (**A**) Subcellular localization of flag-tagged WT or S59N GlialCAM at cell–cell junctions. Scale bar: 20 µm. (**B**) Quantification of WT and S59N GlialCAM at cell–cell junctions. ***$P < 0.001$ when compared with the WT in paired *t*-student test. Graphics represent mean ± SEM. (**C**) Split-TEV assays of GlialCAM WT interaction with different GlialCAM dominant mutants Q56P, S59N and D128N. Protein 4F2 is used as a negative control of protein interaction. Graphics represent mean ± SEM. ns = non significative, *$P < 0.05$ when compared with GlialCAM WT-WT interaction in Bonferroni multiple comparison's test of five different experiments. (**D**) Classification of GlialCAM IgV mutants according to inheritance (dominant or recessive) and the results of a biochemical assay that measures the level of interaction of the mutants with GlialCAM WT. Mutants are coloured according to this classification. Recessive mutants are coloured in green, dominant mutants (D1) that show a reduced oligomerization in red, and dominant mutants (D2) with a normal oligomerization in blue. (**E**) Three-dimensional homology model of the IgV domain of GlialCAM, with the position of the mutations highlighted. (**F**) Quantification of the percentage of GlialCAM WT cell–cell junction targeting when co-expressed with the GlialCAM WT (130 pair of cells counted) recessive mutant p.R92Q (115 pair of cells) dominant p.R92W (128 pair of cells) or dominant p.D128N (119 pair of cells). Graphics represent mean ± SEM. ns = non-significant, **$P < 0.01$ when compared with co-expression with the WT, ## $P < 0.01$ when comparing dominant mutants with recessive mutant p.R92Q with Bonferroni multiple comparison's test of four different experiments. The inset is a schematic representation of the dominance assay performed, where different GlialCAM proteins (WT or mutant) are co-expressed with flag (F)-tagged GlialCAM WT is achieved by the fusion of both proteins through an E2A peptide.

Characterization of a newly developed nanobody that blocks GlialCAM targeting at cell junctions

As indicated in previous studies (9,13), GlialCAM may form homophilic interactions *in cis* (within the same cell) and homophilic interactions *in trans* (with the neighbouring cell) in order to localize at cell–cell junctions. With the aim of getting information about the regions of the GlialCAM molecule that may be important in mediating *trans* interactions, we developed nanobodies recognizing the extracellular side of GlialCAM. Interestingly, the application of one of the developed nanobodies (Nb 139G1) to cells expressing GlialCAM-VFP blocked the localization of GlialCAM at cell–cell junctions in a concentration-dependent manner (Fig. 2A). In contrast, the application of a control nanobody detecting an unrelated protein at the maximal concentration used did not inhibit GlialCAM localization at cell–cell junctions.

To find which regions of the extracellular domain of GlialCAM were recognized by the nanobody, we expressed GlialCAM with deletions in the IgC2 or in the IgV domain and used flow-cytometry to detect the expressed protein. To normalize for expressed protein at the plasma membrane, we used a monoclonal antibody that detects extracellular GlialCAM. Previous immunofluorescence experiments indicated that both mutant forms (lacking either IgV or IgC2 domain) are expressed at the plasma membrane (13). Deleting the IgC2 reduced partially the binding of the monoclonal and the nanobody (Fig. 2B). In clear contrast, deletion of the IgV domain abolished completely the binding of both antibodies, suggesting that both antibodies mainly bind to the IgV domain (Fig. 2B).

We then tested whether MLC2 GlialCAM mutants affect the binding of the nanobody using flow cytometry. We monitored the binding of the monoclonal antibody as a control of surface expression, which was similar for all our mutants of interest (Fig. 2C for p.Q56P). Interestingly, we observed differences in the binding of the nanobody between the different mutations. We represented the mutants and the effect on nanobody binding in the model of GlialCAM monomer (Fig. 2E). Some mutants, such as p.G89D and p.R98C, decreased binding (Fig. 2D and E). On the other hand, other mutants such as p.R92Q and p.R92W increased binding (Fig. 2D and E). Importantly, mutant p.Q56P was the only that showed completely abolished binding of the nanobody (Fig. 2C–E).

Investigating D2 MLC2B mutants reveal a mechanism of dominance

From our previous results using a nanobody that blocked GlialCAM junctional targeting possibly by inhibiting *trans* interactions, we hypothesized that the region close to residue Q56 may be involved in the formation of these *trans* interactions. Accordingly, we reasoned that mutations p.Q56P, p.S59N and p.D128N, which are all very close in space and are all D2 dominant mutants, may affect specifically *trans* interactions. The replacement of a glutamine by a proline may introduce a kink in the beta-strand. Nonetheless, how mutations p.S59N and p.D128N may affect the structure was unclear.

In western blot experiments, we realized that mutants p.S59N and p.D128N showed a higher motility in SDS gels than the WT protein (Fig. 3A). Analyzing the amino acid protein sequence around the mutation, we noticed that in both cases, the mutations putatively introduced new N-glycosylation sites (Fig. 3B). To prove that this was the case, we compared the motility of GlialCAM WT and these mutants after treatment with Endo Glycosidase-F (Endo-F), which removes all N-glycosylation sites (Fig. 3C). The motility of the mutants in SDS after treatment with Endo-F was equal to the motility of the WT protein, indicating that the mutants in fact introduced a new N-glycosylation site. Thus, we speculate that the new glycosylations created by these mutations might affect specifically *trans* interactions within GlialCAM proteins.

After careful analysis of homologous structures, we identified a possible template for *trans* interactions, between the domains 2 and 3 of contactin (PDB 3JXA) (17). This protein has the highest sequence identity with the GlialCAM extracellular domain (30% SI) (Fig. 3D). Therefore, we built a *trans* dimer by superimposing two copies of the GlialCAM monomer model on contactin domains 2 and 3. In this model, the three mutations studied here mapped to the same interface (Fig. 3E). We therefore conclude that D2 mutations are dominant because they specifically disrupt *trans* interactions between opposed molecules, without interfering with GlialCAM homooligomerization in the same cell.

Experiments toward the development of a structural model of GlialCAM dimers

We further aimed to clarify the molecular basis for the dominance of D1 mutants. As happens in other diseases caused by mutations with both recessive and dominant behaviours (18), we reasoned that the dominant mutations might affect specifically protein contact interfaces of the GlialCAM molecule. As previous studies reported a *cis* dimer orientation that was quite conserved in other members of the CAM family (e.g. nectin-1-EC, CAR) (19), we explored whether GlialCAM could adopt the same *cis* dimeric orientation by superimposing two copies of the monomer model on the corresponding subunits of the CAR dimer.

We first aimed to demonstrate using experimental evidence that the resulting template-based *cis* model may be correct. The model suggested the existence of intermolecular interactions between the pair of residues D129-R92 and R64-E86 (Fig. 4A). We performed directed mutagenesis of these residues to change them to cysteines and expressed in HeLa cells alone or together with the predicted corresponding pair, and the presence of GlialCAM dimers was evaluated by western blot in non-reducing conditions.

Unexpectedly (Fig. 4B), the mutants E86C and R92C formed dimers when expressed alone, independently of the co-expression with the predicted pair. Thus, the cysteine cross-linking experiments invalidated this first structural model based on homology modelling.

As the cross-linking experiments suggested that the glutamate 86 (E86) of one GlialCAM monomer was predicted to be close to the glutamate 86 of the other monomer, we reasoned that other closer residues containing a positive charge might form a positive–negative pair. A closer inspection of the template-based model showed lysine 68 (K68) of one monomer in the vicinity of glutamate 86 (E86) of the other monomer (Fig. 4C), which could be even closer after a small re-arrangement of the dimeric interface. In agreement with the hypothesis that E86 is being stabilized by K68, mutating E86 to arginine (p.E86R) abolished GlialCAM protein expression (Fig. 4D), and its expression was recovered by mutating additionally K68 to glutamate (p.K68E) (Fig. 4D). In contrast, expression was not abolished in the protein containing only the mutation K68E (Fig. 4D) and both mutants (i.e. p.K68E and p.K68E-E86R) showed a defective targeting to cell–cell junctions (Supplementary Material, Fig. S1),

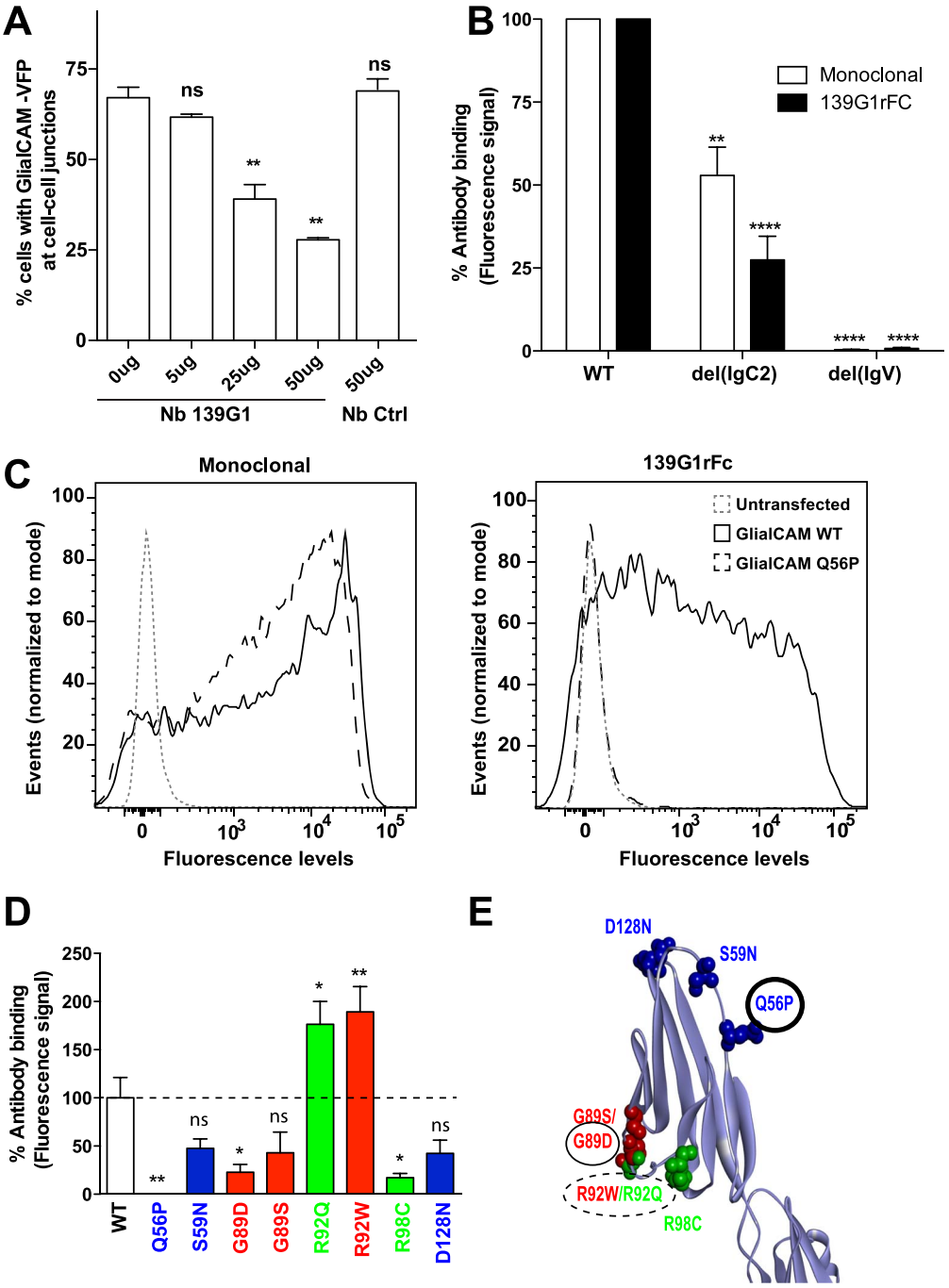

Figure 2. Characterization of a nanobody that blocks GlialCAM localization at cell–cell junctions. (**A**) HeLa cells were transfected with VFP-tagged GlialCAM WT construct and treated with different doses of 139G1 Nb (5, 25 and 50 µg); 181 Nb was used as a negative control. Quantification of the percentage of cells with GlialCAM at cell–cell junctions without Nb was 67.1 ± 2.86% (110 cells), with 5 µg of Nb was 61.7 ± 0.84% (122 cells), 25 µg of Nb was 39.2 ± 4.4% (117 cells), 50 µg of Nb was 27.8 ± 0.5% (111 cells) and 50 µg of Nb control was 68.1 ± 3.4% (104 cells). Graphics represent mean ± SEM. ** $P < 0.01$ in ANOVA Bonferroni multiple comparison test against WT. Data from two independent transfections. (**B**) Quantification of the percentage of antibody binding in HEK293T cells transfected with GlialCAM WT, IgC2 deletion of GlialCAM and IgV deletion of GlialCAM using a flow cytometry assay. Deletions of IgV and IgC2 were performed by PCR resulting in the aminoacid sequence '..TSPVPISRPQV..' for del(IgV) and '..TTVLQGRSLPV..' for del(IgC2). Percentage of antibody binding against del (IgC2) and del (IgV) was normalized with the antibody binding against WT. The mean percentatge of monoclonal antibody (white) against del (IgC2) was 52.8 ± 8.6% ($n = 4$) and against del (IgV) was 0.42 ± 0.07% ($n = 4$). The mean percentage of 139G1 Mb (black) against del (IgC2) was 27.46 ± 7.1% ($n = 4$) and against del (IgV) was 0.74 ± 0.3% ($n = 4$). Graphics represent mean ± SEM. ** $P < 0.01$ ****$P < 0.0001$ in ANOVA Bonferroni multiple comparison test. (**C**) Representative flow cytometry experiments showing the binding of the monoclonal antibody (left) and the 139G1 monobody (right) in untransfected HEK293T cells and cells transfected with WT and p.Q56P GlialCAM. (**D**) Quantification of 139G1 Mb binding by flow cytometry assay in HEK293T cells transfected with different GlialCAM IgV mutants. All the signal of the nanobody for the different GlialCAM IgV mutants were divided by the signal of the monoclonal antibody and normalized with the 139G1 Mb binding against GlialCAM WT. The mean percentage of antibody binding for each mutant was the following: p.Q56P was 0.7 ± 0.4% ($n = 5$); p.S59 N was 47.5 ± 9.9% ($n = 5$); p.G89D was 22.9 ± 8.1% ($n = 4$); p.G89S was 43.1 ± 21.4% ($n = 4$); p.R92Q was 176.3 ± 23.9% ($n = 4$); p.R92W was 189.3 ± 26.3% ($n = 4$); p.R98C was 17.1 ± 4.5% ($n = 3$) and p.D128N was 42.3 ± 13.8% ($n = 5$). Graphics represent mean ± SEM. ns = non-significant; *$P < 0.05$; **$P < 0.01$ in ANOVA Bonferroni multiple comparison test.

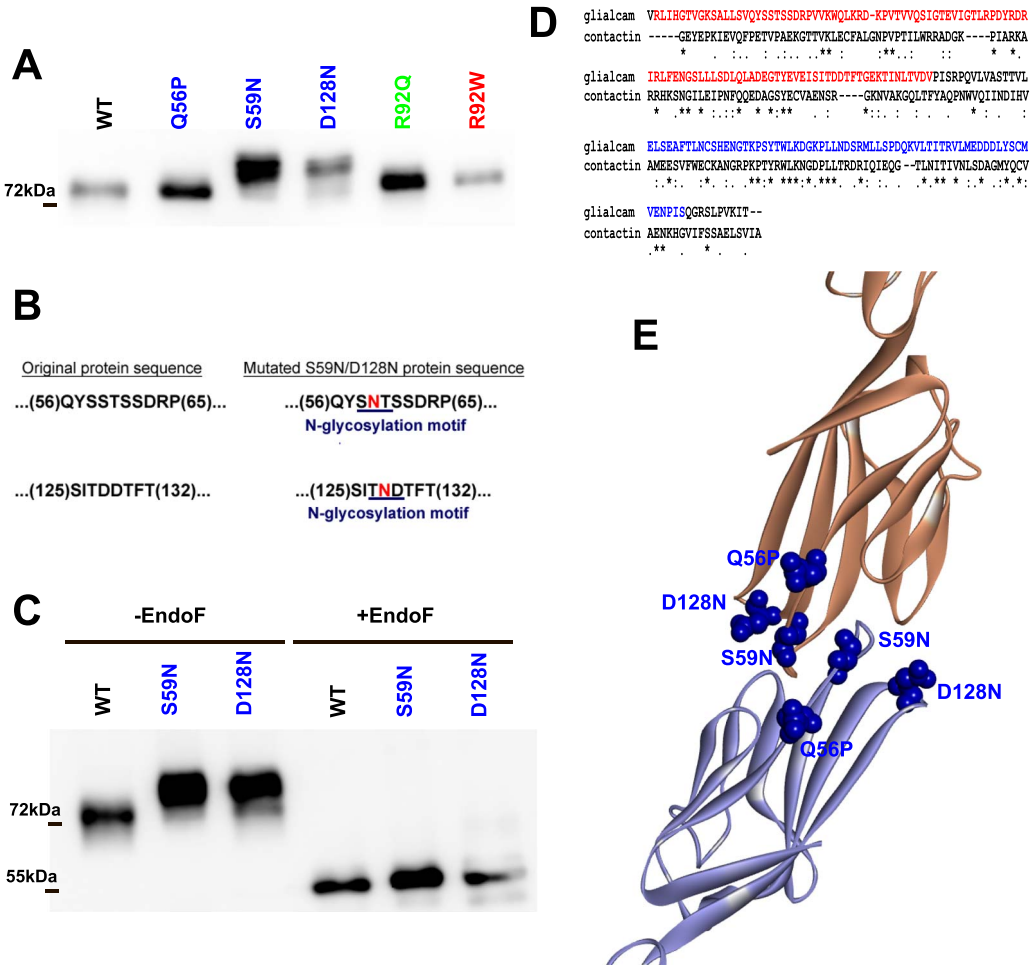

Figure 3. Dominant mutants p.S59N and p.D128N introduce new glycosylation sites in GlialCAM. (**A**) Western blot of transfected cells with flag-tagged GlialCAM WT or carrying dominant or recessive mutations was performed with an antibody detecting the flag epitope. Dominant mutants p.S59N and p.D128N present an increased molecular weight. Another independent experiment gave the same results. (**B**) Predicted *N*-glycosylation motifs that appear in the GlialCAM amino acid sequence due to the p.D128N or the p.S59N dominant mutations. (**C**) Western-blot assay of transfected cells with WT, p.S59N or p.D128N GlialCAM plasmids in control conditions (left) or treated with Endoglycosidase-F (Endo-F) (right) that removes all asparagine-linked mannoses. Treatment with Endo-F results in all GlialCAM constructs presenting the same molecular weight around 50 kDa. Two additional experiments gave the same results. (**D**) Alignment between the Ig domains of contactin and GlialCAM. The IgV domain of GlialCAM is coloured in red and the IgC2 domain in blue. (**E**) Homology model generated to explain the *trans* interaction between the IgV domain of two GlialCAM molecules with key dominant mutants p.Q56P, p.S59N and p.D128N highlighted in blue.

suggesting that E86 may form additional interactions with other residues.

Development of a new structural model of GlialCAM dimerization

Since mutational data and cross-linking experiments did not support the template-based dimer model, we decided to model the *cis* dimer by docking, using the monomer model as input (see Materials and Methods). We selected only docking orientations in which E86 residues from both molecules were within 8 Å distance. From the resulting docking models, the one with the closest E86-K68 distance (6.3 Å) was consistent with all the above mutational data and cross-linking experiments. The new model suggested a large interface formed by the surfaces of the same opposing beta-strands of the IgV domains of two GlialCAM molecules (Fig. 5A, dotted-rectangle in yellow). The interacting segment was formed by residues ranging from Glutamate 86 (E86, in the top) to Arginine 92 (R92, in the bottom) of each GlialCAM molecule (Fig. 5A). To test if this segment (beta strand) from each GlialCAM monomer was interacting in the dimer, we generated new cysteine mutants from the residues of this strand (Isoleucine 88 (I88), Threonine 90 (T90), Leucine 91 (L91)). As a control, we generated the cysteine mutant of Glutamine 81 (Q81), which is also very close, but it is not predicted to be interacting. After expressing these mutants in HeLa cells, we analyzed the formation of GlialCAM dimers by western blot (Fig. 5B). We observed the dimer formation between the pairs of residues E86, I88, T90, L91 and R92, but not with Q81. Treating the extracts with reducing agents (DTT) disrupted the dimers, further confirming that dimers of the cysteine mutants were formed by disulphide bonds (Fig. 5B). In summary, these experiments indicated that the residues from positions 86 to 92 form a specific GlialCAM–GlialCAM interacting segment.

As an additional test that this segment was interacting, we reasoned that introducing a glycosylation site in that segment might work as a dominant mutation. Mutation I88N (Fig. 5C), which increased the motility of GlialCAM because it introduces a new glycosylation (Fig. 5C, inset), caused a dramatic reduction of GlialCAM WT targeting to cell junctions (Fig. 5D). As a control,

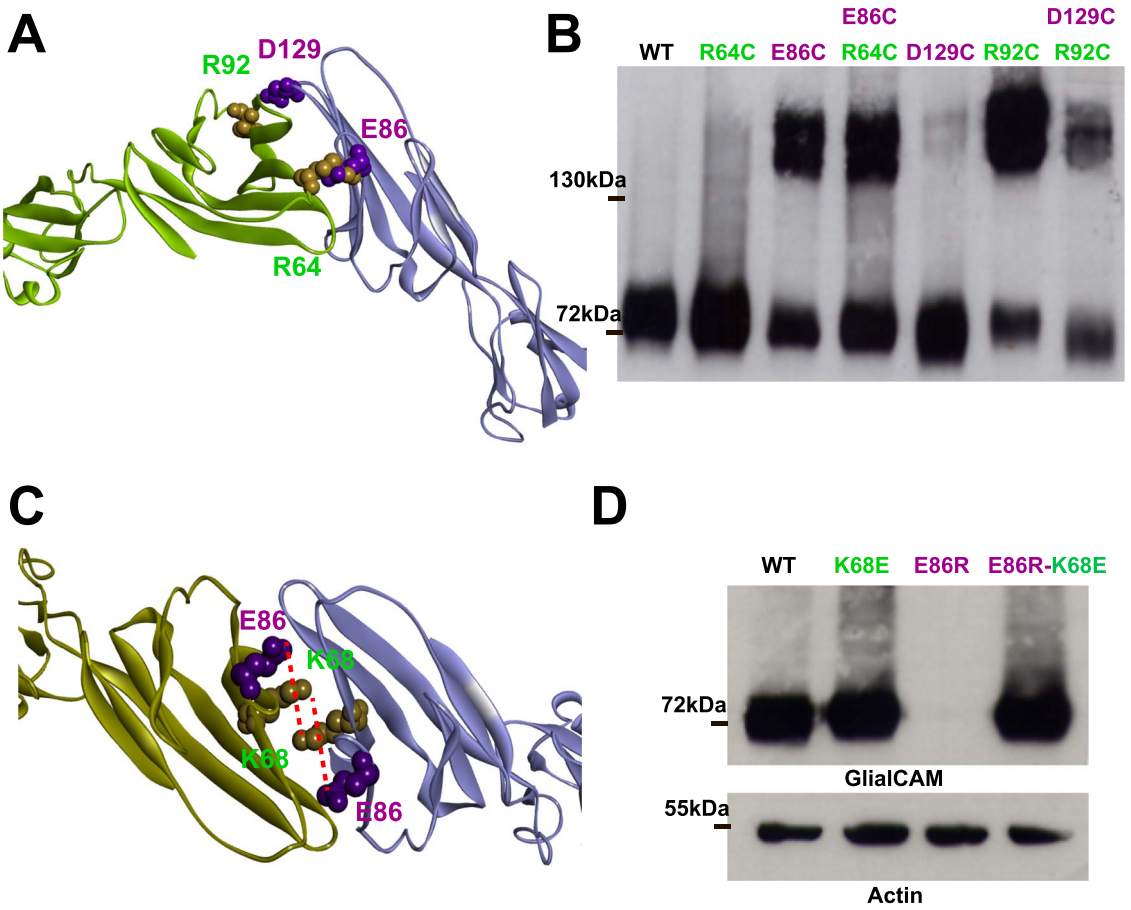

Figure 4. Development and biochemical testing of a structural domain of GlialCAM *cis*-homooligomerization. (**A**) Three-dimensional model of GlialCAM generated by homology modelling using another IgCAM molecule as a template. Possible pairs of interacting residues R64-E86 and R92-D129 are highlighted in orange/purple colours. (**B**) Western blot of GlialCAM WT or mutants changed to Cysteine R64C, E86C, D129C and R92C expressed alone or co-transfected in pairs (R64C + E86C and D129C + R92C) performed to observe Cysteine cross-linked dimerization between the two-paired mutants. Mutants E86C and R92C alone show dimerization, as observed at the 140 kDa band. Representative western blot from three independent experiments. (**C**) Structural representation of the negatively charged residue E86 in the IgV dimer interface. Structural analysis revealed the positively charged residue K68 in the vicinity of E86, which could be even closer after a small interface rearrangement. (**D**) Western blot of transiently transfected cells with GlialCAM WT, K68E mutant, E86R mutant or GlialCAM carrying both aminoacid changes K68E and E86R. While E86R is not expressed, double mutant E86R + K68R protein levels are recovered and similar to protein levels of GlialCAM WT. Data shown are from a representative experiment, out of three independent ones. Actin was used as a loading control.

mutation P76N (Fig. 5C), which also introduces a glycosylation site, reduced only slightly the targeting of GlialCAM WT to cell junctions (Fig. 5D).

Additional characterization of cysteine mutants in the interacting segment provide new keys to differentiate dominant and recessive mutants

We additionally assessed if these cysteine mutants from the GlialCAM interacting segment showed a defect in the targeting to cell–cell junctions (Fig. 6A). Unexpectedly, compared with GlialCAM WT expressed alone, mutant E86C showed an increased targeting to cell–cell junctions, reaching the same values of the co-expression of GlialCAM plus MLC1 (Fig. 6A) (15). In contrast, all the other cysteine mutants (I88C, T90C, R91C and R92C) showed a defect in the targeting to cell–cell junctions.

Given these results, we reasoned that mutation E86C might stabilize the GlialCAM dimer in a more stable conformation, which will result in an increased targeting of the mutant to cell–cell junctions. Then, we decided to explore whether the introduction of the mutation E86C might reverse the trafficking defect caused by recessive or dominant mutations. It was found (Fig. 6B) that the E86C mutation rescued almost completely the trafficking defect caused by the recessive mutation p.R92Q, while it did not increase the targeting of dominant mutants (D1 (p.R92W) and D2 (p.S59N)) to cell junctions (Fig. 6B).

Analyzing the structural mechanism of dominance of some MLC2B mutations

From all *GLIALCAM* mutations identified in MLC2B patients, those affecting their interaction with GlialCAM (i.e p.G89S/D, p.R92W) are found in the identified *cis*-dimerization interacting segment. In contrast, all the MLC2A mutations except p.R92Q are found outside of this segment (p.K68M, p.R98C, p.T132N), suggesting that mutations located in this specific segment will be dominant. To understand the behaviour of the residue R92, we constructed several mutants of this residue to different amino acids, co-expressed them with GlialCAM WT (Fig. 7A) and analyzed whether they behave in a dominant or recessive manner regarding the targeting of GlialCAM WT. Mutation of R92 to the small amino acid alanine (A) did not result in a significant dom-

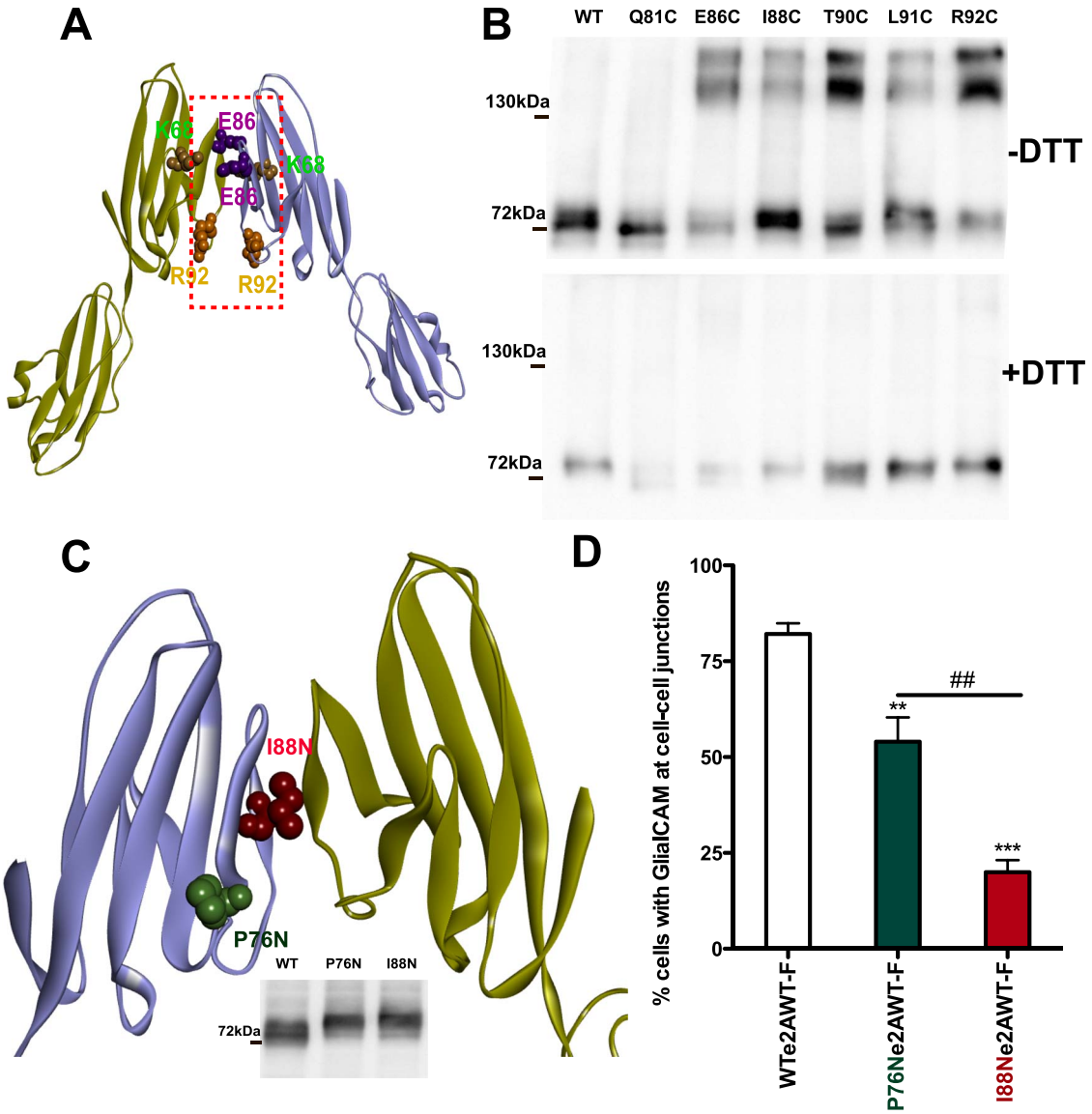

Figure 5. Three-dimensional model of GlialCAM homo-dimerization based on docking. (**A**) Structural representation of the new structural model of GlialCAM dimer based on docking analysis after applying several constraints based on the results from biochemical studies. The interacting surface between the two IgV domains is highlighted in yellow (left). Residues E86 and R92 are paired in close proximity and residue K68 is also highlighted. (**B**) Western-blot assay of cysteine cross-link in the absence or in the presence of 100 mM DTT between the following residues mutated to cysteine: Q81C, E86C, I88C, T90C, L91C and R92C. GlialCAM WT is used as a negative control. Dimers are observed on the mutants E86C, I88C, T90C, L91C and R92C at 140 kDa. Representative western-blot of three independent experiments. (**C**) Scheme of the IgV interaction showing the position of the introduction of two different glycosylation sites, I88N in the interacting segment and P76N as a control. The inset shows a western blot of transfected cells with flag-tagged GlialCAM WT or carrying the introduced glycosylation sites detected with an antibody detecting the flag epitope. Both P76N and I88N present an increased molecular weight. Another experiment gave the same results. (**D**) Biochemical dominance assay of GlialCAM WT targeting to cell–cell junctions co-expressed with different glycosylation mutants. Quantification of flag-tagged GlialCAM at cell–cell junctions (right) when co-expressed in E2A constructs with GlialCAM WT (232 cells), mutant P76N (174 cells) and mutant I88N (176 cells). Graphics represent mean ± SEM. $^{**}P < 0.01$, $^{***}P < 0.001$ when compared with co-expression with the WT. In addition, we also compared with the mutant P76N, to distinguish better between recessive and dominant effects. $^{\#\#}P < 0.01$ when comparing I88N with mutant P76N in Bonferroni multiple comparison's test of three–four different experiments.

inant effect, whereas mutation to tryptophan (W) or tyrosine (Y) was dominant (Fig. 7A). Interestingly, mutants R92 to aspartate (D) or cysteine (C) were also dominant (Fig. 7A). We hypothesized that the dominant mutants of this residue may have the ability to form novel interactions around this region, maybe distorting the native dimer orientation.

By inspecting in the new dimer model residues near to the position of R92 in the other monomer, we found R96 (Fig. 7B). To test the putative interaction of R92 mutants with R96, we focused on the mutant R92D and then constructed the single mutant R96D and the double mutant R92D/R96D and assayed its localization at cell–cell junctions (Fig. 7C). Both R92D and R96D mutants showed a defective targeting to cell–cell junctions (Fig. 7C). In contrast, the double mutant R92D-R96D was targeted to cell junctions as the WT protein.

In summary, our results suggest that there is an interaction segment between residues E86 (located on the top of the beta strand) and R92 (found in the bottom) (Fig. 7D). Although residues E86 from each dimer are close, they are stabilized by its interaction with K68. In the bottom edge, opposed residues

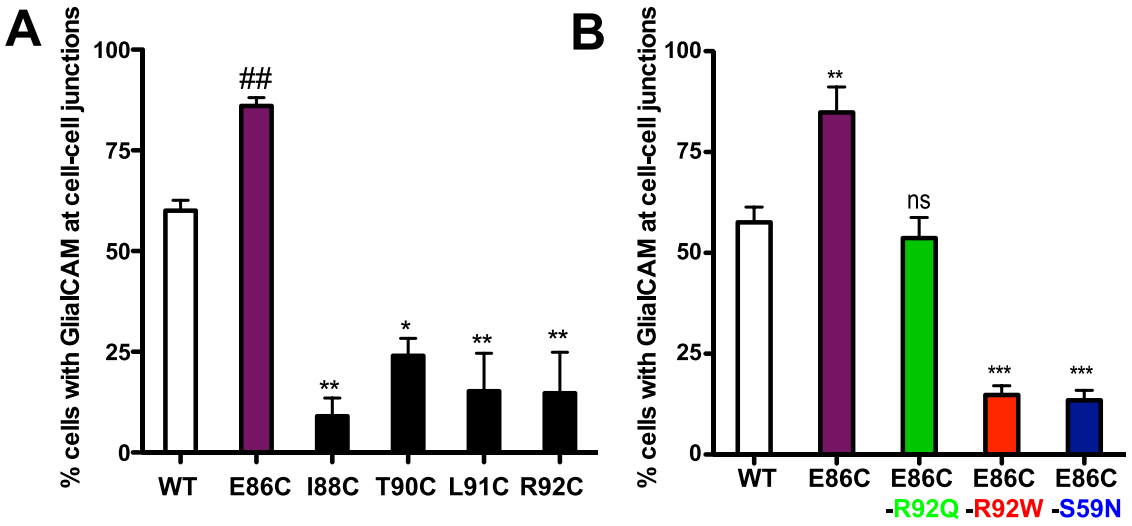

Figure 6. Characterization of the trafficking to cell junctions of GlialCAM cysteine mutants in the interacting segment. (**A**) Percentage at cell–cell junctions of GlialCAM E86C (230 cells) I88C (177 cells) T90C 185 cells) L91C (123 cells) and R92C (91 cells) compared with GlialCAM WT (198 cells). Graphics represent mean ± SEM. $^{*}P < 0.05$, $^{**}P < 0.01$ in Bonferroni multiple comparison test versus WT of three independent experiments. $^{\#\#}P < 0.01$ in T-student test compared with WT in data from four independent experiments. (**B**) Quantification of percentage of cells with GlialCAM in cell junctions for WT (101 cells) E86C (94 cells), E86C-p.R92Q (356 cells), E86C-p.R92W (137 cells) and E86C-p.S59N (147 cells). Graphics represent mean ± SEM. $^{**}P < 0.01$ and $^{***}P < 0.001$ in Bonferroni multiple comparison test, compared with WT. Data from three independent experiments.

R92 may be slightly separated through electrostatic repulsion with R96 (Fig. 7D). The mutation of R92 by charged aspartate can introduce favourable salt bridge with R96 of the other monomer, bringing to a close vicinity this bottom region that in principle was slightly separated in the native protein. Similarly, the introduction of aromatic residues (tryptophan or tyrosine) could introduce novel cation-pi interactions with R96, producing similar effect. The dominant effect of R92C might also be explained by the formation of dipole–dipole interactions or by a disulphide bridge, suggesting that GlialCAM may form oligomers of dimers by lateral interactions (see Discussion). Thus, we speculate that residues in this segment that create aberrant neo-interactions, which might be inducing a different dimer orientation, may be dominant.

Discussion

Our aim was to understand why missense mutations from the first Ig domain (IgV), which are found in MLC2 patients, differentially behave as dominant or recessive. The study of most MLC2B missense dominant mutations that have a trafficking defect has revealed that they can be classified in two groups taking into account regarding whether they display or not a reduced ability to interact with the WT protein. Locating both types of MLC2B mutations in a structural model of the extracellular domain of GlialCAM protein developed in the present work, which takes into account homologous structures, docking energetics and biochemical experiments (Fig. 8), suggested that both types of MLC2B mutations affect GlialCAM-GlialCAM interacting interfaces. In one case (D1), they may affect to interactions involved in GlialCAM–GlialCAM *cis* interfaces, whereas for the other group of mutants (D2), they allegedly affect interactions involved in GlialCAM–GlialCAM *trans* contacts. As it has been shown in other IgCAM molecules (20,21), GlialCAM dimers may be formed first in the endoplasmic reticulum through *cis* mediated interactions that then will travel to the plasma membrane where *trans* interactions may occur. We suggest that MLC2B mutants that showed normal ability to interact with GlialCAM WT may disrupt specifically GlialCAM–GlialCAM *trans* mediated interactions, for instance as in the case of the mutants p.S59N and p.D128N, by creating a new glycosylation site in the mentioned *trans* interaction surface. Possibly, mutant p.Q56P may also disrupt this interaction surface, as proline has a restricted degree of freedom.

Furthermore, GlialCAM is also able to form heterophilic *cis* interactions with MLC1 or ClC-2. It has been previously shown that, although GlialCAM alone reach cell–cell junctions, co-expression with MLC1 increases the percentage of GlialCAM present at cell–cell junctions. Here, we have found a mutant, E86C that also improves the ability of GlialCAM to reach cell–cell junctions. Based on these studies, we suggest that MLC1 may stabilize GlialCAM at cell–cell junctions by changing the conformation of GlialCAM to a similar configuration as the one caused by the mutation E86C.

We analyzed whether mutation E86C could stabilize MLC2A and MLC2B mutants. As the MLC2B p.S59N mutant was not rescued by E86C, we suggest that mutants E86C and p.S59N influence GlialCAM stability by different mechanisms. Contrarily, the double mutant containing E86C and the MLC2A recessive mutation p.R92Q showed a normal targeting to cell–cell junctions, but the double mutant E86C-R92W failed to reach cell–cell junctions. We believe that the MLC2B mutant p.R92W may destabilize *cis* interactions in a different manner than the MLC2A mutant p.R92Q, probably by creating novel interactions, as our experiments with the double mutant R92D-R96D suggest. MLC2B mutant p.R92W may also form novel cation-pi interactions with the residue R96. Thus, we conclude that MLC2B mutants affecting GlialCAM homooligomerization may affect the interacting segment by disrupting extensively the normal pattern of interactions in this segment, as for example, by creating new interactions or by affecting several interactions simultaneously. Using this model, for instance, we could explain why the recently identified p.R92P mutation in MLC2B Chinese patients (22) may

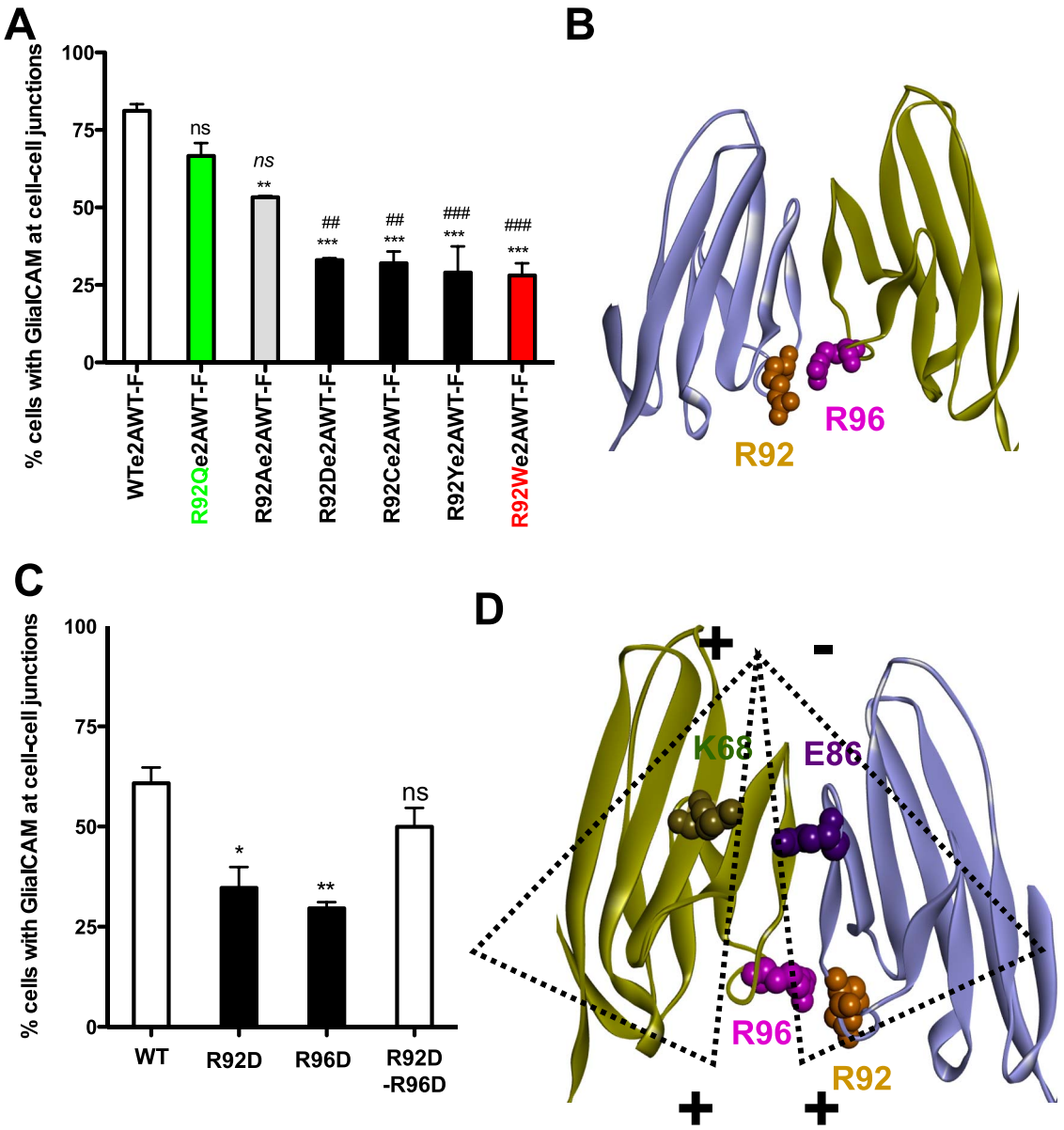

Figure 7. Structural clues on the difference between dominant and recessive mutants at the CIS interacting surface. (**A**) Biochemical dominance assay of GlialCAM WT targeting to cell–cell junctions co-expressed with different R92 mutants (left). Quantification of flag-tagged GlialCAM at cell–cell junctions (right) when co-expressed in E2A constructs with GlialCAM WT (130 cells), mutant p.R92Q (115 cells) R92A (94 cells), R92Y (115 cells), R92D (127 cells), R92C (114 cells) and p.R92W (128 cells). Graphics represent mean ± SEM. ns = no statistical differences, $^{**}P < 0.01$, $^{***}P < 0.001$ when compared with co-expression with the WT. In addition, we also compared with the mutant p.R92Q, to distinguish better between recessive and dominant mutations. ns = no statistical differences, $^{\#\#}P < 0.01$, $^{\#\#\#}P < 0.001$ when comparing with mutant R92Q in Bonferroni multiple comparison's test of three–four different experiments. (**B**) Structural representation of the interaction between two IgV domains in CIS, with focus on the possible interactions between the residue R92 and the residue R96. (**C**) Immunofluorescence of flag-tagged WT and GlialCAM mutants R92D, R96D or double mutant R92D-R96D, where localization at cell–cell junctions is compared with the WT protein. Quantification of percentage of cell–cell junctions in WT (235 cells), R92D (240 cells), R96D (293 cells) or R92D + R96D (278 cells). Graphics represent mean ± SEM. $^{*}P < 0.05$ and $^{**}P < 0.01$, ns = no statistical differences, in Bonferroni multiple comparison test, compared with WT. Data from three independent experiments. (**D**) A proposed model of GlialCAM IgV dimerization indicates that dimer is stabilized both by attracting charges at the top of the IgV interacting segment and by repulsive charges at the bottom.

be also dominant. We also hypothesized that the MLC2B mutants p.G89S and p.G89D may also form new interactions through new hydrogen bonds or by electrostatic effects.

As previous studies have revealed (13), efficient targeting of GlialCAM to cell–cell junctions may require multiple interactions of GlialCAM with GlialCAM forming a GlialCAM dimer in the same or in the opposite cell, but also with the cytoskeleton through the C terminus, and with MLC1 or ClC-2 through unknown interacting surfaces. Moreover, recent work has shown that GlialCAM, MLC1 and ClC-2 may form a ternary complex (23). Considering the volume of the ClC-1 channel (homologous to ClC-2) (24), in the GlialCAM dimer, there is only space for ClC-2, but not for MLC1. Thus, we suggest that GlialCAM dimers may also form lateral interactions with other GlialCAM dimers accommodating ClC-2 or MLC1 within a dimer. The presence of multiple GlialCAM dimers could explain how mutation R92C may be dominant, as the possible formation of a disulphide bridge in one of these different dimers containing two GlialCAM

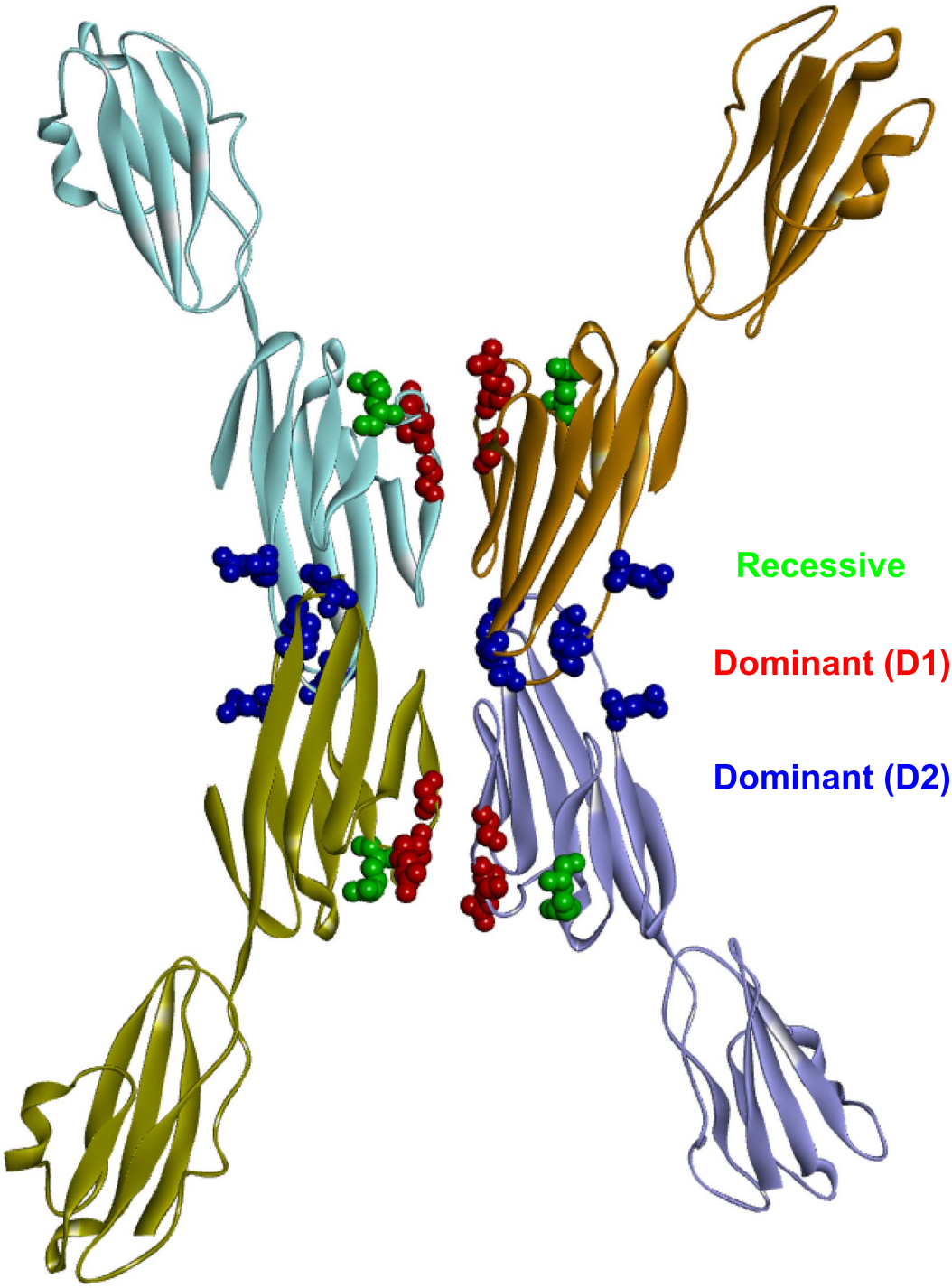

Figure 8. Summary of the structural model proposed for GlialCAM homodimers forming *cis* and *trans* interaction through different surfaces of its IgV domain. *Cis* dimerization is achieved by interactions between two opposing beta-strands of the IgV domain and *trans* interactions occurr between salient loops of both IgV domains. Residues mutated in MLC2A patients (recessive) are shown in green, D1 residues mutated in MLC2B patients are shown in red and D2 residues mutated in MLC2B patients are shown in blue. The classification of D1 and D2 mutants has been explained previously.

molecules with R92 mutated to cysteine may destabilize the overall oligomeric organization at the cell junction. It has been shown that other IgCAM molecules similar to GlialCAM have the ability to form lateral interactions that are also important for clustering through IgC2 domains (20). Therefore, maybe some mutations found in MLC2 patients in the IgC2 domain may affect GlialCAM–GlialCAM lateral interactions.

To conclude, our structural model (Fig. 8) of GlialCAM–GlialCAM dimers mediating *cis* and *trans* interactions could be used to predict the behaviour of new MLC2 mutants (22). For instance, the recently identified MLC2A mutation p.T132N is not found in an interacting surface of GlialCAM, so it may be recessive. The other new mutant identified, p.K68M, may destabilize GlialCAM–GlialCAM interaction by affecting its

electrostatic interaction with E86. Since it is not creating a new interaction, we propose it may also be recessive. In summary, this work provides new insights into the molecular basis of *GLIALCAM* mutations. We believe that this knowledge will be important to help developing therapeutic strategies for MLC patients with *GLIALCAM* mutations.

Materials and Methods

Molecular biology

Plasmids were constructed using standard molecular biology techniques employing recombinant PCR and the Multisite Gateway System (Invitrogen, Carlsbad, CA, USA). For localization studies, all GlialCAM constructs were flag tagged at their C-terminus (three flag copies) and cloned into the pCDNA3 vector. Flag tagged WT GlialCAM was co-expressed with different GlialCAM mutants by generating constructs where both cDNAs were linked to the self-cleavable 2A peptide (E2A). The sequence of the E2A peptide was: *Gly-Ser-Gly-Glu-Gly-Arg-Gly-Ser-Leu-Leu-Thr-Cys-Gly-Asp-Val-Glu-Glu-Asn-Pro-Gly*. The integrity of all cloned constructs was confirmed by sequencing. All cDNAs are from human origin. In the results section, mutations found in patients are mentioned using the genetic nomenclature (for instance p.R92W), whereas other mutants simply describe the mutation (for instance E86C).

Cell transfection

HeLa cells were grown in Dublecco's modified Eagle's medium containing (v/v) 10% foetal bovine serum (FBS, Sigma, St Louis, MO, USA) 1% glutamine and 1% penicillin/streptomycin at 37°C in a humidity controlled incubator with 5% CO_2. Cells were transiently transfected with Transfectin Lipid Reagent (Bio-Rad, Madrid, Spain) following the manufacturer's instructions (https://www.bio-rad.com/webroot/web/pdf/lsr/literature/4106254A.pdf). Experiments were performed 48–72 h after cell transfection. To assay whether a mutant was acting in a dominant manner, cells were co-transfected with GlialCAM WT (or mutant)-E2A- GlialCAM WT-flag tagged plus MLC1. This was done to maximize the percentage of GlialCAM in cell–cell junctions, as it was previously described that MLC1 improves the percentage of GlialCAM in cell–cell junctions (15). In this case, we always detect MLC1 and flag-tagged GlialCAM by immunofluorescence and performed our quantitative analyses on GlialCAM only on cells that express MLC1. To study the effect of mutations on GlialCAM trafficking, GlialCAM WT or mutant flag-tagged were transfected independently.

Immunofluorescence of transfected cells

Twenty four hour transfected HeLa cells were split and transferred onto glass coverslips in Petri dishes, and grown for further 24–48 h. Later, cells were fixed with phosphate-buffered saline (PBS) containing 3% paraformaldehyde (PFA) for 20 min, blocked and permeabilized with 10% FBS and 0.1% Triton X-100 in PBS for 2 h at room temperature (RT). Primary antibodies were diluted in the same solution and incubated 1 h at RT. The antibodies used were mouse anti-flag (1:500) (Sigma) and polyclonal rabbit anti-MLC1 (1:100) (25). Cells were washed and incubated with secondary antibodies for 2 h at RT. Coverslips were mounted in Vectashield medium (Vector Laboratories, Burlingam, CA, USA), with 1.5 µg/mL 4′,6-diamidino-2-phenylindole (DAPI, Sigma) and visualized using a DSU spinning disk confocal microscope (Olympus, Tokyo, Japan). Pairs of immunostained cells were analyzed manually to determine whether or not the staining was present in junctions, as described previously (13).

Split-TEV method

The Split-TEV assay was performed exactly as described previously (Lopez-Hernandez *et al*. 2011*b*; Capdevila- Nortes *et al*. 2012; Jeworutzki *et al*. 2012). Briefly, TEV protease was divided into two fragments: the TEV-N (residues 1–118) and the TEV-C (residues 119–242). TEV-N fragment, the TEV protease recognition site and the chimeric transcription factor GV were fused to the C-terminus of GlialCAM WT in a pCDNA3 vector containing a cytomegalovirus promoter. In addition, we fused the TEV-C fragment to the C-terminus of WT or different GlialCAM mutants. All proteins with the TEV-C fragments were cloned in a pCDNA6.2/V5-pL Dest, containing the herpes simplex virus thymidine kinase promoter, to obtain low to moderate levels of expression. The non-interacting protein 4F2hc was used as a negative control.

Cysteine crosslinking assays, western-blot and glycosylation analysis

For western blot studies, lysates were prepared by cell homogenization in PBS containing 1% Triton X-100 and protease inhibitors: 1 mM pepstatin and leupeptin, 1 mM aprotinin and 1 mM PMSF, incubated for 1 h at 4°C and centrifuged. Proteins in supernatants were quantified using the BCA Kit (Pierce, Thermo Scientific, Rockford, IL, USA) and mixed with SDS loading sample buffer (LSB4X). When processing samples of proteins that may establish disulphide bonds, samples were prepared with LSB4X without reducing agents and boiled for 3 min at 50°C. In order to confirm the disulphide-bound nature of dimeric proteins, protein extracts were treated with 100 mM DTT in SDS loading sample buffer and boiled at 95°C for 5 min.

Western blot analysis was performed as previously described (26). Membranes were incubated with primary antibodies: anti-Flag (1:500) and anti-beta actin (1:5000, Sigma) and secondary antibodies: HRP-conjugated anti-mouse (1:5000; Jackson).

Evaluation of glycosylation status of GlialCAM protein was achieved through denaturing glycosylation assays with PNGase F (New Englan BioLabs, Ipswich, UK). Protein extracts were denatured by heating at 100°C for 10 min with glycoprotein denaturing buffer and treated with PNGase F enzyme for 1 h at 37°C. Finally, treated samples were prepared with LSB4X and analyzed by western blot.

Obtention of nanobodies and minibodies against GlialCAM

The sequence of 139G1 Nb was cloned into the vector pHEN2 that included a hexa-histidine tag at the C-terminus. 139G1 Nb was produced by Hybrigenic Services SAS, Paris, France. Three rounds of phage display selection were carried out using cells expressing GlialCAM. Hybrigenics' synthetic hsd2Ab VHH library of 3.109 clones was expressed at the surface of M13 phage. Hybrigenics' phage display allowed selecting VHHs recognizing the non-adsorbed antigen in a native form. Selected VHHs were validated in non-adsorbed Phage ELISA and were then tested in FACS assay. The 139G1 nanobody plasmid was amplified in the *E. coli* WK6 strain (SBRC, Instruct Integrating Biology, Brussel), as described previously (27). In brief, 3–4 individual colonies of the 139G1 Nb were randomly picked, and those were produced as soluble His- and Capture Select C-tagged proteins (MW

12–15 kDa) in the periplasm of *E. coli*. Inducible periplasmic expression of Nb in *E. coli* WK6 strain produced milligramme amounts of > 95% pure Nb using immobilized Ni/NTA Agarose resin (Qiagen, Hilden, Germany) from the periplasmic extract of a 1-l culture. Purified Nb (2–10 mg ml^{-1}) in 20 mM Tris-Base, NaCl 150 mM, pH 7.4 were frozen in liquid nitrogen and stored at −80°C before use.

The VHH 139G1 coding sequence was inserted in pFuse plasmid (Hybrigenic Services), which included an Fc fragment of rabbit IgG2. The production of 139G1 Minibody (Mb) VHH 139G1 fused at their C-terminus to the Fc fragment of rabbit IgG2 was carried out in HEK 293 T cells. These cells were grown at 37°C in an atmosphere of 5% CO_2 in DMEM (Sigma-Aldrich, St Louis, MO, USA) supplemented with 1 mM sodium pyruvate, 2 mM L-glutamine, 100 U/ml streptomycin, 100 mg/ml penicillin and 5% (v/v) fetal bovine serum. The cells were seeded on 10 cm culture dishes and transiently transfected with 10 µg of 139G1 Mb using Trasfectin reagent (Bio-Rad, Hercules, CA, USA). At 24 h after the transient transfection, the media was exchanged for a serum-free media, and the cell supernatant was collected 1 day later. The presence of the Mb in this supernatant was confirmed by western blot using an HRP-conjugated anti-rabbit antibody (1:5000; Jackson).

Flow cytometry

For flow cytometry, cells were processed as previously described (26). Cells were transfected with the different GlialCAM IgV mutants into six-well plates. Forty-eight hours after transfection, cells were detached using Trypsin-EDTA 1X (Biological Industries, Kibbutz Beit-Hanemek, Israel) and resuspended in 500 µL of DMEM (Sigma-Aldrich, St Louis, MO, USA) supplemented with 1 mM sodium pyruvate, 2 mM L-glutamine, 100 U/ml streptomycin, 100 mg/ml penicillin and 5% (v/v) fetal bovine serum. The following antibodies were used: monoclonal anti-HepaCAM 0.5 mg/ml (1:50; R&D Systems) and the Mb developed in this work 139G1 Mb 0.015 mg/ml (1:1; Hybrigenic Services). These antibodies were added separately to each condition and incubated for 30 min at 4°C. Cells were washed once in 1 mL of 0.2% FBS in PBS and resuspended again in 100 mL of cell culture medium. The secondary antibodies used were: Alexa fluor 488 anti-mouse and Alexa fluor 488 anti-rabbit (1:20; Molecular Probes, Inc., Eugene, OR, USA). Secondary antibodies were added and further incubated for 30 min at 4°C. Cells were rinsed once more and resuspended in 1 mL of 0.2% FBS in PBS. To assess viability, propidium iodide was added to a final concentration of 1 mg/ml immediately before FACS analysis, performed with a Cytometre FACS Canto using the following filter sets: 550 bandpass (GFP) and 620/22 (PI). Untransfected cells and unstained transfected cells were used to set the compensation parameters. Data analysis was performed using DIBA software.

Incubation of cells with the 139G1 nanobody

HeLa cells transiently transfected with VFP-tagged GlialCAM WT construct were seeded on coverslips (100.000 cells) and treated with different doses of 139G1 Nb (5, 25 and 50 µg) for 24 h. Cells were then fixed with PBS containing 4% PFA for 20 min and blocked with 10% FBS in PBS for 2 h at RT. Cells were washed three times and coverslips were mounted in Vectashield medium (Vector Laboratories) with 1.5 µg/ml DAPI (Sigma). For the image acquisition, we worked with an Olympus DSU spinning disk confocal microscope. Experiments were analyzed using ImageJ. Cells incubated with 50 µg with the control nanobody 181Nb (28) were used as a negative control.

Modelling of GlialCAM monomer

A model of extracellular GlialCAM (containing the IgV and IgC2 domains) was built with HHPred (29) based on CAR structure (PDB 3JZ7; 24% SI). There are other available templates for the GlialCAM extracellular domains with 24–30% SI (e.g. 2V5T 24%, 1F97 28%, 3LAF 29%, 3JXA 30%), but none of them yielded better models. Modelling of the IgV alone (with templates 4GOS, 2PKD, 1NEU, 4K55, 3R0N), or using other modelling software (e.g. PSIPRED, genThreader, pDomThreader, pGenThreader, T-coffee), did not improve the models.

Modelling of GlialCAM cis dimer

Previous studies reported a *cis* dimer orientation that was quite conserved in other members of the CAM family (e.g. nectin-1-EC, CAR) (19). We initially explored whether GlialCAM could adopt the same *cis* dimeric orientation by superimposing two copies of the monomer model on the corresponding subunits of the CAR dimer (PDB 3JZ7).

However, mutational data and cross-linking experiments did not support the template-based dimer model, so we also modelled the *cis* dimer by docking, using the monomer model as input. We applied the standard pyDock protocol (30,31). We ran FTDock for exhaustive scanning of protein–protein orientations and then evaluated the energy of the 10 000 resulting docking poses with pyDock scoring function. We finally checked all docking models in search for those that satisfied mutational data.

Modelling of GlialCAM trans dimer

During our analysis of homologous structures, we identified a possible template for interactions, between the domains 2 and 3 of contactin (PDB 3JXA) (17). This protein has the highest sequence identity with GlialCAM extracellular domain (30% SI). Therefore, we built *trans* dimer by superimposing two copies of GlialCAM monomer model on contactin domains 2 and 3.

Supplementary Material

Supplementary Material is available at *HMG* online.

Funding

This work was supported in part by the Spanish *Ministerio de Ciencia e Innovación* (MICINN) (RTI2018-093493-B-I00 to RE) and BIO2016-79930-R to JFR. RE is a recipient of an ICREA Academia prize.

Conflict of Interest: None declared.

References

1. van der Knaap, M.S., Schiffmann, R., Mochel, F. *et al.* (2019) Diagnosis, prognosis, and treatment of leukodystrophies. *Lancet Neurol.*, **18**, 962–972.
2. van der Knaap, M.S.S., Boor, I., Estevez, R. *et al.* (2012) Megalencephalic leukoencephalopathy with subcortical cysts: chronic white matter oedema due to a defect in brain ion and water homoeostasis. *Lancet Neurol.*, **11**, 973–985.

3. Leegwater, P.A., Yuan, B.Q., van der Steen, J. *et al.* (2001) Mutations of MLC1 (KIAA0027), encoding a putative membrane protein, cause megalencephalic leukoencephalopathy with subcortical cysts. *Am. J. Hum. Genet.*, **68**, 831–838.
4. López-Hernández, T., Ridder, M.C., Montolio, M. *et al.* (2011) Mutant GlialCAM causes megalencephalic leukoencephalopathy with subcortical cysts, benign familial macrocephaly, and macrocephaly with retardation and autism. *Am. J. Hum. Genet.*, **88**, 422–432.
5. Hamilton, E.M.C., Cialdella, F., Rappard, V., Di, F. *et al.* (2018) Megalencephalic leukoencephalopathy with subcortical cysts: characterization of disease variants. *Neurology*, **90**, E1395–E1403.
6. Estévez, R., Elorza-Vidal, X., Gaitán-Peñas, H. *et al.* (2018) Megalencephalic leukoencephalopathy with subcortical cysts: a personal biochemical retrospective. *Eur. J. Med. Genet.*, **61**, 50–60.
7. Barrallo-Gimeno, A., Gradogna, A., Zanardi, I. *et al.* (2015) Regulatory-auxiliary subunits of CLC chloride channel-transport proteins. *Austral. J. Phys.*, **593**, 4111–4127.
8. Bugiani, M., Dubey, M., Breur, M. *et al.* (2017) Megalencephalic leukoencephalopathy with cysts: the *Glialcam* -null mouse model. *Ann. Clin. Transl. Neurol.*, **4**, 450–465.
9. Hoegg-Beiler, M.B., Sirisi, S., Orozco, I.J. *et al.* (2014) Disrupting MLC1 and GlialCAM and ClC-2 interactions in leukodystrophy entails glial chloride channel dysfunction. *Nat. Commun.*, **5**, 3475.
10. Capdevila-Nortes, X., López-Hernández, T., Apaja, P.M. *et al.* (2013) Insights into MLC pathogenesis: GlialCAM is an MLC1 chaperone required for proper activation of volume-regulated anion currents. *Hum. Mol. Genet.*, **22**, 4405–4416.
11. Jeworutzki, E., López-Hernández, T., Capdevila-Nortes, X. *et al.* (2012) GlialCAM, a protein defective in a Leukodystrophy, serves as a ClC-2 cl - channel auxiliary subunit. *Neuron*, **73**, 951–961.
12. Jeworutzki, E., Lagostena, L., Elorza-Vidal, X. *et al.* (2014) GlialCAM, a CLC-2 cl(−) channel subunit, activates the slow gate of CLC chloride channels. *Biophys. J.*, **107**, 1105–1116.
13. Capdevila-Nortes, X., Jeworutzki, E., Elorza-Vidal, X. *et al.* (2015) Structural determinants of interaction, trafficking and function in the ClC-2/MLC1 subunit GlialCAM involved in leukodystrophy. *Austral. J. Phys.*, **593**, 4165–4180.
14. Arnedo, T., López-Hernández, T., Jeworutzki, E. *et al.* (2014) Functional analyses of mutations in HEPACAM causing megalencephalic leukoencephalopathy. *Hum. Mutat.*, **35**, 1175–1178.
15. López-Hernández, T., Sirisi, S., Capdevila-Nortes, X. *et al.* (2011) Molecular mechanisms of MLC1 and GLIALCAM mutations in megalencephalic leukoencephalopathy with subcortical cysts. *Hum. Mol. Genet.*, **20**, 3266–3277.
16. Arnedo, T., Aiello, C., Jeworutzki, E. *et al.* (2014) Expanding the spectrum of megalencephalic leukoencephalopathy with subcortical cysts in two patients with GLIALCAM mutations. *Neurogenetics*, **15**, 41–48.
17. Bouyain, S. and Watkins, D.J. (2010) The protein tyrosine phosphatases PTPRZ and PTPRG bind to distinct members of the contactin family of neural recognition molecules. *Proc. Nat. Acad. Sci. U.S.A.*, **107**, 2443–2448.
18. Estévez, R. and Jentsch, T.J. (2002) CLC chloride channels: correlating structure with function. *Curr. Opin. Struct. Biol.*, **12**, 531–539.
19. Narita, H., Yamamoto, Y., Suzuki, M. *et al.* (2011) Crystal structure of the cis-dimer of Nectin-1. *J. Biol. Chem.*, **286**, 12659–12669.
20. Kamiguchi, H. and Lemmon, V. (2000) IgCAMs: bidirectional signals underlying neurite growth. *Curr. Opin. Cell Biol.*, **12**, 598–605.
21. Matthäus, C., Langhorst, H., Schütz, L. *et al.* (2017) Cell-cell communication mediated by the CAR subgroup of immunoglobulin cell adhesion molecules in health and disease. *Mol. Cell. Neurosci.*, **81**, 32–40.
22. Shi, Z., Yan, H.-F., Cao, B.-B. *et al.* (2019) Identification in Chinese patients with GLIALCAM mutations of megalencephalic leukoencephalopathy with subcortical cysts and brain pathological study on Glialcam knock-in mouse models. *World J. Pediatr.*, **15**, 454–464.
23. Sirisi, S., Elorza-Vidal, X., Arnedo, T. *et al.* (2017) Depolarization causes the formation of a ternary complex between GlialCAM, MLC1 and ClC-2 in astrocytes: implications in megalencephalic leukoencephalopathy. *Hum. Mol. Genet.*, **26**, 2436–2450.
24. Wang, K., Preisler, S.S., Zhang, L. *et al.* (2019) Structure of the human ClC-1 chloride channel. *PLOS Biol.*, **e3000218**, 17.
25. Teijido, O., Casaroli-Marano, R., Kharkovets, T. *et al.* (2007) Expression patterns of MLC1 protein in the central and peripheral nervous systems. *Neurobiol. Dis.*, **26**, 532–545.
26. Teijido, O., Martínez, A., Pusch, M. *et al.* (2004) Localization and functional analyses of the MLC1 protein involved in megalencephalic leukoencephalopathy with subcortical cysts. *Hum. Mol. Genet.*, **13**, 2581–2594.
27. Pardon, E., Laeremans, T., Triest, S. *et al.* (2014) A general protocol for the generation of Nanobodies for structural biology. *Nat. Protoc.*, **9**, 674–693.
28. Errasti-Murugarren, E., Fort, J., Bartoccioni, P. *et al.* (2019) L amino acid transporter structure and molecular bases for the asymmetry of substrate interaction. *Nat. Commun.*, **10**, 1807.
29. Soding, J., Biegert, A. and Lupas, A.N. (2005) The HHpred interactive server for protein homology detection and structure prediction. *Nucleic Acids Res.*, **33**, W244–W248.
30. Cheng, T.M.-K., Blundell, T.L. and Fernandez-Recio, J. (2007) pyDock: electrostatics and desolvation for effective scoring of rigid-body protein-protein docking. *Proteins*, **68**, 503–515.
31. Jiménez-García, B., Pons, C. and Fernández-Recio, J. (2013) pyDockWEB: a web server for rigid-body protein–protein docking using electrostatics and desolvation scoring. *Bioinformatics*, **29**, 1698–1699.

Human Molecular Genetics, 2021, Vol. 30, No. 17 1649–1665

https://doi.org/10.1093/hmg/ddab155
Advance Access Publication Date: 7 June 2021
General Article

GENERAL ARTICLE

Identification of the GlialCAM interactome: the G protein-coupled receptors GPRC5B and GPR37L1 modulate megalencephalic leukoencephalopathy proteins

Marta Alonso-Gardón[1,2,#], Xabier Elorza-Vidal[1,2,#], Aida Castellanos[1,2], Gina La Sala[3], Mercedes Armand-Ugon[1], Alice Gilbert[4], Chiara Di Pietro[3], Adrià Pla-Casillanis[1], Francisco Ciruela[5], Xavier Gasull[6], Virginia Nunes[7], Albert Martínez[8], Uwe Schulte[9], Martine Cohen-Salmon[4], Daniela Marazziti[3] and Raúl Estévez[1,2,*,†]

[1]Departament de Ciències Fisiològiques, Genes Disease and Therapy Program IDIBELL - Institute of Neurosciences, Universitat de Barcelona, Barcelona 08036, Spain, [2]Centro de Investigación Biomédica en Red sobre Enfermedades Raras (CIBERER), Instituto de Salud Carlos III, Madrid 28029, Spain, [3]Institute of Biochemistry and Cell Biology, Italian National Research Council (CNR), Monterotondo Scalo, Rome I-00015, Italy, [4]Physiology and Physiopathology of the Gliovascular Unit Research Group, Center for Interdisciplinary Research in Biology (CIRB), College de France, CNRS Unité Mixte de Recherche 724, INSERM Unité 1050, Labex Memolife, PSL Research University, Paris F-75005, France, [5]Pharmacology Unit, Department of Pathology and Experimental Therapeutics, Faculty of Medicine and Health Sciences, Institute of Neurosciences, University of Barcelona-IDIBELL, L'Hospitalet de Llobregat, Barcelona 08036, Spain, [6]Neurophysiology Laboratory, Department of Biomedicine, Medical School, Institute of Neurosciences, University of Barcelona-IDIBAPS, Casanova 143 Barcelona 08036, Spain, [7]Unitat de Genètica, Departament de Ciències Fisiològiques, Universitat de Barcelona, Laboratori de Genètica Molecular, Genes Disease and Therapy Program IDIBELL, L'Hospitalet de Llobregat 08036, Spain, [8]Department of Cell Biology, Physiology and Immunology, Faculty of Biology, University of Barcelona, Barcelona 08028, Spain and [9]Logopharm GmbH, Freiburg 79104, Germany

*To whom correspondence should be addressed at: Facultat de Medicina, Departament de Ciències Fisiològiques, Universitat de Barcelona-IDIBELL, C/Feixa Llarga s/n 08907 L'Hospitalet de Llobregat, Barcelona 08028, Spain. Tel: +34 934039781; Fax: +34 934024268; Email: restevez@ub.edu

Abstract

Megalencephalic Leukoencephalopathy with subcortical Cysts (MLC) is a type of vacuolating leukodystrophy, which is mainly caused by mutations in *MLC1* or *GLIALCAM*. The two MLC-causing genes encode for membrane proteins of yet unknown function that have been linked to the regulation of different chloride channels such as the ClC-2 and VRAC. To gain insight into the role of MLC proteins, we have determined the brain GlialCAM interacting proteome. The proteome

[†]Raúl Estévez, http://orcid.org/0000-0003-1579-650X
[#]These two authors contributed equally to this study and share first authorship.
Received: March 31, 2021. **Revised:** May 31, 2021. **Accepted:** June 1, 2021

includes different transporters and ion channels known to be involved in the regulation of brain homeostasis, proteins related to adhesion or signaling as several G protein-coupled receptors (GPCRs), including the orphan GPRC5B and the proposed prosaposin receptor GPR37L1. Focusing on these two GPCRs, we could validate that they interact directly with MLC proteins. The inactivation of *Gpr37l1* in mice upregulated MLC proteins without altering their localization. Conversely, a reduction of GPRC5B levels in primary astrocytes downregulated MLC proteins, leading to an impaired activation of ClC-2 and VRAC. The interaction between the GPCRs and MLC1 was dynamically regulated upon changes in the osmolarity or potassium concentration. We propose that GlialCAM and MLC1 associate with different integral membrane proteins modulating their functions and acting as a recruitment site for various signaling components as the GPCRs identified here. We hypothesized that the GlialCAM/MLC1 complex is working as an adhesion molecule coupled to a tetraspanin-like molecule performing regulatory effects through direct binding or influencing signal transduction events.

Introduction

Megalencephalic Leukoencephalopathy with subcortical Cysts (MLC) is a rare type of leukodystrophy (1). Patients suffering from MLC present macrocephaly, subcortical cysts and white matter vacuolation, leading to epilepsy as well as motor and cognitive impairments (2). MLC is caused by mutations in either *MLC1* (3) or *GLIALCAM* (also called *HEPACAM*) (4). These genes encode for membrane proteins that form a complex located at cell–cell junctions in brain perivascular astrocytic processes or in Bergmann glia at the cerebellum (5). A reduced number of patients (2%) do not harbor mutations in *MLC1* or *GLIALCAM*, suggesting the existence of other unknown disease genes (6).

The functional role of the GlialCAM/MLC1 complex is still unknown. Nevertheless, different proteins and activities related to brain homeostasis are affected in a GlialCAM or MLC1-dependent manner. Therefore, a role for these proteins in neuronal ion/water homeostasis has been hypothesized. For instance, depletion of MLC1 has been shown to reduce VRAC activity in primary astrocytes (7,8). In addition, GlialCAM and MLC1 have been shown to form a ternary complex with the ClC-2 chloride channel (9). Also, co-expression of human GlialCAM with ClC-2 changes the channel activity from inwardly rectifying to an ohmic channel (10). Furthermore, the Na^+/K^+-ATPase pump has been identified as a MLC1-interacting protein, whereas the overexpression of MLC1 was observed to reduce its activity (11). Finally, Cx43 has been identified as a GlialCAM interacting protein (12) and MLC1 might influence Cx43 stability at gap junctions in astrocytoma cells (13).

It is not clear how GlialCAM and MLC1 affect the activity of different ion channels and transporters. It has been suggested that they might influence signaling cascades by yet undefined mechanisms (14). In this sense, recent work has shown that the overexpression of human MLC1 in astrocytes decreases the phosphorylation of extracellular signal-regulated kinases (ERK), whereas primary astrocytes lacking MLC1 show an increase in ERK phosphorylation (15).

In summary, although it is clear that GlialCAM/MLC1 proteins regulate the activity of different ion channels and transporters that play a role in neuronal brain homeostasis, the mechanisms involved in this process remain unclear. Here, we have determined the GlialCAM interactome from mouse brain and analyzed its interaction with GlialCAM and MLC1. Among the proteins identified as part of this network, we found specific G protein-coupled receptors (GPCRs), concretely the orphan GPRC5B (16) and the proposed prosaposin receptor GPR37L1 (17), which show a dynamic association with GlialCAM and MLC1 and regulate their surface levels. Based on the results of this work, we propose a functional role for GlialCAM and MLC1 proteins.

Results

Identification of the GlialCAM interactome

For comprehensive identification of the GlialCAM interactome, we performed affinity purifications (APs) with four different antibodies specific for GlialCAM on membrane fractions prepared from whole brains from adult rats, wild-type (WT) mice, and *Glialcam* knockout (KO) mice (10). Membranes were solubilized with the detergent buffer CL-47 plus 1 mM Mg^{2+}, as earlier experiments indicated that this detergent mixture was able to maintain the interaction of GlialCAM with MLC1 and ClC-2, two previously validated interactors (4,9). Total eluates of APs with the anti-GlialCAM antibodies or with unspecific immunoglobulins G (IgG) were analyzed by high-resolution nanoflow liquid chromatography-tandem mass spectrometry (LC-MS/MS), which provided data on both the identity and the amount of interacting proteins. Two out of the four anti-GlialCAM antibodies purified their target with high efficiency, allowing for a more detailed analysis of the main target's primary sequence. MS analyses showed that GlialCAM, MLC1 and ClC-2 proteins were retained in all APs with high efficiency, as reflected by the peak volume (PV) values (see Materials and Methods) and the extensive coverage of protein sequences (relative sequence coverage of 72, 53 and 74%, respectively). The other proteins identified by MS were evaluated for both their specifity and consistency of copurification with the GlialCAM protein based on the quantitative data of protein amounts. For each protein, the consistency of enrichment was evaluated with the different antibodies and its quantitative correlation with the purified GlialCAM protein.

Together, these criteria defined a sharp-profiled proteome (Fig. 1A for one GlialCAM antibody and Supplementary Material, Fig. S1 for another GlialCAM antibody), identifying 21 proteins as high-confidence constituents of the GlialCAM interactome in the mouse brain. As summarized in (Fig. 1B), these constituents comprise the aforementioned GlialCAM, MLC1 and ClC-2 and previously identified transport/ion channels proteins interacting with GlialCAM or MLC1. These include the gap junction protein Cx43 (12,13), the glutamate transporters EAAT1/2 and the sodium/potassium ATPase subunits alpha2 and beta2 (11,18). Other proteins that mediate transport or have been related to chloride channel function such as the bicarbonate transporter (NBCe1), the glucose transporter (GLUT1), the sodium/calcium exchanger 1 (NCX1) or the protein tweety-homolog 1 were also identified. In previous APs experiments using MLC1 antibodies, NBCe1 and tweety-homolog 1 were also specifically co-purified with MLC1 (Fig. 1B).

Apart from transporters and ion channels, we identified proteins related to cell adhesion or trafficking such as tetraspanin-9 (CD9), Neuronal membrane glycoprotein M6-a/b (GPM6A/B) or Syntaxin-1A/1B. Interestingly, CD9 was also identified in a membrane yeast two-hybrid (MYTH) screening using human

A

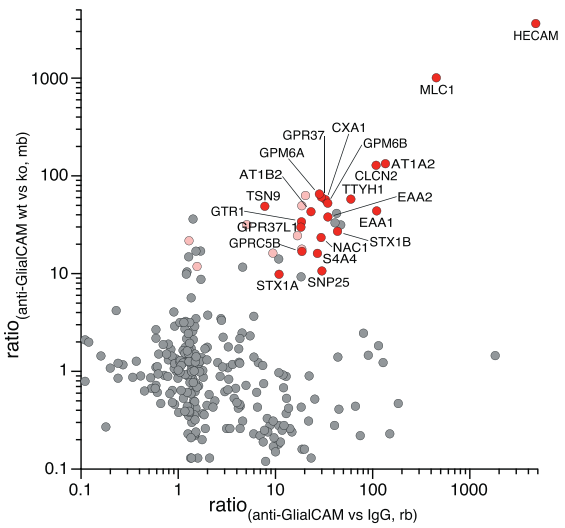

B

Identified proteins	MLC1 IP
HECAM: Hepatocyte cell adhesion molecule	yes
MLC1: Membrane protein MLC1	yes
Transport/Ion channels	
CLCN2: Chloride channel protein 2 (Clc-2)	yes
CXA1: Connexin 43	no
EAA1: Excitatory amino acid transporter 1 (Glast)	yes
EAA2: Excitatory amino acid transporter 2 (Glt-1)	yes
AT1A2: Sodium/potassium-transporting ATPase subunit alpha-2	yes
S4A4: Electrogenic sodium bicarbonate cotransporter 1 (Nbce1)	yes
TTYH1: Protein tweety homolog1	yes
AT1B2: Sodium/potassium-transporting ATPase subunit beta-2	yes
GTR1: Solute carrier family 2, facilitated glucose transporter member 1 (Glut1)	no
NAC1: Sodium/calcium exchanger 1 (Ncx1)	no
Signalling	
GPR37: Prosaposin receptor GPR37	no
GPR37L1: G-protein coupled receptor 37-like 1	no
GPRC5B: G-protein coupled receptor family C group 5 member B	yes*
Adhesion/Junctions/Trafficking	
TSN9: Tetraspanin-9 (CD9)	no*
GPM6A: Neuronal membrane glycoprotein M6-a	yes
GPM6B: Neuronal membrane glycoprotein M6-b	yes
STX1B: Syntaxin-1B	no
STX1A: Syntaxin-1A	no
SNP25: Synaptosomal-associated protein 25	no

* Identified in MYTH screenings using human MLC1 as bait.

Figure 1. Identification of the GlialCAM interactome. (**A**) Specificity map of the GlialCAM interactome with one of the rabbit polyclonal anti-GlialCAM antibodies used that detects a peptide from the C-terminus. Two-dimensional logarithmic abundance-ratio plot illustrating the medians of PV ratios (rPV) obtained for any protein in APs from rat membranes with the *second* anti-GlialCAM antibody used versus IgG (x axis) and in anti-glialCAM APs from mouse membranes of wild-type (WT) versus *Glialcam* KO animals (y axis). Gray bars (rPVs of 10) represent the specificity threshold for this AB on either rPV scale and place specifically purified proteins in the upper-right quadrant. Red dots denote finally annotated GlialCAM constituents (**B**); black dots symbolize all other proteins. (B) List of proteins belonging to the GlialCAM interactome classified according to their assigned function. We indicate if they have been identified in AP using anti MLC1 antibodies and in MYTH screening using human MLC1 as a bait.

MLC1 as a bait, indicating direct interaction. GPM6A/B were also identified in MLC1 APs (Fig. 1B).

Finally, three GPCRs were identified as components of the GlialCAM interactome. One of these, the orphan GPRC5B (also named RAIG2) was also identified in a MYTH using human MLC1 as a bait and also in APs using MLC1 antibodies. Therefore, it can be considered a bona fide interactor. Interestingly, the two other identified GPCRs (GPR37 and GPR37l1) belong to the same protein family (19).

Interactions between GPCRs and GlialCAM/MLC1

GlialCAM and MLC1 have been related to signal transduction changes, but the mechanisms involved in this process remain unresolved (14,15). In this regard, we considered the identified GPCRs as candidates for the signal transduction changes related to GlialCAM/MLC1 and proceeded to characterize their interaction with MLC proteins. As MLC1 is only astrocytic (20), we focused on GPRC5B and GPR37L1 and not on GPR37, which is mainly expressed in oligodendrocytes (21).

We developed a polyclonal antibody which was able to detect specifically GPRC5B by Western blot (Supplementary Material, Fig. S2A–B) and by immunofluorescence on primary astrocytes (Supplementary Material, Fig. S2C). The antibody was validated in siRNA and overexpression experiments. For GPR37L1, we used commercially available antibodies (see Materials and Methods) previously validated using *Gpr37l1* KO animals (22).

Co-localization was tested and observed between MLC1 and GPRC5B (Fig. 2A) or GPR37L1 (Fig. 2B) in primary cultures of astrocytes. We assessed colocalization with MLC1 and not with GlialCAM, as both proteins colocalize perfectly in astrocytes and we have anti-MLC1 polyclonal and monoclonal antibodies directed against the same MLC1 intracellular epitopes (23) and therefore, are suitable for all experiments.

Proximity-ligation assays (PLA) in primary cultures revealed close proximity between GPRC5B or GPR37L1 and MLC1 (Fig. 2C and D). Control experiments in WT cells without the primary antibody or in astrocytes obtained from *Mlc1* KO animals (10) demonstrated the specificity of the PLA signal (Fig. 2C and D).

At a tissular level, we could not detect a specific signal for GPRC5B with the new antibody or with commercially available ones. However, in purified gliovascular units (GVUs), a preparation more accessible to detect astrocytic endfeet proteins (24), we could detect partial co-localization between GPRC5B and MLC1 (Fig. 3A). GPR37L1 is mainly expressed in Bergmann glia (25), where GlialCAM and MLC1 are also expressed. However, co-localization between GPR37L1 and MLC1 in Bergmann glia (Fig. 3B) was low. The fact that the co-localization between the GPCRs and MLC1 was higher in primary cultures could indicate that the accessibility of the antibodies against the GPCRs might be limited in brain tissue preparations.

The ability of human GPRC5B or GPR37L1 to physically interact in living cells with human GlialCAM or MLC1 was then assessed *in vitro* by means of bioluminescence resonance energy transfer (BRET) saturation assays. HEK293T cells were co-transfected with a constant amount of either the GPRC5B-Rluc or the GPR37L1-Rluc plasmids combined with increasing concentrations of the MLC1-VFP (Fig. 4A) or GlialCAM-VFP (Fig. 4B) plasmids. The interaction between GlialCAM and MLC1 (Fig. 4A) was used as positive control, whereas the lack of interaction between LRRC8A [the main subunit of the VRAC channel (26,27)] and either MLC1 (Fig. 4A) or GlialCAM (Fig. 4B) was used as a negative control. A positive BRET signal was detected when GPRC5B or GPR37L1 were co-expressed with MLC1 (Fig. 4A) or with GlialCAM (Fig. 4B). The determination of the $BRET_{50}$ signal allowed to compare the strength of interaction between GPR37L1 or GPRC5B with MLC1 versus the interaction with GlialCAM. The $BRET_{50}$ values for the interaction of GPR37L1 with MLC1 and GPR37L1 with GlialCAM were 2.9 ± 0.9 ($n = 5$) and 2.6 ± 0.4 ($n = 4$), respectively, which were not statistically different ($P = 0.73$). Similarly, the $BRET_{50}$ values for the interaction of GPRC5B with MLC1 and GPRC5B with GlialCAM were 1.2 ± 0.3 ($n = 4$) and 0.7 ± 0.2 ($n = 5$), which were also not statistically different ($P = 0.19$), indicating that GPCRs interact with MLC1 and GlialCAM with similar avidity.

These results demonstrated that GPRC5B or GPR37L1 and the MLC proteins are in close proximity (<10 nm). Together with

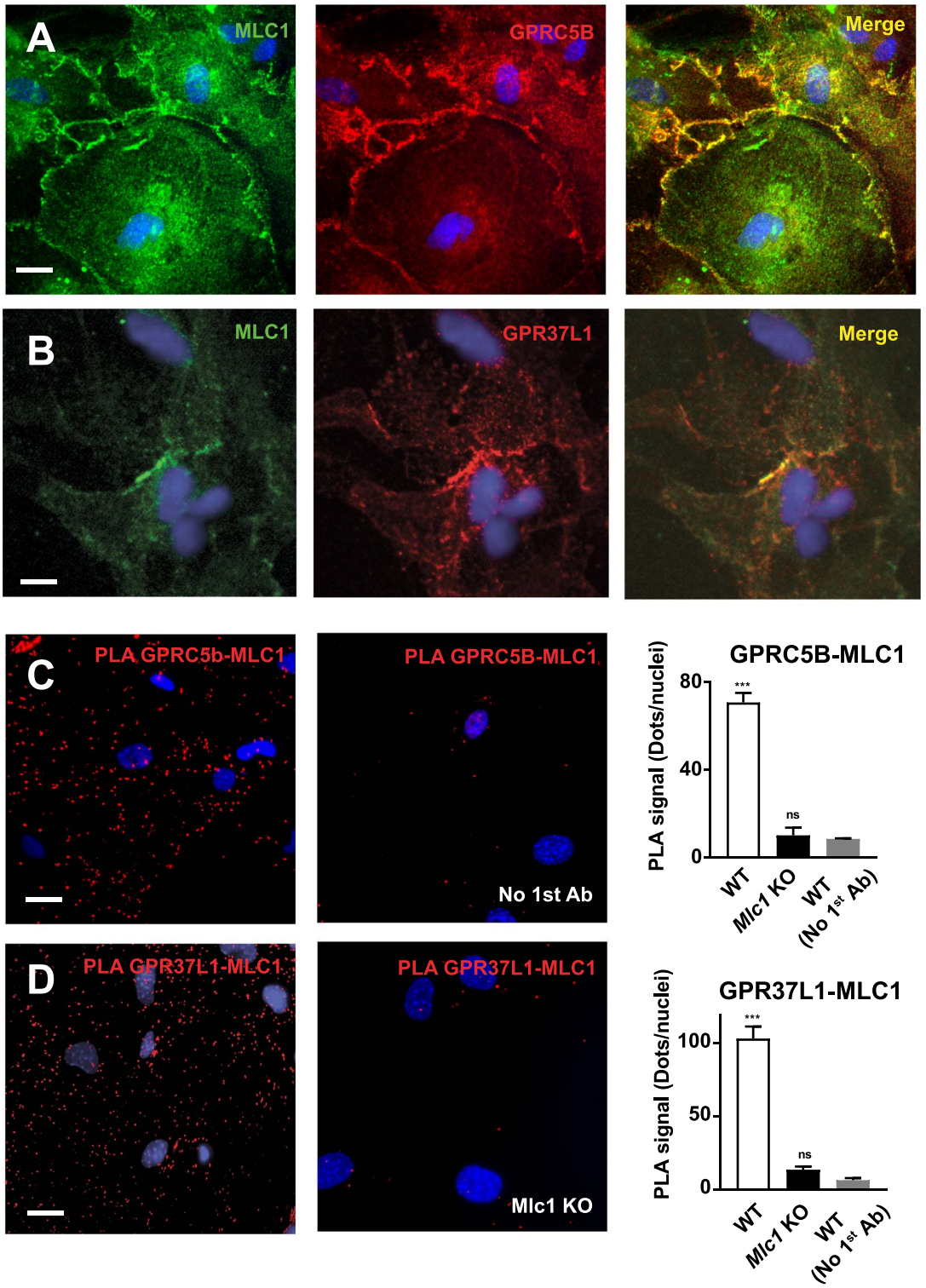

Figure 2. Localization of GPRC5B and GPR37L1 in primary cultures of astrocytes. (**A**) Representative images of immunostaining of MLC1 in green (left), GPRC5B in red (middle) and merged stainings where the two proteins show a certain degree of colocalization at the plasma membrane (right, yellow) from cultured mouse astrocytes. Scale bar, 20 µm (**B**) Representative confocal images of MLC1 (green), GPR37L1 (red), co-immunofluorescence labeling and DAPI staining (blue) in mouse cerebellar primary astrocytes from wild-type (WT) pups. Scale bar, 75 µm. (**C** and **D**) PLA for protein interactions between MLC1 and GPRC5B (C) or GPR37L1 (D) in WT or *Mlc1* KO cultured mouse astrocytes. Cells with only one primary antibody (MLC1 antibody) were used as negative controls. Scale bar, 20 µm. The number of PLA dots was quantified using Image J. Data are mean ± standard error of the mean of three–four independent experiments. For statistical analyses, we performed a one-way analysis of variance plus Dunnet multiple comparison's test versus the negative control. ns, not significant. $^{***}P < 0.001$.

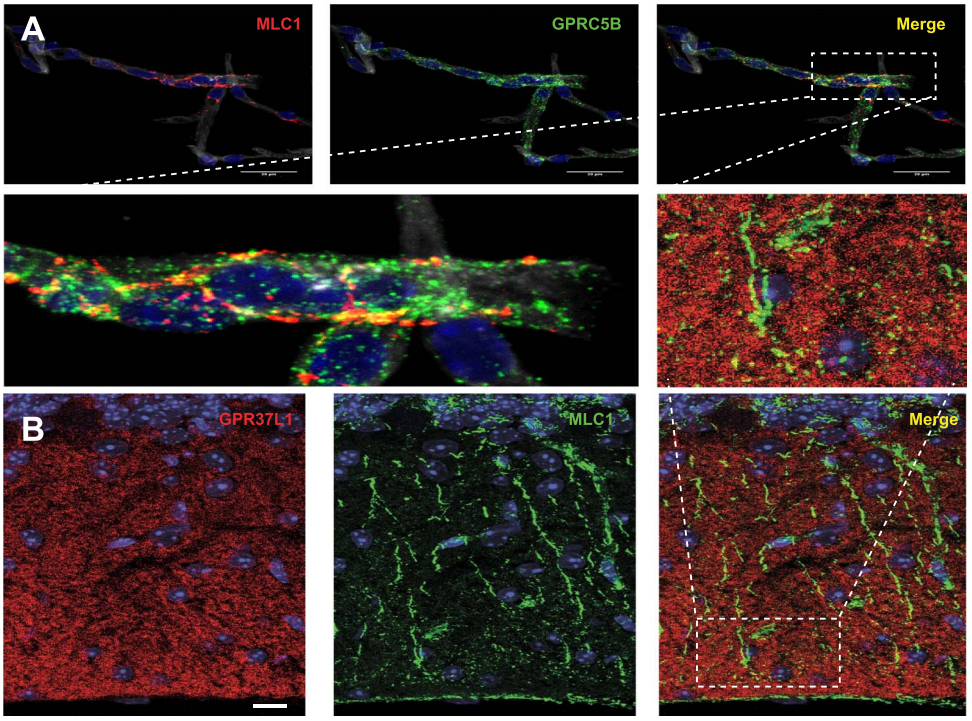

Figure 3. Localization of the identified GPCRs with MLC1 in brain slices. (**A**) The localization of GPRC5B and MLC1 in GVUs. Projection confocal plan of MLC1 (red) and GPRC5B (green) immunolabeled GVUs purified from adult wild-type (WT) brain. Nuclei are labeled with Hoechst (blue) and blood vessel wall with Isolectin B4 (white). Scale bar, 20 µm. (**B**) The localization of GPR37L1 and MLC1 in Bergmann glia. Representative confocal images of GPR37L1 (red), MLC1 (green) co-immunofluorescence labeling and DAPI staining (blue), in cerebellar coronal sections of WT adult mice. Higher magnifications of boxed areas (dashed lines) in (A) and (B) are presented. Scale bar, 20 µm.

our data obtained from slices and cell culture, they support the existence of GPCRs-MLC protein complexes in living cells.

Lack of GPR37L1 increases MLC proteins in vivo

GPR37L1 is expressed exclusively in astrocytes and immature oligodendrocytes within the brain, also being highly expressed in Bergmann glia of the cerebellum (25). *Gpr37l1* KO mice showed no alteration of adult cerebellar layer cytoanatomy and organization and no signs of gliosis. At the functional level, animals presented improved motor functions and advanced cerebellar development (22). Based on the similarities of expression patterns for GlialCAM, MLC1 and GPR37L1 together with the mild phenotype of the KO mice, we reasoned that the analysis of MLC proteins in *Gpr37l1* KO mice may suggest direct effects of GPR37L1 in MLC protein biology.

We first analyzed the consequences of the lack of GPR37L1 on MLC1 and GlialCAM protein levels. Western blot experiments of cerebellum membranes indicated that both proteins were upregulated in the *Gpr37l1* KO (Fig. 5A). Because GlialCAM and MLC1 stabilize ClC-2 at the plasma membrane (28), we then measured ClC-2 protein levels. Similarly, ClC-2 protein levels were increased in the KO animals in a significative manner (Fig. 5A). In contrast, GPRC5B protein levels remained unchanged (Fig. 5A).

An increased signal was observed in tissue samples from KO animals when immunofluorescence experiments detecting MLC1 and GlialCAM at the Bergmann glia were performed. However, MLC proteins showed a more dotted pattern compared with WT signal (Fig. 5B). Similar results were observed for ClC-2 (Supplementary Material, Fig. S3A). Quantification of the fluorescent signal revealed increased amounts of MLC1 in *Gpr37l1* KO mice (Fig. 5B). Similarly, the fluorescent signal of MLC proteins was increased in primary astrocyte cultures from the KO mice (Supplementary Material, Fig. S3B). In contrast, the signal of GPRC5B in astrocyte cultures from KO animals remained unchanged (Supplementary Material, Fig. S3C).

To determine whether MLC1 subcellular localization was altered in *Gpr37l1* KO mice as the immunofluorescence staining suggested, we detected MLC1 by electron microscopy (EM) immunogold experiments (Fig. 5C). These experiments showed that the localization of MLC1 in Bergmann glia (Fig. 5Ca) or in perivascular astrocytic processes was not affected (Fig. 5Cb).

Similarly, we assessed whether the expression of GPR37L1 and GPRC5B depends on MLC1. Western blot experiments revealed that the total amount of GPR37L1 and GPRC5B was the same in the brain and the cerebellum of *Mlc1* KO mice (Supplementary Material, Fig. S4A and B). Likewise, there was no change in the subcellular localization of GPRC5B in the astrocytic endfeet around blood vessels in *Mlc1* KO mice (Supplementary Material, Fig. S4C).

We conclude that the lack of GPR37L1 in mice upregulates MLC protein levels without altering their localization. Moreover, no change is observed for GPRC5B protein.

Knockdown of GPRC5B in primary astrocytes downregulates MLC proteins

We next studied whether the lack of GPRC5B might influence MLC proteins. GPRC5B has been described to be expressed in neurons, oligodendrocytes and astrocytes (16). *Gprc5b* KO mice display gliosis and axonal swellings in the cerebellum caused by increased ROS (29,30). In order to avoid any secondary effect of the loss of GPRC5B, experiments addressing the cellular effects

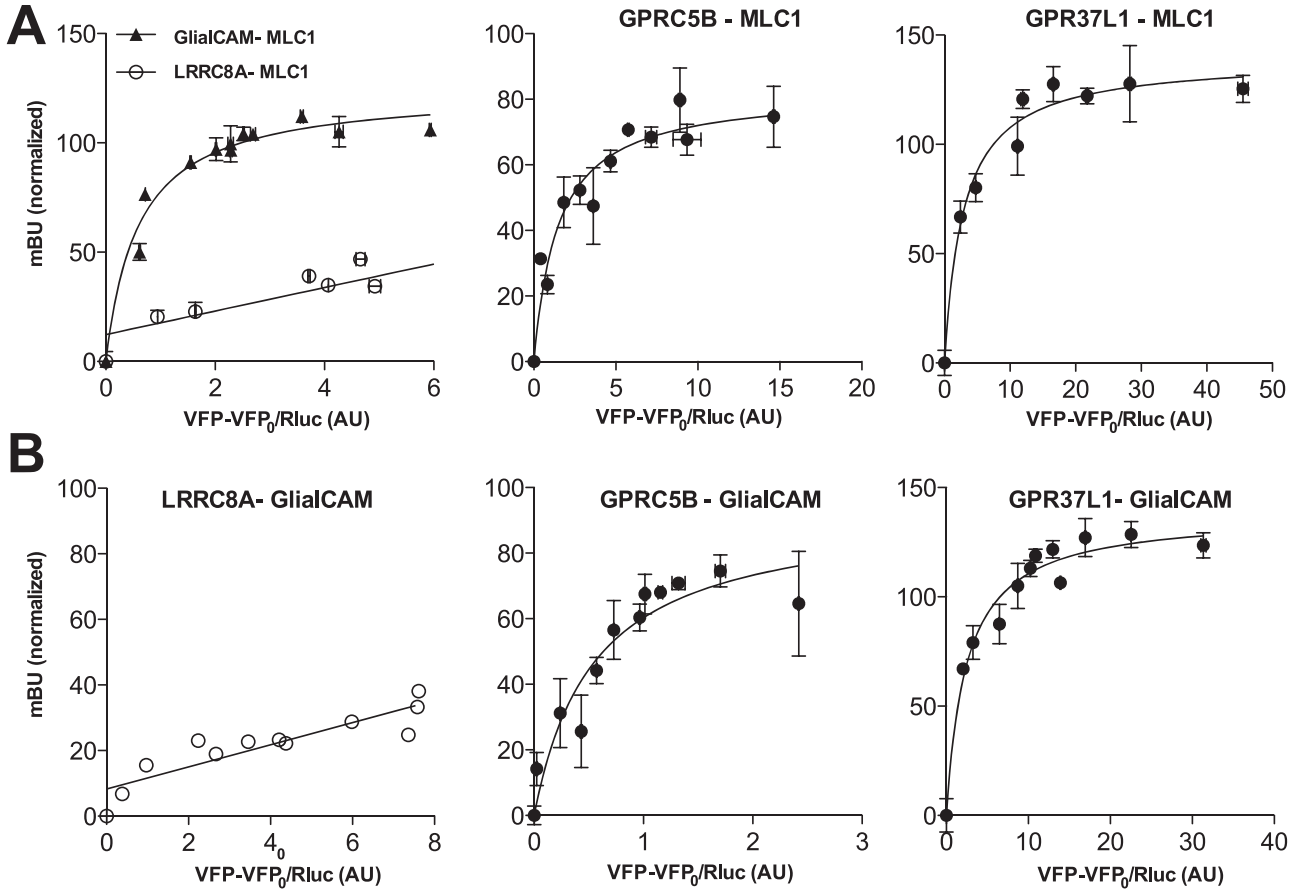

Figure 4. Direct interaction of the human GPCRs with human GlialCAM or human MLC1 by bioluminescence resonance energy transfer (BRET) assays. Representative BRET saturation curve between GPCRs and MLC1 (**A**) or GlialCAM (**B**) from 3 to 5 independent experiments. HEK293T cells were co-expressing a constant amount of GPRC5b-Rluc or GPR37L1-Rluc in presence of increasing concentrations of MLC1-VFP or GlialCAM-VFP. The interaction between GlialCAM-Rluc and MLC1-VFP were analyzed as positive control, and with human LRRC8A as negative control. Plotted on the x axis is the fluorescence value obtained from the VFP, normalized with the luminescence value of the Rluc constructs 10 min after coelenterazine h incubation and the y axis the corresponding BRET ratio (x1000). mBU: mBRET units. Results are expressed as mean ± standard error of mean.

of GPRC5B ablation on MLC proteins were therefore performed on primary cultured astrocytes. For this purpose, we developed adenoviral vectors expressing a shRNA against mouse *Gprc5b* (sh Gprc5b) that were able to nearly deplete GPRC5B levels (Supplementary Material, Figs S2B and C, and 6A). An adenoviral vector expressing a scrambled shRNA was used as control.

In GPRC5B-depleted astrocytes, MLC1 and ClC-2 total protein levels were significantly reduced. In contrast, GlialCAM and LRRC8A protein levels were not altered (Fig. 6A). Because our results have shown that GPRC5B interacts directly with MLC1 and GlialCAM, we reasoned that GPRC5B ablation could influence GlialCAM plasma membrane levels in the absence of MLC1. GPRC5B depletion reduced GlialCAM levels at the plasma membrane in *Mlc1* KO astrocytes (Fig. 6B). Immunofluorescence experiments indicated that GlialCAM was internalized in *Mlc1* KO astrocytes depleted of GPRC5B (Fig. 6C), suggesting that GPRC5B may stabilize GlialCAM at the plasma membrane. In these GPRC5B-depleted astrocytes, complementation with an adenovector expressing human MLC1 rescued GlialCAM localization at the plasma membrane (Fig. 6C), in agreement with previous studies that indicated that MLC1 also stabilizes GlialCAM (31). Hence, GPRC5B might stabilize both MLC1 and GlialCAM at the plasma membrane and thus, it may influence the activity of different chloride channels that have been linked to the presence of GlialCAM and MLC1 in depolarizing (ClC-2) or hypotonic (VRAC) conditions.

In agreement with this hypothesis, the ablation of GPRC5B almost completely abolished the localization of ClC-2 at cell–cell junctions in depolarizing conditions, with a drastic reduction from 47 ± 2 to 7 ± 3 ($n = 3$ experiments, 108 cells counted, $^{***}P < 0.001$) in GPRC5B depleted samples (Fig. 7A). Furthermore, whole cell patch-clamp experiments in rat astrocytes demonstrated that GPRC5B knockdown decreased ClC-2 current activation and prevented its change in rectification observed in depolarizing conditions (Fig. 7B and C), as observed in the measurements of the normalized current (Fig. 7C and D) and the rectification index (Fig. 7E), respectively. Previous studies using VRAC and ClC-2 inhibitors together with shRNA directed against ClC-2 demonstrated that the chloride currents observed in depolarizing conditions are mediated by ClC-2 associated with GlialCAM and MLC1 (23).

Next, we measured VRAC activation by hypotonicity in GPRC5B-depleted astrocytes (Fig. 7F–H). Reduction of GPRC5B expression led to a dramatic reduction of VRAC current measured in hypotonic conditions (Fig. 7F–H).

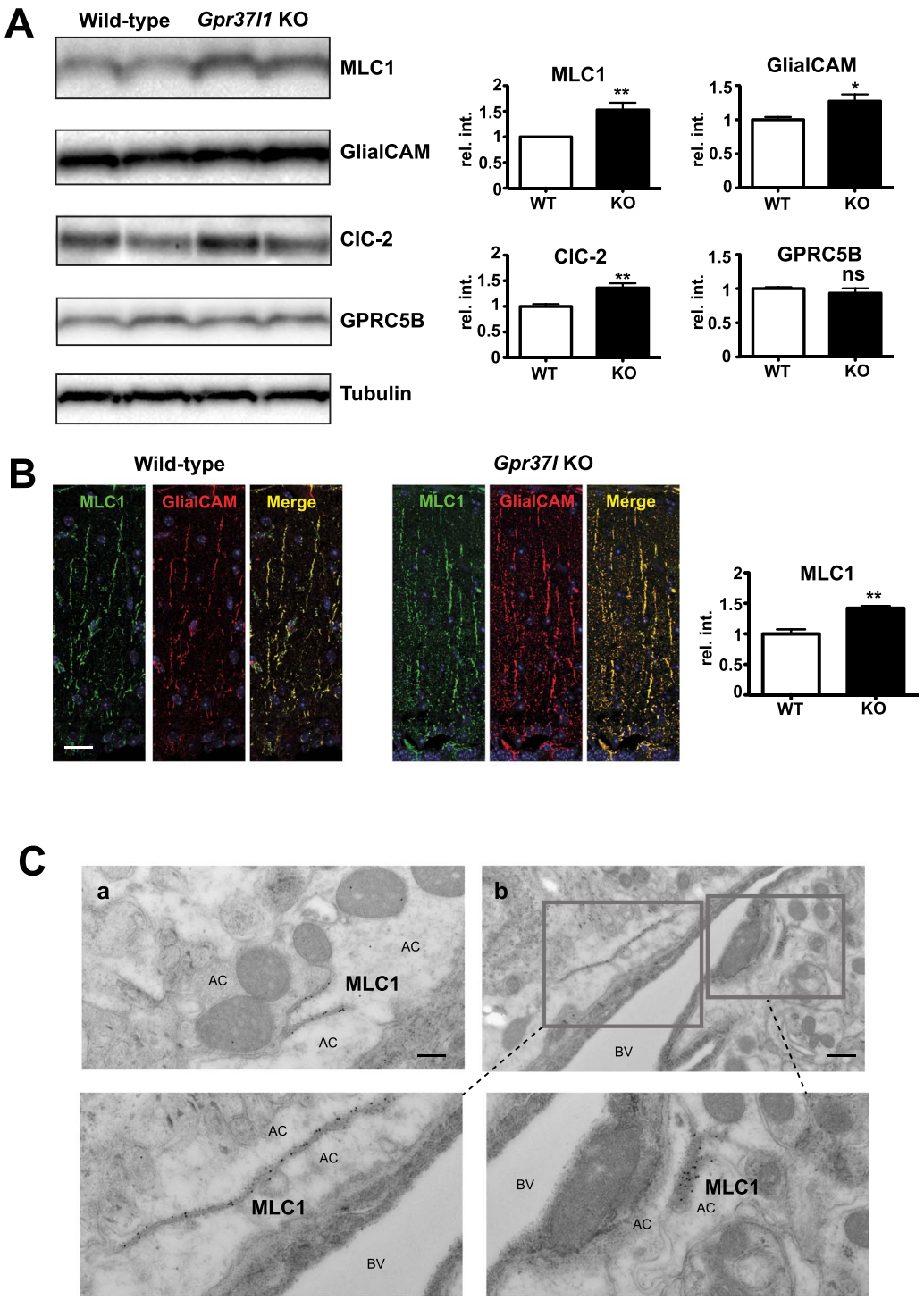

Figure 5. Expression and localization of MLC proteins in *Gpr37l1* KO mice. (**A**) Representative Western blot analysis and densitometric quantification in whole cerebellar extracts from wild-type (WT) and *Gpr37l1* KO adult mice. Data are expressed in arbitrary units (rel.int.: relative intensity) as a ratio to the mean values obtained from WT mice (unpaired *t*-test; $^{*}P < 0.035$; $^{**}P < 0.007$, $n = 6, 7$). (**B**) Representative confocal images of MLC1 (green), GlialCAM (red) co-immunofluorescence labeling and DAPI staining (blue) in cerebellar sections of WT and adult mice (left). Scale bar, 20 µm. The quantification of MLC1 immunostaining intensity (right). Data are expressed in arbitrary units as a ratio to the mean values obtained from WT mice (unpaired *t*-test; $^{**}P \leq 0.0070$; $n = 3$). (**C**) At EM level, MLC1 post-embedding staining in *Gpr37l1* KO showed immunoreactivity in the astrocyte–astrocyte junctions of protoplasmic (a) and perivascular (b) astroglial processes. AC, astrocyte; BV, blood vessel. Higher magnifications of boxed areas (dashed lines) in (b) are presented. Scale bar, a: 0.25 µm; b: 0.5 µm.

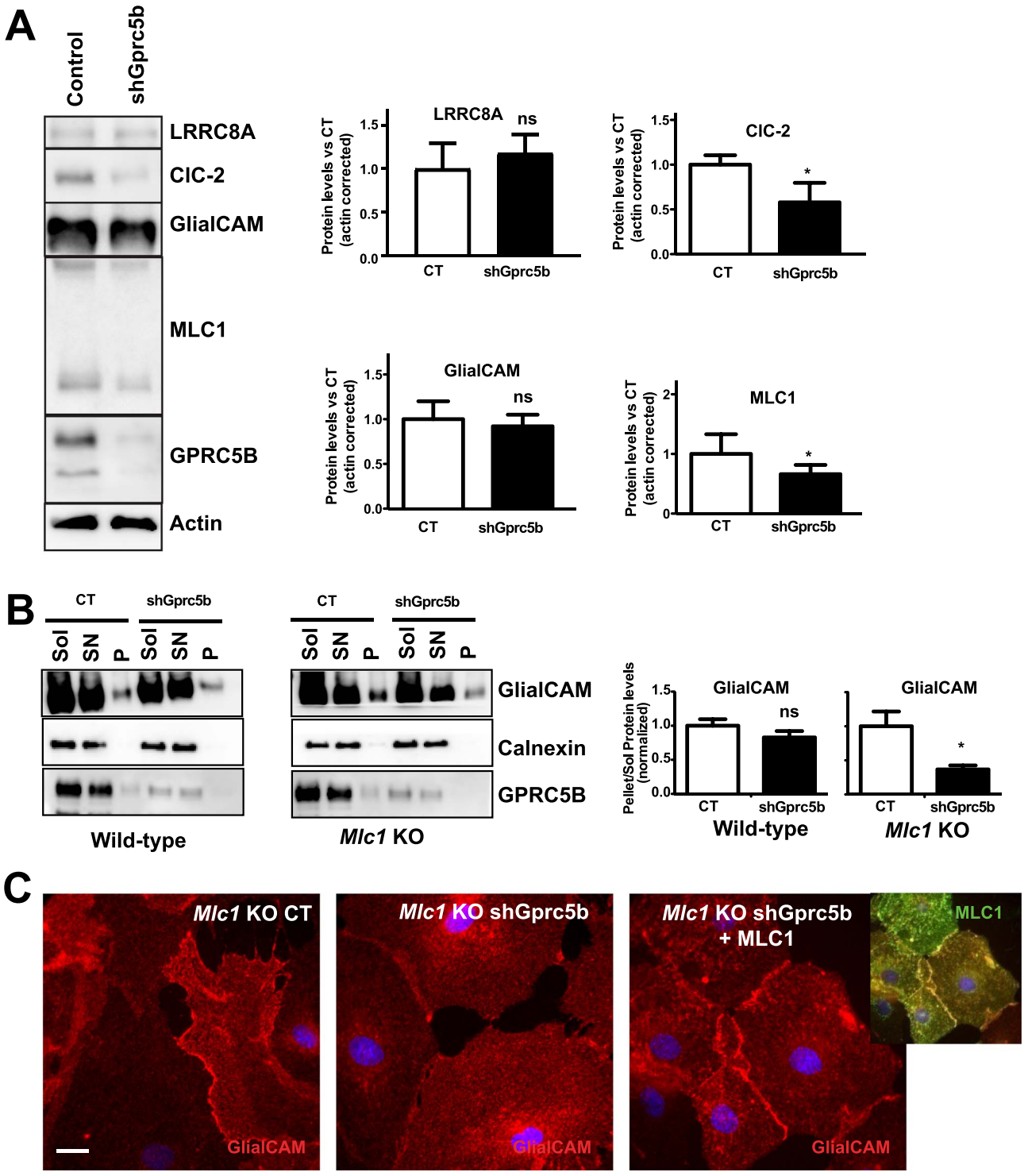

Figure 6. Characterization of GPRC5B depleted primary astrocytes. (**A**) Total protein levels of MLC1, GlialCAM, ClC-2 and LRRC8A were assessed by Western blot (left) in extracts obtained from arrested astrocytes control or infected with shRNA against *Gprc5b*. β-actin was used as a loading control, and GPRC5B was detected to validate the effect of the shRNA. The result shown is representative of four independent experiments. The quantification of these different experiments (right) revealed a decrease in protein levels in the case of ClC-2 and MLC1. $^{*}P < 0.05$ in the Student *t*-test of shRNA versus control. (**B**) Surface levels of GlialCAM in GPRC5B depleted primary astrocytes from wild-type or *Mlc1* KO mice were assessed by biotinylation and subsequent Western blot of the solubilized extract (sol), the supernantant of the purification (SN) and the purification (P). Quantification of the biotynilated fraction (P) revealed a decrease in GlialCAM membrane protein levels only in *Mlc1* KO astrocytes. $^{*}P < 0.05$ in the Student *t*-test of shRNA versus control. Calnexin was detected as a non-plasma membrane (ER) resident protein. (**C**) The misslocalization of GlialCAM in GPRC5B depleted astrocytes from *Mlc1* KO mice is corrected by complementation with human MLC1 overexpressing adenovirus (right). Scale bar: 20 µm. ns, not significant.

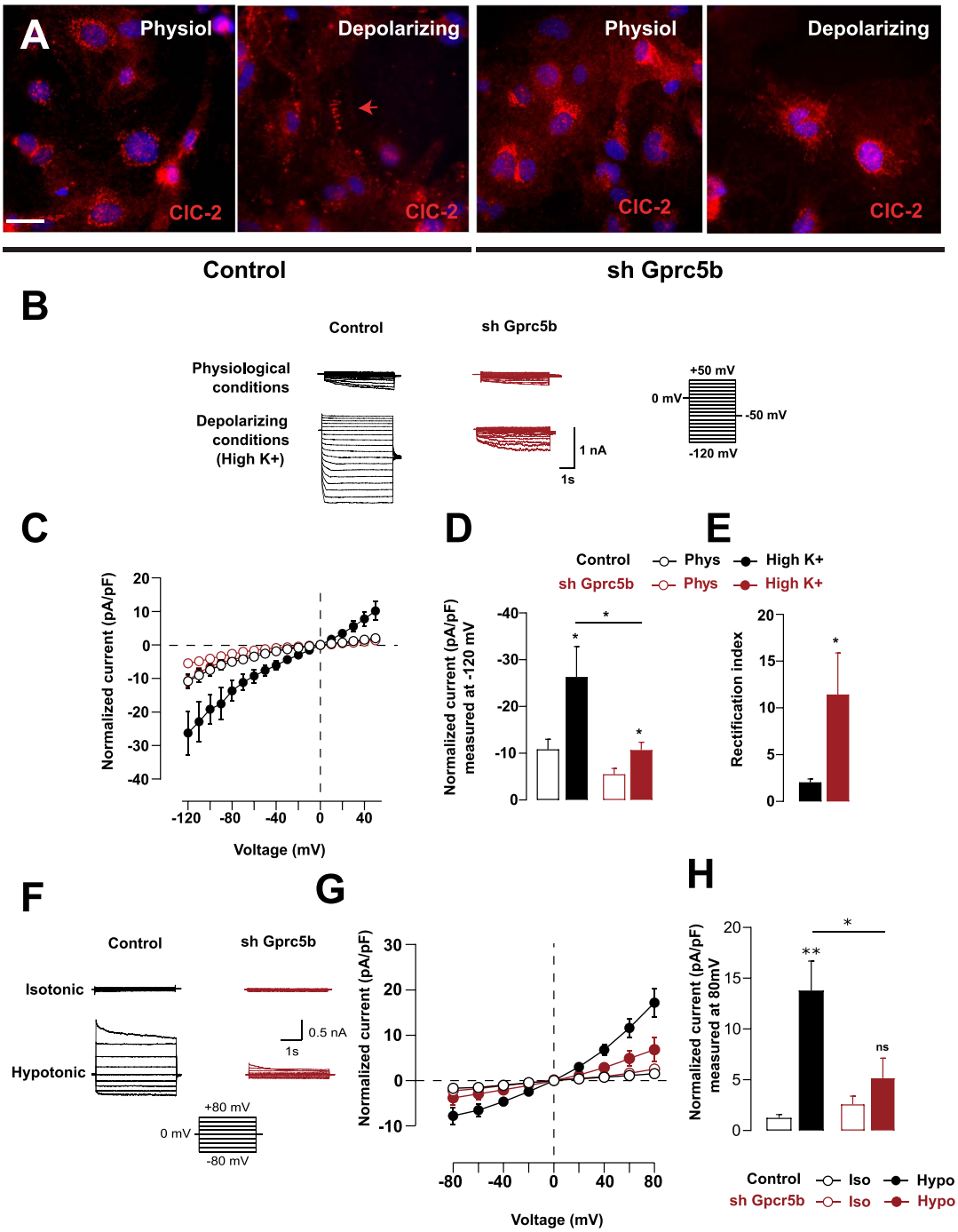

Figure 7. Lack of GPRC5B affects ClC-2 and VRAC activation in depolarizing and hypotonic conditions. (**A**) Immunostainings of ClC-2 in Control or GPRC5B depleted astrocytes treated with physiological or depolarizing solutions. GPRC5B depleted astrocytes showed a markedly reduced ClC-2 trafficking to cell–cell junctions in depolarizing conditions (arrows). $^{***}P < 0.001$ in one-way analysis of variance plus Dunnet multiple comparisons' test versus the depolarizing control. (**B–E**) Reduced activation in depolarizing conditions of the ClC-2 chloride channel in GPRC5B depleted astrocytes. (B) Representative whole-cell recordings from control and GPRC5B-depleted rat astrocytes showing ClC-2 currents evoked by voltage pulses (from −120 to +50 mV) in both physiological and depolarizing conditions. The protocol applied is depicted on the right. (C–E) Current-voltage relationships show the previously described increase in ClC-2 currents when astrocytes are treated with a depolarizing solution and a change in the rectification index. In GPRC5B-depleted astrocytes, however, this increase in the current amplitude is much smaller and no changes in the rectification index can be observed. Quantification of the current measured at −120 mV in both control and GPRC5B-depleted astrocytes can be seen in (D) and changes in the rectification index are depicted in (E). Whole-cell currents shown in (C) and (D) are normalized by cell capacitance. $^{*}P < 0.05$, $^{**}P < 0.01$. The number of experiments is Control phys = 20, Control depolarizing = 14, sh Gprc5b phys = 9, shGprc5b = 11. (**F–H**). (F) Representative whole-cell recordings from control and GPRC5B-depleted rat astrocytes showing VRAC currents evoked by voltage pulses (from −80 to +80 mV) before and after 5 min of hypotonic stimulation. The protocol applied is depicted in the middle. (G and H) Current-voltage relationships showed that current activation upon hypotonicity was not statistically significant in GPRC5B-depleted astrocytes and VRAC currents from these cells were much smaller when compared with those of control astrocytes. Quantification of the current measured at +80 mV can be seen in (H). Whole-cell currents shown in (G) and (H) are normalized by cell capacitance. ns, not significant, $^{*}P < 0.05$, $^{**}P < 0.01$. The number of experiments is Control = 12, sh Gprc5b = 8.

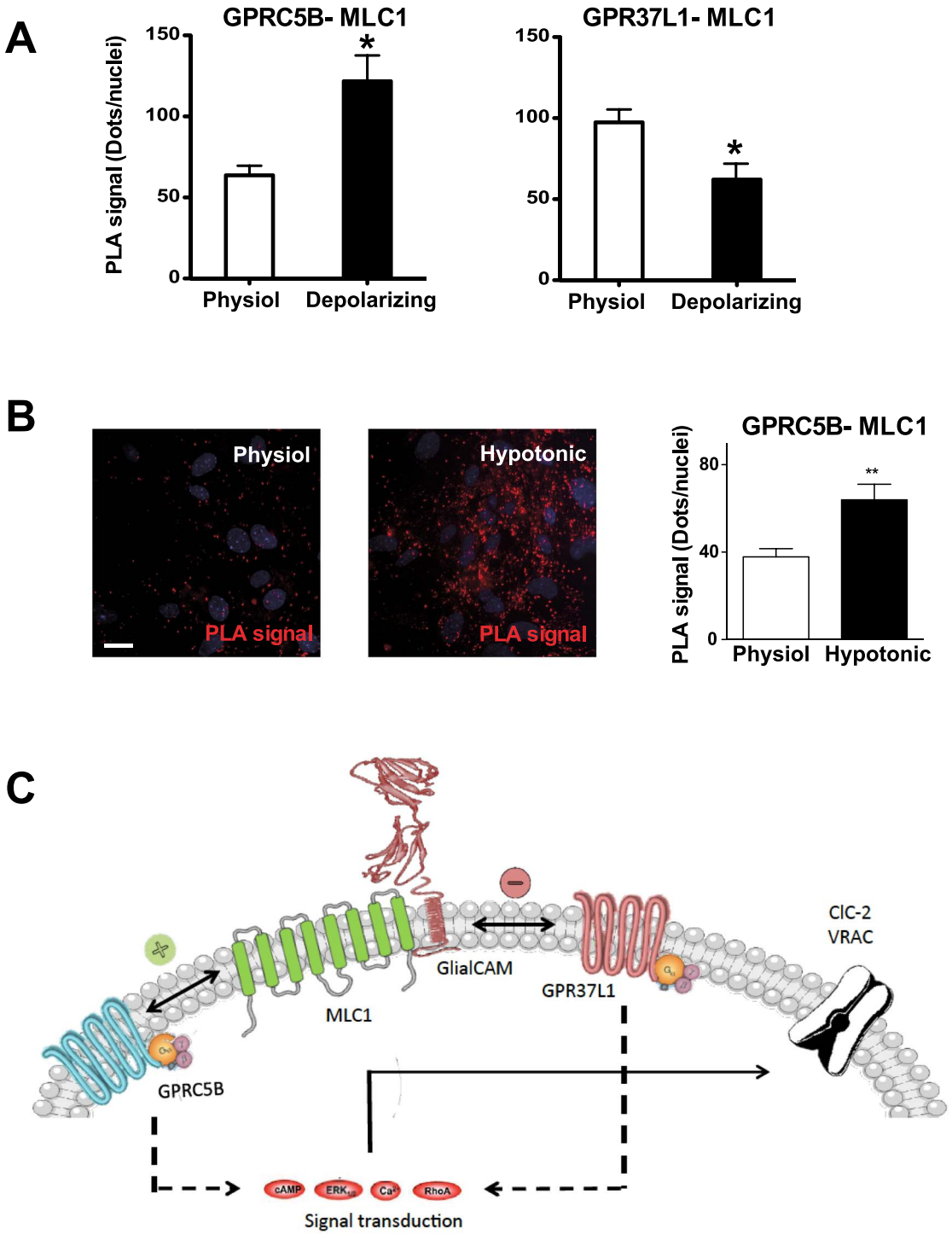

Figure 8. Depolarization and hypotonicity dynamically modulate the interactions between MLC1 and GPCRs. (**A**) The interaction of MLC1 and the GPCRs in depolarizing conditions. Astrocytes were treated with physiological or depolarizing solutions for 4 h, and then PLA between MLC1 and GPRC5B (left) or GPR37L1 (right) was assessed. The number of PLA positive dots was normalized by the negative control and quantified using Image J. Data are mean ± standard error of the mean of three-four independent experiments. $*P < 0.05$ in the Student *t*-test of depolarizing versus physiological conditions. (**B**) The interaction between GPRC5B and MLC1 protein measured by PLA increased by hypotonicity. Wild-type (WT) or *Mlc1* KO mouse cultured astrocytes were treated with physiological or hypotonic solution for 15 min, and then PLA assay between GPRC5B and MLC1 was performed. Assays were performed with mouse monoclonal anti-MLC1 and rabbit polyclonal anti-GPRC5B. *Mlc1* KO mouse astrocytes were used as negative control. Data analyses were from three independent experiments and were corrected subtracting the signal of the negative control. $**P < 0.001$ in two-tailed Student *t*-test. (**C**) Model of the interplay between MLC proteins and two of the GPCRs identified in the GlialCAM interactome. In this model, GlialCAM and MLC1 are negatively and positively regulated by GPR37L1 and GPRC5B, respectively. The interaction between the GPCRs and MLC proteins might activate signal transduction cascades previously linked to Mlc1 or these GPCRs (such as cAMP, ERK1/2, Calcium or RhoA), which will regulate different transporters and channels, as illustrated by the effects seen in this work over the ClC-2 and the VRAC chloride channels.

Depolarization and hipotonicity modulates GPCRs-MLC1 protein interaction

The above results suggested that the lack of GPR37L1 increases MLC proteins levels, whereas the opposite was observed for the lack of GPRC5B. This suggests that these GPCRs may interact with MLC proteins in a dynamic manner. Previous studies indicated that the interaction between GlialCAM/MLC1 and ClC-2 in primary cultured astrocytes was dynamically regulated, and it was observed on depolarizing conditions (23).

Then, we compared the interaction between GPRC5B or GPR37L1 with MLC1 in physiological versus depolarizing conditions in primary astrocyte cultures. PLA indicated that the interaction between MLC1 and GPRC5B was increased in depolarizing conditions whereas the interaction between GPR37L1 and MLC1 was decreased (Fig. 8A). Therefore, these experiments suggested that in depolarizing conditions GPRC5B might be needed for signal transduction responses in a GlialCAM/MLC1-dependent manner.

Subsequently, we assessed whether the interaction between MLC1 and GPRC5B also varies in hypotonic conditions performing PLA. We observed that the interaction between both proteins increased under hypotonic conditions (Fig. 8B).

Discussion

GlialCAM and MLC1 are two membrane proteins linked to a human genetic disease (MLC) and whose biological functions are poorly understood. Previous studies suggested that they might have a role in astrocyte ion/water homeostasis by influencing different ion channels and transporters. In this respect, a direct interaction after astrocyte despolarization has been observed with the chloride channel ClC-2 and it has also been shown to influence VRAC chloride channels and regulatory volume decrease after astrocyte osmotic swelling in an indirect manner. In addition, it has been shown that the overexpression of MLC1 downregulates intracellular signaling pathways controlling astrocyte activation and proliferation. In order to get more insights into the biological role of GlialCAM and MLC1, we have identified GlialCAM-interacting proteins and their association with MLC1 by means of immunoprecipitation and MYTH experiments. Our results revealed that GlialCAM forms a network of ~20 proteins.

Within this proteome there are different proteins, some of them previously identified (such as ClC-2, Cx43 or Na^+/K^+-ATPase), which are related to ion or substrate transport and are involved in the homeostasis of the extracellular media during neuronal activity. Neuronal activity in the central nervous system leads to an increase of potassium in the extracellular space (32). This increase is rapidly buffered by neighboring astrocytes through different molecular mechanisms, including the activity of pumps, transporters and ion channels. One of the most important processes contributing to potassium clearance is its uptake by astrocytes mediated by the Na^+/K^+-ATPase (33). Moreover, the ATPase is activated by intracellular increases in sodium, as occurs in astrocytes during neuronal activity because sodium-coupled glutamate transporters, mainly EAAT2 (or GLT-1) and EAAT1 (or GLAST), remove neurotransmitters from the extracellular media. Potassium may also enter into astrocytes through potassium channels, mainly Kir4.1 (34). Potassium would diffuse to neighboring astrocytes through gap junctions [composed by connexins 30 and 43 (Cx30 and Cx43)] (35,36) in a process that has been defined as spatial buffering (37,38). In addition, potassium can be accumulated inside astrocytes, which is balanced by a parallel transport of chloride to maintain electroneutrality (39). In this case, it has been suggested that chloride might enter astrocytes through ClC-2 chloride channels in association with GlialCAM/MLC1 proteins (10). Within other proteins belonging to the same group of transporter/ion channels, it is interesting to mention the sodium-driven bicarbonate transporter (NBCe1). Astrocytes contribute to the reacidification or basification of the extracellular media during neuronal activity, partly through the activation of NBCe1 (40).

The results presented here suggest that GlialCAM/MLC1 form a protein scaffold for different transporters and ion channels involved in neuronal homeostasis. Previous work has shown that GlialCAM is able to target ClC-2 to glial junctions and modify its gating properties (9). It remains unknown if GlialCAM is also able to modify the functional properties and the localization of the identified proteins. Hence, MLC disease could be caused by impaired activity of some of the proteins found in the GlialCAM interactome.

On the other hand, GlialCAM and MLC1 have been shown to influence intracellular signaling pathways controlling astrocyte activation and proliferation. Several proteins have been identified related to cell signaling within this proteome, such as three different GPCRs (GPR37, GPR37L1 and GPRC5B), a tetraspanin (CD9) (41) and the four transmembrane domain proteins Glycoprotein M6A and M6B (42,43). Considering the role played by GPCRs, we hypothesize that some of the signaling pathways involving MLC proteins might be caused by the activity of these GPCRs.

Within the identified GPCRs, GPR37 and GPR37L1 are part of the rhodopsin (Class A) family, specifically within the endothelin B receptor-like peptide family (44–47). Both GPCRs are highly expressed in the central nervous system. GPR37 is mainly expressed in oligodendrocytes, whereas GPR37L1 is mainly expressed in astrocytes with higher levels in the Bergmann glia of the cerebellum. Studies with KO mice have shown that GPR37 regulates negatively oligodendrocyte differentiation and myelination (21), and that GPR37L1 participates in regulating the development of neuronal and glial cells in the cerebellum (22). Several groups have proposed that prosaposin and derived prosaptides could bind to these GPCRs and activate them, but *in vitro* studies with induced expression of both proteins have so far failed to conclusively prove that these are the cognate ligands (17,19,48–50). It has been indicated that GPR37 and GPR37L1 are coupled to $G\alpha_{i/o}$, which will inhibit adenylate cyclase. Thus, the lack of these GPCRs results in increased cAMP levels and Epac-dependent activation of MAPK cascade, which leads to an increase in phospho-ERK1/2 (21,51). In this sense, *Mlc1* KO cells also show an increase in ERK phosphorylation and its expression is also linked to astrocyte differentiation.

GPRC5B belongs to the family C group IV (metabotropic glutamate receptor-like receptor) of GPCRs (16). GPRC5B is expressed ubiquitously, particularly in the brain, mostly in the cerebellum, adipose tissue and placenta (29). It is subcellularly localized at the plasma membrane, Golgi and exosomes (52). GPRC5B has been implicated in neuronal cell-fate determination, cerebellar motor learning, obesity and inflammation (53–56). There is not a known ligand neither a G protein coupled for GPRC5B, but it seems to recruit the Src-family kinase Fyn through the SH2 domain during its activation, and the activity of Fyn regulates inflammatory responses via NF-kB signaling (53,57). Considering MLC, it has been found that in astrocytoma, the overexpression of MLC1 inhibit the activation of IL-1β-induced inflammatory signals (pERK, pNF-kB) that, conversely, were abnormally upregulated in *Mlc1* KO astrocytes (58).

Thus, considering previous data and the present work, we suggest that these GPCRs could participate in the signaling role previously assigned to GlialCAM and MLC1 (Fig. 8C). First, we have observed that the lack of GPR37L1 upregulates GlialCAM and MLC1 whereas the lack of GPRC5B downregulates it, influencing ClC-2 and VRAC activity. As GPRC5B interacts more with MLC1 in depolarizing and hypotonic conditions, the activity of GPRC5B might be important in metabolic processes related to changes in the ionic composition. In contrast, we hypothesize that signaling through GPR37L1 might be related to differentiation processes. Although future research is needed to understand how GlialCAM and MLC1 modulate GPCR-associated signaling processes, taking into account that they interact *in vitro*, it is possible that they might regulate the activation of the GPCRs through lateral interactions.

Although the exact role played by GlialCAM and MLC1 is still unknown, this work has revealed that the role played by MLC1 is very similar to the work performed by tetraspanins. Tetraspanins are transmembrane proteins that span the plasma membrane four times and that associate with other tetraspanins by homo- and heterooligomerization (59). It has been described in many cases that they form a tight complex with a single-pass transmembrane protein belonging to the immunoglobulin (Ig) superfamily (60). For instance, the tetraspanin CD81 is associated with CD19 (61) or the tetraspanin CD9 with EWI-2 (62). Moreover, these molecules can simultaneously associate laterally at the plasma membrane with numerous integral membrane receptors, modulating their functions and organizing discrete, dynamic plasma membrane compartments (63). Within these partners, there are GPCRs (64) or other cytoplasmatic signaling mediators (65). They might also regulate the trafficking and biosynthetic processing of these partners (66). Considering MLC1, although the sequence homology to tetraspanins is very low (~20%), it passes the membrane eight times, but biochemical studies indicate that each four transmembrane domains can be considered as a duplicate (6). As tetraspanins, MLC1 also oligomerizes with himself and forms a tight complex with GlialCAM, a single-pass transmembrane domain of the Ig family (4). Here, we have also identified the tetraspanin CD9 as a protein forming part of the GlialCAM interactome and a direct interactor of MLC1. As tetraspanins, MLC1 influence the trafficking of diferent partners, as it has been shown for ClC-2 (9) or Cx43 (12). Finally, here we have shown that GlialCAM and MLC1 might be interacting with different GPCRs in a dynamic manner. Therefore, we propose that MLC1 biological role is that of being a tetraspanin-like molecule. Final proof of this hypothesis might need the determination of a 3D structure of the GlialCAM/MLC1 complex.

Understanding the interrelationship between GlialCAM/MLC1 and the GPCRs found here could be crucial not only to the development of therapies for MLC patients but also to unravel the mechanisms conducted by astrocytes to control neuronal homeostasis. In this sense, analyses of the posttranslational modifications of the interactome proteins identified here in MLC mice models as in the *Glialcam* KO, could provide novel insights into regulatory mechanisms. It would be interesting to analyze if the minor percentage of MLC patients without mutations in *GLIALCAM* or *MLC1* harbor mutations in any of the genes coding for the GPCRs identified here.

Materials and Methods

Molecular biology

Plasmids presented herein were constructed using standard molecular biology techniques employing recombinant PCR and the Multisite Gateway System (Invitrogen). The integrity of all cloned constructs was confirmed by DNA sequencing.

Animal procedures

The generation of *Glialcam*$^{-/-}$ and *Mlc1*$^{-/-}$ mice has been previously described (10). *Gpr37l1*$^{-/-}$ mice has also been previously characterized (22). For histological analyses of brains, mice were perfused with 4% PFA/PBS and organs were postfixed overnight. Mouse astrocyte cultures were performed from P0 to P2 mouse pups of the corresponding genotype as previously described (31).

Membrane preparation

Fresh-frozen brains from mouse WT and *Glialcam* KO were homogenized with a glass potter in sucrose buffer (320 mM sucrose, 10 mM Tris, 2 mM $MgCl_2$, 1 mM EGTA, protease inhibitors (5×), pH 7.5; ca. 10 ml/g tissue) and centrifuged for 5 min at 1080 × g. The supernatant (SN) was collected and the procedure was repeated with the pellet using a third of the sucrose buffer volume. Both supernatants were combined and ultracentrifuged (10 min at 200,000 ×g) to collect the crude membrane pellet. The crude membrane pellet was resuspended in hypotonic buffer (50 mM Tris/HCl pH 7.5) and allowed to lyse for 30 min on ice (with gentle stirring). The membrane lysate was then separated on a sucrose step gradient (10 ml 1.3 M sucrose and 10 ml 0.5 M sucrose, each in 10 mM Tris–HCl/1 mM Mg^{2+}/pH 7.5) for 1 h at 200,000 × g. The interface band was collected, diluted 3-fold with 20 mM Tris–HCl/1 mM Mg^{2+}/pH 7.5 and pelleted by ultracentrifugation. The pellets were resuspended in a small volume of 10 mM Tris–HCl/1 mM Mg^{2+}/pH 7.5 and the protein concentration was determined by the Bradford method.

Solubilization and AP

AP was carried out with CL47 supplemented with 1 mM Mg^{2+}. In addition to mouse WT and *Glialcam* KO membranes, a rat brain membrane preparation was used. For each purification experiment, 20 µg of immobilized antibody were incubated with 2 mg membrane solubilized with 1.6 ml CL47 (+1 mM Mg^{2+} and 4× protease inhibitors added). Solubilization was carried out at a protein-detergent ratio of 1:8, incubated for 20 min on ice and cleared by ultracentrifugation at 56,000 rpm/12 min (rotor Sorvall S80-AT3; corresponding to a 200 S cutoff for solubilized particles). After 2 h of incubation with the solubilisate antibodies were washed with CL47 dilution buffer 1 mM Mg^{2+} (2 × 1 ml for 5 min) and eluted with 2 × 7 µl non-reducing Lämmli buffer (100 mM DTT added later).

MS sample preparation and LC-MS/MS analysis

The eluates from APs were shortly run on 10% SDS-PAGE gels and silver-stained. Lanes were excised and split into two parts (> and <50 kDa), each subjected to standard in-gel tryptic digestion. Eluted peptides were vacuum-dried and redissolved in 13 µl 0.5% trifluoroacetic acid prior to MS analysis.

For comprehensive LC-MS/MS analysis, peptides were loaded on a C18 PepMap100 precolumn (5 µm; Dionex) and resolved on an analytical 75 µm × 10 cm C18 column (PicoTip™ Emitter, 75 µm, tip: 8 ± 1 µm, New Objective; self-packed with ReproSilpur 120 ODS-3, 3 µm, Dr Maisch) using an aqueous-organic gradient [UltiMate 3000 HPLC coupled to an Orbitrap XL mass

spectrometer (Thermo Scientific)]. Full spectra (with precursor signals used for quantification) were acquired with a target value of 500 000 and a nominal resolution of 60 000 (scan range 370–1700 m/z).

Up to five data-dependent collision-induced dissociation (CID) fragment spectra per scan cycle were acquired in the ion trap with a target value of 10 000 with dynamic exclusion, preview mode for full precursor scans, charge state screening, monoisotopic precursor selection and rejection charge state 1 enabled. Activation type was CID with default settings.

LC-MS/MS data were extracted and searched against the UniProt Knowledgebase (mouse, rat, human and release 2013-09) using the Mascot search engine (version 2.3.01; Matrix Science) together with anti-GlialCAM AP datasets from a previous round of experiments. For preliminary searches peptide mass tolerance was set to 15 ppm. After linear shift mass recalibration the window was narrowed to ± 5 ppm for final searches. Fragment mass tolerance was set to 0.8 Da. One missed trypsin cleavage and common variable modifications were accepted for peptide identification. Proteins identified by only one specific MS/MS spectrum or representing exogenous contaminations such as keratins or Igs were eliminated.

Analysis of GlialCAM and MLC1 interaction partners

The set of GlialCAM-APs (total of 14) was quantitatively evaluated together with an AP data set from an older experiment (previous study, 4 samples). A label-free evaluation pipeline similar to (67) was used. Briefly, m/z features among LC-MS scans were detected and their intensitied integrated (as intensity × retention time × m/z width = PV) using MaxQuant (Cox and Mann 2008, version 1.3). m/z-corrected features were then aligned between different LC-MS/MS runs and assigned to the peptides identified by Mascot using a home-written software tool with mass tolerance set to 1.5 ppm and a time shift window of 1 min. The resulting assignment showed an even distribution with very high m/z precision and no obvious systematic error (symmetric, no offsets from 0 in either dimension).

Based on the accurately assigned PVs, protein abundance ratios (rPV) in purifications from WT versus control (IgG or *Glialcam* KO) were determined using the TopCorr method (68). Protein-specific peptide PVs were ranked across the evaluated datasets by their consistency using pair-wise linear correlation analysis (Pearson correlation). A maximum of six to a minimum of two peptide PVs were then selected from the best correlating PVs to calculate the abundance ratio as median of the respective peptide PV ratios (referred to as rPV). To ensure validity, sequenced peptides with missed PV assignment were omitted and a minimum of two peptide ratios with total assigned PVs of 80 000 units were required; if no PV could be assigned to a peptide in the AP controls, the detection limit of the spectrometer (3000 PV units with the settings used here) was inserted as a minimum estimate. Distributions of protein rPV values were plotted for each sample pair to derive specificity thresholds. Proteins were considered specifically co-purified when rPV (vs IgG) > threshold (IgG) in both, rat and mouse, and no cross-reactivity was indicated by rPV(vs KO) < threshold (vs KO). For each protein, the consistency of enrichment was evaluated with the different antibodies as well as its quantitative correlation with the purified target GlialCAM_Mouse [based on abundance$_{norm}$ values, (68)].

Finally, the LC-MS/MS data from previous Mlc1 AP experiments were reprocessed and evaluated according to the same improved procedures as described above. Because these datasets did not include target KO controls, specificity could not be evaluated with the same degree of stringency. Rather high thresholds (factor 20–60) for purification rPVs versus IgG were therefore applied.

MYTH screenings

A MYTH screening was performed with the biotech Dualsystems, using the bait vector pBT3-Ste containing human MLC1. A second screening was performed using the human brain DUALmembrane cDNA library in the NubG-x orientation as described (69).

Cell culture and transfection

Human embryonic kidney HEK-293T cells were grown at 37°C in an atmosphere of 5% CO_2 in Dulbecco's modified Eagle's medium (Sigma-Aldrich, St. Louis, MO, USA) supplemented with 1 mM sodium pyruvate, 2 mM L-glutamine, 100 U/mL streptomycin, 100 mg/mL penicillin and 5% (v/v) fetal bovine serum. The cells were seeded into six-well plates containing poly-D-lysine-coated glass coverslips at ∼300 000 cells/well. Cells were transiently transfected with the corresponding cDNA constructs using Transfectin™ (Bio-Rad, Hercules CA, USA) and following the manufacturer's instructions.

Immunological procedures

For immunofluorescence staining, primary cells and tissue sections were fixed and processed as previously described (20,70). The polyclonal rabbit antibodies used were the following: anti-GlialCAM (1:100) (4), anti-MLC1 (1:100) (71), anti-ClC-2 (1:100) (9), anti-LRRC8A (1:100) (A304-175-A, Bethyl antibodies) (15) and the antibody developed in this work anti-GPRC5B against the peptide (C)TIPTAPPSHTGRHHW, using the services provided by Eurogentec. We also used a mouse monoclonal antibody that was developed against the mouse peptide sequence of the N terminus of MLC1 (TREGQFREELGYDRM) (23) and a mouse monoclonal specific for GPR37L1 (1:50 in mouse primary astrocytes, 1:100 in mouse tissue sections, Mab Technologies, Cat. N. scB12). GPR37L1 and MLC1 co-immunostaining was performed in mouse primary astrocytes from *Gpr37l1* WT and KO pups (51), after fixation with 100% methanol at -20°C for 20 min, permeabilizing with 0.1% Triton X-100 and incubating for 1 h at room temperature in blocking buffer containing 0.5% BSA, 0.3 M glycine (Merck, Cat# 104201) and 0.1% Tween-20.

For electron immunogold experiments, small samples of *Gpr37l1* cerebellum KO mice tissue were obtained and fixed in 4% paraformaldehyde and 0.1% glutaraldehyde in 0.12 m phosphate buffer, and processed. They were cryoprotected gradually in sucrose and cryofixed by immersion in liquid propane. Freeze substitution was performed at −90°C during 3 days in an Automatic Freeze Substitution System (AFS, Leica); methanol containing 0.5% uranylacetate was used as a substitution medium. Infiltration was carried out in Lowicryl HM20 at −50°C and then polymerized with UV light. Ultrathin sections were collected, and when needed, processed for post embedding immunostaining. For immunostaining, grids were incubated with rabbit anti-MLC1 (1:10) or antisera. The binding of the primary antibody was visualized by incubating with a secondary antibody conjugated to 18 nm gold particles (British BioCell, International).

In the western blot studies, astrocyte lysates and cerebellar extracts were prepared and processed as previously described

(20,72). The mouse GPR37L1 protein was detected with a goat polyclonal antibody (1:500, Santa Cruz, Cat. N. sc-164532). β-actin or α-tubulin proteins were used as a loading control.

To detect surface levels of GlialCAM, WT or *Mlc1* KO mouse astrocytes were cultured in 6 cm plates. They were washed 3 times with PBS-CM (PBS with 1 mM $CaCl_2$ and 1 mM $MgCl_2$). Subsequently, the astrocytes were incubated on ice for 30 min in PBS-CM containing 2 mg/ml EZ-LinkTM Sulfo-NHS-Biotin (Thermo Scientific). After three washes with PBS-CM, they were quenched for 10 min in PBS Ca/Mg containing 10 mM Lysine. After three additional washes with PBS-CM, the cells were lysed in RIPA buffer (50 mM Tris pH 8, 150 mM NaCl, 1% NP-40, 0.5% deoxycholate, 0.1% SDS, 2 mM EDTA) containing protease inhibitors, for 1 h. After centrifugation for 15 min at 14 000 rpm, the lysate was quantified using the BCA protein assay (Thermo Fisher). Then 2 mg of the solubilized extract in a total volume of 200 µl was incubated with 100 µl of streptavidin agarose (Thermo Fisher) O/N at 4°C. After a brief centrifugation, the SN was taken and the beads were washed three times with RIPA buffer. Biotinylated proteins were eluted with LSB 1× for 15 min at 60°C. Samples of lysate, SN and eluate were analyzed by western blot. To confirm that only membrane proteins were detected in the eluate, we performed a western blot with antibodies to test for the protein calnexin resident in the endoplasmic reticulum.

GVUs purification

GVUs were isolated from whole WT OF1 brains as previously described (24). A selective filtration was performed to enrich vessels of 20 to 100 am diameter (24). For immunostaining, GVUs were plated on a glass slide coated with Cell Tak (Corning, Corning, NY, USA) and fixed in PBS/PFA 4% for 15 min at room temperature. GVUs were immersed in the blocking solution (PBS/NGS 5%/Triton X-100 0.5%) for 1 h at room temperature and incubated with primary antibodies and Isolectin GS-B4 (IB4) diluted in the blocking solution 12 h at 4°C. After 3 PBS washes, slices or GVUs were incubated 2 h at room temperature with secondary antibodies, rinsed in PBS and finally embedded in Fluormount G. GVUs were analyzed using a 63X objective on a confocal microscope.

Quantification of immunofluorescence and western blot labeling

Quantitative analysis of immunofluorescence signals was performed with the Imaris 5.0.2 software (Bitplane). Experiments were carried out with tissue samples obtained from three mice per genotype. Sections of similar size in similar regions were chosen and analyzed. All measurements were performed with the observer blind to the identity of the slides.

Quantification of western blot immunoreactive bands was performed with the Chemidoc XRS+ imager and Image Lab software (Bio-Rad). Experiments were carried out with tissue extracts obtained from six to seven mice per genotype. The intensity of each band was normalized to the intensity of the corresponding α-tubulin band. The average values of each experimental group were expressed in arbitrary units, as a ratio to the mean values obtained from the WT groups.

Primary astrocyte culture, adenoviral transduction and RNA interference

Rat primary quiescent astrocyte cultures were prepared as described previously (20) and maintained in culture in the presence of the mitotic inhibitor AraC for biochemical studies. Dibutyryl-cAMP (dBcAMP) differentiated rat astrocytes obtained as described elsewhere (73), were used for electrophysiological measurements, because they express higher levels of ClC-2 currents and are easier to patch. Immunofluorescence experiments were performed on both types of cultures, with similar results. The physiological solution was: (in mM) NaCl 122, KCl 3.3, $MgSO_4$ 0.4, $CaCl_2$ 1.3, KH_2PO_4 1.2, HEPES 25, Glucose 10 and it had pH 7.4. The osmolarity was 290–300 mOsm and was adjusted with manitol using a vapor-pressure osmometer (Model 3320, Advanced Instruments). In the hypoosmolar solution the osmolarity was adjusted to 180 mOsm/kg. Adenovirus expressing HA-tagged MLC1, and the transduction of astrocytes has been described previously (4). RNAi entry-clone (Gateway, Invitrogen) vectors were prepared using the Block-it PolII miR RNAi EmGFP or the Block-it PolII miR RNAi expression vector kit following the manufacturer's instructions. Entry clones were recombined using LR clonase into the vector pAdVDEST-CMV/V5. Adenoviruses were produced and titrated using fluorescence microscopy detecting EmGFP, which is expressed together with the shRNA, or detecting the viral protein Ad-Hexon. The sequence of the oligo used to knock down mouse GPRC5B expression was: shRNA Gprc5b (shRNA111): 5′ TGGACTGGACCTTCTTCCTCA 3′.

Proximity-ligation assays

Mouse cultured astrocytes seeded on 24 well coverslips were treated with physiological, depolarizing (60 mM K^+) or hypotonic solutions and then were fixed with PFA 3%. Cells were blocked with PBS1x/0.1% Triton X-100/10% FBS for 2 h, and then incubated with the primary antibodies (Mouse monoclonal or Rabbit anti-MLC1 antibody 1:100; Rabbit polyclonal anti-GPRC5B antibody 1:100, Mouse monoclonal anti-GPR37L1 1:100) diluted in blocking solution for 1 h. After 3 washes of 10 min with blocking solution, cells were incubated with the anti-rabbit PLA (+) and the anti-mouse PLA (−) probes (Sigma) diluted 1/5 in blocking solution for 1 h in a 37°C humid chamber. Cells were washed twice with washing buffer A (Sigma) during 5 min. To ligate the PLA probes, cells were incubated in ligation buffer diluted 1/5 in water containing the ligase diluted 1/40 for 1 h in a 37°C humid chamber. After 2 washes with washing buffer A of 2 min, the amplification reaction was performed in ampli RED buffer diluted 1/5 in water containing the polymerase diluted 1/80 for 100 min in a 37°C humid chamber. Cells were washed twice with washing buffer B during 10 min, followed by an additional wash with washing buffer B diluted at 0.01% during 1 min. Finally, coverslips were mounted in DUOLINK DAPI medium and images were acquired using a CellR olympus microscope.

To quantify the PLA signal, images were analyzed using ImageJ (74). First, nuclei were identified and substracted. Then, images were transformed to 8 bit and converted to binary images using the threshold setup. The number of dots/particles corresponding to the PLA signal was quantified using the analyse particle command of the ImageJ submenu, considering that the size (2^) of the particles should be bigger than 5. For each image, we determined the number of dots divided by the number of nuclei.

BRET experiments

HEK293T cells were transfected with a constant amount of GPRC5B-Rluc (200 ng), GPR37L1-Rluc, GlialCAM-Rluc or LRRC8A-Rluc and increasing amounts of MLC1-VFP or GlialCAM-VFP.

Equal DNA ratios were maintained with co-transfection or the empty vector pCDNA3.1, which equilibrated the total amount of transfected DNA. Forty-eight hours post-transfection, cells were washed three times with PBS, detached and resuspended in Hanks balanced salt solution (Thermo Fisher Scientific). An aliquot was used to determine the protein concentrations via the BCA assay, to control the total amount of protein used in the assay. Accordingly, cells were diluted to a density corresponding to a final protein concentration of 600 ng/µl. Cell suspensions (corresponding to 20 µg protein) were distributed in duplicates into white and black 96-well microplates (#3600 and #3650; Corning, Stockholm, Sweden) for $BRET^1$ and fluorescence measurements, respectively. The substrate, h-coelenterazine (Molecular Probes, Eugene, OR, USA) was added at a 5 µM final concentration. After 1 min ($BRET^1$) and 10 min (Rluc total), the signals were measured using the ClarioSTAR microplate reader (BMG Labtech, Ortenberg, Germany) through the sequential integration of signal detection at 475 nm (445–505 nm) and 530 nm (500–560 nm). The net BRET1 ratio was expressed as a ratio of the light intensity at 530 nm over 475 nm by substracting the background signal, which was detected when the Rluc fusion proteins were only expressed with pCDNA3.1. The $BRET^1$ curve was obtained by fitting the data points to a non-linear regression equation assuming a single binding site using GraphPad Prism version 6.00 (San Diego, CA, USA).

Patch-clamp experiments of astrocytes

Three days before the experiment, dB-cAMP-differentiated astrocytes were trypsinized and seeded at a density of $1 - 3 \times 10^4$ cells onto 24-well plates containing a glass coverslip with supplemented DMEM and 250 µM dBcAMP. The glass coverslip was mounted on the stage of inverted microscopy equipped with phase-contrast optics and fluorescence illumination. Patch pipettes were pulled from borosilicate glass capillaries (Clark Electromedical, UK) in a Flaming/Brown micropipettepuller P-97 (Sutter instruments). The electrophysiological recordings were performed with a patch clamp amplifier (Axopatch 200B, Molecular Devices, Union City, CA). The electrodes had a resistance of 4–5 MΩ when filled with intracellular solution (in mM): 144 NMDG-Cl, 2 $MgCl_2$, 5 EGTA, 5 HEPES, 5 Glucose with pH 7.3 and 300 mOsm/kg.

To measure VRAC and ClC-2 currents, the extracellular solution contained (in mM): 144 NMDG-Cl, 2 $CaCl_2$, 2 $MgCl_2$, 5 HEPES, 5 glucose, with pH 7.3 and 300 mOsm/kg. For VRAC, hypotonic extracellular solution (−25%) was obtained by decreasing the NMDG-Cl concentration to 105 mM (220 mOsm/kg). For ClC-2, the depolarizing extracellular solution contained (in mM): 144 NaCl, 11 KCl, 1.3 $CaCl_2$, 0.4 $MgSO_2$, 1.2 KH_2PO_4, 25 HEPES-NaOH, 10 glucose, with pH 7.2 and 300 mOsm/kg. All the solution osmolarities were adjusted with sorbitol. An Ag/AgCl ground electrode mounted in a 3 M KCl agar bridge was used. Membrane currents were recorded in the whole-cell patch clamp configuration, filtered at 2 kHz, digitized at 10 kHz and acquired with pClamp 10 software (Molecular Devices). Data were analyzed with Clampfit 10 (Molecular Devices) and Prism 4 (GraphPad Software, Inc., La Jolla, CA). Whole-cell capacitance and series resistance were compensated with the amplifier circuitry. Series resistance was always kept below 10 MΩ and compensated at 70–80%. All recordings were performed at room temperature (22–23°C). Currents were evoked in 4 s pulses from −120 to +50 mV (Δ10 mV) to measure ClC-2 currents and from −80 to +80 mV (Δ20 mV) to measure VRAC currents. The holding potential was 0 mV.

Statistics

Statistical significance was assessed between two groups using the unpaired or paired Student's test as appropiate. For statistical analyses of multiple groups, one-way analysis of variance and multiple comparison's test (Dunnet) versus control groups were performed.

Supplementary Material

Supplementary Material is available at *HMG* online.

Acknowledgements

This study was supported by MICINN (SAF 2015-70377 and RTI2018-093493-B-I00 and ISCIII (ERARE) to RE. RE was awarded with Icrea Academia prizes (2009 and 2014). A.G. and M.C.S. work has been financed by 'Fondation pour la recherche médicale' (PLP20170939025p60 to A.G.; AJE20171039094 to M.C.S.) and the European Leukodystrophies Association (ELA International) Research Foundation (2019-010 C4A). V.N. was supported by Spanish Health Institute Carlos III Grant PI16/00267-R-FEDER and Generalitat de Catalunya grant SGR2017-191. V.N. and R.E. thanks CERCA Programme/Generalitat de Catalunya for IDIBELL support. It was also funded by European Union, Fondo Europeo de Desarrollo regional, Ministerio de Ciencia e Innovación and Instituto de Salud Carlos III of Spain FIS P17/00296 (XG), RETICS Oftared RD16/0008/0014 (XG), Generalitat de Catalunya 2017SGR737 (XG) and Maria de Maeztu MDM-2017-0729 to Institut de Neurociencies, Universitat de Barcelona.
We thank Thomas Jentsch for providing brains from *Glialcam* KO mice and two different GlialCAM antibodies. We thank Esther prat for managing the colonies of KO mice.

Conflict of Interest statement. None declared.

References

1. van der Knaap, M.S.S., Boor, I. and Estévez, R. (2012) Megalencephalic leukoencephalopathy with subcortical cysts: chronic white matter oedema due to a defect in brain ion and water homoeostasis. *Lancet Neurol.*, **11**, 973–985.
2. Hamilton, E.M.C., Tekturk, P., Cialdella, F. *et al.* (2018) Megalencephalic leukoencephalopathy with subcortical cysts. *Neurology*, **90**, e1395–e1403.
3. Leegwater, P.A., Yuan, B.Q., van der Steen, J. *et al.* (2001) Mutations of MLC1 (KIAA0027), encoding a putative membrane protein, cause megalencephalic leukoencephalopathy with subcortical cysts. *Am. J. Hum. Genet.*, **68**, 831–838.
4. López-Hernández, T., Ridder, M.C., Montolio, M. *et al.* (2011) Mutant GlialCAM causes megalencephalic leukoencephalopathy with subcortical cysts, benign familial macrocephaly, and macrocephaly with retardation and autism. *Am. J. Hum. Genet.*, **88**, 422–432.
5. Lopez-Hernandez, T., Sirisi, S., Capdevila-Nortes, X. *et al.* (2011) Molecular mechanisms of MLC1 and GLIALCAM mutations in megalencephalic leukoencephalopathy with subcortical cysts. *Hum. Mol. Genet.*, **20**, 3266–3277.
6. Bosch, A. and Estévez, R. (2021) Megalencephalic leukoencephalopathy: insights into pathophysiology and perspectives for therapy. *Front. Cell. Neurosci.*, **14**, 627887.
7. Capdevila-Nortes, X., López-Hernández, T., Apaja, P.M. *et al.* (2013) Insights into MLC pathogenesis: GlialCAM is an MLC1 chaperone required for proper activation of volume-regulated anion currents. *Hum. Mol. Genet.*, **22**, 4405–4416.

8. Ridder, M.C., Boor, I., Lodder, J.C. *et al.* (2011) Megalencephalic leucoencephalopathy with cysts: defect in chloride currents and cell volume regulation. *Brain*, **134**, 3342–3354.
9. Jeworutzki, E., López-Hernández, T., Capdevila-Nortes, X. *et al.* (2012) GlialCAM, a protein defective in a leukodystrophy, serves as a ClC-2 Cl - channel auxiliary subunit. *Neuron*, **73**, 951–961.
10. Hoegg-Beiler, M.B., Sirisi, S., Orozco, I.J. *et al.* (2014) Disrupting MLC1 and GlialCAM and ClC-2 interactions in leukodystrophy entails glial chloride channel dysfunction. *Nat. Commun.*, **5**, 3475.
11. Sugio, S., Tohyama, K., Oku, S. *et al.* (2017) Astrocyte-mediated infantile-onset leukoencephalopathy mouse model. *Glia*, **65**, 150–168.
12. Wu, M., Moh, M.C. and Schwarz, H. (2016) HepaCAM associates with connexin 43 and enhances its localization in cellular junctions. *Sci. Rep.*, **6**, 36218.
13. Lanciotti, A., Brignone, M.S., Belfiore, M. *et al.* (2020) Megalencephalic leukoencephalopathy with subcortical cysts disease-linked MLC1 protein favors gap-junction intercellular communication by regulating connexin 43 trafficking in astrocytes. *Cell*, **9**, 1425.
14. Lanciotti, A., Brignone, M.S., Visentin, S. *et al.* (2016) Megalencephalic leukoencephalopathy with subcortical cysts protein-1 regulates epidermal growth factor receptor signaling in astrocytes. *Hum. Mol. Genet.*, **25**, 1543–1558.
15. Elorza-Vidal, X., Sirisi, S., Gaitán-Peñas, H. *et al.* (2018) GlialCAM/MLC1 modulates LRRC8/VRAC currents in an indirect manner: implications for megalencephalic leukoencephalopathy. *Neurobiol. Dis.*, **119**, 88–99.
16. Hirabayashi, Y. and Kim, Y.J. (2020) Roles of GPRC5 family proteins: focusing on GPRC5B and lipid-mediated signalling. Roles of GPRC5 family proteins: focusing on GPRC5B and lipid-mediated signalling. *J. Biochem.*, **167**, 541–547.
17. Smith, N.J. (2015) Drug discovery opportunities at the endothelin B receptor-related orphan g protein-coupled receptors, GPR37 and GPR37L1. Drug discovery opportunities at the endothelin B receptor-related orphan g protein-coupled receptors, GPR37 and GPR37L1. *Front. Pharmacol.*, **6**, 275.
18. Brignone, M.S., Lanciotti, A., Macioce, P. *et al.* (2011) The beta1 subunit of the Na,K-ATPase pump interacts with megalencephalic leucoencephalopathy with subcortical cysts protein 1 (MLC1) in brain astrocytes: new insights into MLC pathogenesis. *Hum. Mol. Genet.*, **20**, 90–103.
19. Meyer, R.C., Giddens, M.M., Schaefer, S.A. *et al.* (2013) GPR37 and GPR37L1 are receptors for the neuroprotective and glioprotective factors prosaptide and prosaposin. *Proc. Natl. Acad. Sci. U. S. A.*, **110**, 9529–9534.
20. Duarri, A., Lopez de Heredia, M., Capdevila-Nortes, X. *et al.* (2011) Knockdown of MLC1 in primary astrocytes causes cell vacuolation: a MLC disease cell model. *Neurobiol. Dis.*, **43**, 228–238.
21. Yang, H.J., Vainshtein, A., Maik-Rachline, G. *et al.* (2016) G protein-coupled receptor 37 is a negative regulator of oligodendrocyte differentiation and myelination. *Nat. Commun.*, **7**, 10884.
22. Marazziti, D., Di Pietro, C., Golini, E. *et al.* (2013) Precocious cerebellum development and improved motor functions in mice lacking the astrocyte cilium-, patched 1-associated Gpr37l1 receptor. *Proc. Natl. Acad. Sci. U. S. A.*, **110**, 16486–16491.
23. Sirisi, S., Elorza-Vidal, X., Arnedo, T. *et al.* (2017) Depolarization causes the formation of a ternary complex between GlialCAM, MLC1 and ClC-2 in astrocytes: implications in megalencephalic leukoencephalopathy. *Hum. Mol. Genet.*, **26**, 2436–2450.
24. Boulay, A.C., Saubaméa, B., Declèves, X. *et al.* (2015) Purification of mouse brain vessels. *J. Vis. Exp.*, (105), e53208.
25. Jolly, S., Bazargani, N., Quiroga, A.C. *et al.* (2018) G protein-coupled receptor 37-like 1 modulates astrocyte glutamate transporters and neuronal NMDA receptors and is neuroprotective in ischemia. *Glia*, **66**, 47–61.
26. Qiu, Z., Dubin, A.E., Mathur, J. *et al.* (2014) SWELL1, a plasma membrane protein, is an essential component of volume-regulated Anion Channel. *Cell*, **157**, 447–458.
27. Voss, F.K., Ullrich, F., Münch, J. *et al.* (2014) Identification of LRRC8 heteromers as an essential component of the volume-regulated anion channel VRAC. *Science*, **344**, 634–638.
28. Gaitán-Peñas, H., Apaja, P.M., Arnedo, T. *et al.* (2017) Leukoencephalopathy-causing CLCN2 mutations are associated with impaired Cl− channel function and trafficking. *J. Physiol.*, **595**, 6993–7008.
29. Sano, T., Kim, Y.J., Oshima, E. *et al.* (2011) Comparative characterization of GPRC5B and GPRC5C LacZ knockin mice; behavioral abnormalities in GPRC5B-deficient mice. *Biochem. Biophys. Res. Commun.*, **412**, 460–465.
30. Sano, T., Kohyama-Koganeya, A., Kinoshita, M.O. *et al.* (2018) Loss of GPRC5B impairs synapse formation of Purkinje cells with cerebellar nuclear neurons and disrupts cerebellar synaptic plasticity and motor learning. *Neurosci. Res.*, **136**, 33–47.
31. Sirisi, S., Folgueira, M., López-Hernández, T. *et al.* (2014) Megalencephalic leukoencephalopathy with subcortical cysts protein 1 regulates glial surface localization of GLIALCAM from fish to humans. *Hum. Mol. Genet.*, **23**, 5069–5086.
32. Larsen, B.R., Assentoft, M., Cotrina, M.L. *et al.* (2014) Contributions of the Na+/K+-ATPase, NKCC1, and Kir4.1 to hippocampal K+ clearance and volume responses. *Glia*, **62**, 608–622.
33. Larsen, B.R., Stoica, A. and MacAulay, N. (2016) Managing brain extracellular K+ during neuronal activity: the physiological role of the Na+/K+-ATPase subunit isoforms. Managing brain extracellular K+ during neuronal activity: the physiological role of the Na+/K+-ATPase subunit isoforms. *Front. Physiol.*, **7**, 141.
34. Djukic, B., Casper, K.B., Philpot, B.D. *et al.* (2007) Conditional knock-out of Kir4.1 leads to glial membrane depolarization, inhibition of potassium and glutamate uptake, and enhanced short-term synaptic potentiation. *J. Neurosci.*, **27**, 11354–11365.
35. Rouach, N., Koulakoff, A. and Giaume, C. (2004) Neurons set the tone of gap junctional communication in astrocytic networks. *Neurochem. Int.*, **45**, 265–272.
36. Pannasch, U., Vargova, L., Reingruber, J. *et al.* (2011) Astroglial networks scale synaptic activity and plasticity. *Proc. Natl. Acad. Sci.*, **108**, 8467–8472.
37. Bellot-Saez, A., Kékesi, O., Morley, J.W. *et al.* (2017) Astrocytic modulation of neuronal excitability through K+ spatial buffering. *Neurosci. Biobehav. Rev.*, **77**, 87–97.
38. Kofuji, P. and Newman, E.A. (2004) Potassium buffering in the central nervous system. *Neuroscience*, **129**, 1043–1054.
39. MacAulay, N. (2020) Molecular mechanisms of K+ clearance and extracellular space shrinkage—glia cells as the stars. Molecular mechanisms of K+ clearance and extracellular space shrinkage—glia cells as the stars. *Glia*, **68**, 2192–2211.

40. Theparambil, S.M., Hosford, P.S., Ruminot, I. *et al.* (2020) Astrocytes regulate brain extracellular pH via a neuronal activity-dependent bicarbonate shuttle. *Nat. Commun.*, **11**, 5073.
41. Charrin, S., Jouannet, S., Boucheix, C. *et al.* (2014) Tetraspanins at a glance. *J. Cell Sci.*, **127**, 3641–3648.
42. Ito, Y., Honda, A. and Igarashi, M. (2018) Glycoprotein M6a as a signaling transducer in neuronal lipid rafts. *Neurosci. Res.*, **128**, 19–24.
43. Zhang, X., Xie, H., Chang, P. *et al.* (2019) Glycoprotein M6B interacts with TβRI to activate TGF-β-Smad2/3 signaling and promote smooth muscle cell differentiation. *Stem Cells*, **37**, 190–201.
44. Zeng, Z., Su, K., Kyaw, H. *et al.* (1997) A novel endothelin receptor type-B-like gene enriched in the brain. *Biochem. Biophys. Res. Commun.*, **233**, 559–567.
45. Marazziti, D., Golini, E., Gallo, A. *et al.* (1997) Cloning of GPR37, a gene located on chromosome 7 encoding a putative g- protein-coupled peptide receptor, from a human frontal brain EST library. *Genomics*, **45**, 68–77.
46. Marazziti, D., Gallo, A., Golini, E. *et al.* (1998) Molecular cloning and chromosomal localization of the mouse Gpr37 gene encoding an orphan G-protein-coupled peptide receptor expressed in brain and testis. *Genomics*, **53**, 315–324.
47. Valdenaire, O., Giller, T., Breu, V. *et al.* (1998) A new family of orphan G protein-coupled receptors predominantly expressed in the brain. *FEBS Lett.*, **424**, 193–196.
48. Liu, B., Mosienko, V., Vaccari Cardoso, B. *et al.* (2018) Glio- and neuro-protection by prosaposin is mediated by orphan G-protein coupled receptors GPR37L1 and GPR37. *Glia*, **66**, 2414–2426.
49. Lundius, E.G., Vukojevic, V., Hertz, E. *et al.* (2014) GPR37 protein trafficking to the plasma membrane regulated by prosaposin and GM1 gangliosides promotes cell viability. *J. Biol. Chem.*, **289**, 4660–4673.
50. Meyer, R.C., Giddens, M.M., Coleman, B.M. *et al.* (2014) The protective role of prosaposin and its receptors in the nervous system. The protective role of prosaposin and its receptors in the nervous system. *Brain Res.*, **1585**, 1–12.
51. La Sala, G., Di Pietro, C., Matteoni, R. *et al.* (2020) Gpr37l1/prosaposin receptor regulates Ptch1 trafficking, Shh production, and cell proliferation in cerebellar primary astrocytes. *J. Neurosci. Res.*. doi: 10.1002/jnr.24775.
52. Kwon, S.H., Liu, K.D. and Mostov, K.E. (2014) Intercellular transfer of GPRC5B via exosomes drives HGF-mediated outward growth. *Curr. Biol.*, **24**, 199–204.
53. Kim, Y.J., Sano, T., Nabetani, T. *et al.* (2012) GPRC5B activates obesity-associated inflammatory signaling in adipocytes. *Sci. Signal.*, **5**, ra85.
54. Zambrano, S., Möller-Hackbarth, K., Li, X. *et al.* (2019) GPRC5B modulates inflammatory response in glomerular diseases via NF-κB pathway. *J. Am. Soc. Nephrol.*, **30**, 1573–1586.
55. von Samson-Himmelstjerna, F.A., Freundt, G., Nitz, J.T. *et al.* (2019) The orphan receptor GPRC5B modulates inflammatory and fibrotic pathways in cardiac fibroblasts and mice hearts. *Biochem. Biophys. Res. Commun.*, **514**, 1198–1203.
56. Kim, Y.J. and Hirabayashi, Y. (2018) Caveolin-1 prevents palmitate-induced NF-κB signaling by inhibiting GPRC5B-phosphorylation. *Biochem. Biophys. Res. Commun.*, **503**, 2673–2677.
57. Kim, Y.-J., Greimel, P. and Hirabayashi, Y. (2018) GPRC5B-mediated sphingomyelin synthase 2 phosphorylation plays a critical role in insulin resistance. i*Science*, **8**, 250–266.
58. Brignone, M.S., Lanciotti, A., Serafini, B. *et al.* (2019) Megalencephalic leukoencephalopathy with subcortical cysts Protein-1 (MLC1) counteracts astrocyte activation in response to inflammatory signals. *Mol. Neurobiol.*, **56**, 8237–8254.
59. Hemler, M.E. (2005) Tetraspanin functions and associated microdomains. Tetraspanin functions and associated microdomains. *Nat. Rev. Mol. Cell Biol.*, **6**, 801–811.
60. Robert, J.M.H., Amoussou, N.G., Le Mai, H. *et al.* (2021) Tetraspanins: useful multifunction proteins for the possible design and development of small-molecule therapeutic tools. Tetraspanins: useful multifunction proteins for the possible design and development of small-molecule therapeutic tools. *Drug Discov. Today*, **26**, 56–68.
61. Susa, K.J., Rawson, S., Kruse, A.C. *et al.* (2021) Cryo-EM structure of the B cell co-receptor CD19 bound to the tetraspanin CD81. *Science*, **371**, 300–305.
62. Oosterheert, W., Xenak, K.T., Neviani, V. *et al.* (2020) Implications for tetraspanin-enriched microdomain assembly based on structures of CD9 with EWI-F. *Life Sci. Alliance*, **3**, e202000883.
63. Barreiro, O., Zamai, M., Yáñez-Mó, M. *et al.* (2008) Endothelial adhesion receptors are recruited to adherent leukocytes by inclusion in preformed tetraspanin nanoplatforms. *J. Cell Biol.*, **183**, 527–542.
64. Little, K.D., Hemler, M.E. and Stipp, C.S. (2004) Dynamic regulation of a GPCR-Tetraspanin-G protein complex on intact cells: central role of CD81 in facilitating GPR56-Gαq/11 association. *Mol. Biol. Cell*, **15**, 2375–2387.
65. Termini, C.M. and Gillette, J.M. (2017) Tetraspanins function as regulators of cellular signaling. Tetraspanins function as regulators of cellular signaling. *Front. Cell Dev. Biol.*, **5**, 34.
66. Yang, Y., Liu, X.R., Greenberg, Z.J. *et al.* (2020) Open conformation of tetraspanins shapes interaction partner networks on cell membranes. *EMBO J.*, **39**, e105246.
67. Schwenk, J., Harmel, N., Brechet, A. *et al.* (2012) High-resolution proteomics unravel architecture and molecular diversity of native AMPA receptor complexes. *Neuron*, **74**, 621–633.
68. Bildl, W., Haupt, A., Müller, C.S. *et al.* (2012) Extending the dynamic range of label-free mass spectrometric quantification of affinity purifications. *Mol. Cell. Proteomics*, **11**, M111.007955.
69. Sokolina, K., Kittanakom, S., Snider, J. *et al.* (2017) Systematic protein–protein interaction mapping for clinically relevant human GPCRs. *Mol. Syst. Biol.*, **13**, 918.
70. La Sala, G., Marazziti, D., Di Pietro, C. *et al.* (2015) Modulation of Dhh signaling and altered Sertoli cell function in mice lacking the GPR37-prosaposin receptor. *FASEB J.*, **29**, 2059–2069.
71. Teijido, O., Martinez, A., Pusch, M. *et al.* (2004) Localization and functional analyses of the MLC1 protein involved in megalencephalic leukoencephalopathy with subcortical cysts. *Hum. Mol. Genet.*, **13**, 2581–2594.
72. Di Pietro, C., La Sala, G., Matteoni, R. *et al.* (2019) Genetic ablation of Gpr37l1 delays tumor occurrence in Ptch1 +/− mouse models of medulloblastoma. *Exp. Neurol.*, **312**, 33–42.
73. Ferroni, S., Marchini, C., Nobile, M. *et al.* (1997) Characterization of an inwardly rectifying chloride conductance expressed by cultured rat cortical astrocytes. *Glia*, **21**, 217–227.
74. Schneider, C.A., Rasband, W.S. and Eliceiri, K.W. (2012) NIH image to ImageJ: 25 years of image analysis. *Nat. Methods*, **9**, 671–675.

International Journal of
Molecular Sciences

MDPI

Review

GPR37 Receptors and Megalencephalic Leukoencephalopathy with Subcortical Cysts

Adrià Pla-Casillanis [1,†], Laura Ferigle [1,†], Marta Alonso-Gardón [1], Efren Xicoy-Espaulella [1], Ekaitz Errasti-Murugarren [2,3], Daniela Marazziti [4] and Raúl Estévez [1,3,*]

1 Unitat de Fisiologia, Departament de Ciències Fisiològiques, Genes Disease and Therapy Program IDIBELL-Institute of Neurosciences, Universitat de Barcelona, L'Hospitalet de Llobregat, 08907 Barcelona, Spain; adria.pla9@gmail.com (A.P.-C.); laura.ferigle@ub.edu (L.F.); malonsga@gmail.com (M.A.-G.); efrenxicoyespaulella@gmail.com (E.X.-E.)
2 Unitat de Genètica, Departament de Ciències Fisiològiques, Genes Disease and Therapy Program IDIBELL-Institute of Neurosciences, Universitat de Barcelona, L'Hospitalet de Llobregat, 08907 Barcelona, Spain; ekaitz_errasti@ub.edu
3 Centro de Investigación en Red de Enfermedades Raras (CIBERER), ISCIII, 28029 Madrid, Spain
4 Institute of Biochemistry and Cell Biology, Italian National Research Council (CNR), I-00015 Rome, Italy; daniela.marazziti@cnr.it
* Correspondence: restevez@ub.edu; Tel.: +34-944-039-781; Fax: +34-934-024-268
† These authors contributed equally to this work.

Abstract: Megalencephalic leukoencephalopathy with subcortical cysts (MLC) is a rare type of vacuolating leukodystrophy (white matter disorder), which is mainly caused by defects in MLC1 or glial cell adhesion molecule (GlialCAM) proteins. In addition, autoantibodies to GlialCAM are involved in the pathology of multiple sclerosis. *MLC1* and *GLIALCAM* genes encode for membrane proteins of unknown function, which has been linked to the regulation of different ion channels and transporters, such as the chloride channel VRAC (volume regulated anion channel), ClC-2 (chloride channel 2), and connexin 43 or the Na^+/K^+-ATPase pump. However, the mechanisms by which MLC proteins regulate these ion channels and transporters, as well as the exact function of MLC proteins remain obscure. It has been suggested that MLC proteins might regulate signalling pathways, but the mechanisms involved are, at present, unknown. With the aim of answering these questions, we have recently described the brain GlialCAM interactome. Within the identified proteins, we could validate the interaction with several G protein-coupled receptors (GPCRs), including the orphan GPRC5B and the proposed prosaposin receptors GPR37L1 and GPR37. In this review, we summarize new aspects of the pathophysiology of MLC disease and key aspects of the interaction between GPR37 receptors and MLC proteins.

Keywords: megalencephalic leukoencephalopathy with subcortical cysts; GlialCAM; MLC1; GPRC5B; GPR37L1; GPR37; glia; ion; water homeostasis

Citation: Pla-Casillanis, A.; Ferigle, L.; Alonso-Gardón, M.; Xicoy-Espaulella, E.; Errasti-Murugarren, E.; Marazziti, D.; Estévez, R. GPR37 Receptors and Megalencephalic Leukoencephalopathy with Subcortical Cysts. *Int. J. Mol. Sci.* **2022**, *23*, 5528. https://doi.org/10.3390/ijms23105528

Academic Editor: Ross Bathgate

Received: 21 April 2022
Accepted: 13 May 2022
Published: 16 May 2022

1. Introduction

Megalencephalic leukoencephalopathy with subcortical cysts (MLC) is a rare genetic type of leukodystrophy (OMIM 604004). It is a childhood-onset hereditary disease characterized by white matter vacuolation and macrocephaly, which is developed during the first year of life. Most MLC patients present a progressive loss of motor functions with ataxia and spasticity, cognitive decline and epileptic seizures [1]. Symptomatology often worsens after fever or mild head trauma [2].

Magnetic Resonance Imaging (MRI), which is used for diagnostics, shows that patients display diffuse signal abnormality and swelling of the cerebral white matter together with the presence of subcortical cysts, mainly in the anterior temporal regions [3]. Furthermore, MRI together with the histopathology of the brain of an MLC patient revealed

that myelin contains water-filled vacuoles [4]. Up to date, MLC has no cure. Treatment is symptomatic in combination with supportive care.

Two different phenotypes of MLC disease have been described: a classical and a remitting phenotype [5]. The classical phenotype is the most commonly found in patients. It is caused by autosomal recessive mutations in either the *MLC1* or the hepatic cell adhesion molecule (*HEPACAM*) genes, resulting in two disease subtypes, namely MLC1 or MLC2A. The remitting phenotype, named MLC2B, is caused by dominant mutations in *HEPACAM* [6]. Approximately 76% of patients present mutations in *MLC1*, 22% in *HEPACAM* and 2% of MLC cases cannot be explained by mutations in these two genes, suggesting that others might be implied in the disease [2].

MLC1 encodes for a membrane protein with eight predicted transmembrane domains whose function remains unknown. It is expressed exclusively in the brain in astrocytes surrounding blood vessels and Bergmann glia in the cerebellum [7]. More than 50 mutations have been described for *MLC1*, including missense, deletions, insertions and nonsense mutations [1].

On the other hand, *HEPACAM* encodes for a cell adhesion molecule of the immunoglobulin (Ig) family named GlialCAM, which is expressed predominantly in neurons, astrocytes and oligodendrocytes [6]. GlialCAM was first identified in hepatic cancer, where it was downregulated, but it is predominantly expressed in glial cells [8]. GlialCAM can form interactions with other GlialCAM molecules in *cis* (within the same cell) or *trans* (between different cells) [9]. GlialCAM acts as an endoplasmic reticulum (ER) chaperone for MLC1 [10] and it also helps MLC1 to reach astrocyte-astrocyte junctions where both proteins co-localize [6,11]. Apart for being involved in MLC, recently, it has been described that autoantibodies recognizing GlialCAM might be involved in the development of multiple sclerosis [12].

The pathophysiological mechanisms leading to MLC are still unclear [13]. Even though the function of the MLC1/GlialCAM complex is unknown, it has been hypothesized that it may have a role in the regulation of ion/water homeostasis, as it interacts with different transporters and ion channels. Thus, it has been shown that the complex interacts directly with the chloride channel 2 (ClC-2) [14], the gap junction alpha 1 protein (connexin 43, Cx43) [15–17], Na^+/K^+-ATPase [18,19], and it is thought to regulate indirectly the activity of volume-regulated anion channel (VRAC) [10,20,21] or the calcium-permeable channel TRPV4 [22]. Recent bioinformatics developments have suggested new potential functions for the GlialCAM/MLC1 complex (see Section 2).

2. Novel Insights into GlialCAM/MLC1 Function by Alphafold Structural Models

Powerful sequence-alignment methodologies have been used to identify possible functional MLC1 homologues. The underlying assumption of these sequence-based methods is that proteins with similar sequences adopt a similar fold. As protein folding determines function, the detection of evolutionary relationships between proteins can be used to predict functions of non-annotated protein sequences. Thus, MLC1 sequence identity analysis by BLAST/PSI-BLAST algorithm identified the voltage gated potassium channel Kv1.1 alpha subunit (KCNA1) as the protein with the highest sequence identity (less than 20% amino acid identity) [23], suggesting that MLC1 could act as an ion channel. In agreement with this hypothesis, it is known that MLC1 can form homo-oligomers, a characteristic found in many ion channels proteins [24]. Moreover, MLC patients may present epileptic seizures, which is a common feature in ion channel diseases, but not in leukodystrophies [25]. Taking all these data into consideration, the first hypothesis regarding MLC1 function was that it could act as an ion channel. Nevertheless, voltage-clamp measurements in *Xenopus* oocytes did not detect any changes in the conductance and neither did patch clamp measurements in HEK293T or HeLa transfected cells. For those experiments, different pulse protocols and various pulse durations were applied and no conductivity of MLC1 was detected, even in the presence of GlialCAM [26].

The functional characterization of MLC1 is necessary to understand its physiological relevance. As the 3D structure of a protein is believed to be responsible for its biological function, protein structure can provide a better insight into which protein fragments contribute most to the functionality of a protein compared to the primary sequence. In fact, residues located far apart in primary sequence may be close in the 3D structure. Recently reported MLC1 structural models [27,28] suggest a protein fold based on a 4 + 4 structural repeat, involving transmembrane regions (TMs) 1–4 and 5–8 (Figure 1A,B). Interestingly, although mutations found in MLC patients are spread through all the protein sequence, a significant number of identified missense MLC1 mutations are mainly localized on the interphase between MLC1 internal repeats (Figure 1C). As MLC1 mutations have been reported to cause protein instability, which consequently causes its degradation at the endoplasmic reticulum or lysosomes [29–31], we propose that proper interaction between MLC1 internal repeats is of key relevance for proper protein folding and endoplasmic reticulum sorting. Similarly, recently reported MLC1 homo-trimeric complex in detergent micelles and proteoliposomes [24], suggests that mutations affecting MLC1 monomers interaction would also affect protein stability. However, the lack of a 3D structure at atomic resolution precludes the identification of putative protein-protein interaction regions.

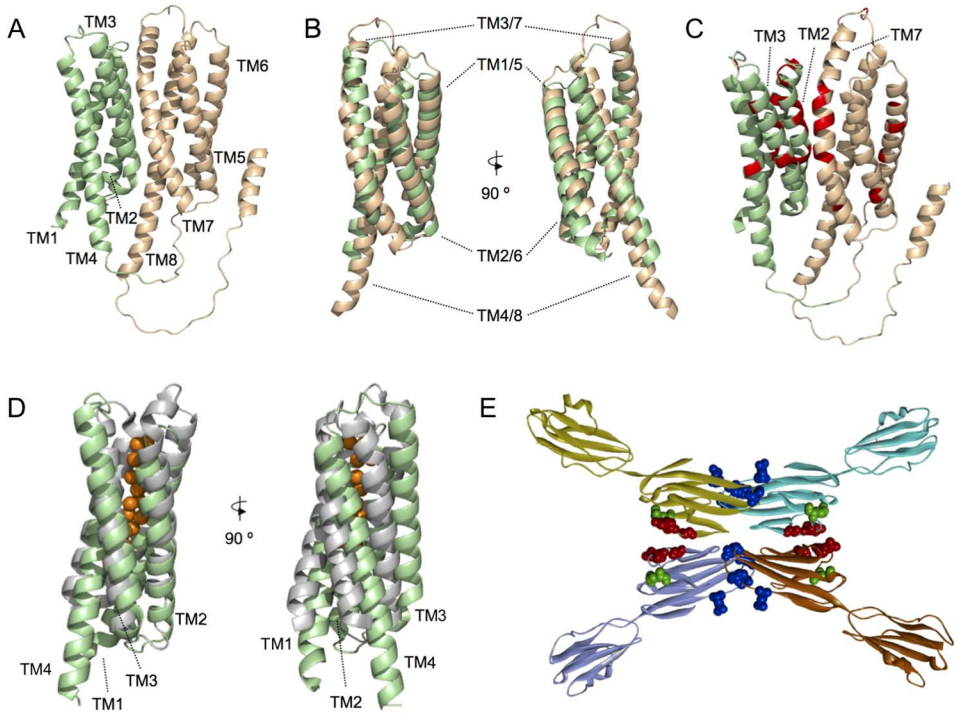

Figure 1. Structural models of MLC1 and GlialCAM proteins. (**A**) Alphafold structural model of monomeric MLC1. Helices 1 to 4 and 5 to 8 are coloured pale green and wheat, respectively. (**B**) Structural superimposition of the two MLC1 subdomains, comprised of TMs 1 to 4 (pale green) and 5 to 8 (wheat), respectively. Two different views, rotated by 90°, are shown. (**C**) MLC causing mutations (red) depicted in the MLC1 structural model. Preferential localization of mutated residues is located in the interaction surface defined by the two MLC1 subdomains (TMs 1 to 4 (pale green) and 5 to 8 (wheat)). (**D**) Structural superimposition of MLC1 structural model TM1 to 4 (pale green) and a prokaryotic soluble copper storage protein from *Streptomyces lividans* (light grey) (PDB ID 6Q6B). Two different views, rotated by 90°, are shown. (**E**) Summary of the structural model proposed for GlialCAM homodimers forming *cis* and *trans* interaction through different surfaces of its IgV domain. *Cis* dimerization is achieved by interactions between two opposing beta-strands of the IgV domain and *trans* interactions occur between salient loops of both IgV domains. Residues mutated in MLC2A patients (recessive) are shown in green, Residues mutated in MLC2B patients are shown in red or blue (affecting blue the interactions in *trans* only).

The growing number of known protein structures and structural models has motivated the interest into developing approaches that aim to identify the protein functions from the structure. Among them, methods comparing the global fold of a query protein with other template proteins of known function are commonly used. Identification of proteins similarly folded to whole MLC1 and TM1-4 MLC1, using the PDBeFold algorithm [32], revealed both prokaryotic and eukaryotic proteins with a similar 3D fold. Particularly, PDBeFold analysis of the TM1-4 MLC1 subdomain resulted in the identification of a prokaryotic soluble copper storage protein from *Streptomyces lividans* (PDB ID 6Q6B) (Figure 1D), suggesting that maybe MLC1 would be involved in ion sensing. However, further research should be conducted to solve this issue.

In addition, based on the identification of the interactome of GlialCAM and MLC1, we recently proposed that MLC1 could act as a tetraspanin-like molecule [16]. Tetraspanins are cell-surface proteins with four transmembrane domains, which can homo- and hetero-oligomerize. They participate in a wide variety of cellular processes such as adhesion, differentiation and cell activation [33]. In many cases, they also form a tight complex with proteins belonging to the Ig superfamily, as it happens with MLC1 and GlialCAM.

Our recent work based on 3D models combined with biochemical analyses indicated that GlialCAM forms interactions in *cis* through an interaction surface comprising residues Glutamate 86 to Arginine 92 in the IgV domain [9] (Figure 1E). Furthermore, two other loops might also be involved in the formation of *trans*- interactions, which are blocked by a nanobody generated against GlialCAM. Residues causing dominant MLC are located in these two interaction surfaces (Figure 1E). It remains to be determined whether the IgC2 domain contributes to the formation of lateral interactions as it has been observed in other Ig proteins, or if it also mediates interaction with the MLC1 protein.

3. Physiological Processes Affected in MLC Deduced from Animal Models of MLC

The main characteristic observed in MLC patients is that the brain is enlarged with increased water accumulation. Water is accumulated in subcortical cysts but also, in a general manner, in the outer part of myelin [4] and in astrocytes surrounding blood vessels [34]. Similarly, the lack of MLC1 or GlialCAM in knockout (KO) mice [18,35–37] or KO zebrafish [7,38] leads to an increased brain water content and cerebellar white matter vacuolation, although no cysts are observed. Moreover, in humans, the oedema is localized mainly in the subcortical white matter, while vacuoles are found in the cerebellum of KO mice. Although vacuoles of water in myelin sheaths that enwrap axons of central neurons can be observed in both patient biopsies and mice samples, still the developmental myelination process is not altered. Considering astrocytes, histological studies revealed that *Mlc1* KO mice presented abnormal astrocytes with thicker cell processes, swollen cell bodies and enlarged end-feet, although the length and number of these cells were not altered [34]. Primary astrocytes from *Mlc1* KO showed an increase in the number of vacuoles [7]. In summary, although there are differences between human and animal models, they show in common an increase in the content of water in the brain, which is accumulated in the form of vacuoles in myelin or in astrocytes.

Why does the lack of MLC1 lead to an increased water content in the brain? The first hypothesis was that MLC1 functions as a water or ion channel, and its defect causes water accumulation due to osmotic alterations linked to neuronal activity [23]. However, this activity has not been detected after expressing the MLC1 protein alone or together with GlialCAM in different cell systems [26]. Thus, a search for other proteins interacting with MLC1 and/or GlialCAM to find a connection with the patient's brain phenotype was developed. Unsurprisingly, several transporters and ion channels were identified by different groups (for review [13]). In an extensive proteomic analysis [16], we have recently identified the following interactor proteins: the chloride channel ClC-2, the gap junction protein Cx43, the glutamate transporter EAAT1/2, the alpha2 and beta2 subunits of the sodium/potassium ATPase, the sodium bicarbonate transporter NBCe1, the glucose transporter GLUT1, and the sodium calcium exchanger. Furthermore, although not appearing as MLC interacting

proteins, other activities have been shown to be affected by the lack of MLC1 such as the volume regulated anion channel (VRAC) or the calcium-permeable channel TRPV4. It has been clearly demonstrated that the activity of the chloride channels ClC-2 [37] and VRAC [21,35] and of the gap junction protein Cx43 [15] are affected in vivo. Thus, one possible hypothesis is that the lack of activity of some of these proteins is the reason that explains myelin vacuolization. In agreement with these hypotheses, a *Clcn2* KO mouse model displayed widespread vacuolization, including the cerebellum [37]. Similarly, defects of connexins have also been linked to myelin vacuolization [39]. As LRRC8 proteins of VRAC channels are involved in cell volume regulation and their absence cause cell vacuolation in several tissues, it will be important to analyse whether a conditional (because the complete KO is deleterious [40]) astrocyte KO of LRRC8A [41] (the main constituent of the VRAC channel [42,43]) also displays astrocyte and myelin vacuolization.

In contrast to other leukodystrophies, MLC patients can suffer from seizures [25]; still the underlying mechanism that links MLC to epilepsy is not known. In this sense, both *Glialcam* and *Mlc1* KO mice present an abnormal extracellular K^+ dynamics and neuronal network activity, as they had an epileptiform brain activity and a lowered seizure threshold [44]. As described previously, defects in either the MLC1 or GlialCAM interacting proteins' function might also affect extracellular potassium dynamics. Astrocyte uptake is mainly mediated by the Na^+/K^+ ATPase pump [45], an interactor of MLC1 [16,18,19]. In *Mlc1* KO mice, there is a reduced expression of the inward rectifier potassium channel Kir4.1 involved in potassium clearance [35], whose absence is known to lead to hyperexcitability and epilepsy [46]. The interaction of GlialCAM with the ClC-2 chloride channel increases total current amplitudes and abolishes the rectification of ClC-2, which is thus opened at positive voltages [14]. In addition, this interaction opens the ClC-2 common gate, which is closed by acidic pH. This reduction in the inward rectification will allow the influx of chloride, which may be needed to maintain the electroneutrality after potassium intake in glial cells [47]. Connexins are also essential to disperse local high potassium concentrations through a glial syncytium. It must be considered that disturbed astrocyte regulation of water homeostasis in MLC affecting the VRAC channel might also cause hyperexcitability of neuronal networks and seizures.

Importantly, perivascular astrocytes by itself, where MLC1 expression is higher and can even be considered a marker of these cells [48], are essential to the maintenance of an adequate blood brain barrier, which is also important for the clearance of potassium [49]. In this sense, it has recently been shown that the lack of MLC1 affects the perivascular astrocytic processes' molecular maturation and organization. In *Mlc1* KO mice, an accumulation of fluid in the brain occurs, although this does not alter the blood-brain barrier integrity and neither the organization of the endothelial network. It has been determined that MLC1 might play a role in contractile maturation of vascular smooth muscle cells, arterial perfusion, and neurovascular coupling. Its absence disturbs the postnatal acquisition of contractile properties by vascular smooth muscle cells and disrupts blood perfusion, vessel diameter and neurovascular coupling [50]. Thus, not only affecting different ion channels and transporters in astrocytes can cause water increase and it might be that disruption of gliovascular unit by itself might contribute also to the increase in water content and seizures observed in MLC patients.

Another important aspect to consider in the pathophysiology of MLC is that MLC1 is expressed in astrocytes, whereas its auxiliary subunit GlialCAM is expressed in astrocytes, oligodendrocytes, and neurons [15,37]. Importantly, GlialCAM regulates astrocyte competition for territory and morphological complexity in the developing mouse cortex [15]. It has been shown that the lack of MLC1 causes GlialCAM mislocalization by an unknown mechanism in astrocytes [7], but also in oligodendrocytes [37], possibly because astrocytic GlialCAM interacts in *trans* through the IgV domain with oligodendrocytic GlialCAM. Moreover, the mislocalization of GlialCAM also affect to the localization of ClC-2 in oligodendrocytes, as shown by immunofluorescence and electrophysiological measurements of ClC-2 activity in oligodendrocytes on cerebellar slices [37]. In line with these studies, it has

been recently shown that the lack of GlialCAM in astrocytes in vivo decreases synaptic inhibition and, therefore, increases excitation, which may also explain seizures [15]. As ClC-2 and GlialCAM are also expressed in inhibitory synapses, this change in synaptic function might also be related to disorganization of GlialCAM (astrocyte)-GlialCAM (neuron) trans contacts. It could also be related to the mislocalization of other interacting partners such as Cx43, which in turn might also interact with connexins present in oligodendrocytes (connexin 47) [51] and/or neurons.

As previously stated in this review, the functional role of the GlialCAM/MLC1 complex is still unknown. Nevertheless, it has been described that several proteins and processes related to brain homeostasis are affected in a GlialCAM or MLC1-dependent manner and it is not clear how GlialCAM and MLC1 exert this effect on the activity of different ion channels and transporters. A suggested hypothesis argues that they might influence signalling cascades by yet undefined mechanisms [52], which may regulate these channels or transporters. In this regard, GlialCAM and MLC1 have been related to signal transduction changes. For instance, it has been described that the overexpression of human MLC1 in astrocytes decreases the phosphorylation of extracellular signal-regulated kinases (ERK), whereas primary astrocytes lacking MLC1 show an increase in phosphorylation [21]. Nonetheless, the mechanisms involved in this process remain unresolved.

In summary, GlialCAM and MLC1 seem to regulate the activity of many different transporters and ion channels in different cell types (Figure 2), possibly by regulating phosphorylation of these proteins. An anomalous activity of these proteins might contribute to the defects observed in the regulation of the extracellular water and ionic homeostasis, which could explain the increased water content and seizure susceptibility of MLC patients.

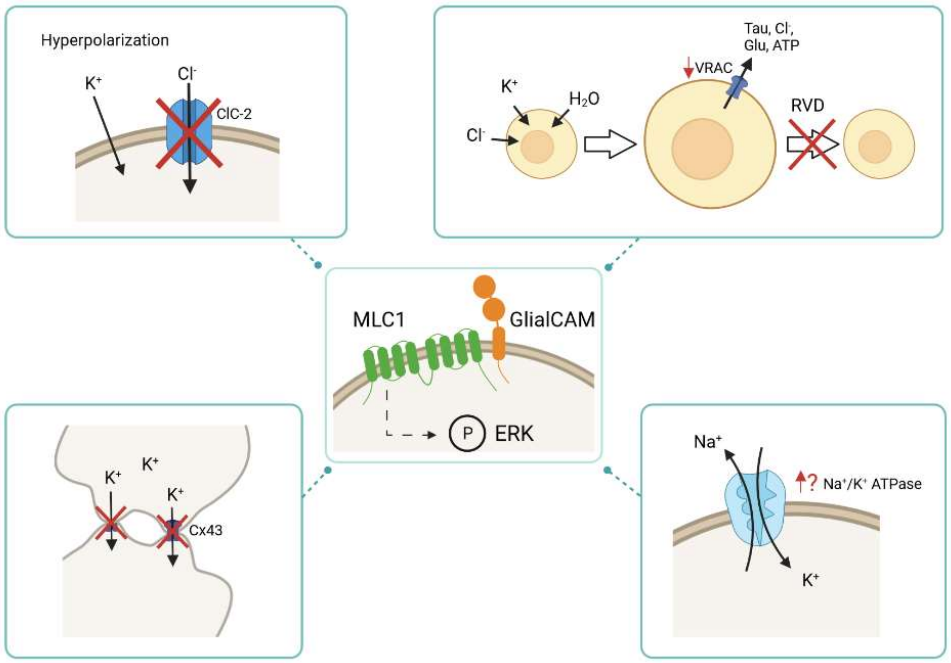

Figure 2. Physiological alterations caused by the lack of MLC1 and/or GlialCAM. MLC1/GlialCAM might regulate the activity of different transporters and ion channels through phosphorylation of ERK signalling transduction cascade. In the absence of MLC proteins, the activity of different transporters and ion channels is altered, such as the activity of ClC-2, VRAC, Cx43 and Na^+/K^+ ATPase. During the hyperpolarization phase of a neuronal action potential, the activity of the chloride channel ClC-2 is decreased in the absence of MLC1/GlialCAM. The lack of MLC proteins diminishes VRAC activity, which leads to an impaired regulatory volume decrease (RVD) response: an important mechanism to shrink cells after cell swelling. The Cx43 localization in the absence of MLC1/GlialCAM is affected as it is internalized and it is no longer located at cell-cell junctions. It is thought that the activity of the Na^+/K^+ ATPase is altered when MLC proteins are not present.

4. Regulation Mechanism of Different Transporters and Ion Channels by MLC Proteins: Is a GPCR Link the Answer?

Recently, our research group identified the GlialCAM interactome through an approach based on affinity purifications (APs) [16]. Four different antibodies specific for GlialCAM were used on samples consisting of membrane fractions prepared from whole brains from adult animals. These included wild type (WT) rats and mice, as well as *Glialcam* KO mice. The previously validated interactors MLC1, ClC-2 and GlialCAM itself were retained in all APs with high efficiency, reinforcing the robustness of this approach. We could identify as many as 21 proteins within the GlialCAM interactome in the rodent brain, some of them already linked to MLC as mentioned above. Within the proteins identified as part of the network of GlialCAM, there were three specific G protein-coupled receptors (GPCRs). Specifically, we retrieved the orphan receptors GPRC5B [53], which we suggested that mutations in this gene could be found in MLC patients without mutations in *MLC1* and *HEPACAM*, and the proposed binders of prosaposin GPR37 and GPR37L1 [54,55]. It is interesting to note that the latter two GPCRs belong to the same protein family. Therefore, we proceeded to determine the potential interaction and the relationship between these GPCRs and MLC-related proteins (GlialCAM/MLC1 and ClC-2). As the purpose of this review is to update the knowledge of the GPR37 family, we will focus on these two proteins.

The GPR37 and GPR37L1 proteins are part of class A rhodopsin-like family of GPCRs, which comprises 80% of all identified GPCRs [56]. Both are considered orphan receptors as no ligand has conclusively been linked to them in vitro [55]. The two GPCRs are widely expressed in the CNS [57]. GPR37 is mainly expressed in the cerebellum, corpus callosum, medulla, putamen, caudate nucleus, substantia nigra and the hippocampus [58–61]. Specifically, oligodendrocytes are the cell type displaying a higher expression of GPR37 together with certain subsets of neurons like dopaminergic neurons in the substantia nigra [62]. On the other hand, GPR37L1 is exclusively expressed in glial cells within the brain, in particular Bergmann glia astrocytes in the cerebellum [63], as well as immature oligodendrocytes [64].

Studies carried out in *Gpr37* KO mice revealed that GPR37 acts as a negative regulator of oligodendrocyte differentiation and myelination. The lack of GPR37 leads to premature differentiation of pre-myelinating oligodendrocytes to myelin producing cells. This alteration is a cause of central nervous system hypermyelination in these mice, already at a very young age and up until adult stages [64]. Furthermore, experiments performed both in primary oligodendrocytes and in brain-derived samples obtained from *Gpr37* KO mice show an increase in ERK1/2 phosphorylation. Pharmacological inhibition of MEK1/2 and ERK1/2 seemed to stop premature differentiation of oligodendrocytes in the absence of GPR37. This inhibition, however, did not affect normal cell proliferation [65]. In addition, adenylyl cyclase inhibition resulted in the impairment of ERK1/2 translocation to the nucleus. Taken together, these data suggested that this pathway is indeed responsible for GPR37 activation during oligodendrocyte differentiation.

Regarding GPR37L1, several studies have highlighted its relevance in the developing brain. One study showed that the lack of Gpr37l1 led to altered cerebellar development in mice [63]. The animals displayed a reduction in neuronal granule cell precursors together with premature maturation of Bergmann glia and Purkinje neurons. Cerebellar layer formation was also altered. However, the authors observed that KO mice seemed to perform better in motor tasks. Motor learning was improved both in juvenile and adult stages, while the adult animals also showed better coordination skills. Furthermore, it has been suggested that Gpr37l1 could play a role in recovery after ischemic injuries, possibly by modulating glutamate transporters [66], which also form part of the GlialCAM interactome [16].

5. Biochemical Relationship between the GPR37/GPR37L1 and MLC Proteins

As detailed above, these two GPCRs, that were identified as members of the GlialCAM interactome, play an important role in mediating a variety of processes in the central

nervous system. Hence, our research group was particularly interested in the analysis of the potential role of these GPCRs in MLC pathophysiology. The first experiments that were carried out aimed to validate the proteomics data regarding the interaction between these proteins and GlialCAM/MLC1 [16]. As MLC1 and GPR37L1 are both expressed in astrocytes, we initially focused our studies on this GPCR. We could establish that there was co-localization between GPR37L1 and MLC1 by immunofluorescence in mouse primary astrocytes. Furthermore, both proteins were in proximity in the same cells, as assessed by Proximity Ligation Assay (PLA) [16]. Moreover, the ability of each of the two GPCRs to directly interact with either MLC1 or GlialCAM was monitored by split-tobacco etch virus (TEV) assays for GPR37 (Figure 3) and bioluminescence resonance energy transfer (BRET) studies in HEK293T cells for GPR37L1 [16].

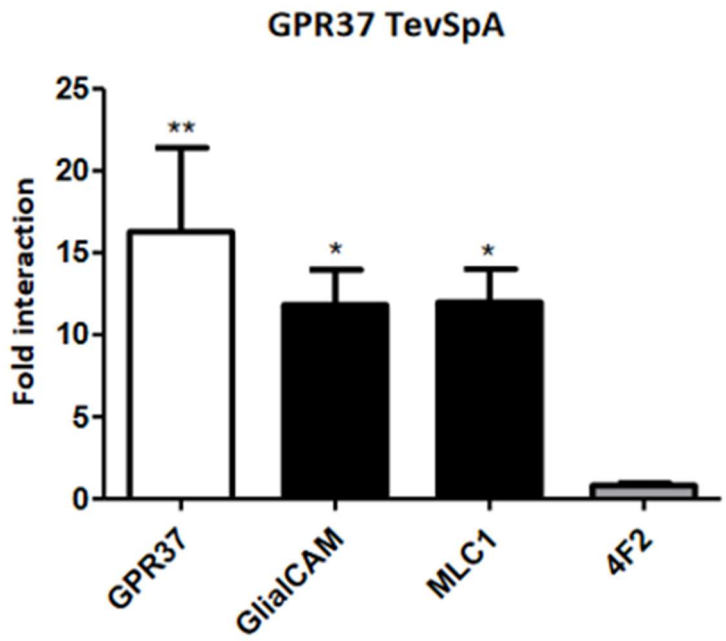

Figure 3. Direct Interaction between GPR37 and GlialCAM/MLC1. Results of split-TEV interaction assays in HeLa cell using GPR37 C-terminally tagged with the N-terminal part of the TEV protease (TevSpA). They were co-transfected with different constructs (GPR37, GlialCAM, MLC1 and 4F2 as a negative control) C-terminally tagged with the C-terminal part of the TEV protease. Plotted data combine the results from three independent experiments. Statistical significance was obtained comparing the interaction within each group to the interaction with the negative control in Bonferroni's multiple comparison test (* $p < 0.05$, ** $p < 0.01$ in the test versus 4F2). Results show that GPR37 is able to homo-oligomerize and hetero-oligomerize with GlialCAM and MLC1, in the same manner as shown for GPR37L1 by BRET.

The above summarized results support the formation of complexes between the GPCRs and MLC-related proteins in living cells. More work was carried out to further characterize the nature of the relationship between these proteins and the physiological role of these complexes. In collaboration with the group led by Daniela Marazziti, we started to address these questions using the *Gpr37l1* constitutive KO mice [63]. As the animals showed no alteration of adult cerebellar layer cytoanatomy and organization and there was no apparent sign of gliosis, it was considered that the analysis of MLC proteins in *Gpr37l1* KO mice could elucidate direct effects of GPR37L1 on MLC protein expression and function.

Biochemically, the first step was to analyse the consequences of the lack of GPR37L1 on MLC1 and GlialCAM protein levels [16]. Western blot experiments of cerebellar membrane fractions indicated that both proteins were upregulated in the *Gpr37l1* KO samples. Likewise, ClC-2 protein levels were also increased. Similarly, in immunofluorescence la-

belling experiments of MLC1 and GlialCAM in cerebellar Bergmann glia samples, an increased signal was observed. These in tissue results were consistent with what was observed in primary astrocytes derived from these mice, in which an increased signal for MLC-related proteins was revealed. However, the MLC proteins and ClC-2 showed a more dotted pattern compared to the WT signal. To determine whether MLC1 subcellular localization was altered in *Gpr37l1* KO mice, we proceeded to detect MLC1 by electron microscopy (EM) immunogold experiments. These experiments showed that the localization of MLC1 in Bergmann glia or in perivascular astrocytic processes was not affected. In summary, we concluded that the lack of GPR37L1 in mice upregulates MLC protein levels without altering their localization [16]. No studies have so far been performed in *Gpr37* KO mice.

6. Possible Role of GPR37 and GPR37L1 in MLC Pathophysiology

As the lack of GPR37L1 increases MLC proteins levels, it was suggested that GPR37L1 might be a negative regulator of MLC proteins in astrocytes (Figure 4). Interestingly, previous studies [67] have suggested that GPR37 interacts and negatively regulates dopamine transporters by regulating their endocytosis and trafficking. As stated previously, GPR37 has been described to act as a negative regulator of myelin formation [64]. As the proper expression of GlialCAM/MLC1 is necessary for myelin homeostasis, we could hypothesize that GPR37L1 would exert a similar negative effect regulating the GlialCAM/MLC1 complex during development (Figure 4).

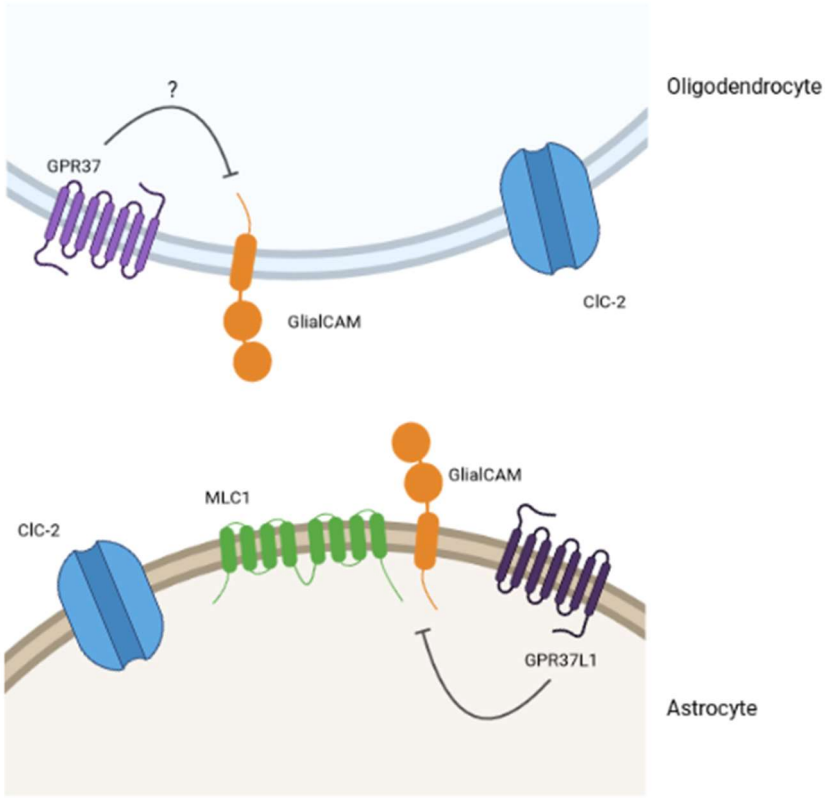

Figure 4. Model for the interplay between GPCRs and MLC-related proteins. The existing pieces of evidence in the literature and the results from our lab lead us to think that GPR37 and GPR37L1 would be part of an interplay with MLC-related proteins. Specifically, we hypothesize (question mark for GPR37 in oligodendrocytes) that these GPCRs would be negative regulators of the physiological MLC1/GlialCAM complex activity.

Previous studies indicated that the interaction between GlialCAM/MLC1 and ClC-2 in primary cultured astrocytes was dynamically regulated, and it was observed only

in depolarizing conditions [47]. Then, we addressed whether the interaction between GPR37L1 and MLC1 was also regulated in a dynamic manner, and compared the interaction between GPR37L1 with MLC1 in physiological versus depolarizing conditions in primary astrocyte cultures [16]. The PLA assays indicated that the interaction between GPR37L1 and MLC1 was decreased, whereas the interaction with the orphan GPCR5B was increased. As GPRC5B interacts more with MLC1 in depolarizing and hypotonic conditions, the activity of GPRC5B might be important in metabolic processes related to changes in the ionic composition. In contrast, we hypothesize that signalling through GPR37L1 might be related to cell differentiation processes. In line with this hypothesis, as mentioned previously, the lack of GPR37L1 resulted in an increase of phospho-ERK1/2, which has also been seen in *Mlc1* KO cells [21].

Another similar correlation has been found recently between MLC proteins and GPR37L1. As mentioned previously, MLC patients [25] and *Mlc1* KO mice [44] show increased seizure susceptibility. A homozygous GPR37L1 variant (c.1047G > T [Lys349Asp]) has been found in a patient with myoclonus epilepsy [68]. Furthermore, both *Gpr37* and *Gpr37l1* KO mice showed an increase in seizure susceptibility [68]. These results are consistent with a possible functional link between these GPCRs and MLC disease. However, it is important to state that future research is needed to understand how GlialCAM and MLC1 modulate GPCR-associated signalling processes.

Funding: This research was funded by MICINN (RTI2018-093493-B-I00).

Institutional Review Board Statement: Not applicable.

Informed Consent Statement: Not applicable.

Data Availability Statement: Not applicable.

Conflicts of Interest: The authors declare no conflict of interest.

References

1. Van der Knaap, M.S.; Boor, I.; Estevez, R. Megalencephalic leukoencephalopathy with subcortical cysts: Chronic white matter oedema due to a defect in brain ion and water homoeostasis. *Lancet Neurol.* **2012**, *11*, 973–985. [CrossRef]
2. Knaap, M.S.; van der Abbink, T.E.M.; Min, R. Megalencephalic Leukoencephalopathy with Subcortical Cysts. In *Brain Imaging with MRI and CT: An Image Pattern Approach*; Cambridge University Press: Cambridge, UK, 2018; pp. 47–48, ISBN 9780521119.
3. Singhal, B.S.; Gursahani, R.D.; Udani, V.P.; Biniwale, A.A. Megalencephalic leukodystrophy in an Asian Indian ethnic group. *Pediatric. Neurol.* **1996**, *14*, 291–296. [CrossRef]
4. Van der Knaap, M.S.; Barth, P.G.; Vrensen, G.F.; Valk, J. Histopathology of an infantile-onset spongiform leukoencephalopathy with a discrepantly mild clinical course. *Acta Neuropathol.* **1996**, *92*, 206–212. [CrossRef] [PubMed]
5. Van der Knaap, M.S.; Lai, V.; Kohler, W.; Salih, M.A.; Fonseca, M.J.; Benke, T.A.; Wilson, C.; Jayakar, P.; Aine, M.R.; Dom, L.; et al. Megalencephalic leukoencephalopathy with cysts without MLC1 defect. *Ann. Neurol.* **2010**, *67*, 834–837. [PubMed]
6. López-Hernández, T.; Ridder, M.C.; Montolio, M.; Capdevila-Nortes, X.; Polder, E.; Sirisi, S.; Duarri, A.; Schulte, U.; Fakler, B.; Nunes, V.; et al. Mutant GlialCAM causes megalencephalic leukoencephalopathy with subcortical cysts, benign familial macrocephaly, and macrocephaly with retardation and autism. *Am. J. Hum. Genet.* **2011**, *88*, 422–432. [CrossRef] [PubMed]
7. Sirisi, S.; Folgueira, M.; López-Hernández, T.; Minieri, L.; Pérez-Rius, C.; Gaitán-Peñas, H.; Zang, J.; Martínez, A.; Capdevila-Nortes, X.; De La Villa, P.; et al. Megalencephalic leukoencephalopathy with subcortical cysts protein 1 regulates glial surface localization of GLIALCAM from fish to humans. *Hum. Mol. Genet.* **2014**, *23*, 5069–5086. [CrossRef] [PubMed]
8. Favre-Kontula, L.; Rolland, A.; Bernasconi, L.; Karmirantzou, M.; Power, C.; Antonsson, B.; Boschert, U. GlialCAM, an immunoglobulin-like cell adhesion molecule is expressed in glial cells of the central nervous system. *Glia* **2008**, *56*, 633–645. [CrossRef]
9. Elorza-Vidal, X.; Xicoy-Espaulella, E.; Pla-Casillanis, A.; Alonso-Gardón, M.; Gaitán-Peñas, H.; Engel-Pizcueta, C.; Fernández-Recio, J.; Estévez, R. Structural basis for the dominant or recessive character of GLIALCAM mutations found in leukodystrophies. *Hum. Mol. Genet.* **2020**, *29*, 1107–1120. [CrossRef]
10. Capdevila-Nortes, X.; López-Hernández, T.; Apaja, P.M.; de Heredia, M.L.; Sirisi, S.; Callejo, G.; Arnedo, T.; Nunes, V.; Lukacs, G.L.; Gasull, X.; et al. Insights into MLC pathogenesis: GlialCAM is an MLC1 chaperone required for proper activation of volume-regulated anion currents. *Hum. Mol. Genet.* **2013**, *22*, 4405–4416. [CrossRef]
11. Xu, H.; Isenmann, S.; López-Hernández, T.; Estévez, R.; Lukacs, G.L.; Apaja, P.M. Control of membrane protein homeostasis by a chaperone-like glial cell adhesion molecule at multiple subcellular locations. *Sci. Rep.* **2021**, *11*, 18435. [CrossRef]

12. Lanz, T.V.; Brewer, R.C.; Ho, P.P.; Moon, J.S.; Jude, K.M.; Fernandez, D.; Fernandes, R.A.; Gomez, A.M.; Nadj, G.S.; Bartley, C.M.; et al. Clonally expanded B cells in multiple sclerosis bind EBV EBNA1 and GlialCAM. *Nature* **2022**, *603*, 321–327. [CrossRef] [PubMed]
13. Bosch, A.; Estévez, R. Megalencephalic Leukoencephalopathy: Insights Into Pathophysiology and Perspectives for Therapy. *Front. Cell Neurosci.* **2021**, *22*, 14. [CrossRef] [PubMed]
14. Jeworutzki, E.; Lopez-Hernandez, T.; Capdevila-Nortes, X.; Sirisi, S.; Bengtsson, L.; Montolio, M.; Zifarelli, G.; Arnedo, T.; Muller, C.S.; Schulte, U.; et al. GlialCAM, a protein defective in a leukodystrophy, serves as a ClC-2 Cl^- channel auxiliary subunit. *Neuron* **2012**, *73*, 951–961. [CrossRef]
15. Baldwin, K.T.; Tan, C.X.; Strader, S.T.; Jiang, C.; Savage, J.T.; Elorza-Vidal, X.; Contreras, X.; Rülicke, T.; Hippenmeyer, S.; Estévez, R.; et al. HepaCAM controls astrocyte self-organization and coupling. *Neuron* **2021**, *109*, 2427–2442. [CrossRef] [PubMed]
16. Alonso-Gardón, M.; Elorza-Vidal, X.; Castellanos, A.; La Sala, G.; Armand-Ugon, M.; Gilbert, A.; Di Pietro, C.; Pla-Casillanis, A.; Ciruela, F.; Gasull, X.; et al. Identification of the GlialCAM interactome: The G protein-coupled receptors GPRC5B and GPR37L1 modulate megalencephalic leukoencephalopathy proteins. *Hum. Mol. Genet.* **2021**, *30*, 1649–1665. [CrossRef] [PubMed]
17. Wu, M.; Moh, M.C.; Schwarz, H. HepaCAM associates with connexin 43 and enhances its localization in cellular junctions. *Sci. Rep.* **2016**, *6*, 36218. [CrossRef] [PubMed]
18. Sugio, S.; Tohyama, K.; Oku, S.; Fujiyoshi, K.; Yoshimura, T.; Hikishima, K.; Yano, R.; Fukuda, T.; Nakamura, M.; Okano, H.; et al. Astrocyte-mediated infantile-onset leukoencephalopathy mouse model. *Glia* **2017**, *65*, 150–168. [CrossRef] [PubMed]
19. Brignone, M.S.; Lanciotti, A.; Macioce, P.; Macchia, G.; Gaetani, M.; Aloisi, F.; Petrucci, T.C.; Ambrosini, E. The beta1 subunit of the Na,K-ATPase pump interacts with megalencephalic leucoencephalopathy with subcortical cysts protein 1 (MLC1) in brain astrocytes: New insights into MLC pathogenesis. *Hum. Mol. Genet.* **2011**, *20*, 90–103. [CrossRef]
20. Ridder, M.C.; Boor, I.; Lodder, J.C.; Postma, N.L.; Capdevila-Nortes, X.; Duarri, A.; Brussaard, A.B.; Estévez, R.; Scheper, G.C.; Mansvelder, H.D.; et al. Megalencephalic leucoencephalopathy with cysts: Defect in chloride currents and cell volume regulation. *Brain* **2011**, *134*, 3342–3354. [CrossRef]
21. Elorza-Vidal, X.; Sirisi, S.; Gaitán-Peñas, H.; Pérez-Rius, C.; Alonso-Gardón, M.; Armand-Ugón, M.; Lanciotti, A.; Brignone, M.S.; Prat, E.; Nunes, V.; et al. GlialCAM/MLC1 modulates LRRC8/VRAC currents in an indirect manner: Implications for megalencephalic leukoencephalopathy. *Neurobiol. Dis.* **2018**, *119*, 88–99. [CrossRef]
22. Lanciotti, A.; Brignone, M.S.; Molinari, P.; Visentin, S.; De Nuccio, C.; Macchia, G.; Aiello, C.; Bertini, E.; Aloisi, F.; Petrucci, T.C.; et al. Megalencephalic leukoencephalopathy with subcortical cysts protein 1 functionally cooperates with the TRPV4 cation channel to activate the response of astrocytes to osmotic stress: Dysregulation by pathological mutations. *Hum. Mol. Genet.* **2012**, *21*, 2166–2180. [CrossRef] [PubMed]
23. Teijido, O.; Martínez, A.; Pusch, M.; Zorzano, A.; Soriano, E.; del Río, J.A.; Palacín, M.; Estévez, R. Localization and functional analyses of the MLC1 protein involved in megalencephalic leukoencephalopathy with subcortical cysts. *Hum. Mol. Genet.* **2004**, *13*, 2581–2594. [CrossRef] [PubMed]
24. Hwang, J.; Park, K.; Lee, G.-Y.; Yoon, B.Y.; Kim, H.; Roh, S.H.; Lee, B.-C.; Kim, K.; Lim, H.-H. Transmembrane topology and oligomeric nature of an astrocytic membrane protein, MLC1. *Open Biol.* **2021**, *11*, 210103. [CrossRef] [PubMed]
25. Hamilton, E.M.C.; Tekturk, P.; Cialdella, F.; Van Rappard, D.F.; Wolf, N.I.; Yalcinkaya, C.; Çetinçelik, Ü.; Rajaee, A.; Kariminejad, A.; Paprocka, J.; et al. Megalencephalic leukoencephalopathy with subcortical cysts: Characterization of disease variants. *Neurology* **2018**, *90*, E1395–E1403. [CrossRef]
26. Estévez, R.; Elorza-Vidal, X.; Gaitán-Peñas, H.; Pérez-Rius, C.; Armand-Ugón, M.; Alonso-Gardón, M.; Xicoy-Espaulella, E.; Sirisi, S.; Arnedo, T.; Capdevila-Nortes, X.; et al. Megalencephalic leukoencephalopathy with subcortical cysts: A personal biochemical retrospective. *Eur. J. Med. Genet.* **2018**, *61*, 50–60. [CrossRef]
27. Jumper, J.; Evans, R.; Pritzel, A.; Green, T.; Figurnov, M.; Ronneberger, O.; Tunyasuvunakool, K.; Bates, R.; Žídek, A.; Potapenko, A.; et al. Highly accurate protein structure prediction with AlphaFold. *Nature* **2021**, *596*, 583–589. [CrossRef]
28. Varadi, M.; Anyango, S.; Deshpande, M.; Nair, S.; Natassia, C.; Yordanova, G.; Yuan, D.; Stroe, O.; Wood, G.; Laydon, A.; et al. AlphaFold Protein Structure Database: Massively expanding the structural coverage of protein-sequence space with high-accuracy models. *Nucleic Acids Res.* **2022**, *50*, D439–D444. [CrossRef]
29. Duarri, A.; Teijido, O.; López-Hernández, T.; Scheper, G.C.; Barriere, H.; Boor, I.; Aguado, F.; Zorzano, A.; Palacín, M.; Martínez, A.; et al. Molecular pathogenesis of megalencephalic leukoencephalopathy with subcortical cysts: Mutations in MLC1 cause folding defects. *Hum. Mol. Genet.* **2008**, *17*, 3728–3739. [CrossRef]
30. Lanciotti, A.; Brignone, M.S.; Camerini, S.; Serafini, B.; Macchia, G.; Raggi, C.; Molinari, P.; Crescenzi, M.; Musumeci, M.; Sargiacomo, M.; et al. MLC1 trafficking and membrane expression in astrocytes: Role of caveolin-1 and phosphorylation. *Neurobiol. Dis.* **2010**, *37*, 581–595. [CrossRef]
31. Petrini, S.; Minnone, G.; Coccetti, M.; Frank, C.; Aiello, C.; Cutarelli, A.; Ambrosini, E.; Lanciotti, A.; Brignone, M.S.; D'Oria, V.; et al. Monocytes and macrophages as biomarkers for the diagnosis of megalencephalic leukoencephalopathy with subcortical cysts. *Mol. Cell Neurosci.* **2013**, *56*, 307–321. [CrossRef]
32. Mary Rajathei, D.; Selvaraj, S. Analysis of sequence repeats of proteins in the PDB. *Comput. Biol. Chem.* **2013**, *47*, 156–166. [CrossRef] [PubMed]
33. Pols, M.S.; Klumperman, J. Trafficking and function of the tetraspanin CD63. *Exp. Cell Res.* **2009**, *315*, 1584–1592. [CrossRef] [PubMed]

34. Duarri, A.; Lopez de Heredia, M.; Capdevila-Nortes, X.; Ridder, M.C.; Montolio, M.; López-Hernández, T.; Boor, I.; Lien, C.F.; Hagemann, T.; Messing, A.; et al. Knockdown of MLC1 in primary astrocytes causes cell vacuolation: A MLC disease cell model. *Neurobiol. Dis.* **2011**, *43*, 228–238. [CrossRef] [PubMed]
35. Dubey, M.; Bugiani, M.; Ridder, M.C.; Postma, N.L.; Brouwers, E.; Polder, E.; Jacobs, J.G.; Baayen, J.C.; Klooster, J.; Kamermans, M.; et al. Mice with megalencephalic leukoencephalopathy with cysts: A developmental angle. *Ann. Neurol.* **2015**, *77*, 114–131. [CrossRef]
36. Bugiani, M.; Dubey, M.; Breur, M.; Postma, N.L.; Dekker, M.P.; ter Braak, T.; Boschert, U.; Abbink, T.E.M.; Mansvelder, H.D.; Min, R.; et al. Megalencephalic leukoencephalopathy with cysts: The *Glialcam* -null mouse model. *Ann. Clin. Transl. Neurol.* **2017**, *4*, 450–465. [CrossRef]
37. Hoegg-Beiler, M.B.; Sirisi, S.; Orozco, I.J.; Ferrer, I.; Hohensee, S.; Auberson, M.; Gödde, K.; Vilches, C.; De Heredia, M.L.; Nunes, V.; et al. Disrupting MLC1 and GlialCAM and ClC-2 interactions in leukodystrophy entails glial chloride channel dysfunction. *Nat. Commun.* **2014**, *5*, 3475. [CrossRef]
38. Pérez-Rius, C.; Folgueira, M.; Elorza-Vidal, X.; Alia, A.; Hoegg-Beiler, M.B.; Eeza, M.N.H.; Díaz, M.L.; Nunes, V.; Barrallo-Gimeno, A.; Estévez, R. Comparison of zebrafish and mice knockouts for Megalencephalic Leukoencephalopathy proteins indicates that GlialCAM/MLC1 forms a functional unit. *Orphanet J. Rare Dis.* **2019**, *14*, 268. [CrossRef]
39. Schiza, N.; Sargiannidou, I.; Kagiava, A.; Karaiskos, C.; Nearchou, M.; Kleopa, K.A. Transgenic replacement of Cx32 in gap junction-deficient oligodendrocytes rescues the phenotype of a hypomyelinating leukodystrophy model. *Hum. Mol. Genet.* **2015**, *24*, 2049–2064. [CrossRef]
40. Wilson, C.S.; Dohare, P.; Orbeta, S.; Nalwalk, J.W.; Huang, Y.; Ferland, R.J.; Sah, R.; Scimemi, A.; Mongin, A.A. Late adolescence mortality in mice with brain-specific deletion of the volume-regulated anion channel subunit LRRC8A. *FASEB J.* **2021**, *35*, e21869. [CrossRef]
41. Yang, J.; del Carmen Vitery, M.; Chen, J.; Osei-Owusu, J.; Chu, J.; Qiu, Z. Glutamate-Releasing SWELL1 Channel in Astrocytes Modulates Synaptic Transmission and Promotes Brain Damage in Stroke. *Neuron* **2019**, *102*, 813–827. [CrossRef]
42. Qiu, Z.; Dubin, A.E.; Mathur, J.; Tu, B.; Reddy, K.; Miraglia, L.J.; Reinhardt, J.; Orth, A.P.; Patapoutian, A. SWELL1, a plasma membrane protein, is an essential component of volume-regulated anion channel. *Cell* **2014**, *157*, 447–458. [CrossRef] [PubMed]
43. Voss, F.K.; Ullrich, F.; Münch, J.; Lazarow, K.; Lutte, D.; Mah, N.; Andrade-Navarro, M.A.; Von Kries, J.P.; Stauber, T.; Jentsch, T.J. Identification of LRRC8 heteromers as an essential component of the volume-regulated anion channel VRAC. *Science* **2014**, *344*, 634–638. [CrossRef] [PubMed]
44. Dubey, M.; Brouwers, E.; Hamilton, E.M.C.; Stiedl, O.; Bugiani, M.; Koch, H.; Kole, M.H.P.; Boschert, U.; Wykes, R.C.; Mansvelder, H.D.; et al. Seizures and disturbed brain potassium dynamics in the leukodystrophy megalencephalic leukoencephalopathy with subcortical cysts. *Ann. Neurol.* **2018**, *83*, 636–649. [CrossRef]
45. Larsen, B.R.; Assentoft, M.; Cotrina, M.L.; Hua, S.Z.; Nedergaard, M.; Kaila, K.; Voipio, J.; Macaulay, N. Contributions of the Na^+/K^+-ATPase, NKCC1, and Kir4.1 to hippocampal K+ clearance and volume responses. *Glia* **2014**, *62*, 608–622. [CrossRef]
46. Kinboshi, M.; Ikeda, A.; Ohno, Y. Role of Astrocytic Inwardly Rectifying Potassium (Kir) 4.1 Channels in Epileptogenesis. *Front. Neurol.* **2020**, *11*, 1832. [CrossRef] [PubMed]
47. Sirisi, S.; Elorza-Vidal, X.; Arnedo, T.; Armand-Ugón, M.; Callejo, G.; Capdevila-Nortes, X.; López-Hernández, T.; Schulte, U.; Barrallo-Gimeno, A.; Nunes, V.; et al. Depolarization causes the formation of a ternary complex between GlialCAM, MLC1 and ClC-2 in astrocytes: Implications in megalencephalic leukoencephalopathy. *Hum. Mol. Genet.* **2017**, *26*, 2436–2450. [CrossRef]
48. Morales, J.E.; De, A.; Miller, A.A.; Chen, Z.; McCarty, J.H. Mlc1-Expressing Perivascular Astrocytes Promote Blood-Brain Barrier Integrity. *J. Neurosci.* **2022**, *42*, 1406–1416. [CrossRef]
49. MacAulay, N. Molecular mechanisms of K+ clearance and extracellular space shrinkage—Glia cells as the stars. *Glia* **2020**, *68*, 2192–2211. [CrossRef]
50. Gilbert, A.; Elorza-Vidal, X.; Rancillac, A.; Chagnot, A.; Yetim, M.; Hingot, V.; Deffieux, T.; Boulay, A.C.; Alvear-Perez, R.; Cisternino, S.; et al. Megalencephalic leukoencephalopathy with subcortical cysts is a developmental disorder of the gliovascular unit. *eLife* **2021**, *10*, e71379. [CrossRef]
51. May, D.; Tress, O.; Seifert, G.; Willecke, K. Connexin47 protein phosphorylation and stability in oligodendrocytes depend on expression of Connexin43 protein in astrocytes. *J. Neurosci.* **2013**, *33*, 7985–7996. [CrossRef]
52. Lanciotti, A.; Brignone, M.S.; Visentin, S.; De Nuccio, C.; Catacuzzeno, L.; Mallozzi, C.; Petrini, S.; Caramia, M.; Veroni, C.; Minnone, G.; et al. Megalencephalic leukoencephalopathy with subcortical cysts protein-1 regulates epidermal growth factor receptor signaling in astrocytes. *Hum. Mol. Genet.* **2016**, *25*, 1543–1558. [CrossRef] [PubMed]
53. Hirabayashi, Y.; Kim, Y.J. Roles of GPRC5 family proteins: Focusing on GPRC5B and lipid-mediated signalling. *J. Biochem.* **2020**, *167*, 541–547. [CrossRef] [PubMed]
54. Meyer, R.C.; Giddens, M.M.; Schaefer, S.A.; Hall, R.A. GPR37 and GPR37L1 are receptors for the neuroprotective and glioprotective factors prosaptide and prosaposin. *Proc. Natl. Acad. Sci. USA* **2013**, *110*, 9529–9534. [CrossRef] [PubMed]
55. Smith, N.J. Drug discovery opportunities at the endothelin B receptor-related orphan g protein-coupled receptors, GPR37 and GPR37L1. *Front. Pharmacol.* **2015**, *6*, 275. [CrossRef] [PubMed]
56. Hu, G.M.; Mai, T.L.; Chen, C.M. Visualizing the GPCR Network: Classification and Evolution. *Sci. Rep.* **2017**, *7*, 15495. [CrossRef] [PubMed]

57. Valdenaire, O.; Giller, T.; Breu, V.; Ardati, A.; Schweizer, A.; Richards, J.G. A new family of orphan G protein-coupled receptors predominantly expressed in the brain. *FEBS Lett.* **1998**, *424*, 193–196. [CrossRef]
58. Donohue, P.J.; Shapira, H.; Mantey, S.A.; Hampton, L.L.; Jensen, R.T.; Battey, J.F. A human gene encodes a putative G protein-coupled receptor highly expressed in the central nervous system. *Mol. Brain Res.* **1998**, *54*, 152–160. [CrossRef]
59. Marazziti, D.; Golini, E.; Gallo, A.; Lombardi, M.S.; Matteoni, R.; Tocchini-Valentini, G.P. Cloning of GPR37, a gene located on chromosome 7 encoding a putative g- protein-coupled peptide receptor, from a human frontal brain EST library. *Genomics* **1997**, *45*, 68–77. [CrossRef]
60. Takahashi, R.; Imai, Y. Pael receptor, endoplasmic reticulum stress, and Parkinson's disease. *J. Neurol.* **2003**, *250* (Suppl. S3), 25–29. [CrossRef]
61. Zeng, Z.; Su, K.; Kyaw, H.; Li, Y. A novel endothelin receptor type-B-like gene enriched in the brain. *Biochem. Biophys. Res. Commun.* **1997**, *233*, 559–567. [CrossRef]
62. Imai, Y.; Soda, M.; Inoue, H.; Hattori, N.; Mizuno, Y.; Takahashi, R. An unfolded putative transmembrane polypeptide, which can lead to endoplasmic reticulum stress, is a substrate of Parkin. *Cell* **2001**, *105*, 891–902. [CrossRef]
63. Marazziti, D.; Di Pietro, C.; Golini, E.; Mandillo, S.; La Sala, G.; Matteoni, R.; Tocchini-Valentini, G.P. Precocious cerebellum development and improved motor functions in mice lacking the astrocyte cilium-,patched 1-associated Gpr37l1 receptor. *Proc. Natl. Acad. Sci. USA* **2013**, *110*, 16486–16491. [CrossRef] [PubMed]
64. Yang, H.-J.; Vainshtein, A.; Maik-Rachline, G.; Peles, E. G protein-coupled receptor 37 is a negative regulator of oligodendrocyte differentiation and myelination. *Nat. Commun.* **2016**, *7*, 10884. [CrossRef] [PubMed]
65. Keshet, Y.; Seger, R. The MAP kinase signaling cascades: A system of hundreds of components regulates a diverse array of physiological functions. *Methods Mol. Biol.* **2010**, *661*, 3–38.
66. Jolly, S.; Bazargani, N.; Quiroga, A.C.; Pringle, N.P.; Attwell, D.; Richardson, W.D.; Li, H. G protein-coupled receptor 37-like 1 modulates astrocyte glutamate transporters and neuronal NMDA receptors and is neuroprotective in ischemia. *Glia* **2018**, *66*, 47–61. [CrossRef]
67. Marazziti, D.; Mandillo, S.; Di Pietro, C.; Golini, E.; Matteoni, R.; Tocchini-Valentini, G.P. GPR37 associates with the dopamine transporter to modulate dopamine uptake and behavioral responses to dopaminergic drugs. *Proc. Natl. Acad. Sci. USA* **2007**, *104*, 9846–9851. [CrossRef]
68. Giddens, M.M.; Wong, J.C.; Schroeder, J.P.; Farrow, E.G.; Smith, B.M.; Owino, S.; Soden, S.E.; Meyer, R.C.; Saunders, C.; LePichon, J.B.; et al. GPR37L1 modulates seizure susceptibility: Evidence from mouse studies and analyses of a human GPR37L1 variant. *Neurobiol. Dis.* **2017**, *106*, 181–190. [CrossRef]